Mathematical Modelling and Signal and System Design for Spectrally Efficient Future Wireless Communications

Hedaia Ghannam

A thesis submitted for the degree of Doctor of Philosophy

of

University College London.

Communications and Information Systems Research Group

Department of Electronic and Electrical Engineering

University College London

August 15, 2019

I, Hedaia Ghannam, confirm that the work presented in this thesis is my own. Where information has been derived from other sources, I confirm that this has been indicated in the work.

Abstract

This thesis addresses engineering studies and design of a multi-carrier signalling format known as spectrally efficient frequency division multiplexing (SEFDM), in which higher spectral efficiency compared to conventional orthogonal frequency division multiplexing (OFDM) is achieved by compressing the spacing between subcarriers below the orthogonality limit. Work reported in this thesis comprises: *i*) Critical revision of existing studies of multi-carrier modulation formats and techniques developed for improving the spectral efficiency, with special emphasis on SEFDM system. *ii*) Mathematical modelling of interference in SEFDM and its potential capacity advantages. *iii*) The introduction of powerful channel coding techniques to mitigate the effect of interference in SEFDM, and the design of successive interference cancellation method, with a special case for broadband and broadcasting applications (DVB-S2) being considered. *iv*) A novel channel estimation scheme is developed to enhance channel estimation accuracy and to reduce its complexity for SEFDM signals for 5G systems. *v*) An experimental demonstration of successful SEFDM signals transmission over the E-Band frequency range 81-86 GHz. The systems proposed are described in detail with numerical simulations of the newly proposed system models to compare their performance to conventional OFDM systems. It is shown that SEFDM with the aforementioned techniques can achieve significant spectral efficiency gains at the expense of moderate increase in receiver complexity or increase in the transmitted power level compared to OFDM. Overall, theoretical, simulation and experimental results show key advantages of SEFDM signals and systems over other signal formats, thus paving the way to practical inclusion of SEFDM in future wireless standards.

Impact Statement

This research contributes to the study, design and practical implementation of spectrally efficient communication systems. Due to the ever increasing and unprecedented demands on the limited radio frequency (RF) spectrum, the proposed designs are expected to have impact on future cellular networks (5G and beyond), satellite broadcast systems (DVB-S2, DVB-S2X) and millimetre wave communication systems.

Towards the ultimate goal of considering spectrally efficient systems in future wireless standardisation, this thesis adapts and modifies existing SEFDM part-systems into full system design and practical implementation. Such will impact innovations in communication systems design, mathematical modelling, software simulation, hardware implementation and experimental verification. Over the past four years, this research has produced results that bridged existing research gaps, through the application of channel coding and derivation of new techniques for channel estimation, to enhance performance. Such techniques will significantly impact SEFDM real time channel estimation and signal detection, this facilitating serious consideration of SEFDM practical systems.

Collaboration with Chalmers University of Technology in Sweden led to the implementation of the worlds first E-band SEFDM practical system transmission, showing the potential of the SEFDM for future millimetre wave systems. This particular work, having considered full system design and implementation, is expected to lead to further research and development efforts in the area of high frequency, high bit rate and long distance SEFDM systems, including transmission in the beyond 100 GHz D-Band.

Much of the research and experimental work presented in the thesis was reported in 15 papers, many of cross disciplinary nature, which I have authored and co-authored and which appeared in leading international journals and conference proceedings. The transmitter, the detector and the channel estimator designs developed in this work, may be utilised in various wired and wireless systems such as 5G and beyond, DVB-S2, VLC, optical fibre systems and fast-DSL. The successful application of SEFDM in these systems makes it a serious signal contender in future networks and paves the way for new research and possible implementation in future commercial communication systems.

In 2018 and with funding from the UKs Engineering and Physical Sciences Research Council (EPSRC)/ UCL Innovation and Enterprise and with further funding and support from British Telecom, I undertook an internship for 6 months at BT's Global Research and Development Headquarters. The aim was to introduce this PhD research work to industry and gain a better insight into industry's requirements and limitations. Various use cases are studied including future wireless systems and the application of SEFDM signals to DSL twisted copper lines with multi Gbit/s.

SEFDM has already had academic impact in wireless, optical and satellite system designs at universities worldwide; in China (Fudan, BUPT, Sun Yat-sen and Jinan); Hong Kong (HK Poly-U), University of Luxembourg; McGill University in Canada; St. Petersburg Polytechnic University in Russia; Tokyo University of Agriculture and Technology in Japan. The research reported in this thesis is already being tracked by various researchers in the field and is expected to lead to further academic impact at the universities above and perhaps others in the future.

Acknowledgements

First, I would like to express my sincere gratitude to my supervisor Prof Izzat Darwazeh for the great supervision, motivation and friendship. It would have never been possible for me to take this PhD to completion without his constant guidance and support. Being your student has been a real privilege and all what I will accomplish in the future is because of you.

I would like to thank Mr Dhecha Nopchinda and Prof Herbert Zirath, from Chalmers University of Technology, Gothenburg, Sweden, about the collaborative work, which resulted in a journal publication and is introduced in Chapter 7 of this thesis.

I would like to thank Dr Tongyang Xu and Mr Waseem Ozan for the long discussions about the system and the collaborative work to test the proposed channel estimation scheme of Chapter 6 on National Instrument's USRPs, which resulted in two conference publications. I would like to thank Dr Ioannis Kanaras and Dr Safa Isam for the use of the fixed sphere decoder implemented by them to SEFDM systems in Chapter 8. I also appreciate Dr Arman Shojaeifard help and support, especially in Latex and Dr Ryan Grammenos for all the insightful conversations we had.

I would like to thank Dr Michel Fitch for giving me the opportunity to do my internship in BT research labs, Ipswich. I met excellent researchers and people who have helped me to improve my knowledge, especially about standards and industry. Special thanks to Dr Anvar Tukmanov for his guiding that led to the second part of Chapter 8 presented in this thesis. I would also like to thank Dr Marcus Perrett for giving me the opportunity to work in Cobalt on my last year in my PhD.

I am also grateful to my UCL colleagues and to UCL staff, especially to Sephora Madjiheurem and Silvia Rossi, for providing a supportive, stimulating and enjoyable living experience during the course of my study. My deepest thanks are to my partner Dr Adrian Garcia for accompanying me in this challenging and stimulating experience with all its ups and downs. A very special and warm thanks to my friend Ola Anabtawi for being with me in every step along this journey. I am very grateful to my wonderful friends Lucy Garbett, Zeina Amro, Dia Bargouthi, Dina Amro, Wafi Belal, Haneen Qolagasi and Noor Khaled for being my family here in London.

Last but not least, I would like to express my deepest gratitude to my family who supported me through the course of the PhD studies. I am greatly indebted to my wonderful parents Nabeela and Omar and my siblings Ibrahim, Hadeel and Rand whose love and support now and throughout my life has led me to all that I accomplished. I am also grateful to my uncle Nabeel Isleem for his absolute support through my PhD.

During the course of this work I have been funded by the Overseas Research Student (ORS) Award and the UCL Dean of Engineering Sciences Award for three years of study. My internship in BT for six months was funded by BT and the Engineering and Physical Sciences Research Council (EPSRC) UCL Innovation and Enterprise Impact Acceleration Account (IAA) Award.

Contents

List of Figures

List of Tables

Glossary

$\mathbb{C}$	Set of complex numbers
$\mathbb{Z}$	Set of integer numbers
$\mathbf{\Phi}$	Modulator matrix
$(.)^{\mathrm{H}}$	Hermitian operator
$\mathbf{I}_x$	Identity matrix of size x
η	Spectral efficiency
α_t	Time acceleration factor
α	Frequency compression factor
$\lfloor . \rfloor$	Floor operation
$\lceil . \rceil$	Ceiling operation
$\lfloor . \rceil$	Slice function
$\mathbf{\Lambda}$	Correlation matrix
ρ	Oversampling factor
σ	Variance (second moment)
μ	Mean (first moment)
$Q(.)$	Tail distribution function
$\|\|.\|\|$	Euclidean norm
$\mathrm{E}[.]$	Expectation operator

ζ	Spectral efficiency gain
$\Re\{.\}$	Real part of a complex number
Υ	Interference canceller matrix
$\odot$	Element-wise multiplication
.	Element-wise division
mod	Modulo operation
$\mathscr{H}$	Sphere decoder search subspace
A	Uppercase bold character denotes a matrix
a	Lowercase bold character denotes a vector
min	Minimum

Abbreviations

ADC	Analog to digital converter
ALCR	Adjacent channel leakage ratio
APP	*aposteriori* probability
AWG	Arbitrary waveform generator
AWGN	Additive white Gaussian noise
BCH	Bose-Chaudhuri-Hocquenghem
BCJR	Bahl, Cocke, Jelinek and Raviv
BER	Bit error rate
BLER	Block error rate
BP	Belief propagation
BPSK	Binary phase shift keying
CCDF	Complementary cumulative distribution function
CDMA	Code-division multiple access
CFR	Channel frequency response
CP	Cyclic prefix
CSI	Channel state information
CRS	Channel reference symbol
CSR	Cell-specific reference
DAC	Digital to analog converter
DFT	Discrete Fourier transform
DSP	Digital signal processing
DVB-S2	Digital video broadcast-second generation
eMBB	Enhanced mobile broadband

EP	Expectation propagation
EPA	Extended pedestrian A model
ESE	Effective spectral efficiency
EVM	Error vector magnitude
FBMC	Filter-bank multi-carrier
FDM	Frequency division multiplexing
FEC	Forward error correction
FFT	Fast Fourier transform
FOFDM	Fast OFDM
f-OFDM	Filtered OFDM
FPGA	Field programmable gate arrays
FSD	Fixed sphere decoder
FTN	Faster than Nyquist
GB	Guard band
GFDM	Generalised frequency division multiplexing
GSD	Generalized sphere decoder
HPA	High power amplifier
ICI	Inter-carrier interference
IDFT	Inverse discrete Fourier transform
IFFT	Inverse fast Fourier transform
IMUX	Input multiplexer
ISI	Inter-symbol interference
ITU	International telecommunications union
LDPC	Low-density parity-check
LLR	Log-likelihood ratio
LoS	Line of sight
LPF	Low pass filter
LS	Least square
LTE	Long term evolution
LTE-A	LTE-Advanced

MAP	Maximum $a-posteriori$
M-ASK	M-array amplitude shift keying
MCM	Multi-carrier modulation
MFTN	Multistream-FTN
MIMO	Multi-input multi-output
ML	Maximum likelihood
MMSE	Minimum mean square error
mMTC	Massive machine type communications
M-PSK	M-array phase shift keying
MSE	Mean square error
NOFDM	Non-orthogonal OFDM
NOMA	Non-orthogonal multiple access
NR	New radio
OFDM	Orthogonal frequency division multiplexing
OMA	Orthogonal multiple access
OMUX	Output multiplexer
OOBE	Out-of-band emission
O-QAM	Offset-QAM
PAPR	Peak to average power ratio
PCCC	Parallel concatenated convolutional code
PCE	Partial channel estimation
PDF	Probability density function
PDSCH	Physical downlink shared channel
PER	Packet error rate
PSD	Power spectral density
P/S	Parallel to serial
QAM	Quadrature amplitude modulation
QI	Quality index
QoS	Quality of service
QPSK	Quadrature phase shift keying

RB	Resource block
RCP	Robust channel processor
RLS	Recursive least square
RMS	Root mean square
RRC	Root-raised cosine
RS	Reed-Solomon
RSCC	Recursive systematic convolutional code
SCM	Single carrier modulation
SD	Sphere decoder
SDP	Semi definite programming
SEFDM	Spectrally efficient frequency division multiplexing
SIC	Successive interference cancellation
SISO	Soft-input/soft-output
SLW	Selective windowing
SNR	Signal to noise ratio
SoDeMA	Soft defined multiple access
SoDeFDM	Soft defined FDM
SOVA	Soft output Viterbi algorithm
S/P	Serial to parallel
TDL	Tapped delay line
TFP	Time-frequency packing
TSVD	Truncated singular value decomposition
VA	Viterbi algorithm
VCCM	Variable coding compression and modulation
VCM	Variable coding and modulation
VLC	Visible light communication
VMP	Variational message passing
V2V	Vehicle to vehicle
UE	User equipment
UFMC	Universal filter multi-carrier

URLLC	Ultra reliable low latency communications
USRP	Universal software radio peripheral
W-OFDM	Windowed OFDM
WPAN	Wireless personal area network
ZF	Zero forcing
ZP	Zero padding
2G	Second generation
3GPP	3rd generation partnership project
5G	Fifth generation

Chapter 1

Introduction

The rapid development of communications technologies and the explosive growth in users and machines demand for broadband wireless access push the current wireless spectrum towards saturation. Consequently, much research interest is focused on searching for new higher spectral efficient communication methods and techniques, such as orthogonal frequency division multiplexing (OFDM); massive multi-input multi-output (MIMO); non orthogonal multiple access (NOMA) and pulse shaping techniques, to enhance spectrum utilisation by providing higher spectral efficiency. These techniques are found in today's mobile communication standards, such as the 4th generation (4G) [1] and future 5th generation (5G) [2] cellular systems, in addition to other wireless systems such as 802.11*ac* and in broadcast systems (e.g. DVB). Moreover, research interest is currently exploring mm waves and THz frequencies to benefit from the larger available bandwidth for future 2030 6th generation (6G) cellular system [3].

The advantages of OFDM made it (and its variants) key technologies for the physical layer of 5G [4]. The special interest in OFDM signal format is mainly motivated by its spectrum structure with overlapping subcarriers, which not only enhances bandwidth efficiency but also significantly improves immunity against multipath propagation effects, when compared to single carrier transmission [5]. In addition, the ease of implementation of OFDM transmitters and receivers made it attractive for a wide variety of wired and wireless applications [3], [4].

A key question is: Can the spectral efficiency of OFDM be improved without

sacrificing its key advantages? One contribution in this direction was the development of spectrally efficient frequency division multiplexing (SEFDM), first proposed in 2003 [6]. SEFDM is a multi-carrier system that achieves spectral efficiency gains by packing the subcarriers closer (relative to OFDM), while compromising the orthogonality. Despite the non-orthogonality, different detection methods have been demonstrated where the error performance of SEFDM gets reasonably close to OFDM, with spectral efficiency improvement greater than 25% [7], [8], [9]. The Faster than Nyquist (FTN) technique initially proposed in 2009 [10], is SEFDM's time domain counterpart and has similar spectral efficiency gains. Another spectrally efficient technique, which combines SEFDM with FTN to what is termed time-frequency packing (TFP), where the time and frequency spacing are chosen to maximize the spectral efficiency [11].

This thesis reviews the work that has been done so far on SEFDM and explores and designs new techniques to tackle SEFDM signals generation, detection and channel estimation problems. Furthermore, mathematical models are designed and experiments are reported to verify the proposed solutions. In the following sections, aim and motivation of this work are presented, followed by the main contributions and the structure of the thesis.

1.1 Aim and Motivations

The work in this thesis focuses on the SEFDM system of [6]. SEFDM system enhances spectral efficiency by compressing the subcarriers closer, compared to OFDM, while maintaining the same transmission rate per subcarrier. Notwithstanding, the deliberate collapse of orthogonality generates significant interference between the subcarriers that turns the overall system model into a complex problem [8].

The main research focus on SEFDM so far has been on lowering SEFDM detector complexity, while maintaining good error performance. Such research resulted in practical detector designs, such as fixed sphere decoder [12], iterative equaliser [13] and other detectors summarised in [14]. Towards the ultimate goal

of considering SEFDM in future wireless standardisation, this thesis aims to take part systems into full system design and practical implementation. Motivated by this and for the first time, existing channel coding techniques currently used and others proposed for future wireless systems have been applied to SEFDM systems, either on its own or as part of a successive interference canceller, to guarantee a low complex and good error performance detector.

Most published research articles on SEFDM signals assume perfect knowledge of the channel and the existing estimation schemes suffer from high complexity, such as the time-domain estimation scheme in [15] and the frequency domain with interpolation estimation scheme in [16]. The work in this thesis aims to bridge this gap by developing a new robust and low complexity frequency domain channel estimation scheme, that can be used in practical systems.

Inspired by the new leading technique power NOMA in 5G, a preliminary work in this thesis investigate the application and advantages of applying power allocation to SEFDM. Finally, motivated by increased research interest in the high frequency spectrum, the worlds first testbed is designed and tested, to transmit SEFDM at the mm-wave E-band frequency range 81-86 GHz.

1.2 Contributions

This thesis documents work in different areas of SEFDM signals and systems, covering system modelling, transmission, detection, channel estimation and performance investigations. The benefits of techniques reported are substantiated by theoretical analyses, simulations and experimental results. The main contributions presented in this document may be divided into two main parts: fundamentals and new design concepts; and implementation and practical systems.

- **Fundamentals and new design concepts:**
  - Derived the statistical model for interference in SEFDM signals to complement the well-known SEFDM deterministic model. The model was used to derive a closed form to compute SEFDM systems probability of error with a matched filter and to calculate SEFDM potential capacity

and spectral efficiency upper bound. This work was published in [17] and appears in Chapter 3 in this thesis.

- Designed the first SEFDM system with different channel coding techniques, namely Reed-Solomon (RS) coding; turbo coding and serially concatenated coding, to mitigate interference impairments. This study included an investigation of the effect of different channel coding parameters on SEFDM systems and evaluated the advantage of interleavers in SEFDM coded systems. This work was published in [18] and in [19] and appears in Chapter 4 in this thesis.
- Designed a new method of successive interference cancellation (SIC) with low-density parity-check (LDPC) coding and verified its efficacy by mathematical modelling. This work was published in [20] and appears in Chapter 5 of the thesis.
- Developed a new robust frequency domain channel estimation scheme distinguished by its estimation accuracy and low complexity, compared to existing channel estimation schemes. This work was published in [21] and in [22], also was presented in [23] and appears in Chapter 6 in the thesis.
- Proposed a new method of generating and adding cyclic prefix to SEFDM signals, to maintain the cyclic prefix continuity property. This work was published in [24] and appears in Chapter 6 in the thesis.
- Introduced the concept of power allocation to SEFDM signal format, such as different subcarriers are allocated with different power levels, to overcome the ill-conditioned issue of SEFDM and to reduce detector complexity. This work was published in [25] and in [26] and appears in Chapter 8 in the thesis.

- **Implementation and practical systems:**
  - Applied SEFDM to digital video broadcast-second generation (DVB-S2) satellite system with LDPC and SIC to provide more degrees of freedom

in optimising the system, by adding a compression variable to variable coding and modulation parameter. This work was published in [20] and appears in Chapter 5 in the thesis.

- Designed and implemented the world's first transmission of SEFDM in the mm-wave E-band frequency range 81-86 GHz. The newly developed channel estimation scheme is used here to solve the channel and phase offset estimation and equalization issues, while LDPC is used to improve system error performance. The work reported highest transmission rate of 12 Gbps (experimental). This work was published in [27] and appears in Chapter 7 in the thesis.
- Applied SEFDM signals to 5G new radio system model. A proposal was given for a single reconfigurable transmitter design capable of generating SEFDM symbols with continuous cyclic prefix, as well as the pilot symbols of the new channel estimation scheme. This work was published in [24] and appears in Chapter 6 in the thesis.
- Applied SEFDM signals to LTE physical downlink channel with different transmission modes, to increase spectral efficiency compared to OFDM signals. Power allocation was used to boost the power level of the reference signals compared to data signals, to enhance channel estimation accuracy. This work appears in Chapter 8 in the thesis.

1.3 Structure of the Thesis

This thesis consists of 9 chapters and three appendices. Subsequent to this introductory chapter, the thesis organisation follows the description below.

Chapter 2 contains a detailed literature review on multi-carrier modulation formats, to establish the significance of the work done as part of this PhD thesis and to identify the place where the new contributions are made. The chapter starts with a description of single and multi-carrier modulations, then focuses on OFDM system, signal generation, modulation and demodulation. A discussion of waveforms candidates for 5G systems is provided and a table comparing the main features of the

different candidates is given. Finally, the concept of non-orthogonal modulation formats is introduced and the main signals within this special format are summarised.

Chapter 3 presents a comprehensive survey on SEFDM signals and systems. It starts with a detailed mathematical model of SEFDM signal generation, modulation and demodulation. A statistical model of the interference in SEFDM signals is derived and mathematical simulations are provided to validate the system model. The effect of the compression level and number of subcarriers in the interference variance is investigated. Upon these results, the interference statistical model is used to derive a closed form expression of the probability of error in SEFDM systems. To prove the advantage of SEFDM signals, SEFDM potential capacity and spectral efficiency upper bound are calculated and compared to OFDM. To conclude the overview, after the mathematical modelling, a comprehensive survey of the development history of SEFDM signals since 2003 is presented, covering wireless and optical communications concepts, circuit design and experimental testbeds. The main challenges of SEFDM and the developed ongoing work to solve them are addressed, including the work reported in this thesis.

Chapter 4 is dedicated to the basics of coded SEFDM systems, where different channel coding techniques are applied to enhance SEFDM error rates. The capability of RS, convolutional, turbo and serially concatenated codes, in eliminating the interference effect in SEFDM, is investigated. As the results expectedly favour turbo coding over the other techniques, a study of the effect of different parameters of turbo codes in dealing with the interference in SEFDM is provided, such as the number of decoder iterations and coding rate. Afterwards, the application and benefits of using an external interleaver (to interleave the coded bits of SEFDM signals) is given. Finally, a fair comparison between OFDM and SEFDM is held, given that both have the same spectral efficiency and the same simulation parameters, to evaluate SEFDM signals performance and limitations with channel coding.

The conclusions of Chapter 4 has led to the development and design of a successive interference canceller in Chapter 5. The new SEFDM receiver design is introduced to DVB-S2 satellite systems, to add more flexibility by introducing ad-

justable compression level variable, besides the coding rate and modulation cardinality variables. A mathematical model and simulation studies are presented, to prove the gains achieved for introducing the compression level in SEFDM transmission with interference cancellation and LDPC channel coding.

Chapter 6 proposes a novel frequency domain channel estimation scheme for SEFDM signals, which is distinguished by its implementation simplicity, low computational complexity and high accuracy. A mathematical model of SEFDM transmission over multipath frequency selective channels is demonstrated. To confirm the benefits of the proposed scheme, comparisons are held between it and other existing channel estimation schemes. In order to provide further insights, simulation studies are done about the application of the developed scheme to SEFDM 5G new radio frames using 5G defined channel model standards. As part of this study, a new transmitter design was proposed, which is capable of generating pilot signals for the developed estimation scheme and continuous cyclic prefix for SEFDM signals.

Chapter 7 describes the design of the experiment of SEFDM signals transmission over mm-wave 81-86 GHz frequency range. The testbed components and setup are detailed and the complete chain of digital signal processing is explained. The channel estimation scheme proposed in Chapter 6 is used to solve the channel and phase offset estimation and equalisation issues, while LDPC channel coding is employed to achieve low error rates.

Chapter 8 proposes the application of power allocation to SEFDM signals. This implication of power allocation to SEFDM systems is tested from two perspectives: signal detection and channel estimation. Regarding signal detection, a new system architecture based on double stage detection technique with a fixed sphere decoder is designed and the advantages of such design are explored. On the other hand, for power allocation effect on channel estimation, a simulation study is presented for a specific scenario of SEFDM-LTE physical downlink channel dedicated to transmit user data.

Chapter 9 summarises the work in this thesis and highlights the significance of the proposed techniques. In addition, the chapter presents future research lines to

follow from the work of this thesis.

The thesis includes three appendices; Appendix A explains the mathematics of MAP decoding, for which it was used to build and simulate MAP decoding functions in MATLAB; Appendix B details the circuit design and performance of the transmitter and receiver E-band chips used in the experiment setup in Chapter 7. In Appendix C, a flow chart is drawn to show the steps followed to convert between SNR and E_b/N_0.

1.4 Publications

The aforementioned contributions resulted in 3 journal publications and 12 conference publications and presentations and one award, listed below in chronological order.

- Journal Publications

    1. H. Ghannam and I. Darwazeh. SEFDM over Satellite Systems with Advanced Interference Cancellation. *IET Communications*, 12(1):59–66, January 2018.
    2. H. Ghannam T. Xu and I. Darwazeh. Practical Evaluations of SEFDM: Timing Offset and Multipath Impairments. *Infocommunications Journal*, January 2019.
    3. H. Ghannam, D. Nopchinda, M. Gavell, H. Zirath, and I. Darwazeh. Experimental Demonstration of Spectrally Efficient Frequency Division Multiplexing Transmissions at E-Band. *IEEE Transactions on Microwave Theory and Techniques*, 67(5):1911–1923, March 2019.

- Conference Publications

    1. H. Ghannam and I. Darwazeh. Comparison of Turbo Decoder and Turbo Equalizer for Spectrally Efficient FDM System. In *IEEE Proc. 10th Int. Symp. Commun. Syst. Networks and Digital Signal Process. (CSNDSP), Prague*, pages 1–6, July 2016.

2. H. Ghannam and I. Darwazeh. Turbo Coding and Iterative Interference Cancellation of Spectrally Efficient FDM Systems. In *IEEE Wireless Communications and Networking Conference ((WCNC) - Student Outreach Program-Poster, San Francisco*, March 2017.

3. H. Ghannam and I. Darwazeh. Signal Coding and Interference Cancellation of Spectrally Efficient FDM Systems for 5G Cellular Networks. In *2017 IEEE Proc. 24th Int. Symp. International Conference on Telecommunications (ICT), Cyprus*, pages 1–6, May 2017.

4. H. Ghannam and I. Darwazeh. Low Complexity Channel Estimation Scheme for Spectrally Efficient FDM Systems in 5G Cellular Networks. In *Wireless World Research Forum (WWRF) Meeting 39 Workshop, Castelldefels, Barcelona*, October 2017.

5. W. Ozan, H. Ghannam, P. A. Haigh, and I. Darwazeh. Experimental Implementation of Real-time Non-orthogonal Multi-carrier Systems in a Realistic Fading Channel. In *IEEE proc. Radio and Wireless Symposium (RWS), California*, pages 121–124, January 2018.

6. H. Ghannam and I. Darwazeh. Robust Channel Estimation Methods for Spectrally Efficient FDM Systems. In *IEEE 87th Vehicular Technology Conference VTC (Spring) workshop; Technology Trials and Proof-of-Concept Activities for 5G and Beyond 2018 (TPoC5G 2018), Porto*, June 2018.

7. I. Darwazeh, H. Ghannam, and T. Xu. The First 15 Years of SEFDM: A Brief Survey. In *IEEE Porc. 11th International Symposium on Communication Systems, Networks Digital Signal Processing (CSNDSP), Budapest*, pages 1–7, July 2018.

8. H. Ghannam and I. Darwazeh. SEFDM: Spectral Efficiency Upper Bound and Interference Distribution. In *IEEE Proc. 11th International Symposium on Communication Systems, Networks Digital Signal Processing (CSNDSP), Budapest*, pages 1–6, July 2018.

9. W. Ozan, H. Ghannam, T. Xu, P. A. Haigh, and I. Darwazeh. Experimental Evaluation of Channel Estimation and Equalisation in Non-Orthogonal FDM Systems. In *IEEE 11th Proc. International Symposium on Communication Systems, Networks Digital Signal Processing (CSNDSP), Budapest*, July 2018.

10. H. Ghannam and I. Darwazeh. Power Allocation for Detection Performance Enhancement of SEFDM Signals. In *2018 IEEE 29th Annual International Symposium on Personal, Indoor and Mobile Radio Communications (PIMRC), Bologna*, pages 584–585, September 2018.

11. H. Ghannam and I. Darwazeh. Design and Performance of SEFDM Signals with Power Allocation. In *IEEE Proc. Wireless Communications and Networking Conference (WCNC), Marrakech*, April 2019.

12. H. Ghannam and I. Darwazeh. A Proposal for Scalable 5G New Radio Frames with Enhanced Throughput. In *IEEE 89th Vehicular Technology Conference (Spring), Kuala Lumpur*, April 2019.

- Awards

1. Turing Institute Prize for best student poster, Barlow lecture, UCL, 2017. Poster title: “Turbo Coding and Iterative Interference Cancellation of Spectrally Efficient FDM Systems”.

Chapter 2

Spectrally Efficient Modulation Schemes: Orthogonal & Non-Orthogonal Waveforms

This chapter presents a review of the state of the art in the research areas relevant to this thesis. In particular, the focus is on spectrally efficient multi carrier waveforms with the objective of enhancing the spectral efficiency of wireless communications. The chapter starts with a description of single and multi carrier modulations, then OFDM signal main features and its mathematical model are provided in section 2.2. Section 2.3 summarises fifth generation (5G) network waveforms candidate. Section 2.4 outlines non-orthogonal modulation systems similar to SEFDM, which is the main focus of this thesis. Finally, conclusions are drawn in section 2.5.

2.1 Single Carrier & Multi Carrier Modulation

single carrier modulation (SCM) was dominant over the years for data and voice transmission in the first and second generations of mobile wireless networks. By that time, the data was limited to text and multimedia messages and few kbit/s rates was sufficient. However, mobile phone revolution, such as video calls and real time applications, required a more reliable and efficient forms of data communication (i.e. higher bitrate and shorter delay) [5]. To meet higher bitrate requirement, two straight forward methods may be used; i) increasing the modulation size (order) to

carry more bits per symbol; ii) transmitting the symbols faster in time, or in other words, use a higher symbol rate and shorter symbol interval [31]. Regarding the first method, if the transmitted power level is maintained, a higher modulation size will cause error performance degradation and will lower system reliability [31]. In the second method, symbol duration is limited by the wireless channel characteristics, because symbol duration must be larger than the delay spread of a dispersive fading channel to avoid inter-symbol interference (ISI) [31]. To deal with such ISI impairments, a waiting gap, with a minimum duration equals the delay spread of the channel, can be inserted between transmission of adjacent symbols. However, this solution reduces the effective transmission rate [31]. Another solution to reduce ISI is the employment of multi carrier modulation (MCM) instead of SCM. In 1957, the idea of MCM was firstly proposed for a special single-sideband voice channel over wires [32]. In MCM, instead of transmitting the data over a single carrier that occupies the whole channel available bandwidth, the channel is divided into narrow subchannels (subcarriers). All subcarriers transmit, in parallel, at a lower data rate to maintain the aggregate high data rate transmission and to increases the symbol duration to combat ISI effects [33]. The OFDM survey in [5], provides a thorough review of different MCM methods invented and studied over the years. This chapter concentrates on the most prominent and successful MCM signal model, which is OFDM. The following section describes the OFDM signal and its advantages over other MCM signals.

2.2 OFDM

Orthogonal frequency division multiplexing is defined as a parallel multiplexed data signal, where multi streams of data are transmitted simultaneously on non-interfering (i.e. orthogonal) subcarriers, so that each subcarrier only occupies a small part of the available bandwidth. By a sufficient selection of number of subcarriers, the OFDM symbol duration can become much larger than the time dispersion of the channel, thus, ISI impairments encountered by frequency selectivity can be made arbitrarily small [5].

In conventional MCM signals, the total signal frequency band is divided into N non-overlapping frequency subcarriers, each subcarrier is modulated with a separate symbol and the N subcarriers are frequency multiplexed. In OFDM, a more efficient use of bandwidth is obtained by permitting the individual subcarriers to overlap, with specific orthogonality constraints. Adjacent subcarriers are orthogonal when the frequency separation between them is the reciprocal of their signalling duration [31]. Further details of the mathematical model of OFDM modulation and demodulation processes is provided in the next section.

2.2.1 OFDM System Model

A general descriptive block diagram of baseband OFDM system model is given in Fig. 2.1. The message bits $\mathbf{b} \in \{0,1\}$ are generated, then each $\log_2 M$ bits are mapped into a complex symbol $z \in \mathbb{C}$, given M is the mapper cardinality order. The mapped symbols are divided into K streams each of size equal to the desired OFDM symbol size N. The k^{th} stream is converted from a serial to a parallel stream using a serial to parallel (S/P) converter. Afterwards, each element of this stream modulates one of the N subcarriers of the OFDM symbol. The resultant signal $x_k(t)$ is transmitted over a channel, which in this case is an additive white Gaussian noise (AWGN) channel. At the receiver, the received signal $y_k(t)$ is processed by an OFDM demodulator. At the last stage, the demapper makes a hard decision and retrieves the received bits $\hat{\mathbf{b}}$.

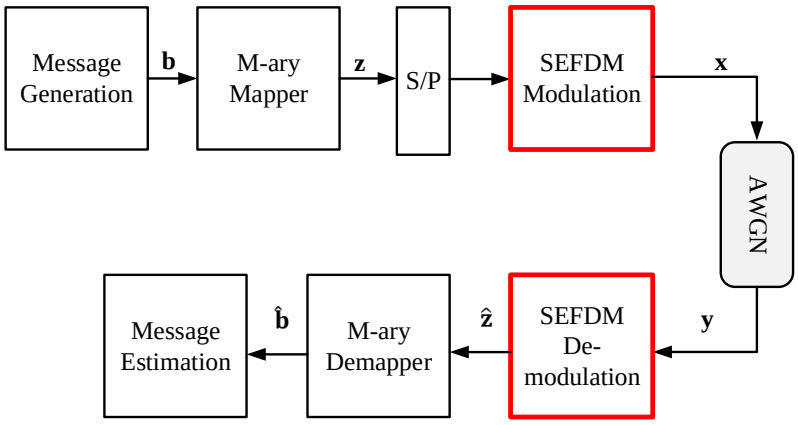

Figure 2.1: General descriptive OFDM baseband transceiver block diagram.

If T_s is the symbol interval in a SCM signal, the symbol interval of an OFDM signal of N subcarriers is $T = N \times T_s$. The frequency separation between adjacent subcarriers (Δf) is the reciprocal of the signalling duration (T), to enable independent separation among subcarriers at the receiver side by using coherent detection [31]. The complex envelope of the k^{th} baseband OFDM modulated signal can be presented by

$$x_k(t) = \frac{1}{\sqrt{T}} \sum_{n=0}^{N-1} z_{k,n} \exp\left(j2\pi n \Delta f g(t-kT)\right), \quad 0 \leq t \leq T \tag{2.1}$$

where $g(t)$ is time domain rectangular pulse of duration T, given by

$$g(t) = \begin{cases} 1/T, & 0 \leq t \leq T \\ 0, & \text{otherwise.} \end{cases} \tag{2.2}$$

The normalised OFDM spectrum of $x_k(t)$, for $N = 1024$ subcarriers, is shown in Fig. 2.2 (a) and of 8 subcarriers is shown in Fig. 2.2 (b). A rect pulse in the time domain is translated into a Sinc shaped subcarrier in the frequency domain, where $\text{Sinc}(x) = \text{Sin}(\pi x)/(\pi x)$. From Fig. 2.2 (b): *i*) orthogonality can be noticed, as at the maximum point of any subcarrier, the rest of the subcarriers are zero; *ii*) the main lobe of any subcarrier is from a null to a null $(1/T)$ Hz. Adjacent sidelobes levels of Sinc-shaped subcarriers are relatively high and do not decay rapidly, hence, frequency guard band is inserted between OFDM symbols.

Assuming the signal is only impaired by AWGN, i.e. the noise $w(t)$ mean is zero and variance is $\sigma_n^2 = N_0$, where $N_0/2$ is the noise power spectral density (PSD). Then, the received signal is

$$y(t) = x(t) + w(t). \tag{2.3}$$

At the receiver, a coherent detector with a matched filter is used for a symbol-by-symbol decision to demodulate the OFDM signal. If the transmitted signal is impaired only by AWGN, the orthogonality condition ($\triangle f = 1/T$) makes a simple

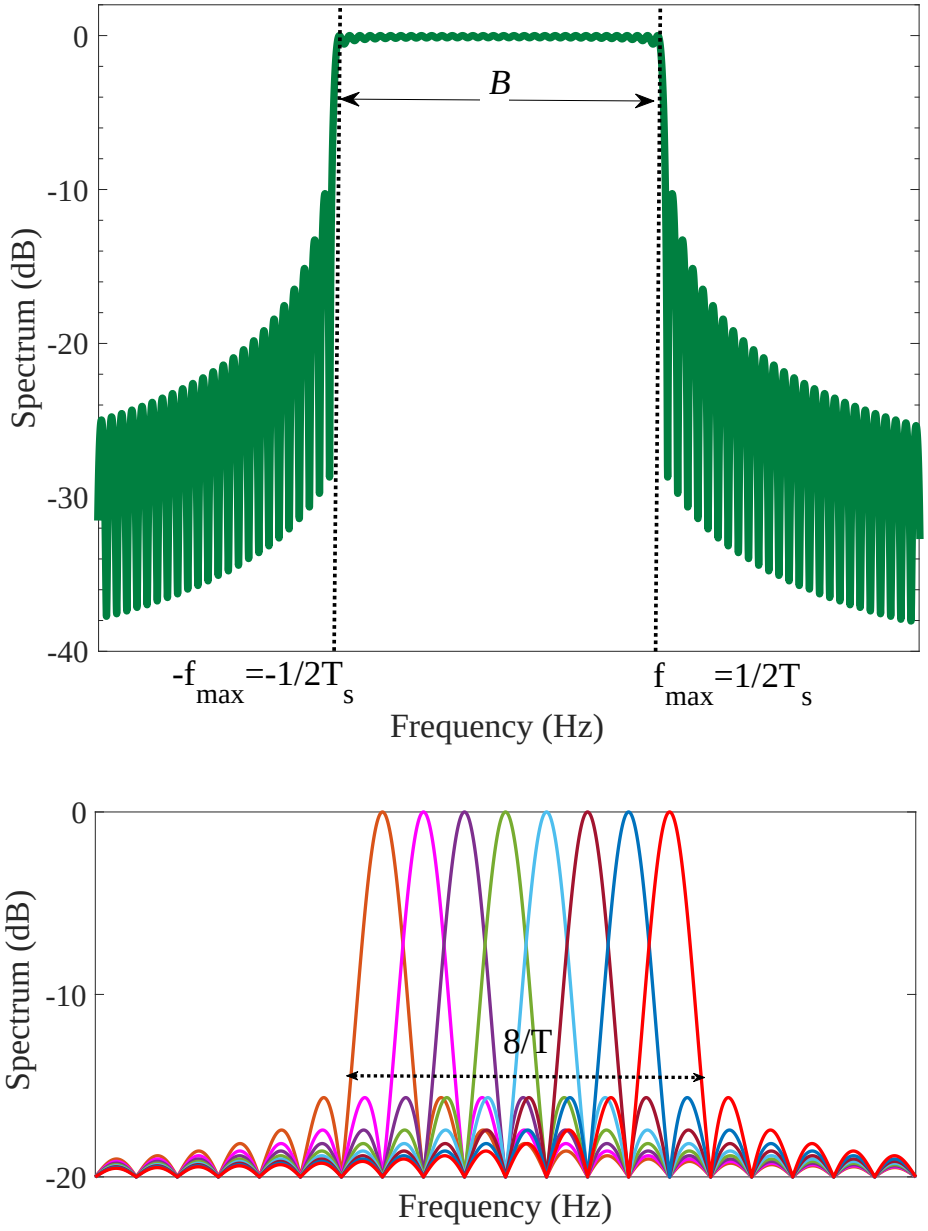

Figure 2.2: OFDM Spectrum for (a) $N = 1024$, (b) $N = 8$.

matched-filter detector sufficient. The estimated symbol $\hat{z}_{k,n}$ is given by

$$\hat{z}_{k,n} = \frac{1}{\sqrt{T}} \int_T y_k(t) \exp\left(-j2\pi n \Delta f (t - kT)\right) dt. \quad 0 \leq n \leq N \tag{2.4}$$

In current systems, baseband processes occur in the digital domain, thus it is essential to convert the above processes from analogue to digital. The signal bandwidth of the band-limited baseband signal $x_k(t)$ is $f_{max} = B/2 = 1/2T_s$, as shown in Fig. 2.2.

Following Nyquist, the signal is to be sampled at a minimum rate of double the symbol rate, to allow the reconstruction of the signal from its samples at the receiver (i.e. $f_s = 2f_{max} = B = 1/T_s$). Consequently, by sampling the signal in (2.1) at a regular interval of $\tau = T_s$, the total number of samples is $Q = T/\tau = N$. Therefore, $Q \geq N$ samples are required. The sampled version $x_k(qT/Q)$ of (2.1), or simply $x_{k,q}$ is

$$\begin{aligned} x_{k,q} &= \frac{1}{\sqrt{Q}} \sum_{n=0}^{N-1} z_{k,n} \exp\left(j2\pi n\Delta f \left(\frac{qT}{Q} - kT \right) \right) \\ &= \frac{1}{\sqrt{Q}} \sum_{n=0}^{N-1} z_{k,n} \exp\left(j2\pi \frac{qn}{Q} \right) \times \exp(-j2\pi kn) \\ &= \frac{1}{\sqrt{Q}} \sum_{n=0}^{N-1} z_{k,n} \exp\left(j2\pi \frac{qn}{Q} \right), \quad q = 0, 1, ..., Q-1 \end{aligned} \tag{2.5}$$

where the factor $1/\sqrt{Q}$ in (2.5) is employed for normalization purpose [1]. Following the same method, the discrete demodulated signal at the receiver side is [5]

$$\hat{z}_{k,n} = \frac{1}{\sqrt{Q}} \sum_{q=(k-1)Q}^{kQ-1} y_{k,q} \exp\left(-j2\pi \frac{qn}{Q} \right), \quad n = 0, 1, ..., N-1. \tag{2.6}$$

Initially, the combination of (2.5) and (2.6) used a bank of modulators each tuned at a certain frequency. However, such generations are complex, and even get more complex when the number of subcarriers is large. Taking another look at (2.5) and (2.6), they are actually the inverse discrete Fourier transform (IDFT) of the transmitted symbols $\mathbf{z}$ and the discrete Fourier transform (DFT) of the received symbols $\mathbf{y}$, respectively. In practice, they are implemented in the digital domain by means of inverse fast Fourier transform (IFFT) and fast Fourier transform (FFT), at the transmitter and receiver, respectively.

It is convenient to describe the process by a linear model. The system in (2.5)

[1] For simplicity, the condition that indicates $Q \geq N$ is omitted in subsequent discussion of this thesis.

can be expressed in matrix form as [2]

$$\mathbf{x} = \Phi\, \mathbf{z}, \tag{2.7}$$

where $\mathbf{x} = \{x_0, x_1, ..., x_{Q-1}\}$ is a vector of transmitted samples of $x(t)$ in (2.5) and Φ is a $Q \times N$ matrix, whose elements are given by

$$\phi_{q,n} = \frac{1}{\sqrt{Q}} \exp\left(j2\pi \frac{qn}{Q}\right), \quad 0 \leq n \leq N-1, 0 \leq q \leq Q-1. \tag{2.8}$$

The received signal is

$$\mathbf{y} = \Phi\mathbf{z} + \mathbf{w}, \tag{2.9}$$

where $\mathbf{w}$ is a $Q \times 1$ vector, which represents the AWGN samples. The output of the FFT at the receiver is

$$\hat{\mathbf{z}} = \Phi^{\mathrm{H}}\Phi\mathbf{z} + \Phi^{\mathrm{H}}\mathbf{w}, \tag{2.10}$$

where $(.)^{\mathrm{H}}$ is the Hermitian operator to obtain the conjugate transpose of the modulation matrix Φ. In (2.10), due to the orthogonality condition, the term $\Phi^{\mathrm{H}}\Phi$ turns into an identity matrix of size $N \times N$ ($\mathbf{I}_N$).

To summarise, the OFDM transceiver is simple and efficient. The next section calculates the spectral efficiency of OFDM and compares it to that of SCM.

2.2.2 OFDM Spectral Efficiency

The term spectral efficiency (η) measured in b/s/Hz refers to the bit transmission rate (R_b) in b/s, transmitted over a channel of bandwidth (B) in Hz, for a given communication system. The spectral efficiency of an SCM system (η_s) is given by [3] [31]

$$\eta_s = \frac{\log_2 M / T_s}{B} = \log_2 M \tag{2.11}$$

where B in this case is the reciprocal of symbol duration T_s (considering the bandwidth to equal the frequency distance from zero to the first null of an ideal Sinc

[2] For presentation simplicity, the index that indicates the OFDM block is not stated in subsequent discussion of this thesis.

[3] Channel coding and other redundant signals (e.g. cyclic prefix (CP) and zero padding) are not taken into consideration here as they affect all modulation signals in a similar manner.

spectrum) and M is the cardinality order.

The calculation of OFDM spectral efficiency is not straight forward. First, to calculate the bit rate, each subcarrier is of duration $T = N \times T_s$, as was shown earlier. Thus, each subcarrier transmits at a bit rate of $\log_2 M/NT_s$ b/s [31]. Consequently, the total bit rate for transmitting on all subcarriers simultaneously is

$$R_b = \frac{\log_2 M}{NT_s} \times N = \log_2 M/T_s. \tag{2.12}$$

Second, to calculate the bandwidth B [31]

$$B = f_{N-1} - f_0 + 2\delta, \tag{2.13}$$

where $f_{N-1} - f_0 = (N-1)\Delta f = N - 1/NT_s$, δ is the one sided bandwidth of subcarriers at the edges and it is half the bandwidth of the subcarrier's bandwidth (i.e. $1/2NT_s$). Consequently, divide (2.12) by (2.13) to calculate OFDM spectral efficiency [31]

$$\eta_m = \frac{\log_2 M/T_s}{\frac{N-1}{NT_s} + \frac{2}{2NT_s}} = \log_2 M. \tag{2.14}$$

Comparing (2.14) with (2.11), OFDM does not have any spectral efficiency gain over single carrier transmission. However, in comparison to conventional FDM methods which utilizes at least twice the bandwidth of OFDM and single carrier, OFDM doubles the spectral efficiency. Furthermore, in a flat fading channel scenario (i.e. AWGN), both OFDM and SCM systems have identical bit error rate (BER) performance [5]. The advantages of OFDM over SCM appear in the case of high data rate transmission over multipath channels. In the following section, the performance of OFDM over wireless channels is investigated.

2.2.3 OFDM over Wireless Channels

Given the harsh wireless communication environment and the scarcity of available spectrum, it is desirable to consider signalling formats which provide good performance and that are also bandwidth efficient.

The most common scenarios in wireless mobile systems is when the user

equipment (UE) moves in the multipath field or when other structures around move. Such movement produces rapid random amplitude and phase variations in the received signal known as frequency selective channel. The multipath propagation arises from multiple scattering and reflections by obstacles, such as buildings, obstacles and other structures [31]. In addition, the movement of the UE at a certain speed results in a spread in time arrivals of the different frequency components of the UE signal, resulting in a signal spectrum broadening. This phenomena is known as Doppler spread [34]. Frequency selectivity and Doppler spread results in ISI between OFDM symbols, as well as, inter-carrier interference (ICI) between the subcarriers within an OFDM symbol. [34].

The variations due to multipath propagation effects and Doppler shift are stated under the name micro (small) signal variations. Besides this, other impairments in a cellular mobile system degrades the overall performance. A large scale variation (i.e. higher signal power losses) results in cellular systems from attenuation related to distance and shadowing, which is caused by large obstacles blocking the transmission path [31].

An additional critical impairment in cellular systems is termed co-channel interference. In order to increase the system capacity, the available spectrum is used more efficiently by reusing the same radio channels (frequencies) at different locations within the overall cellular service area. Therefore, mobiles simultaneously assigned with same channels in different locations interfere with each other [34].

In this study, the effect of large scale variations and co-channel interference are not taken into consideration because they are independent of the signalling format used, unlike small signal variations, which is the key motivation behind OFDM [34].

To reduce the multipath propagation effects, the delay spread of the wireless channel has to be much smaller than the transmitted symbol period. The normalized delay spread factor D_s in (2.15) gives a good idea about the channel status, where τ_c is the delay of the channel, and T_{sym} is the transmitted symbol duration.

$$D_s = \frac{\tau_c}{T_{sym}} \tag{2.15}$$

Consequently, in order to reduce D_s for a given channel, a longer symbol has to be transmitted, thus the symbol rate will be reduced. However, the OFDM approach has the advantage of spreading out the total signalling interval, thereby reducing the sensitivity of the system to delay spread, without reducing the symbol rate. Furthermore, OFDM has the advantage of spreading out a fade over multi symbols. Thus, instead of a symbol being severely distorted, few symbols are only distorted, as shown in Fig. 2.3, where the multipath channel results in deep fading. The utilization of OFDM over SCM allows recovery of distorted symbols with the aid of error correction methods, such as channel coding [31].

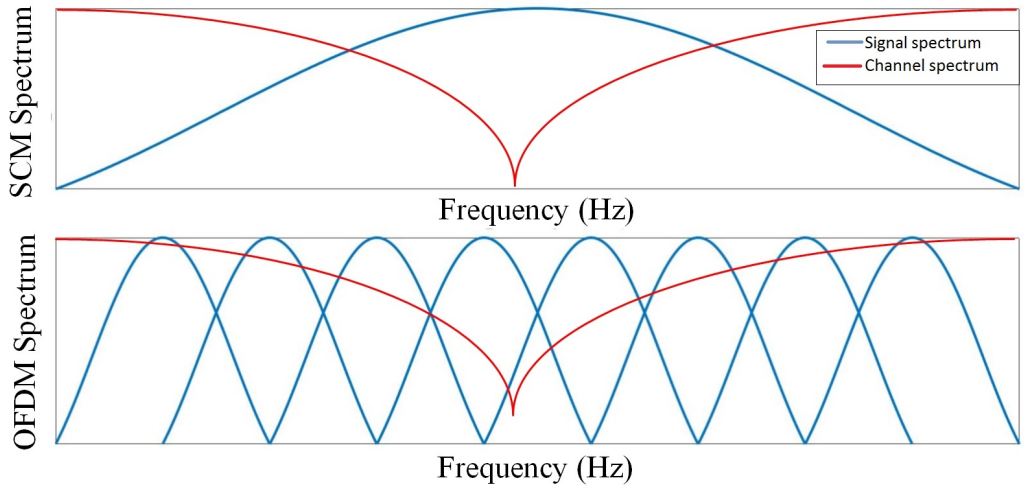

Figure 2.3: The effect of deep fading of a multi-path channel on SCM and OFDM signals.

It is important to emphasize that although D_s is N times smaller for OFDM than in SCM, still ISI effect is not totally eliminated [5]. Fig. 2.4, shows the effect of OFDM signal $x(t)$ transmission over a multipath channel, where in addition to the line of sight path (shortest time delay), the transmitted signal arrives from two other different paths. As a result, the received symbols are distorted by ISI (the red shaded area in the figure).

Zero padding (ZP) or CP is normally inserted between adjacent OFDM symbols to avoid ISI [5]. ZP pads the end of the OFDM symbol by zeros of duration $T_g \geq D_s$, while CP copies the end of OFDM symbol of length $T_{cp} \geq D_s$ as a prefix to the same symbol to maintain signal continuity, which is essential for channel one

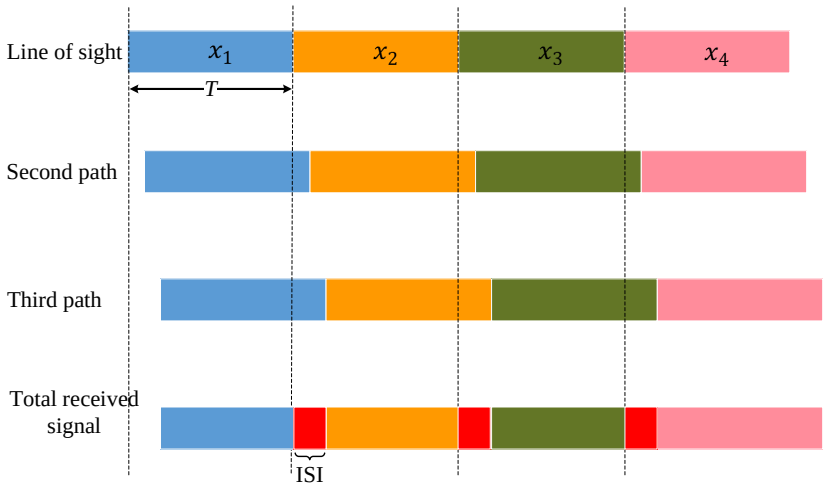

Figure 2.4: OFDM signal transmission over a multipath channel, without CP.

tap frequency equalisation used in practical OFDM systems [5] [34].

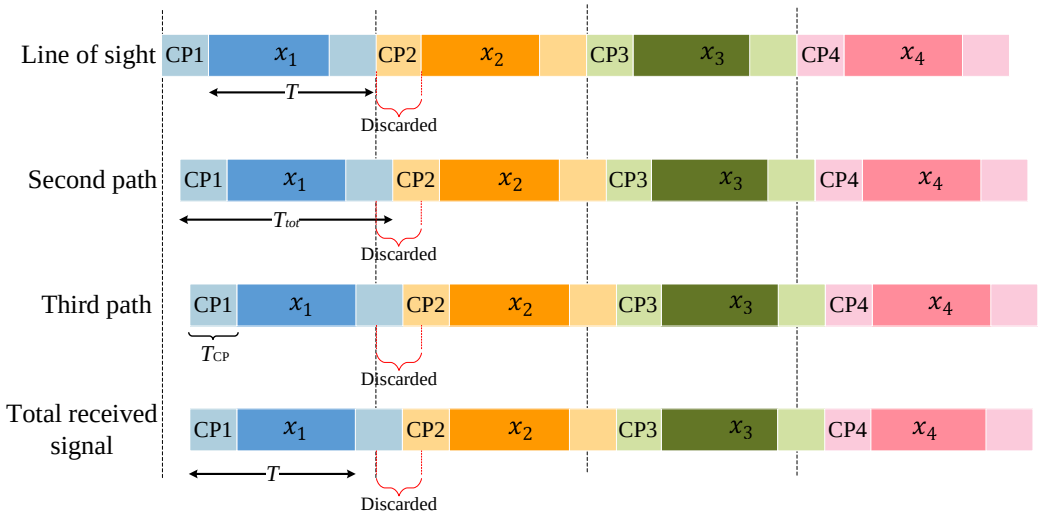

Figure 2.5: CP-OFDM signal transmission over a multipath channel.

In Fig. 2.5, each OFDM symbol duration is extended to $T_{tot} = T + T_{cp}$, where T_{cp} is the CP length. A sufficient CP has at least the same length of the channel delay spread D_s to eliminate totally ISI. The transmitted signal $x(t)$ of (2.1) becomes

$$x(t) = \frac{1}{\sqrt{T}} \sum_{n=0}^{N-1} z_n \exp\left(j2\pi n\Delta f t\right), \quad -T_{cp} \leq t \leq T. \tag{2.16}$$

At the receiver, the last samples of each OFDM symbol of length T_{cp} are discarded, because they form the part of the signal distorted by ISI.

CP and ZP reduce the effective data rate, as redundant data is transmitted between symbols. Thus, the utilisation of these is a trade-off between effective data rate and system reliability.

To conclude, the benefit of OFDM over SCM system results from its property of extending the symbol duration of the transmitted signals, which results in better performance over multipath channels. Furthermore, OFDM has key features that make it preferable over other waveforms, such as low complexity and its support to high order modulation. Yet, OFDM is not the optimal choice, because the time-frequency localisation is far from the optimal case and it suffers from high spectral sidelobes [2]. Therefore, OFDM requires a relatively large guard band (e.g. 10% in long term evolution (LTE)) and CP to meet the spectrum mask and adjacent channel leakage ratio (ALCR) requirement [35]. Next section discusses alternative candidates, which were nominated for future cellular 5G networks to improve spectral efficiency conditions of OFDM signals.

2.3 Alternative Waveforms for 5G

5G is referred to as (IMT-2020) in industry and international telecommunications union (ITU) working groups, with the goal of being commercially deployed in 2020 [4]. The vision of 5G network, summarised in Fig. 2.6 is: Enhanced mobile broadband (eMBB) to support up to three times higher than the current LTE data rate; ultra reliable low latency communications (URLLC); massive machine type communications (mMTC) with lower energy consumption [36]. In light of these requirements, the transition to 5G has to cope with the qualities of OFDM used for 4G, but at the same time try to overcome its existing drawbacks [4].

According to the Balian-Low theorem [37]: “ There is no waveform that satisfies the following three conditions simultaneously: 1. Mutual orthogonality in the complex domain; 2. best time-frequency localization; 3. symbol density 1”. Condition 1 means the signal is ICI and ISI free, while the second condition is

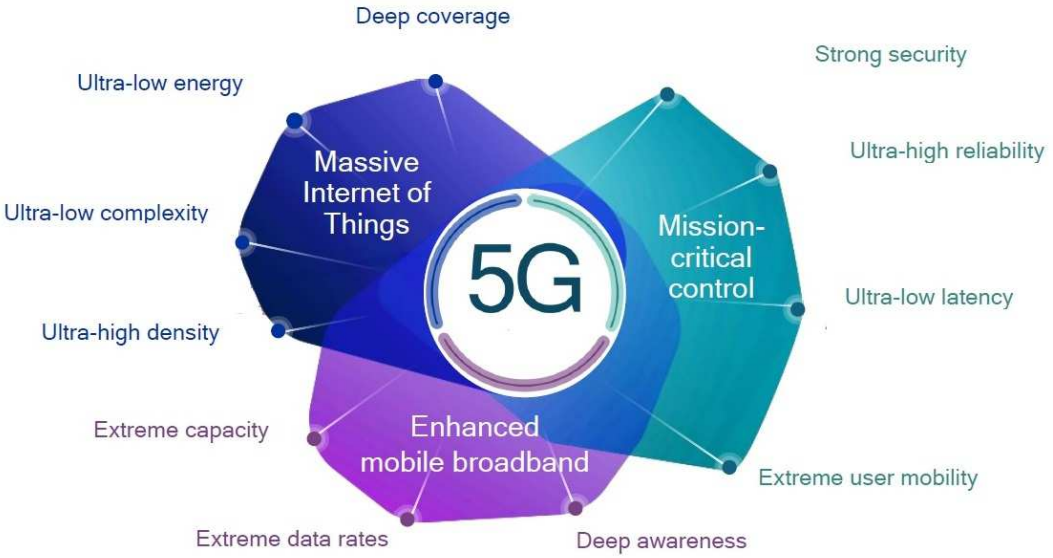

Figure 2.6: Target requirements for the envisioned 5G use cases [36].

related to the uncertainty principle equality of time-frequency dispersion product. The symbol density, in condition 3, is defined as $(1/T\Delta f)$, where T is the symbol transmission period and Δf is the subcarrier spacing. Depending on the application, the waveform is chosen as a trade-off between these three conditions [38].

Back to 2014, the authors of the key paper (What 5G will be?) [2] suggested that the best 5G format is the adjustable CP-OFDM numerology, where the FFT block size, subcarrier spacing and CP length are flexible and can change with the channel conditions. For instance, in scenarios with small delay spread (e.g. small cells and mm-wave channels) or URLLC services (1 ms round trip time constraint), the subcarrier spacing could grow, while the FFT size (number of subcarriers) and the CP could be significantly shortened for lower latency, shortened CP length and reduce computational complexity. In channels with longer delay spreads, that could revert to narrower subcarriers, longer FFT blocks, and longer CP [2]. 3rd generation partnership project (3GPP) standards adopted this waveform in releases 14 & 15 [39] [40].

One of the methods to reduce OFDM guard band length and improve OFDM time-frequency localisation condition is windowing the CP-OFDM symbol from both edges to smooth the transition between adjacent symbols, thus, reduce the

guard band length. This is referred to as windowed OFDM (W-OFDM) [41]. The simplicity of windowing operation at the transmitter and receiver (time domain multiplication and addition operations) is the main advantage of this waveform. However, its out-of-band emission (OOBE) suppression is limited and it reduces the length of the effective CP, hence, worsens the performance in multipath channels with a relatively long delay spread [41]. W-OFDM second condition is slightly better than CP-OFDM.

Trying to maintain the low complexity, universal filter multi-carrier (UFMC) is another attempt to reduce the OOBE by filtering fixed bandwidth sub-bands (e.g. filtering each LTE resource block 180 KHz) [41]. UFMC replaces the CP by a ZP to prevent ISI. The advantage of UFMC is in its simplicity, as the filter length cannot exceed the ZP length to prevent overlapping. Without CP, to account for the linear convolution of the signal with the channel impulse response, a double-sized FFT is typically used at the receiver, resulting in increased complexity and noise enhancement compared to CP-OFDM [2] [41].

In filtered OFDM (f-OFDM) [4], the sub-band filtering granularity is configurable to any value larger than a physical resource block (RB) bandwidth (180 KHz in LTE). This feature makes f-OFDM favourable in large bandwidth applications, unlike UFMC where its complexity increases rapidly by increasing bandwidth. Moreover, f-OFDM uses CP and the filter length is not limited by the CP length [42]. This results in better OOBE suppression at the cost of increased complexity by increasing the filter length [41]. Another issue with f-OFDM is that a one-tap equaliser may be used only if the CP length is longer than the filter order, which is not a spectrally efficient solution. Consequently, a more complex channel equaliser, like zero forcing (ZF) or minimum mean square error (MMSE), might be used as shown in [42]. UFMC and f-OFDM do not satisfy Balian conditions 1 and 3, while condition 2 is better than CP-OFDM.

The aforementioned waveforms can be generated with a small adjustment to the existing CP-OFDM transceiver architecture. This simplifies its potential co-

[4] In filtered OFDM, f is written in lowercase letter to distinguish it from fast OFDM (F-OFDM).

existence with the 4G/ 5G CP-OFDM transceivers. On the other hand, the following 5G waveform candidates require new transceivers and this is one of their key limitations, because this demand more efforts in standardization.

Filter-bank multi-carrier (FBMC) applies designed pulse shaping filters on subcarrier level. FBMC provides excellent frequency domain localisation by extending the pulse duration in the time domain to multiple times of a symbol duration, thus, the adjacent symbols overlap in time [41]. However, the edge-smoothed pulse shape of subcarriers make the waveform less sensitive to multi-path spreading, even without CP and guard band overhead [41]. The long filters at both transmitter and receiver increases the OOBE suppression level and the system complexity. FBMC satisfies Balian condition 3 and condition 2 is much better than CP-OFDM.

Offset-QAM (O-QAM) was firstly introduced to FBMC to reduce ICI. O-QAM is capable of maintaining the signal orthogonality in the real domain only. Communication channels are inherently complex, this implies that unless an ideal channel estimator and equalizer at the receiver is adopted, a good performance cannot be guaranteed [38]. Furthermore, O-QAM makes the pilot design, equalisation and MIMO application complicated and challenging. Another alternative to O-QAM in FBMC, is to use quadrature amplitude modulation (QAM) and apply different filters for different subcarriers (e.g. even and odd). In this case, MIMO application and pilot design can be as simple as CP-OFDM systems. QAM-FBMC can support high modulation orders (64-QAM), but with a large power penalty to maintain CP-OFDM error performance. Moreover, sophisticated receivers and time-domain least square (LS) with interpolation denoising after filtering is used for estimation, while equalisation is done in the oversampled domain (before the FFT) which increases the complexity of ZF and MMSE equalisers even more [38].

Generalised frequency division multiplexing (GFDM) also applies filtering on the subcarrier level, but in a block-wise and circular manner to avoid inter-burst tails. GFDM attains the optimal time-frequency localisation (condition 2) and can achieve lower OOBE compared to other waveforms [41]. In addition, block-wise CP is added to eliminate inter-block interference in multipath channels. GFDM is

generally non-orthogonal and the same pilot design and MIMO transmission issues of O-QAM FBMC, applies to GFDM [43]. GFDM receiver complexity is high, as a result of the large size FFT and the SIC at the detector. Consequently, this discards the option of using GFDM for low-latency and URLLC applications.

Finally, inspired by the table in [41] and [44], an extended table is provided in the following to summarise the key features of each waveform. Although, SEFDM will be discussed in the next chapter, its features are summarised in the table too, to ease the comparison later on.

The aforementioned waveforms above have a common goal; achieve higher spectral efficiency by improving CP-OFDM time-frequency localisation condition. Another approach to improve spectral efficiency is compressing the signal and violating its orthogonality in time and/or frequency domain. A summary of the leading waveforms in this area is given in the following section.

2.4 Non-Orthogonal Waveforms

In 1975, Mazo showed that, in a single carrier Sinc-pulse shape scenario with binary phase shift keying (BPSK) modulation and optimum detector, a 25% gain in spectral efficiency can be obtained at the same BER and energy per bit (E_b) [45]. This limit, according to [46] is called Mazo limit.

Mazo's work had little attention till the early 2000s when interest started developing in non-orthogonal MCM signals. fast OFDM (FOFDM) concept first appeared in 2002 [47], where the spectral efficiency of OFDM is doubled by occupying only half of the OFDM bandwidth, for a given symbol rate. This is achieved by halving the frequency separation between subcarriers (i.e. $\Delta f/2$) [47]. The k^{th} FOFDM modulated signal is presented as

$$x_k(t) = \frac{1}{\sqrt{T}} \sum_{n=0}^{N-1} z_{k,n} \exp\left(j2\pi n \frac{\Delta f}{2}(t - kT) \right), \quad 0 \leq t \leq T. \tag{2.17}$$

FOFDM maintains the signal orthogonality but only for its real part. Therefore, FOFDM uses only one-dimensional modulation, i.e. BPSK or M-array amplitude shift keying (M-ASK) [47]. For instance, FOFDM proved to be beneficial in im-

Table 2.1: A summary table to compare the main features of 5G waveform candidates.

	CP-OFDM [5]	CP-SEFDM [6]	W-OFDM [41]	UFMC [2]	f-OFDM [4]	OQAM-FBMC [38]	QAM-FBMC [38]	GFDM [44]
New transceiver	NA	No	No	No	No	Yes	Yes	Yes
Orthogonality	Yes	No	Yes	No	Yes	Yes (real field only)	No	No
Transmitter filter length	NA	NA	NA	Short	Long	Long	Long	Long
Filtering level	Na	NA	NA	Sub-band	Sub-band	Subcarrier	Subcarrier	Subcarrier
Support high modulation order	Yes	No	Yes	Yes	Yes	No	Moderate	No
CP /ZP	CP	CP	CP	ZP	CP	Null	Null	CP
Transmitter complexity	IFFT	IFFT	IFFT, multiplication & addition operations	IFFT & Short filters	Simple IFFT with long filters	Bank of modulators with long filters	Bank of modulators with long filters	IFFT with long filters
Receiver Complexity	FFT	FFT & SIC	receiver Windowing	Double-sized FFT	FFT & Filtering	Bank of modulators and Filtering	Bank of modulators and Filtering	FFT & SIC
OOBE suppression	Non	Non	Limited	Limited	High	High	High	High
The effect on CP	NA	NA	Reduce effective CP	NA	NA	NA	NA	NA
Pilot design	Simple	Simple with overhead	Simple	Simple	Simple	Complex	Simple	Complex
Equalisation	One-tap equaliser	One-tap equaliser	One-tap equaliser	Complex	One-tap equaliser	Complex	Complex	Complex
MIMO Application	Straight forward	Needs further investigation	Straight forward	Straight forward	Difficult	Difficult	Straight forward	Difficult
Tolerance to async. access	No	No	No	No	Yes	Yes	Yes	No
Support low latency app.	Yes	Yes	Yes	No	No	No	No	No

proving optical communication systems spectral efficiency, where one-dimensional modulation is commonly used [48]. On the other hand, in complex (two dimensional) FOFDM systems, ICI cannot be avoided.

SEFDM signals, first proposed in 2003, is a multi-carrier signal that achieves spectral efficiency gains by packing the subcarriers closer (relative to OFDM), while compromising the orthogonality. SEFDM symbols are generated in a similar manner of OFDM using modified IFFT structures [49], yet they require more complex receiver structures [50]. Despite the non-orthogonality, different detection methods have been demonstrated where the error performance of SEFDM is reasonably close to OFDM, with spectral efficiency improvement greater than 25% [8]. The focus of this PhD thesis is SEFDM signals, thus, SEFDM features, mathematical characteristics, obstacles and a summary on the ongoing research are given separately in the next chapter.

Other non-orthogonal waveforms similar to SEFDM were proposed and studied. The IEEE proceeding paper [46] summarises the leading systems in this area. Faster than Nyquist is SEFDM's time domain counterpart, where the data transmission rate is higher than Nyquist rate [51]. FTN results in ISI because pulses are no longer uncorrelated [10]. The SCM FTN signal is [46]

$$x(t) = \sum_{k} z_k g(t - k\alpha_t T), \tag{2.18}$$

where $g(t)$ is a Sinc pulse and $0 < \alpha_t \leq 1$ is the time acceleration factor. A trellis-structured based on Viterbi algorithm (VA) decoder is suggested to decipher the received FTN signal to overcome ISI [46]. FTN detector complexity increases even more for coded FTN, as it has at least two decoders, one for decoding and the other one for detection. Turbo equaliser improves FTN system performance, where soft information is exchanged between the two decoders for a given number number of iterations [46].

An extension to FTN called frequency-FTN [5] was introduced first in [52],

[5] frequency-FTN is similat to SEFDM concept but appeared two years after SEFDM was firstly introduced.

which has the same subcarriers compression concept of SEFDM to save bandwidth, while multistream-FTN (MFTN) compresses the signal in both time and frequency domains [46].

TFP is another non-orthogonal waveform, which optimises the spacing between adjacent signals to maximise the achievable spectral efficiency. TFP uses root-raised cosine (RRC) pulse shaping, where time packing uses the roll-off factor of the RRC shaping filter and frequency packing is achieved by reducing the frequency spacing between subcarriers [11].

To summarise, non orthogonal modulation systems is based on packing the signal in time and/or frequency. Mazo developed this concept first for single carrier system, then other waveforms, such as FOFDM, SEFDM, FTN, MFTN and TFP were developed.

2.5 Conclusions

The main goal of this chapter was to set the scene for the work in this thesis. At the start, OFDM advantages of being able to support high data rates and being immune to fading, compared to SCM systems, were demonstrated. Brief descriptions of OFDM transmission and reception were provided, in addition to OFDM spectral efficiency calculations. Then, a summary was provided of other 5G waveforms candidates, which aim to enhance OFDM spectral efficiency by improving its time and frequency localisation. Finally, the concept of using non orthogonal overlapped signal to achieve higher spectral efficiency was introduced and similar proposals to SEFDM signals were outlined. The next chapter provides a detailed review of SEFDM system mathematical model and addresses the main challenges this thesis aims to solve.

Chapter 3

SEFDM Signals & Systems

The aim of this chapter is to establish the foundations of SEFDM signals, which are the focus of this thesis. The feasibility of SEFDM is hindered by many design and implementation obstacles due to orthogonality violation. Previous work focused on SEFDM signal generation and detection, however, other issues have not been fully tackled. For instance, SEFDM signals mathematical models were limited to deterministic models in previous work. Therefore, a new statistical model of ICI in SEFDM is derived in this chapter, to complement the well-known SEFDM deterministic model and to facilitate system design under different channel conditions. Thereafter, to set the main theme of this work and identify the gaps where contributions can be made, an extensive survey of the active research work on SEFDM is provided.

The outline of this chapter is: Section 3.1 explains SEFDM signals generation and detection and its main impairment (ICI). In section 3.2, a thorough study of the statistical distribution of ICI in SEFDM is presented. Thereafter, the statistical model is used to calculate the error lower bound and capacity for SEFDM signals in sections 3.3 and 3.4, respectively. Finally, section 3.5 presents a comprehensive survey on the development history of SEFDM since 2003, covering wireless and optical communications theory, circuit design and experimental testbed design. The survey covers SEFDM main challenges and the developed ongoing work to solve them, including the work reported in this thesis.

3.1 SEFDM Waveform

Spectrally efficient frequency division multiplexing is defined as a parallel multiplexed data system, which offers possibilities of improving spectral efficiency of communication systems, by intentionally violating OFDM subcarriers orthogonality [6]. SEFDM achieves spectral gains by reducing the subcarriers spacing beyond orthogonality. This reduction in bandwidth comes at the cost of interference and increased complexity at the transmitting and receiving ends.

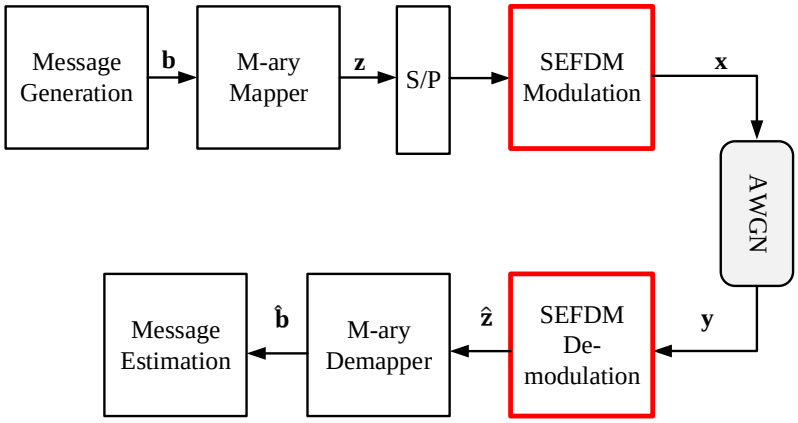

Figure 3.1: General descriptive SEFDM baseband transceiver block diagram.

A general descriptive block diagram of an SEFDM baseband system model is given in Fig. 3.1. This model is similar to that of OFDM in Fig. 2.1 and the differences are in the highlighted modulator and demodulator blocks. At the transmitter, the message bits $\mathbf{b} \in \{0,1\}$ are generated. Each $\log_2 M$ bits are mapped into a complex symbol $z \in \mathbb{C}$. Then, the mapped symbols are divided into K streams each of size equal to the desired SEFDM symbol size N. The k^{th} stream is converted from a serial to a parallel stream using a S/P converter. Afterwards, each element of this stream modulates one of the N^{th} subcarriers of the SEFDM symbol.

If T_s is the symbol interval in a SCM system, the symbol interval in an SEFDM system of N subcarriers is $T = N \times T_s$, which is similar to OFDM modulation. However, in SEFDM, the subcarriers spacing Δf is reduced by multiplying the frequency spacing by a compression factor ($0 < \alpha \leq 1$), where $\alpha = 1$ for OFDM.

The complex envelope of the k^{th} baseband SEFDM modulated signal becomes

$$x_k(t) = \frac{1}{\sqrt{T}} \sum_{n=0}^{N-1} z_{k,n} \exp\left(j2\pi n\alpha\Delta f g(t-kT)\right), \quad 0 \leq t \leq T \tag{3.1}$$

where $g(t)$ is time domain rectangular pulse given in (2.2). A normalized SEFDM spectrum of $x_k(t)$, for $N = 1024$ subcarriers and different compression levels is shown in Fig. 3.2. Clearly, SEFDM in Fig. 3.2 (b-d), saves $(1-\alpha) \times 100\%$ of bandwidth, relative to OFDM Fig. 3.2 (a) for the same transmission rate. The OOBE level of SEFDM signals is slightly higher than OFDM. To avoid ISI, a guard period or filtering and windowing may be used.

SEFDM can be beneficial in another scenario, where the system throughput is increased while maintaining OFDM bandwidth. The number of SEFDM subcarriers increases to $\lfloor N/\alpha \rfloor$, where $\lfloor . \rfloor$ denotes the floor operation. Resultantly, the system throughput is boosted up by a factor of $(1-\alpha)/\alpha \times 100\%$.

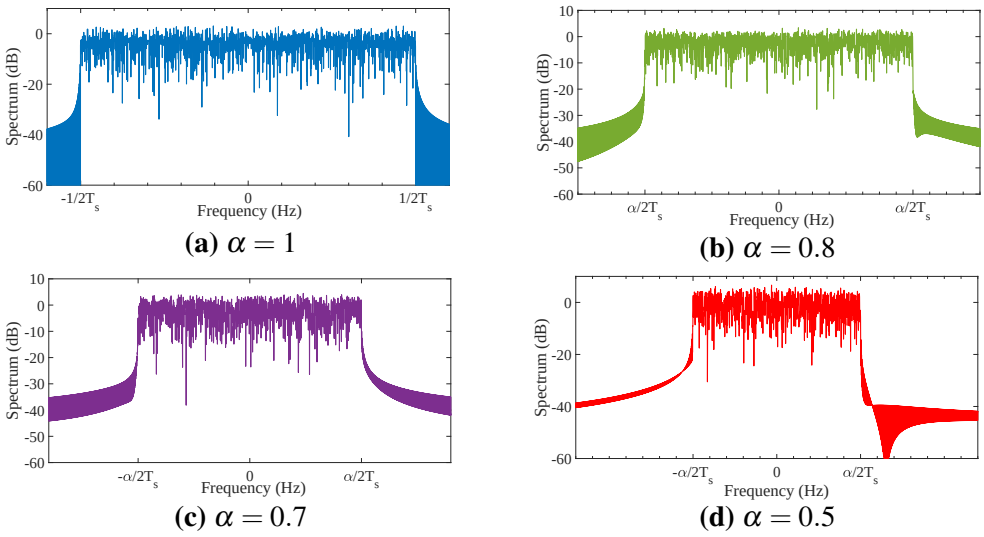

(a) $\alpha = 1$ **(b)** $\alpha = 0.8$

(c) $\alpha = 0.7$ **(d)** $\alpha = 0.5$

Figure 3.2: The frequency spectrum of $x_k(t)$, for $N = 1024$ subcarriers with different compression factor values.

ICI in SEFDM is visualised in Fig. 3.3 for $\alpha = 0.8$ and for two cases; $N = 8$ and $N = 10$. If the spectrum is compared to the OFDM spectrum in Fig. 2.2 (b), the SEFDM signal either occupies 20% less bandwidth for the same number of subcarriers of OFDM, or occupies two extra subcarriers within the same OFDM bandwidth, as shown in Fig. 3.3 (a) and (b), respectively. Looking at the peak

value of any of the subcarriers, unlike OFDM, the rest of the subcarriers are non-zero. The power level of other subcarriers, at the peak value of a specific subcarrier presents ICI, with the dominant interference on a given subcarrier resulting from the main lobes of adjacent subcarriers. Hence, ICI suppression by pulse shaping will be limited.

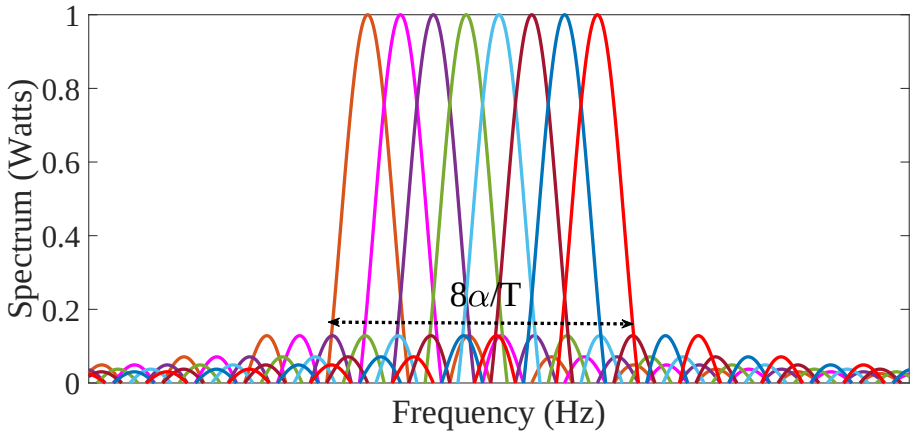

(a) Bandwidth saving scenario $N = 8$.

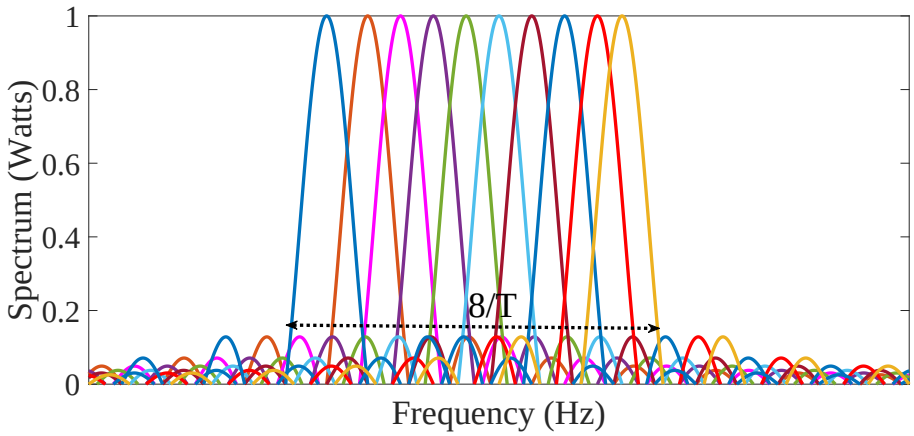

(b) Throughput improvement scenario $N = 10$.

Figure 3.3: A zoom-in caption of SEFDM Spectrum for $\alpha = 0.8$.

The resultant signal $x_k(t)$ is sent over an AWGN channel, then the received signal $y_k(t)$ is the input to the SEFDM demodulator, which is used to estimate the transmitted symbols. Finally, a demapper retrieves the received bits $\hat{\mathbf{b}}$. The demodulated SEFDM signal, which is the output of the coherent detector with a matched

filter, is given by

$$\hat{z}_{k,n} = \frac{1}{\sqrt{T}} \int_T y_k(t) \exp\left(-j2\pi n\alpha\Delta f g(t-kT)\right)dt, \quad 0 \leq n \leq N \tag{3.2}$$

where $\hat{z}_{k,n}$ is the estimated symbol on the n^{th} subcarrier of the k^{th} SEFDM symbol. However, a symbol-by-symbol decision is no longer optimal for SEFDM, due to ICI. Thus, SEFDM detection becomes more complex as will be shown later.

To generate discrete SEFDM symbols, the same method mentioned before for the case of OFDM in (2.5) is applied to get

$$x_{k,q} = \frac{1}{\sqrt{Q}} \sum_{n=0}^{N-1} z_{k,n} \exp\left(j2\pi\alpha\frac{qn}{Q}\right), \quad q = 0,1,...,Q-1, \tag{3.3}$$

while SEFDM discrete demodulated signal, after the matched filter is

$$\hat{z}_{k,n} = \frac{1}{\sqrt{Q}} \sum_{q=0}^{Q-1} y_{k,q} \exp\left(-j2\pi\alpha\frac{qn}{Q}\right), \quad n = 0,1,...,N-1. \tag{3.4}$$

The linear model of SEFDM signals is the same as OFDM. However, at the output of the demodulator, the demodulated symbol will be distorted by ICI, such as

$$\hat{\mathbf{z}} = \Phi^{\mathrm{H}}\Phi\mathbf{z} + \Phi^{\mathrm{H}}\mathbf{w} \tag{3.5}$$

$$= \Lambda\mathbf{z} + \Phi^{\mathrm{H}}\mathbf{w}. \tag{3.6}$$

The term $\Phi^{\mathrm{H}}\Phi$ does not yield to an identity matrix as the case of OFDM, due to the presence of interference terms. The term $\Lambda = \Phi^{\mathrm{H}}\Phi$ is referred to as the correlation matrix, where Λ has a diagonal of ones, representing auto-correlation and non-diagonal elements ($\Lambda_{m,n}$) representing the interference from subcarrier n on subcarrier m and its value is given by [53]

$$\Lambda(m,n) = \exp(j\pi\alpha(m-n)) \times \exp(\frac{-j\pi\alpha(m-n)}{Q}) \left[\frac{\mathrm{sinc}(\alpha(m-n))}{\mathrm{sinc}\left(\frac{\alpha(m-n)}{Q}\right)}\right]. \tag{3.7}$$

From the above formula, it can be perceived that ICI depends on SEFDM symbol

size (i.e. the number of subcarriers N), the oversampling factor ρ where $Q = \rho N$ and α. The correlation power level increases by reducing α and becomes zero when $\alpha(m-n) \in \mathbb{Z}$, which indicates that subcarriers m and n are orthogonal. For a detailed mathematical treatment of ICI in SEFDM, readers are referred to [53].

Since the innovation of SEFDM signals, the mathematical model has been studied thoroughly as a deterministic problem, because the ICI in SEFDM is intentionally introduced. In a perfect noiseless channel, the deterministic model (i.e. the correlation matrix) is enough, however, in a realistic scenario, to have a full understanding of the system, a statistical model becomes important. In the next section the statistical model of SEFDM signals is derived.

3.2 The Statistical Characteristics of ICI in SEFDM

The statistical model of OFDM signals suffering from ICI has been studied widely. ICI in SEFDM is similar, but more severe than ICI resulting from OFDM signal propagation through a frequency selective channel. The procedure followed in [54] to derive the statistical model of ICI in OFDM is followed in this chapter to derive SEFDM signals ICI statistical model. The realization of the statistical nature of SEFDM signals helps in answering the following fundamental questions:

- In which scenarios do SEFDM signals outperform OFDM signals?
- Which signal to noise ratio (SNR) regions do SEFDM signals outperform OFDM signals?
- What are the limitations of SEFDM signals?
- Is there an error floor SEFDM signals?
- How can maximise SEFDM signals spectral efficiency benefits be maximised?

As the main focus of this work is ICI in SEFDM signals, two assumptions are made: i) Zero ISI between adjacent SEFDM symbols by using long guard band or cyclic prefix; ii) the channel is noiseless (i.e. $\mathbf{w} = 0$ in (3.6)). It is noteworthy that

the ICI term (Λ) on its own, given in (3.7), is deterministic for a given set of system parameters (α, N). In (3.6), Λ is multiplied by the transmitted symbol z, which belongs to a random variable set Z, thus, the resultant $\hat{z}$ will belong to a random variable set too. According to the central limit theorem, if the number of interfering signals is high (i.e. relatively high N), then, the interference can be approximated to a Gaussian process. Consequently, ICI can be modelled by a Gaussian process characterised by its first and second moments, which are the mean and variance, respectively.

In the following, the symbol z_n modulating the n^{th} subcarrier belongs to a quadrature phase shift keying (QPSK) random variable set $Z = \{1+j, 1-j, -1+j, -1-j\}$ of mean $\mu_z = 0$ [1]. Multiplying the random variable Z by a constant value Λ in (3.6), results in multiplying the mean of Z by that constant. Hence, the ICI mean will be $\mu_I = 0$.

The ICI variance $\sigma^2_{I,n}$ is non-zero because of the interference on the n^{th} subcarrier from all other subcarriers, such as [54]

$$\sigma^2_{I,n} = \sum_{m=0, m\neq n}^{N-1} \sigma^2_{m,z} \times |\Lambda_{m,n}|^2, \tag{3.8}$$

where $\sigma^2_{m,z}$ is the variance of the data symbol z. Consequently, the total ICI variance within one SEFDM symbol is equal to

$$\sigma^2_I = \sum_{n=0}^{N-1} \sigma^2_{I,n}. \tag{3.9}$$

For normalization purposes, if the total variance is divided by the transmitted signal power ($N \times \sigma^2_z$), then the scalar quantity $\tilde{\sigma}_I$ represents the normalized variance function. Therefore, if the signal is transmitted with power P, then, the total interference in this case will be ($P \times \tilde{\sigma}_I$) Watt.

The accuracy of the proposed ICI statistical model can be examined by simulating the SEFDM system of Fig. 3.1 and then plotting the probability density func-

[1] The mean and variance of a complex number is calculated separately for the real and imaginary parts

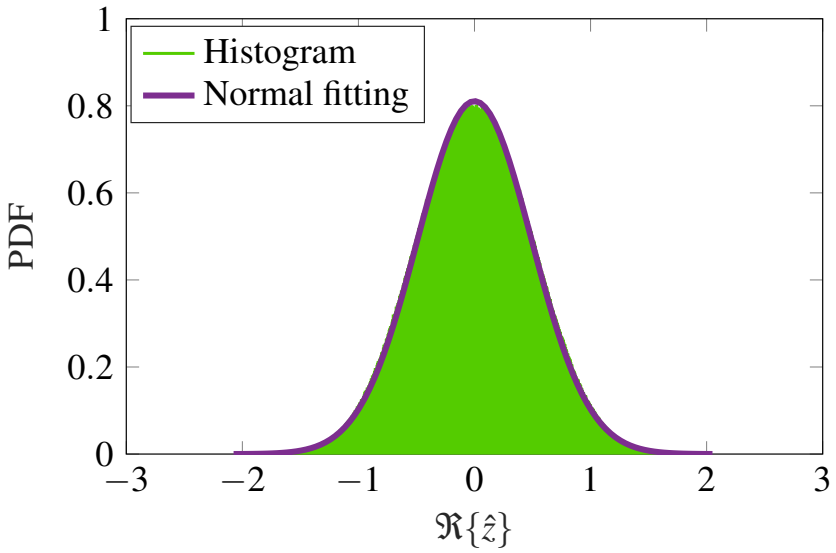

Figure 3.4: PDF of ICI, $\alpha = 0.8$, $N = 128$, zero noise.

tion (PDF) of the received symbols $\hat{\mathbf{z}}$ in (3.6) without noise (i.e. $\mathbf{w} = 0$). Fig. 3.4 shows the histogram of $\Re\{\hat{\mathbf{z}}\}$ for the case of QPSK symbols transmission, where $N = 128$ and $\alpha = 0.8$. Expectedly, this has a normal distribution using distribution fitting tool from MATLAB, where the mean and variance are 0 and 0.2422, respectively. Furthermore, the effects of α and N on the variance σ_I^2 are tested individually, by fixing one of them at a time as shown in Fig. 3.5 (a) and (b). The simulated and theoretical results using the derived equations (3.8) and (3.9) match. Clearly, N does not have a major influence on the value of σ_I^2 (i.e. 10% in the worst case), unlike the effect of α (above 90%), because ICI mainly comes from the neighbouring subcarriers on both sides of a given subcarrier.

To sum up the results of σ_I^2, Fig. 3.6 shows the variance for $\alpha \in [0.5, 1)$ and $N \in \{16, 32, 64, 128, 256, 512, 1024\}$. Fig. 3.6 will be used in the next sections to calculate SEFDM signals error bounds and spectral efficiency upper bounds.

3.3 Probability of Error Bounds

The PDF of the combined AWGN and ICI impairments will also be Gaussian. The mean and variance of this Gaussian PDF is the summation of AWGN and ICI means and variances [54]. For instance, referring to Fig. 3.4 and given the white noise mean is zero, while the variance is set to be constant ($\sigma_n^2 = 0.2$), the total variance of

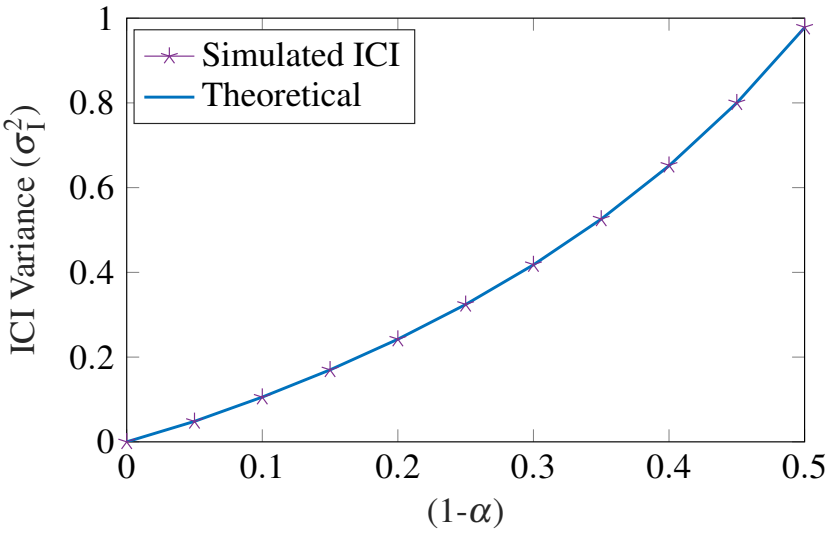

(a) $\sigma_I^2, N = 128$.

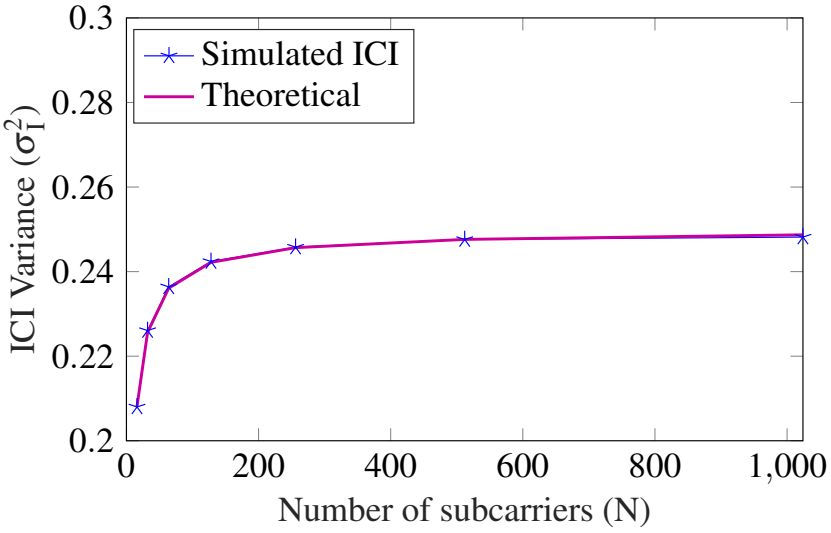

(b) $\sigma_I^2, \alpha = 0.8$.

Figure 3.5: ICI statistical model examination.

Fig. 3.7 is $\sigma_t^2 = 0.4423$ and this is approximately the summation of $\sigma_n^2 = 0.2, \sigma_I^2 = 0.2422$.

When a matched filter is used at the receiver to estimate the transmitted symbols as shown before in Fig. 3.1, the theoretical probability of error (P_e) value for QPSK-OFDM is given by [34]

$$P_e = Q\left(\sqrt{\frac{2E_b}{N_0}}\right), \tag{3.10}$$

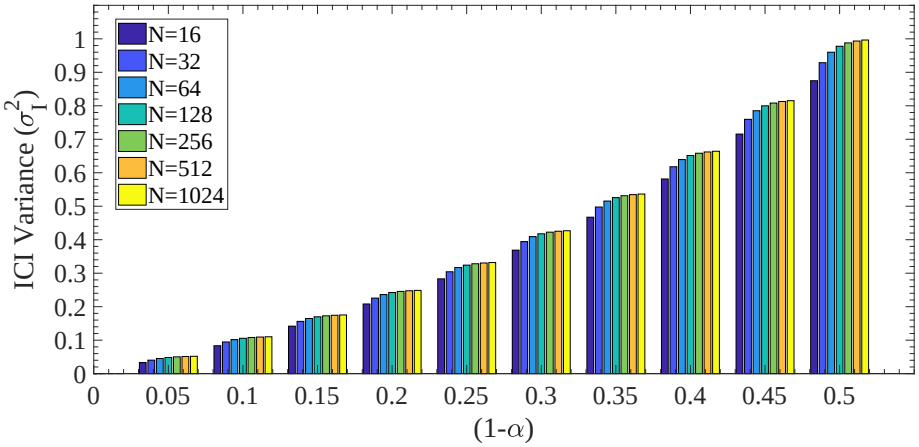

Figure 3.6: The ICI variance for different α and N.

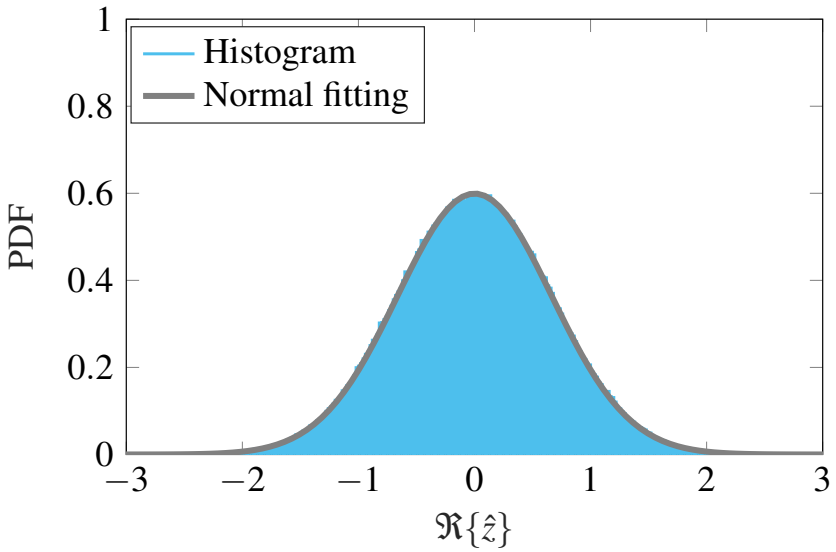

Figure 3.7: PDF of the received signal with $\alpha = 0.8$, $N = 128$ and $\sigma_n^2 = 0.2$.

where E_b/N_0 is the ratio of energy per bit over the noise spectral density and $Q(.)$ is the tail distribution function [34].

However, for $\alpha < 1$, the probability of error is higher, because the total variance of the received signal increases due to ICI as shown before. Therefore, the P_e for this specific case becomes

$$P_e = Q\left(\sqrt{\frac{2E_b}{N_0 + 2E_b \times \tilde{\sigma_I^2}}}\right). \tag{3.11}$$

Clearly (3.11) turns into (3.10) when $\alpha = 1$ as $\tilde{\sigma}_I^2 = 0$. To prove the validity of

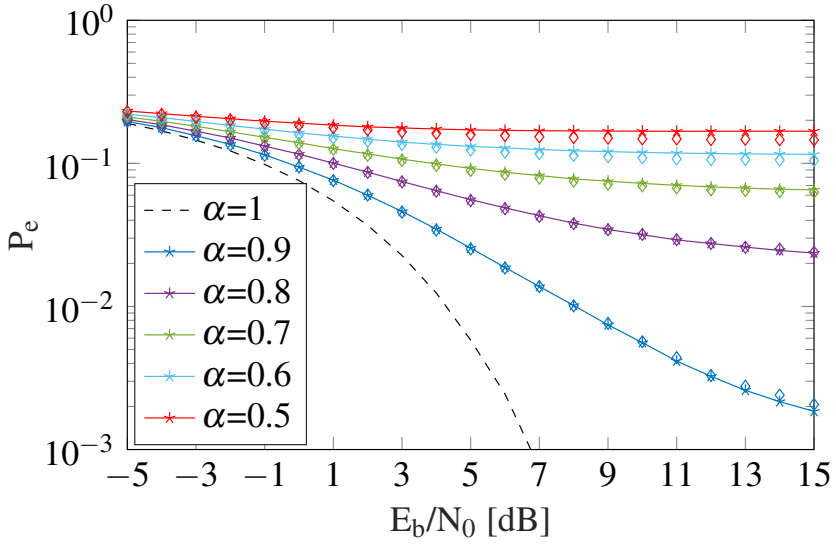

Figure 3.8: P_e vs. E_b/N_0 for QPSK-SEFDM signals, $N = 128$.

(3.11), P_e is simulated for the system in Fig. 3.1, when $N = 128$, and compared to the theoretical results for QPSK symbols transmission in Fig. 3.8. The following can be observed from the results:

1. The theoretical prediction (diamonds marks) matches the simulation results (stars marks).

2. An error floor appears in SEFDM, because as evident in (3.11), the interference level increases by increasing the signal power. Thus, unlike white noise, the ICI variance is signal dependent.

3. The error floor level increases by increasing the compression level of SEFDM signals. To mitigate the ICI effect, a more sophisticated and complex receiver is required; such as a sphere decoder [16] or an iterative interference canceller for the case of coded systems [20]. The ideal scenario is to remove the interference completely in (3.11), then, the error rate of SEFDM becomes equal to that of OFDM.

Next section will calculate capacity and spectral efficiency upper bound for SEFDM with and without ICI cancellation.

3.4 SEFDM Capacity & Spectral Efficiency Upper bound

This work is not the first attempt to calculate SEFDM system capacity. For instance, the recent Nature Scientific Report paper [48] derives the capacity of SEFDM signals (termed as non-orthogonal OFDM (NOFDM) in the report) and shows that non-orthogonal signals potentially achieve higher capacity, when compared to orthogonal signals. The main contribution of this work is in its SEFDM capacity formula derivation given by

$$C \leq \frac{1}{\alpha} \times B \log_2 \left[1 + \frac{P_s}{P_N + P_{ICI}} \right], \tag{3.12}$$

where C is the system capacity in bit/s, B is the channel bandwidth, P_S, P_N, P_{ICI} are the signals, white noise and ICI power levels, respectively. From the equation, clearly, SEFDM signal capacity depends on P_{ICI}, while P_{ICI} depends on both the signal power level and the ICI second moment (variance) derived in the previous section.

Earlier, another attempt to calculate SEFDM capacity from information theoretic perspective was reported in [55]. The work quantifies the capacity benefits of SEFDM signals transmission with different pulse shaping, when compared to an equivalent OFDM transmission. The expression for the capacity of SEFDM signals is found by normalizing the mutual information between the transmitted and received SEFDM symbol over the SEFDM symbol duration [55]. However, the results are inconsistent for two reasons:

1. Results indicate that at high SNR, SEFDM capacity is higher than that of OFDM, even with no ICI cancellation. This mistake is due to the mutual information calculation, where the interference level variable is independent of the signal level. Logically, by increasing the power level of the subcarriers, the interference coming from them to other subcarriers will increase too.

2. The compression level considered in the work is non-realistic, as the authors

are not considering the practicality of the systems used, i.e. α takes a value between 0.1 and 0.5. For these compression levels, even with the most complex detector, the transmitted signals cannot be recovered, especially, when the transmitted symbols belong to a two dimensional modulation format (e.g. M-PSK, M-QAM) .

Usually, the capacity of a communication system has to be calculated at the front end of its detector, which in this case is at the input of the demapper. For instance, consider an OFDM signal transmitting information at a rate equal to the Nyquist rate (i.e. $R_s = 2B$ sample/sec), where R_s is the sample rate. The channel capacity (C), based on Shannon's original definition [56], in bits per use is

$$C = \frac{1}{2}\log_2\left[1 + \frac{P}{(N_0/2)\times B}\right] \text{bits per use}, \tag{3.13}$$

where P is the transmitted power level. For a fair comparison and to ensure that the total transmitted power of both OFDM and SEFDM systems are equal, if SEFDM higher throughput scenario in Section 3.1 is applied, the power level per SEFDM subcarrier is reduced by a factor of $N/\lfloor N/\alpha \rfloor$ [55].

The multiplication of (3.13) by the number of times the channel is used per unit time gives the capacity in b/s [56]. This factor is equal to the ratio of number of samples transmitted within time T to this time duration T. Owing to the increase in the number of subcarriers in SEFDM, the number of samples transmitted in T seconds is equal to $(R_s \times T/\alpha)$ samples, thus, the system capacity becomes

$$C = \frac{B}{\alpha}\log_2\left[1 + \frac{P}{(N_0/2)\times B + P\times \tilde{\sigma_I^2}}\right], \tag{3.14}$$

where the interference of SEFDM appears here as $P \times \tilde{\sigma_I^2}$. A meaningful performance measure for comparison between different systems is represented by the spectral efficiency (η) b/s/Hz, which is found by dividing the capacity of (3.14)

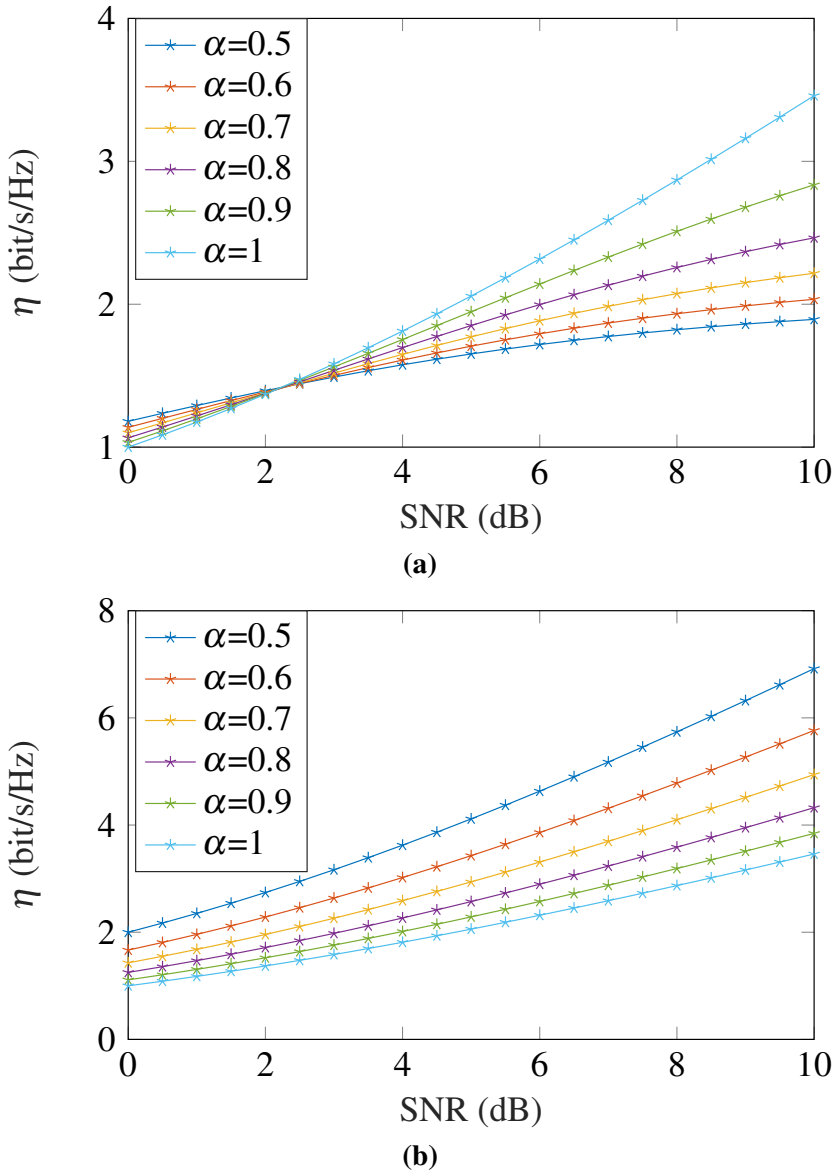

Figure 3.9: η vs. SNR for SEFDM signals, $N = 128$, (a) without ICI cancellation; (b) with ICI cancellation.

by the channel bandwidth, such as

$$\eta = \frac{1}{\alpha}\log_2\left[1+\frac{P}{(N_0/2)\times B + P\times\tilde{\sigma}_I^2}\right]. \tag{3.15}$$

In Fig. 3.9(a), η is plotted versus signal to noise ratio (SNR $= P/((N_0/2)B)$ without ICI cancellation. The results can be divided into two regions: *i*) low SNR region, where the noise is dominant and SEFDM spectral efficiency is higher than that of

OFDM; *ii*) high SNR region, where the ICI is dominant and it limits the spectral efficiency of SEFDM, with no advantage of transmitting with higher SNR.

This information is important when considering the utility of SEFDM. For instance, powerful channel codes; such as turbo and LDPC codes, allow reliable information transmission with low SNR. Thus, SEFDM in such a case is more efficient, when compared to OFDM. Conversely, by considering the ideal case of 100% ICI elimination in (3.15), the maximum η becomes as shown in Fig. 3.9(b). Clearly, the capacity advantage of SEFDM is higher with ICI cancellation, especially in high SNR regions. Different ICI cancellation methods have been suggested, as will be shown in the next section and upcoming chapters.

To finish this overview of SEFDM signals, after the mathematical modelling, the next section presents a comprehensive survey of the development history of SEFDM since 2003, covering wireless and optical communications theory, circuit design and experimental testbed design. The main challenges of SEFDM and the developed ongoing work to solve them are addressed, including the work reported in this thesis.

3.5 SEFDM Survey

The feasibility of SEFDM was hindered by few issues. Firstly, signal detection was very complex, because it was based on maximum likelihood (ML) with exponential algorithmic complexity $O(M^N)$ over the constellation cardinality M and number of subcarriers N. The second issue is in signal generation and detection, which requires an adjustment to the existing OFDM transmitter and receiver design to allow adaptive subcarriers compression based on the value of α. Third issue is the high peak to average power ratio (PAPR) compared to single carrier systems and the last issue is channel estimation. Since SEFDM concept was invented, different methods have been developed to overcome these issues to benefit from SEFDM advantages. In the following, each issue is addressed with the work have been done so far.

3.5.1 SEFDM Signal Generation and Transmission

Two approaches to generate SEFDM signals, based on IDFT, were proposed in [57]. These approaches aim to facilitate an easy SEFDM migration and/or coexistence with OFDM at the transmitters. For the ease of explaining, refer to Fig. 3.10, which shows the real part of the four components ($N = 4$) of the transmitted signal $x(t)$ in the time domain over one symbol duration T, for OFDM and SEFDM ($\alpha = 0.8$). From the figure, when comparing the two signals, in SEFDM, the symbol duration T is maintained the same as OFDM, but because the frequency separation is reduced, T is not long enough to complete an integer number of cycles and extra samples are required to cover the $T(1/\alpha - 1)$ duration. In the first approach, if the sampling rate is to be maintained as OFDM, an IDFT of size (Q/α) is taken which will result in orthogonal N subcarriers but with frequency spacing α/T. To make the output signal non-orthogonal, $((1-\alpha)/\alpha) \times Q$ samples from the output of the IDFT are punctured at any position. However, if it is desired to maintain the IDFT size of OFDM, the $((1-\alpha)/\alpha) \times Q$ are punctured from the output of the IDFT, which results in fewer samples compared to OFDM, thus, lower sampling rate, under the condition of Q being greater than N to satisfy Nyquist criterion.

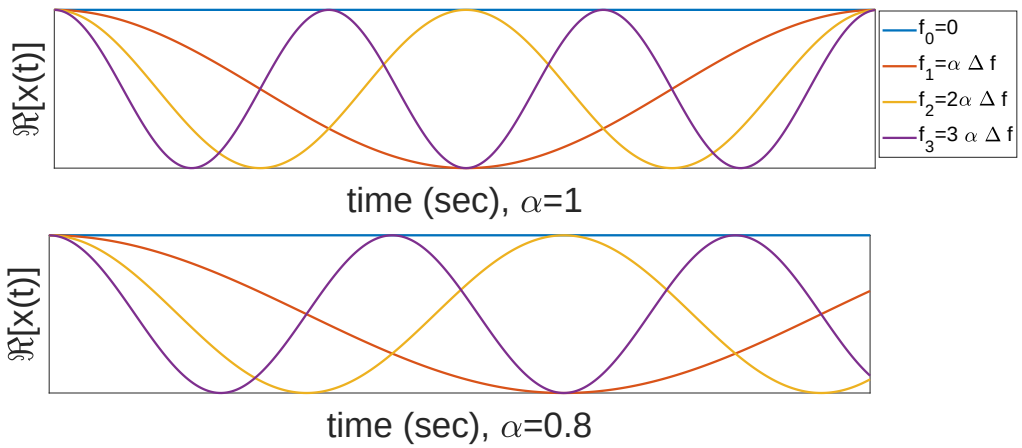

Figure 3.10: The real part of transmitted signal $x(t)$ components in the time domain, for $N = 4$, $\alpha = 1$ and $\alpha = 0.8$, respectively.

The idea behind the second approach in [57] is based on the correlation (or ICI) equation given in (3.7). For any two arbitrarily chosen subcarriers (m and n), when the product $\alpha(m-n)$ is an integer, this indicates that the m^{th} and n^{th} subcarriers

are orthogonal. This method looks at SEFDM signal as a combination of multiple smaller OFDM systems overlapping in frequency to reduce the spacing between subcarriers. Thus, signal generation is done using multiple shorter IDFTs are used in parallel instead of one IDFT.

Results in [49] and [57] show that the aforementioned methods decrease the computational complexity drastically compared to conventional bank of modulators generation scheme. It was found that the first scheme computational complexity is lower than that of the second scheme [49]. However, the second scheme is better suited to hardware implementation using IFFT blocks, if the sampling rate is to be maintained, because in the first scheme IDFT size (Q/α) often results in non integer and/or non power of two values needed for the IFFT, therefore, it is limited for certain values that makes $(Q/\alpha) \in 2^n, n \in \mathbb{Z}$ [49].

After SEFDM signal generation, the next stage at the transmitter is adding CP to reduce ISI effects resulting from multi-path channel effects. Conventionally, CP addition in SEFDM was implemented in the same way as OFDM. However, the resultant signal suffers from non-continuity, leading to higher OOBE level, thus, higher ISI between SEFDM symbols. In Chapter 6, the generation of 5G resource blocks, based on SEFDM signals, with continuous CP using a single IFFT is discussed and proven.

To prove the practicability of SEFDM systems, a hardware platform that facilitates the implementation of signals generation in real-time system was designed in field programmable gate arrays (FPGA). In [58], [59] the generation of SEFDM signals was implemented based on the multiple IDFTs method [57]. Then, the SEFDM transmitters have been synthesised, placed and routed in CMOS process technology in [49]. The results of this study confirm the feasibility of SEFDM transmitters and report SEFDM challenges, mostly the chip area and power dissipation overhead compared to conventional OFDM, which turns to demand more manufacturing cost and power [49].

3.5.2 SEFDM Signal Detection

SEFDM main aim is to improve spectral efficiency. Though as system capacity moves closer toward Shannon capacity, both storage and computation grow rapidly and it is important to decide whether the given closeness is worth the penalty or not [46].

As is the case for most systems, optimal performance for SEFDM in AWGN channel is achieved by ML detection [34]. The estimate of transmitted symbols based on ML detection is

$$\hat{\mathbf{z}} = \underbrace{\arg\min}_{\mathbf{z}} \left\{ \|(\mathbf{y} - \Lambda\mathbf{z})\|^2 \right\} \tag{3.16}$$

where $\|.\|$ denotes the Euclidean norm. However, the computational complexity of ML is impractically complex. The complexity of ML increases exponentially with N and the constellation cardinality M, i.e. it is of order $O(M^N)$, making the use of ML limited to small size systems.

Therefore, aiming to trade complexity versus detector optimality, other alternatives were investigated over the years to overcome ICI impairments with lower complexity. It was demonstrated that the linear detection techniques such as; ZF and MMSE perform significantly worse than ML, for $\alpha \leq 0.8$ and/or $N \geq 8$ [50]. The detectability of the signals is restricted by the ill-conditioning of the SEFDM correlation matrix Λ. The correlation matrix eigenvalues degrade as the number of the SEFDM subcarriers N increases and/or their frequency separation decreases. Consequently, Λ becomes severely ill-conditioned matrix and the detection turns into an ill-posed problem [50].

Matrix regularisation is used to reduce the condition number for ill-conditioned matrices. In [60], truncated singular value decomposition (TSVD) regularisation method is proposed to overcome the ill-conditioning problem, outperforming linear detectors (ZF and MMSE) while maintaining a linear system complexity. Although results show a reduction in the condition number of Λ, still, it is very high when compared to OFDM. In addition to this, it is true that TSVD performs better than ZF and MMSE [60], however, TSVD BER performance is comparable to that of

a matched filter without any ICI cancellation methods. Thus, the elimination of TSVD ICI canceller, at the receiver, has no performance penalty.

Approaching the problem from another angle, to reduce the so called relaxation gap between sub-optimum solutions and ML detection, a two steps detection method commonly known as boxed ML was investigated. In this method, ML detection is performed in a neighbouring area defined by a less complex detector, such as semi definite programming (SDP) [61] and MMSE [62]. The boxed detectors of MMSE-ML [62] and SDP-ML [61] show a drastic reduction in detector complexity compared to conventional ML, because the complexity of MMSE is of order $O(N^3)$ and SDP has polynomial complexity of order $O((2N)^{3.5})$ over the number of subcarriers N, followed by an ML operating on the neighbouring area and is of complexity order, at least, $N \times \log_2 M$, depending on the area size. The MMSE-ML method has two limitations: First, any linear detection for SEFDM, even if combined with other non-linear detectors, is always limited by the signal dimension N and the levels of bandwidth compression α, hence, the matrix Λ singularity remains a fundamental limitation in MMSE signal detection of FDM systems operating below the orthogonality limit [62]. Second, for two-dimensional modulation, such as QPSK, even with increase of the size of the MMSE neighbourhood, the BER system enhancement is limited compared to standalone MMSE linear detector [62]. On the other hand, the SDP-ML detector shows a small error penalty when compared to optimal ML for a moderate number of subcarriers and reported a spectral efficiency advantage of SEFDM over OFDM for the same transmitted power level.

Inspired by the successful deployment of sphere decoder (SD) in MIMO systems, which has a matrix similar in structure to the SEFDM correlation matrix, SD has been applied to SEFDM, firstly, in [50]. SD is a mathematical algorithm based on VA and achieves ML error performance with a reduced complexity. SD solves the ML problem described in (3.16) as [50]

$$\|(\mathbf{y} - \Lambda\mathbf{z})\|^2 = \|\Lambda(\hat{\mathbf{z}}_{ZF} - \mathbf{z})\|^2 \leq D \tag{3.17}$$

where $\hat{\mathbf{z}}_{ZF} = \Lambda^{-1}\mathbf{y}$ is the ZF estimate of $\mathbf{z}$ and D is a constant. Although SD achieves

optimum BER performance, its applicability is limited by two problems. First, SD mainly depends on the invertiblity of the ill-conditioned correlation matrix Λ, thereby limiting its efficacy to SEFDM systems with small number of subcarriers and ($\alpha \geq 0.8$). Second, the SD practicability is limited due to the dependence of its complexity on the noise level and system condition (i.e. α and N) [50]. Thenceforth, different versions of conventional SD are investigated to overcome its limitations.

In [50], generalized sphere decoder (GSD) is used to improve the condition number of the correlation matrix, through regularization based on Cholesky decomposition. Reported results show an enhancement in system performance compared to SD, but still with random complexity and applicability limited to low noise values and $N \leq 32, \alpha \geq 0.75$. In order to solve the random complexity problem of SD, the utilization of fixed sphere decoder (FSD) for SEFDM systems detection was studied in [63]. FSD has a fixed complexity because it fixes the number of nodes visits at each level of the search tree. Logically, by increasing the tree width, the BER performance improves and the complexity increases [63]. Although SD outperforms FSD in terms of BER performance, FSD eradicates the problem of random complexity of SD, making it better suited to hardware implementation [63].

Thereafter, FSD detectors have been used to detect SEFDM signals. For example, a combination of TSVD with FSD is implemented, where TSVD is used instead of ZF in conventional SD to calculate the initial estimate of transmitted symbols which helps in setting the sphere radius [60]. An iterative FSD has been applied to detect SEFDM signals transmitted over optical network in [64]. Results showed that SEFDM is more prone to non-linearity impairments in the optical channel, compared to higher-order OFDM signals.

The boxed SDP-SD detector of [65], achieves a quasi-optimal error performance for limited signal size and compression factor with a fractional computational effort compared to conventional boxed ML with SDP [65]. Also, in [66], a precoding method is implemented based on zero forcing, where the effect of ICI is reveresed before transmission. In [66], an ML detector was used but not on all

subcarriers, as it was proven that $(1-\alpha)N$ of the subcarriers have high Eigenvalue, thus, they can be detected directly by simple methods like ZF, while other subcarriers are detected by ML. Other techniques, based on good enough heuristic were proposed in the early work on SEFDM [6] and in [67]. Little work has been done in this area since, however, emerging techniques of machine learning based detection [68] and optimisation may lead to renewed efforts in this area.

To sum up, the aforementioned detectors may be considered as the first generation of SEFDM system detectors. The focus here was to reduce the detection complexity relative to ML. However, all suggested systems have restrictions on N, α and the modulation order M is limited to QPSK, because even with SD the complexity becomes impractical for higher M. To make SEFDM a valid competitor and a good applicant for the implementation of communication systems, the above restrictions were addressed. For instance, LTE was launched a few years after the invention of SEFDM and its OFDM symbol size is $N = 1200$ with up to 16-QAM and a simple one-tap frequency equaliser [1]. These were the motivations to get a forward step towards SEFDM practical implementation.

Channel coding was first introduced to SEFDM in 2014 [13]. In this study, convolutional code of rate $R_c = 1/2$ is used. An iterative turbo equaliser detector is implemented, that subtracts the interference gradually at each iteration, aiming to reach the correct $a-posteriori$ information for each transmitted bit after a certain number of iterations. The advantage of the turbo equalizer is in the absence of any matrix inversion, thus, avoiding the ill-conditioned SEFDM system problem. Consequently, the restrictions on α and N are relaxed, while maintaining the spectral efficiency improvement over OFDM.

Turbo equalisation was proved to be beneficial in different SEFDM scenarios. In [69], an experimental test bed is designed to evaluate the performance of LTE-Advanced (LTE-A) like SEFDM with carrier aggregation. Radio over fiber test beds were implemented at 2.4 GHz and 60 GHz in [70] and [71], respectively. It is shown in these experiments that SEFDM outperforms OFDM with the same spectral efficiency in terms of BER performance, however, a more complex iterative receiver

was needed to eliminate the ICI gradually from SEFDM signals [69].

The work in [18]and [19] and of Chapter 4 of this thesis, further investigate the employment of various channel coding techniques, such as convolutional, turbo, RS and serial concatenation codes for different coding rates. A new system architecture with block interleaving has been studied to improve the overall system performance, which benefits from channel coding to ameliorate the effects of ICI. Results show that the use of turbo coded SEFDM can drastically increase the spectral efficiency by up to 67% with a power penalties below 3 dB.

In [20] and Chapter 5 of this thesis, to increase the spectral efficiency of the design of high spectral efficiency satellite communication systems, the employment of a finite constellation SEFDM signals, coupled with LDPC channel coding and advanced interference cancellation processing via SIC, is investigated. A special case for broadband and broadcast applications (DVB-S2) is considered, where SEFDM provides more degrees of freedom in optimising the system, compared to orthogonal signals, by introducing compression level to the variable coding and modulation operating parameter. Results show that SEFDM saves bandwidth when compared to OFDM and requires less power while preserving the same BER performance. For high spectral efficiency values, interference cancellation becomes necessary to gain SEFDM advantages.

In addition to this, the current trend for 5G and beyond systems is to employ windowing and pulse shaping [72]. Following this, in [73], Nyquist RRC filtering is introduced to SEFDM, to reduce the OOBE power emission in a similar way to FBMC. However, the difference here is in the subcarriers being closer to each other in SEFDM. The concern with this design is in the increase of transceiver complexity. In 2015, it was proven that the bandwidth compression problem in SEFDM can be alleviated using optimum envelope forms and the OOBE is therefore constrained [74] [75]. The interference introduced by waveform shaping can be mitigated using interference cancellation approach, since interference is largely limited to adjacent subcarriers [73].

A new design idea inspired by power non-orthogonal multiple access (NOMA)

technique was implemented and reported in [25] and [26] and in Chapter 8 of this thesis. In this work, subcarriers within the same SEFDM symbol are allocated different power levels. Results show that such power allocation is beneficial to SEFDM in enhancing the overall system stability, reducing SEFDM detector complexity, enhancing channel estimation quality and improving PAPR behaviour.

Finally, the last obstacle to underline for SEFDM detectors, is its real time implementation. The growth in integrated circuits capability to cope with highly complex operations in real time, makes SEFDM implementation more promising. However, until now, only two detectors have been designed using FPGAs. The first one is a TSVD detector in [76]. Although TSVD is not an optimum solution in terms of BER performance, this technique has low complexity which allows it to be implemented in real-time system [76]. The second FPGA design is for an FSD combined with TSVD for the special case of $\alpha = 0.8$ and $N = 16$ [77]. The turbo equaliser used in the aforementioned experiments is an off-line detector simulated in MATLAB, and its real-time implementation is still in its early stages, however, further hardware implementations of SEFDM detectors seem to be just around the corner.

3.5.3 Peak-to-Average Power Ratio (PAPR)

PAPR holds information about the range of power variation in the signal, which is vital in the design optimisation process to choose system components. PAPR is generally defined as [78]

$$\text{PAPR} = \frac{\max|x(t)|^2}{\text{E}[|x(t)|^2]}, \tag{3.18}$$

where E[.] is the expectation operator to find the average, while $\max|x(t)|^2$ and $\text{E}[|x(t)|^2]$ are the peak and average power of the transmitted signal $x(t)$, respectively.

In a multi-carrier system, the nature of the signal might result in a constructive addition of the powers of different subcarriers, resulting in a higher $\max|x(t)|^2$. Consequently, a multi-carrier system is more prone to high PAPR compared to single carrier [78].

Results in [78] show that the probability of constructive addition of subcarriers

for SEFDM is lower than that of OFDM and further degradation occurs with higher bandwidth compression (i.e. lower α). Thus, SEFDM signals are less prone to non-linear effects when amplifiers are used, which is considered as an added advantage to SEFDM, besides improving the spectral efficiency. Recently, [79] and [80] investigated the PAPR behaviour of MFTN signals, which is similar to an SEFDM case with RRC shaped subcarriers [75]. The results agree with the previous conclusion of [78] that SEFDM and MFTN signals PAPR behaviour is better than that of OFDM signals. Further enhancement in PAPR is achieved by applying the newly suggested power allocation method, as shown in Chapter 8. For further PAPR reduction, different methods were introduced for SEFDM and MFTN, such as selective windowing (SLW) [78]; partial transmit sequence [79]; and tone reservation PAPR reduction algorithm [81].

3.5.4 Channel Estimation

The non-orthogonality nature of SEFDM signals further complicates the channel estimation problem. Two time domain channel estimation schemes for SEFDM systems were proposed in [15] and another in [82]. These schemes show acceptable performance, however, their complexity limits their practical utilisation because they require matrix inversions. Frequency domain channel estimation was therefore proposed in [16]. However, this scheme suffers from the disadvantage of interpolation, which increases the estimation complexity and reduces its accuracy [16].

The work in Chapter 6 of this thesis (also reported in [21]), devises a robust frequency domain channel estimation scheme for SEFDM signals, where the transmitted block is divided into orthogonal and non-orthogonal multiplexing regions. Specifically, the pilot is sent over orthogonally spaced subcarriers as an OFDM symbol, while information symbols are sent over SEFDM; both using the same number of subcarriers and the same subcarrier spacing. Therefore, this new scheme does not require channel interpolation and results in accurate channel estimation at the expense of slightly increased pilot duration overhead. Results demonstrate that this new scheme maintains an accurate estimation of the channel, regardless of the compression factor of SEFDM, the number of subcarriers and channel state. In addition,

substantial reduction in computational complexity and implementation simplicity are achieved compared to other schemes. The overhead (added redundancy) of the OFDM pilot results from extending the pilot symbol period compared to SEFDM symbol to maintain its orthogonality. The added redundancy of this scheme depends on how frequent the pilot is sent. For instance, if the pilot is sent every G information symbols, then, the added redundancy is $((1-\alpha)/(G+1)) \times 100\%$. Therefore, this scheme fits better in slow varying or static environments, where the pilot symbol may be sent less frequently. For fast varying channels, the same technique may be applied but with more frequent pilot transmission leading to more overhead [21].

This new channel estimation scheme impacted the practicality of SEFDM signals, as it made it possible to build real-time SEFDM systems and this has been verified experimentally in [30]. In this experiment, an LTE-alike SEFDM testbed was built, which consists of universal software radio peripheral (USRP) transceivers (NI USRP RIO N2395R) and a Spirent VR5 channel emulator, generating LTE channels that are estimated and equalised in real time using the new method [30]. Thereafter, a combination of the aforementioned channel estimation scheme and LDPC channel coding were utilised in the experiment of SEFDM transmission over E-band frequency range reported in Chapter 7. The experiment verifies SEFDM advantages through the design and testing of a multi Gbit/s communication link operating in the 81-86 GHz region. The highest transmission rate reported is 12 Gbps over bandwidths ranging from 4 GHz for a non compressed system down to 2.67 GHz for an SEFDM system.

3.6 Conclusions

The focus of this chapter was on SEFDM signals, where a new statistical mathematical model was derived and the signal characteristics were explained. Theoretical and empirical results concluded that ICI in SEFDM follows a Gaussian distribution, of a variance which depends largely on the compression level and to a lesser extent on the number of subcarriers. The developed ICI model was used to derive a closed form of SEFDM probability of error bounds, when a simple matched filter receiver

and AWGN channel are assumed. Results indicated that increasing the power level in SEFDM systems does not guarantee better error performance, because ICI results in an error floor level that increases by decreasing α. Therefore, a powerful interference cancellation method is required to benefit from SEFDM spectral efficiency advantages. In the final part of signal mathematical studies, SEFDM upper-bound spectral efficiency was derived using the statistical signal model and showed the advantage of SEFDM over OFDM, for different signal powers and system operating conditions.

Finally, the last section of this chapter presents a survey on the advancements achieved in SEFDM systems and summarises main areas of active work and highlights unresolved issues to set the foundation to the work in the subsequent chapters. The work in this thesis focuses on SEFDM systems, however, the findings of this chapter can be generalised to other non-orthogonal systems, similar to SEFDM, with appropriate modifications.

Chapter 4

The Application of Channel Coding to SEFDM Systems

Channel coding aims to approach Shannon's capacity limit, as introduced in Shannon's famous landmark paper in 1948 [83], by generating and adding redundant bits to protect information bits from communication systems disturbances. Therefore, the application of channel coding results in error rate reduction, at the cost of lower effective spectral efficiency for a given modulation cardinality.

Conventionally, only transmission impairments were taken into account when design and test performance of different channel coding techniques. However, after the wide application of channel coding in wired and wireless systems, researchers explored the capability of channel coding in eliminating other system impairments effects. For instance, the work in [84] and [85], explored the advantages of using convolutional codes and turbo codes, respectively, to overcome ICI and ISI effects, when OFDM signals are transmitted over multipath channels. Furthermore, convolutional coding is used to attain a more accurate estimation of channel state information at the receiver in [86].

Inspired by the aforementioned work and considering the main disturbance in SEFDM is ICI, the focus of this chapter is on the application of various channel coding techniques to eliminate ICI effects in SEFDM systems; specifically RS block codes, convolutional codes and turbo codes. A serial concatenation of RS and turbo codes is also implemented to further improve ICI effects elimination.

Moreover, the efficacy of different coding parameters in reducing the ICI effect is explored, through study of effects of puncturing and the number of turbo decoder iterations. A new method is developed in this chapter to enhance coded SEFDM error performance, especially with high compression level, where a block interleaver is implemented to interleave coded bits.

As a side note, it is worth mentioning that in this thesis, channel coding is not limited to the coding techniques described in this chapter. In the following chapters, depending on the application SEFDM is serving, other channel coding techniques are used and introduced in the subsequent chapters.

The outline of this chapter is: In section 4.1, an introduction to channel coding is provided, with a main focus on convolution and turbo coding. The spectral efficiency of coded SEFDM systems is evaluated in section 4.2, then the system model on which this chapter new designs are based is described in section 4.3. Investigation of different channel coding types and parameters is provided in section 4.4. Thereafter, the concept of block external interleaver is introduced to coded SEFDM systems and the advantages of this proposed design are explored in section 4.5. To summarise, section 4.6 runs a fair comparison between OFDM and SEFDM systems, which leads to the conclusions drawn in section 4.7.

4.1 Channel Coding Preliminaries

Shannon theorem relates the maximum error free transmission bit rate (or capacity (C) b/s) that can be achieved over a given channel with bandwidth (B) Hz and certain noise characteristics, such as [56]

$$C = B\log_2(1+SNR). \tag{4.1}$$

The ratio of C to B is effectively the maximum spectral efficiency (η) b/s/Hz that may be achieved. Fig. 4.1 shows η versus E_b/N_0 and highlights three main regions ($R_b < C, R_b = C, R_b > C$). Existing communication systems operate in the lower-right region of Fig. 4.1, where the transmission rate is less than Shannon capacity (i.e. $R_b < C$). The advent of channel coding techniques allows systems to operate

closer to Shannon limit (i.e. $R_b = C$), compared to uncoded systems. This gap between coded and uncoded systems is referred to as channel coding gain.

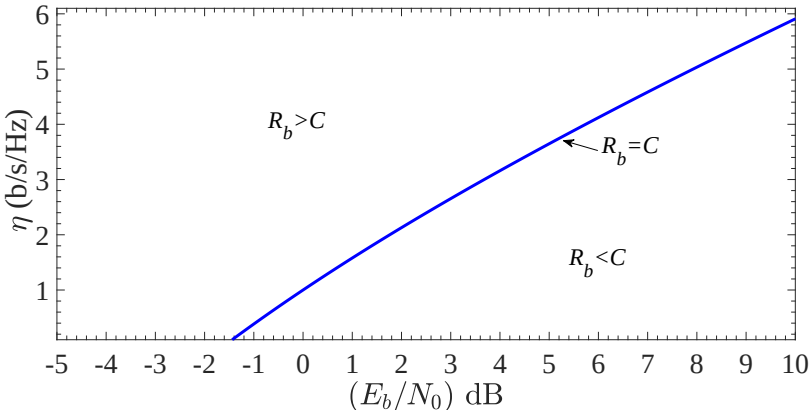

Figure 4.1: Maximum achievable η versus E_b/N_0.

Channel coding is characterised by three parameters (n_c, k_c, R_c). The input sequence of the encoder is of length k_c, while the encoder output sequence is of length $n_c \geq k_c$. The coding rate parameter defined as $R_c = k_c/n_c$ is usually used in spectral efficiency calculations, to reflect the effect of channel coding on system spectral efficiency. Another parameter may be used to describe channel coding is d, which is the minimum Hamming distance between any two distinct codewords, i.e. the minimum number of coordinates in which any two codewords differ [87].

There are two main categories of channel coding; algebraic and probabilistic coding. Algebraic coding became the focus directly after Shannon's theory, with the aim of finding codes that maximise d for a given k_c and n_c. There are two types of algebraic coding; binary (e.g. Bose-Chaudhuri-Hocquenghem (BCH)) and non-binary (e.g. RS). In contrast to algebraic coding, research on probabilistic coding aim is to find classes of codes that optimise average performance as a function of coding and decoding complexities. The first probabilistic coding type to appear was convolutional coding [88], then, turbo and LDPC coding. Over the years, probabilistic codes proved to be much more powerful, when compared to algebraic codes. Consequently, probabilistic codes are currently used in most transmission systems, either by its own or serially concatenated with algebraic coding [87] [89]. Known applications of convolutional codes are GSM and WiFi 802.11 a/g, while

turbo codes are used in UMTS, LTE and IEEE 802.16 (WiMAX). LDPC codes are adopted in IEEE 802.3an (10 Gbit/s Ethernet) standards and in DVB-S2, serially concatenated with BCH codes. Furthermore, LDPC codes are chosen for the future 5G systems and IEEE 802.11 ac standards.

As the main focus of this chapter is the application of convolutional and turbo codes to cope with SEFDM ICI impairment, in the following sections, a general overview of these two codes is provided.

4.1.1 Convolutional Coding

A convolutional encoder generates an output of length n_c from k_c inputs and m_c previous inputs stored in the encoder registers. Convolutional coding is also called feed-forward register, because at each stage, the bits in the memory registers are shifted one step towards the output and not back into the input [34].

Table 4.1: A summary of convolutional coding main parameters

Parameter	Value
Input sequence size	k_c
Output sequence size	n_c
Memory size	m_c
Constraint length	$L_c = m_c + 1$
Number of states	$S = 2^{m_c}$
Coding rate	$R_c = k_c/n_c$
Generator sequence length	L_c

Table. 4.1 summarises the main parameters of convolutional coding. Each bit stays m_c stages and affect the output during the m_c stages, plus when it is the input bit before entering the memory. The constraint length L_c is defined as the extent to which one input bit can affect the output, thus, $L_c = m_c + 1$. A convolutional encoder has generator sequences (g), given in octal form and each of length L_c. The encoder in Fig. 4.2 is for a special design of convolutional encoder called recursive systematic convolutional code (RSCC) of parameters (5, 7, 3)[1]. The encoder constraint length is three and has two outputs; systematic bit s, which is identical to the information bit, and parity bit p. The generator sequence for the parity bit

[1]The description of RSCC is usually presented as $(g_1, g_2, ..., m_c)$.

p depends on both the feed-forward ($(101)_{oct.} = 5$) and feedback ($(111)_{oct.} = 7$) generator sequences and is given by [34]

$$g(D) = \frac{1+D^2}{1+D+D^2}, \tag{4.2}$$

where g here is in the polynomial D domain. This type of encoder is called recursive because of the feedback connection and systematic because the codeword $\mathbf{c}$ contains s. The advantage of the feedback connection is that for the same memory and block lengths, the encoder can achieve higher minimum Hamming distance [34] [90]. For example, the RSCC of Fig. 4.2, achieves the maximum free distance d for a three memory stages encoder, which is 5 [34]. Thus, the rest of this work will utilise RSCC (5,7,3). A table in [34] summarises the optimum generator sequences for each constraint length in RSCC and [90] confirms these results by simulation.

To attain the optimum performance of the encoder, the initial and final states of the encoder need to be known. Thence, code termination takes place after coding the input sequence $\mathbf{b}$, to return the encoder to its initial zero state.

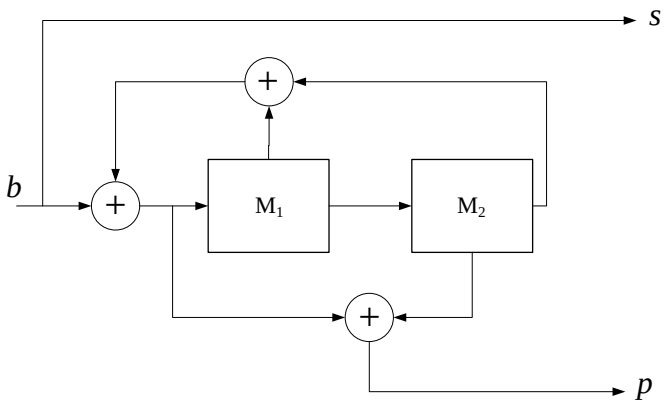

Figure 4.2: Block diagram of (5,7,3) RSCC with $R_c = 1/2$.

At the receiver, there are two types of convolutional decoders: Viterbi decoder with hard-output and maximum $a-posteriori$ (MAP) decoder with soft-output. Viterbi decoder finds the most likely path the input takes through a trellis diagram to reach the output. The complexity of the Viterbi decoder is given by $(k_c \times 2^{m_c})$ [90] [91]. On the other hand, a MAP decoder, firstly invented in 1974 by Bahl, Cocke,

Jelinek and Raviv (BCJR), estimates the *aposteriori* probability (APP) of the trellis states and the transitions between them [92]. Given that the Viterbi decoder output is hard, it does not perform well when the decoder is part of an iterative detector because soft information must be circulated. Soft output Viterbi algorithm (SOVA) overcomes this limitation, but when compared to the MAP decoder, MAP decoder achieves better BER performance with lower complexity [90] [87]. For further information about the trellis diagram and how the Viterbi and MAP decoders work, readers are encouraged to refer to Appendix A.

4.1.2 Turbo Coding

The name turbo comes from the iterative nature of its decoder. Berrou *etal*. proposed this class of codes in 1993, where they showed that using the BCJR decoding algorithm, turbo codes outperform other codes in single carrier signals transmission over flat and frequency selective fading channels [93]. A turbo encoder combines two identical rate RSCC in a parallel concatenation arrangement, with an internal pseudo-random interleaver ($\Pi_{\text{int.}}$) of size k_c bits between them, as shown in Fig. 4.3. The source bits **b** are the input to the first constituent encoder, while the sec-

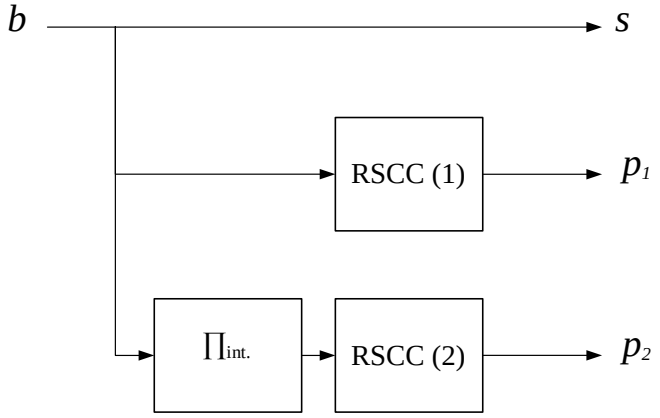

Figure 4.3: Turbo encoder block diagram.

ond encoder is fed by an interleaved version of the original data $\acute{\mathbf{b}}$ [90] [94]. The output of the turbo encoder consists of: systematic bits **s**; parity bits from the first encoder $\mathbf{p}_1$; parity bits from the second encoder $\mathbf{p}_2$. Therefore, the coding rate is

$R_c = 1/3$, as for each information bit, three bits are transmitted. In practice, to enhance the transmission system spectral efficiency, puncturing is used to achieve a higher R_c, by reducing the amount of redundant information sent [94]. Punctured codes are classified as systematic, partially systematic or non-systematic according to whether all, some or none of the systematic bits are transmitted, respectively [95]. However, when it comes to turbo coding, most of the Hamming weight resides in the parity bits. Consequently, if excessive puncturing is applied to the parity bits, the effective minimum distance degrades significantly for higher code rates.

At the receiver, a turbo decoder is used to estimate the transmitted message bits from the received coded bit stream. Fig. 4.4 shows the block diagram of a turbo de-

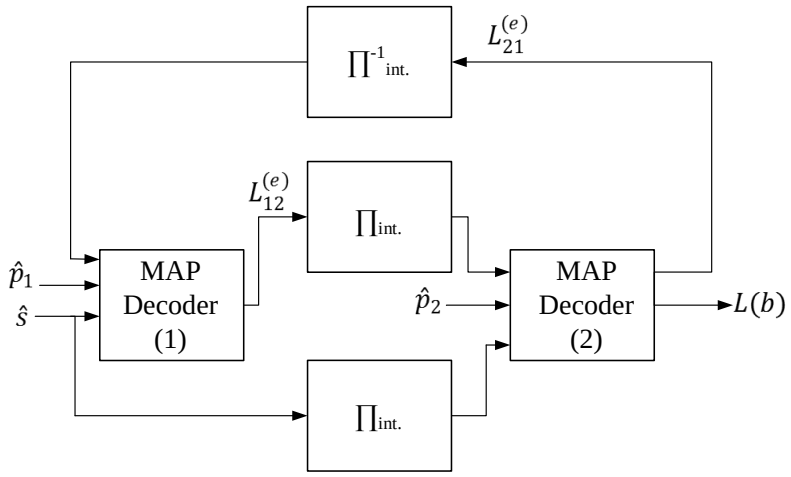

Figure 4.4: Turbo decoder block diagram.

coder, which consists of two MAP decoders to produce soft estimates of the source bits. For the case where puncturing is used, the mean value of $\mathbf{b}$ is inserted at the positions of the punctured bits. The first decoder is fed by three inputs; received systematic bits $\hat{\mathbf{s}}$, received first parity bits $\hat{\mathbf{p}}_1$, and $a-priori$ information $\mathbf{L}_1(\mathbf{b})$ to produce soft estimates of the transmitted bits. Next, it evaluates the extrinsic information $\mathbf{L}_{12}^{(e)}$ from the soft estimates, interleaves it and feeds it to the second decoder as $a-priori$ probabilities $\mathbf{L}_2(\mathbf{b})$, in addition to the interleaved received systematic bits $\acute{\hat{\mathbf{s}}}$ and second parity bits $\hat{\mathbf{p}}_2$. The extrinsic information is generated from the second decoder $\mathbf{L}_{21}^{(e)}$ by subtracting the $a-priori$ information from the decoder output.

Following this, $\mathbf{L}_{21}^{(e)}$ is de-interleaved and used as $a-priori$ information $\mathbf{L}_1(\mathbf{b})$ to the first decoder in the next iteration. This process continues for a given number of iterations or until a certain condition is met. Then, a hard decision is made upon the sign of $L(b)$ [89]. By increasing the number of iterations, a better error performance is achieved to a certain extent, at the cost of increased decoder latency and complexity.

After this general review about convolutional and turbo coding, next section calculates the spectral efficiency of coded SEFDM systems, which will be used later in this chapter to evaluate SEFDM system performance.

4.2 Coded SEFDM Systems Spectral Efficiency

In coded SEFDM, the spectral efficiency η, is expressed in terms of the compression factor α, the modulation cardinality M, coding rate R_c, number of subcarriers N, symbol rate R_s in symbol/Hz and the channel bandwidth B Hz as in

$$\eta = \frac{R_s \times R_c \times \log_2(M)}{\alpha \times B}, \tag{4.3}$$

where $B = N \times \Delta f$. The related spectral efficiency gain ζ (relative to OFDM) is simply defined as

$$\begin{aligned} \zeta &= \frac{\eta_{\text{SEFDM}} - \eta_{\text{OFDM}}}{\eta_{\text{OFDM}}} \times 100\% \\ &= \left(\frac{1}{\alpha} - 1\right) \times 100\%. \end{aligned} \tag{4.4}$$

Fig 4.5 plots ζ versus α. Obviously, lower α results in a reduced occupied bandwidth and higher ζ. The maximum spectral efficiency gain shown here is 67% when $\alpha = 0.6$, because signal detection becomes really difficult when lower α and two dimensional mapping is used. In the following section, the coded SEFDM system model is described.

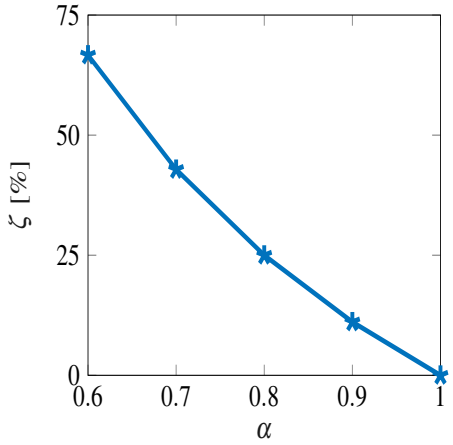

Figure 4.5: SEFDM spectral efficiency improvement percentage (ζ) vs. α.

4.3 System Model with Coding

The work done on channel coding application to SEFDM systems are published in [18] and [19]. Consider SEFDM system architecture block diagram depicted in Fig. 4.6, where blocks with dashed edges are not within the initial simulated system in [18] and they will be introduced later in this chapter. At the far left end of the transmitter, a stream of bits $\mathbf{b}$, $b \in \{0,1\}$, of length k_c is encoded by the channel encoder, followed by a mapper which maps each $\log_2 M$ bits to a symbol $z \in \mathbb{C}$ from the M-ary symbol alphabet, where $M = 4$ for QPSK. The sequence $\mathbf{z}$ is then

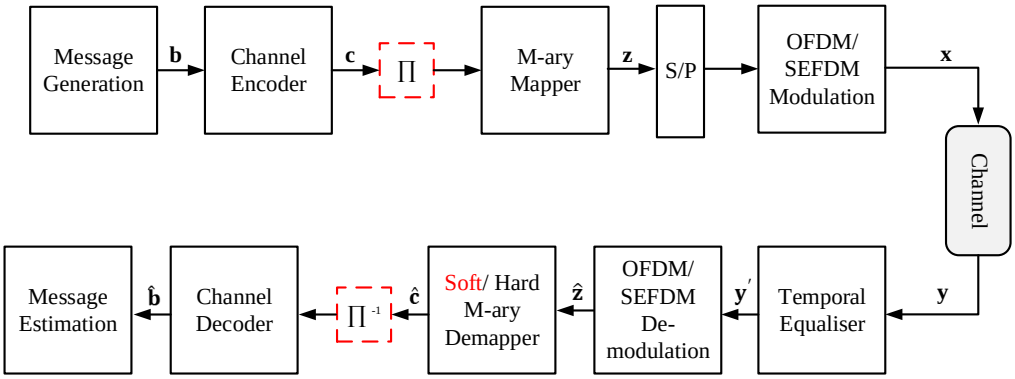

Figure 4.6: SEFDM system block diagram.

divided into parallel streams, each of size N. Each parallel stream is modulated by SEFDM subcarriers as was shown in (3.3). A simplified illustrative SEFDM signal generation is described in this block diagram while the exact details of different

methods of SEFDM generation are described in [57] [24] and Chapter 6. Finally, the sampled parallel output of the IFFT is multiplexed to **x**.

For proof of concept, initially, a system only impaired by AWGN is considered and then the treatment is extended into SEFDM operating in a static multipath frequency selective channel. A static frequency selective channel is chosen with an impulse response of [96]

$$h(t) = 0.8765\delta(t) - 0.2279\delta(t - T_s) + 0.1315\delta(t - 5T_s) - 0.4032e^{\frac{i\pi}{2}}\delta(t - 7T_s), \tag{4.5}$$

where $\delta(t)$ is the Dirac delta function. At the receiver, perfect synchronisation and perfect channel estimation with a sufficient CP that totally eliminates ISI are assumed. A temporal zero forcing channel equalisation is used to reverse the channel effect, such as

$$\acute{\mathbf{y}} = \mathbf{H}^{-\mathbf{1}} \times \mathbf{y}, \tag{4.6}$$

where $\mathbf{H}$ is the $Q \times Q$ circulant channel matrix of a multipath channel of length L, Q is the number of samples in one SEFDM symbol. Following ZF temporal channel equalisation, the equalised SEFDM symbols are demodulated to obtain $\hat{\mathbf{z}}$, as was shown in (3.4). Then, the symbols are demapped into their associated code bits. The demapped hard bits are decoded using the channel decoder.

Fig. 4.7 plots BER versus E_b/N_0 of turbo coded OFDM and SEFDM ($\alpha = 0.8$) for two different channel conditions; an AWGN channel and the aforementioned static frequency selective channel. The system parameters are $N = 1024$, $R_c = 1/2$ and the number of decoder iterations is 8. By looking at the results, SEFDM reaches an error floor in the AWGN case and the power penalty of SEFDM is more than 4 dB, when compared to OFDM for 20% bandwidth savings. In Fig. 4.7(b), 7 dB is considerably a high power level for turbo coded systems, yet, SEFDM BER curve has not converged yet. Such error performance diminishes the advantage of SEFDM.

To enhance SEFDM error performance, the above experiment limitations were labelled: First, the demapper feeds hard bits to the decoder, however, to cope

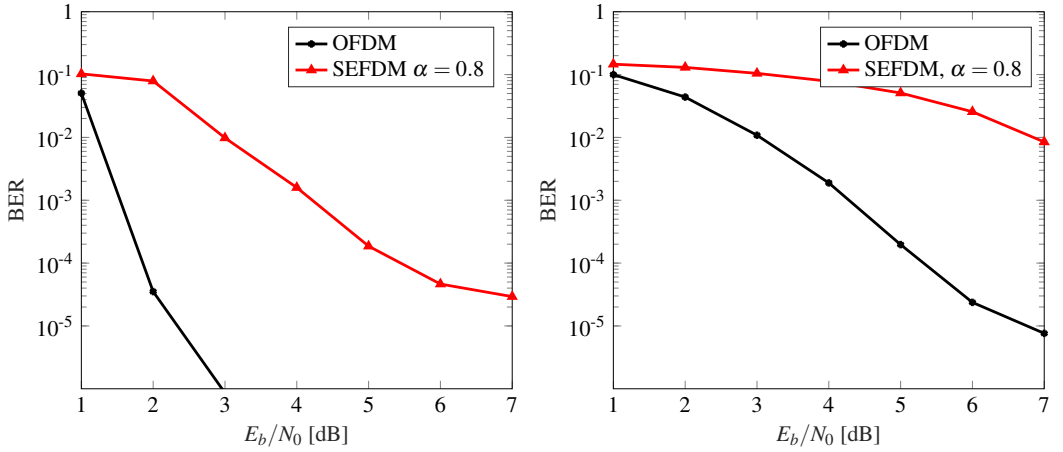

(a) AWGN channel **(b)** Frequency selective channel

Figure 4.7: BER performance of turbo encoded SEFDM ($\alpha = 0.8$) and OFDM signals, $N = 1024$, with turbo decoder system of 8 iterations.

with the deteriorative effect of ICI, the replacement of hard demapper with a soft demapper becomes essential [97]. The soft demapper feeds the decoder with log-likelihood ratio (LLR) values that indicates the reliability of the decision by considering how far it is from the decision threshold. Second, to attain the optimum performance of the decoder, the initial and final states of the encoder need to be known. Trellis termination is performed by padding with tail bits after encoding information bits to return the encoder to its all zeros state at the end of each input block. However, due to the feedback connection of the RSCC in the turbo encoder, the termination is not simply done by terminating the information bits with zeros, but it needs to be done in a more complex two-stages termination criteria, as explained in detail in Release 13 version 13,1.0 of the 3GPP standards [98].

Consequently, the above issues were addressed and a drastic enhancement in system performance is reported in [19]. This study is not limited to turbo codes only, other channel coding types are tested and a concatenation of block coding with turbo coding is evaluated. Furthermore, a temporal MMSE equaliser is used instead of ZF equaliser to take into account the noise variance. The MMSE equaliser reverses the channel distortion through the application of a linear filter to the received signal time samples $\mathbf{y}$. The filter coefficients are determined according to MMSE criterion

using [99]

$$\mathbf{G}_{\text{MMSE}} = \mathbf{H}^{-1}\left(\mathbf{I}_Q + \sigma_n^2 \mathbf{I}_Q\right)^{-1}, \tag{4.7}$$

and yielding the output simply expressed in

$$\acute{\mathbf{y}} = \mathbf{G}_{\text{MMSE}} \times \mathbf{y}, \tag{4.8}$$

where $\mathbf{I}_Q$ is an identity matrix of size $Q \times Q$ and ${\sigma_n}^2$ is the noise variance.

Also, an external block interleaver ($\prod_{\text{ext}}$) and de-interleaver ($\prod_{\text{ext}}^{-1}$) of size equivalent to encoded bits **c** length n_c, were introduced at the transmitter and receiver, respectively, as shown in Fig. 4.6. There are two reasons for using the external interleaver; first it is used to insure that the assumption of **c** being independent approximately holds for several iterations for the turbo equalisation application. Second, in SEFDM system due to ICI, it has a burst error performance similar to OFDM over frequency selective channels, thus, it scatters the error as will be shown later. Unless otherwise stated, the results in this section are for the parameters shown in Table 4.2.

Table 4.2: SEFDM with coding system parameters

Modulation	QPSK
Turbo encoder	(5,7,3), $R_c = 1/3$ with zero biting(8 bits), Inner interleaver size 2048, and output block size $(2048 \times 3 + 8) = 6152$
Turbo encoder with puncturing	(5,7,3), $R_c = 1/2$ with zero biting(8 bits), Inner interleaver size 2048, and output block size $(2048 \times 2 + 8) = 4104$
Convolutional coding	(5,7,3), $R_c = 1/2$
Systematic RS block code	(223,255,32), $R_c = 223/255$
Serial concatenated coding	outer RS (223,255,32), internal turbo, $R_c = \frac{223}{255} \times \frac{1}{3} = \frac{223}{765}$
Turbo decoder	Log-MAP decoder
Turbo decoder iterations	8
Convolutional decoder	Viterbi Algorithm
SEFDM Symbol Size (N)	16
Channel (I)	Additive white Gaussian noise (AWGN)
Channel (II)	(4.5)

The next section analyses the effect of several system parameters by examining the BER performance and spectral efficiency.

4.4 Channel Coding Type

Different types of channel codes are explored in this study. RSCC rate $(1/2)$; RS block code $(223, 255, 32)$; turbo code of original rate $(1/3)$ and the serial concatenation of RS with turbo code. Fig. 4.8(a-d), shows the BER versus E_b/N_0 results for AWGN channels. In each figure, OFDM is used as a reference to evaluate the efficacy of using a particular coding method for the SEFDM case. The results of Fig. 4.8(a) proves the inability of block coding to correct the errors caused by ICI. This is particularly evident from the error floor at high E_b/N_0 and for higher spectral efficiency gains (lower α). Hence, the option of using RS with SEFDM is discarded.

Looking at RSCC ($R_c = 1/2$) of Fig. 4.8(b), it fares better compared to RS, but still cannot cope with high level of interference for lower values of α. A 25% improvement in η for ($\alpha = 0.8$) has a power penalty of 3 dB compared to OFDM, which is similar to the BER performance of uncoded OFDM, thus, if we calculate η for both it is 2 b/s/Hz and 1.25 b/s/Hz for uncoded OFDM and convolutional coded SEFDM ($\alpha = 0.8$), respectively. To sum up, there is no benefit of RSCC with SEFDM over uncoded OFDM, unless, the successive interference canceller of [13] is utilized, where the concept of multi soft iterations is used with ICI cancellation. A more detailed explanation of this turbo equaliser is discussed in the next chapter.

Turbo coding in Fig. 4.8(c) performs better than the aforementioned coding schemes. For instance, the results of using turbo encoder of rate ($R_c = 1/3$) and 8 turbo decoder iterations indicate that for $\alpha = 0.8$, a power penalty of 1 dB is required, compared to OFDM. Also, the turbo coded SEFDM is superior to uncoded OFDM even with 67% improvement in η. Unlike the aforementioned channel coding types, there is an advantage of using turbo coding with SEFDM.

Looking up for further performance enhancement, a serial concatenation of turbo with the outer block code of type RS is implemented. The coding rate of RS

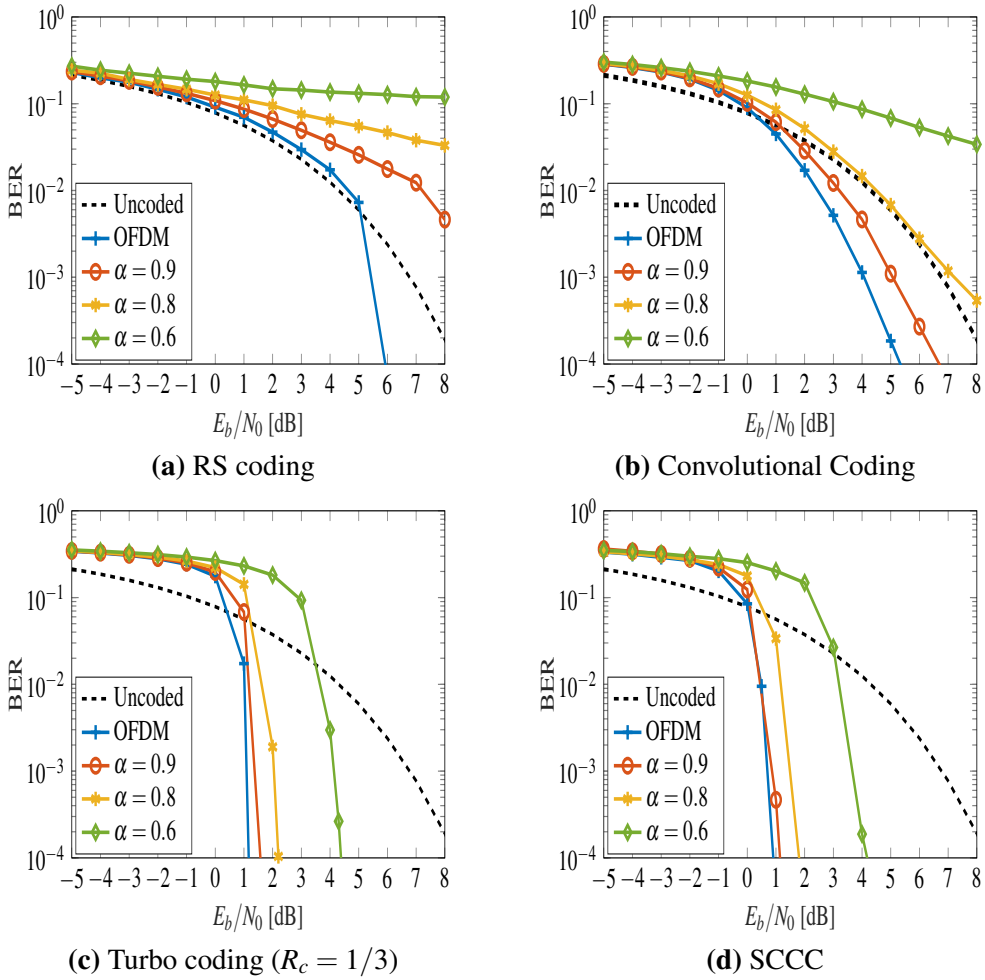

(a) RS coding

(b) Convolutional Coding

(c) Turbo coding ($R_c = 1/3$)

(d) SCCC

Figure 4.8: SEFDM system QPSK BER performance with different coding algorithms

.

is ($R_c = 223/255$) thus, as shown in Table. 4.2, the resultant coding rate becomes ($R_c = 1/3 \times 223/255 = 223/785$), which means a reduction in η. The results of the serially concatenated RS-Turbo coding in Fig. 4.8(d) shows a negligible improvement when compared to turbo coding.

Given the better performance of turbo coding, in the following, further investigations are undertaken to evaluate the impact of puncturing and number of decoder iterations on ICI mitigation capabilities of turbo coding.

4.4.1 Coding Rate

Adaptive modulation and coding (AMC) is commonly employed to improve system throughput and to optimise resources utilisation, by selecting the modulation

and coding rates depending on the channel condition. Consider the BER results

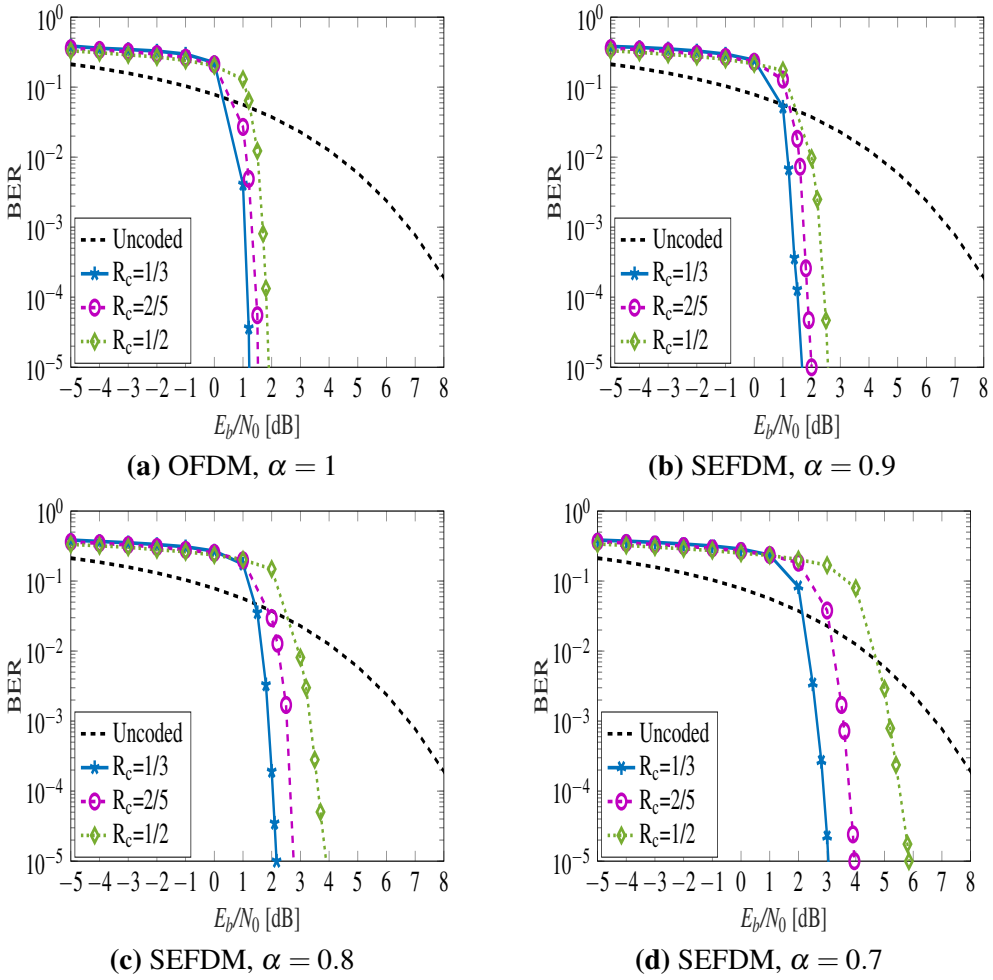

(a) OFDM, $\alpha = 1$ **(b)** SEFDM, $\alpha = 0.9$

(c) SEFDM, $\alpha = 0.8$ **(d)** SEFDM, $\alpha = 0.7$

Figure 4.9: QPSK coded SEFDM system BER performance for different R_c and α with 8 turbo decoder iterations.

given in Fig. 4.9, for three different coding rates and compression levels. The different coding rates are achieved by puncturing the parity bits of an original turbo code of rate $R_c = 1/3$. Puncturing the parity bits is introduced to increase R_c, for example, in the case of $R_c = 1/2$, two bits are transmitted for each information bit, one systematic and one parity. On the other hand, for $R_c = 2/5$ it means that for each two information bits, 5 bits are transmitted where two of them are systematic and the other three are parity bits.

Looking at the results, the system performance degrades by increasing the coding rate, because the number of redundant bits transmitted per information bit is reduced. Therefore, there is a higher chance of erroneous detection at the receiver.

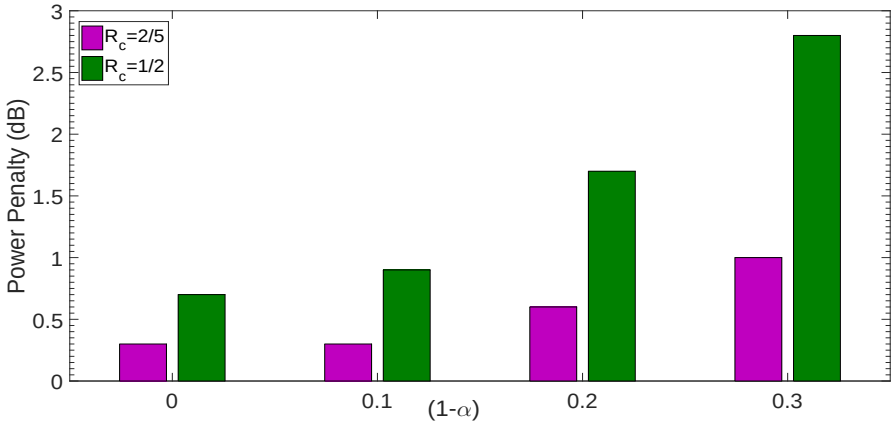

Figure 4.10: Power penalty in dB due to puncturing the turbo encoder output, versus $(1-\alpha)$.

In addition, it is noticed that by lowering α, the system becomes more sensitive to puncturing. This is summarised in the chart of Fig. 4.10, showing the power penalty in dB, due to puncturing, versus $(1-\alpha)$. To sum up, SEFDM is more prone to puncturing compared to OFDM.

4.4.2 Number of Iterations

In a turbo coded system, by increasing the number of decoder iterations, better BER performance is achieved, or in other words, the BER curve gets closer to Shannon limit boundary [91]. Fig. 4.11 demonstrates the effect of increasing the number of iterations on the BER performance for different compression factors. From the results, expectedly, an enhancement in the performance is achieved by increasing the number of iterations up to a limit where the benefit becomes negligible.

In pursuit of Mazo's work [45], the same BER performance might be possible for almost the same E_b/N_0, using a more complex receiver, which in this case is higher number of iterations. This can be seen by looking at Fig. 4.11 again, to compare SEFDM to OFDM with lower number of iterations. For instance, SEFDM $\alpha = 0.8$ and 8 decoder iterations, has the same error performance of OFDM with 3 iterations.

In conclusion, SEFDM improves OFDM spectral efficiency, at the cost of higher transmission power or higher number of decoder iterations (more complex

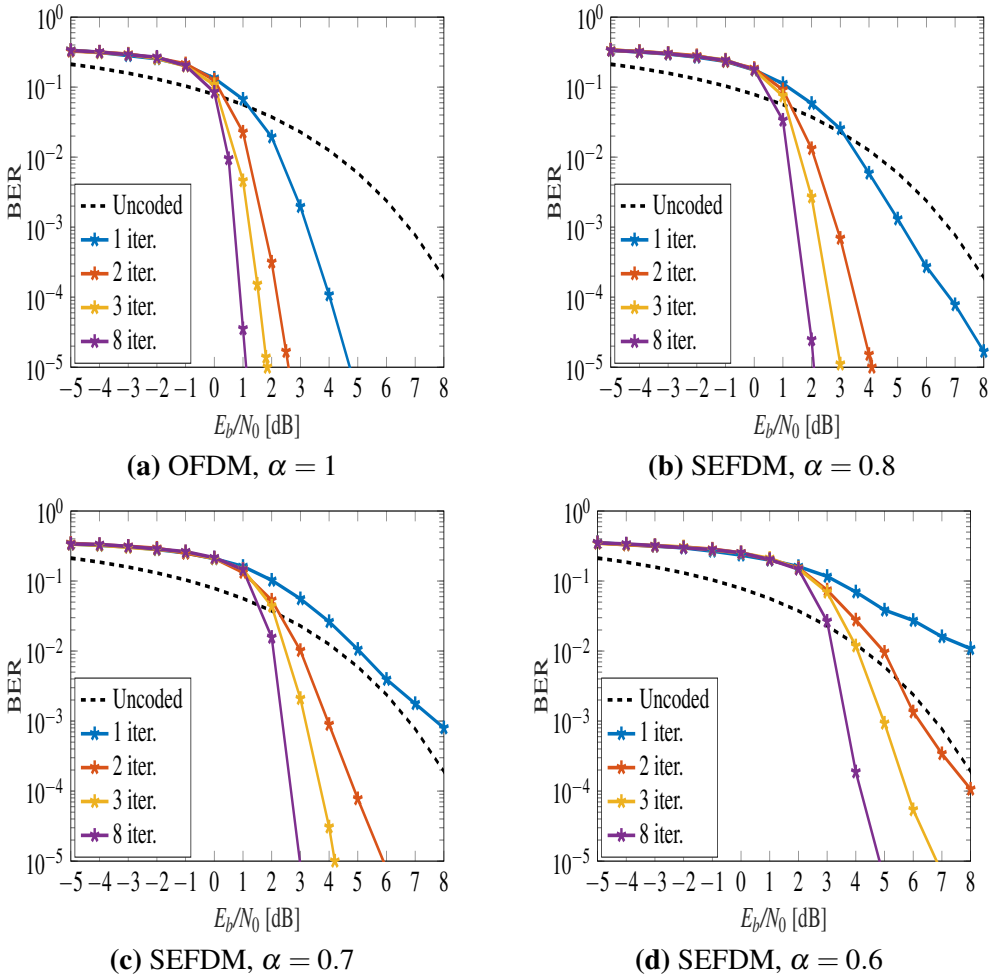

(a) OFDM, $\alpha = 1$ **(b)** SEFDM, $\alpha = 0.8$

(c) SEFDM, $\alpha = 0.7$ **(d)** SEFDM, $\alpha = 0.6$

Figure 4.11: Turbo coded QPSK SEFDM system BER performance for $R_c = 1/3$ and different number of iterations

detector). To improve coded SEFDM system performance further, in the next section, an external interleaver is introduced.

4.5 External Interleaver

Conventionally, interleavers have been used in communication systems with channel coding to scatter error bursts caused by a fading channel. However, in SEFDM, even with a flat channel, due to the interference between its subcarriers and the variation of the interference level, according to the location of the subcarrier, interleavers become beneficial.

Based on the ICI formula in SEFDM given in (3.7), the amplitude of ICI on each subcarrier versus the subcarrier index is given in Fig. 4.12 for unmodulated

SEFDM system for $N = 16$ and $N = 1024$. From the figure, the correlation is not

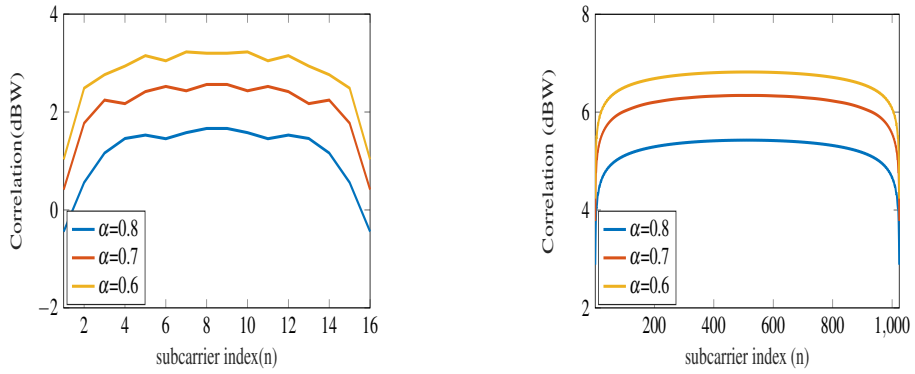

(a) $N = 16$ **(b)** $N = 1024$

Figure 4.12: ICI amplitude versus subcarrier index for unmodulated SEFDM system with $N = 16, 1024$.

equal and the subcarriers in the middle experience more interference compared to those on the edges. Furthermore, by reducing α, the interference amplitude increases.

In any channel coded system, one of the important assumptions is that the coded bits are independent. However, in SEFDM due to the ICI, this condition is missed. To overcome this, a second stage external interleaver is used to enhance the reliability of the coded system, where the coded bits are interleaved before mapping [34]. This interleaver is of no benefit for uncoded systems and coded OFDM over a flat fading channel.

An interleaver can be of two forms, a convolutional or block interleaver. In this proposed system, the block interleaver is a rectangular array of the same size of turbo encoder output $n_c = 6152$ ($i \times j = 769 \times 8$), by which it interleaves the encoded bits by sequentially increasing the row number for each successive bit, and filling the columns. The interleaved source data is then read out row-wise and fed to the modulator. This has the effect of separating the original bits by 769-bit period [34].

Fig. 4.13 presents the results obtained for the same turbo coded SEFDM of the previous section, but with an external interleaver. A comparison between Fig. 4.13 and Fig. 4.11 shows the advantage of the external interleaver. For OFDM,

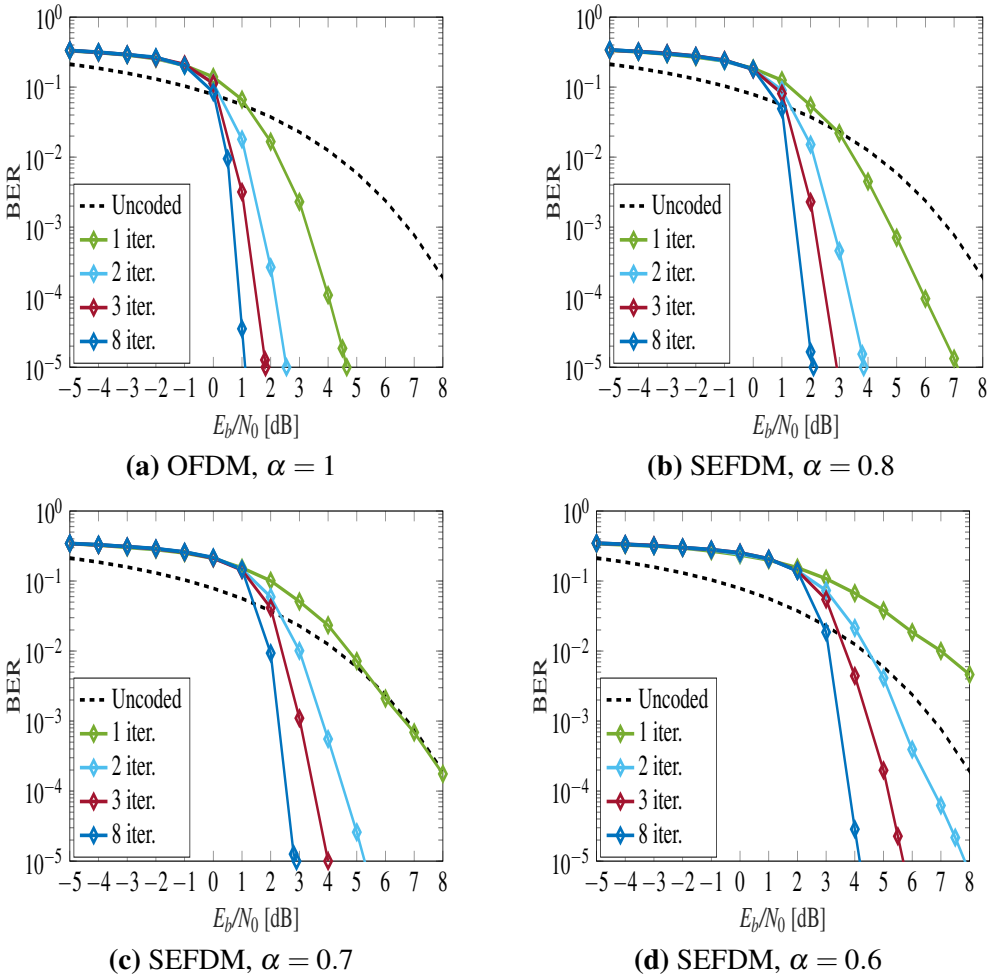

(a) OFDM, $\alpha = 1$ **(b)** SEFDM, $\alpha = 0.8$

(c) SEFDM, $\alpha = 0.7$ **(d)** SEFDM, $\alpha = 0.6$

Figure 4.13: SEFDM turbo coded QPSK system BER performance with external interleaver for $R_c = 1/3$ and different number of iterations

unfailing the above argument, the interleaver has no effect at all because there is no ICI. In SEFDM for $\alpha = 0.8$ and high number of iterations, no major enhancement is reported as well. However, for SEFDM $\alpha = 0.6$, due to the high ICI, even with 8 iterations, an approximately 1 dB power enhancement is achieved at BER$= 10^{-5}$.

Finally, to compare this system model performance to the BER results previously shown in Fig. 4.7(b), when the signal propagates through the multipath channel given in (4.5), the optimal parameters from the above investigations are considered. BER results shown in Fig. 4.14 are for turbo coded signals of $R_c = 1/3$ and 8 decoder iterations and the external interleaver is used. Furthermore, the temporal MMSE equaliser, discussed before in the system design is used to mitigate the multipath channel effect. Results show a drastic enhancement in SEFDM and

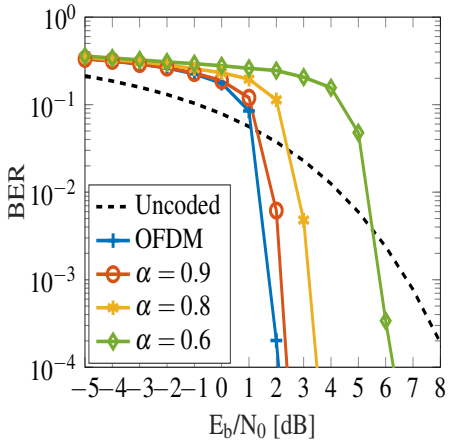

Figure 4.14: Turbo coded rate (1/3) QPSK SEFDM system BER performance over multi-path channel.

OFDM performances, when compared to the turbo initial system model results in Fig. 4.7(b). However, there is still performance degradation relative to the AWGN case for both OFDM and SEFDM in Fig. 4.13. Moreover, SEFDM with lower α becomes more prone to the multipath channel effect resulting in a higher power penalty.

4.6 SEFDM versus OFDM

To summarise the work done in this chapter, a fair comparison between OFDM and SEFDM is held given that both have the same spectral efficiency. The LTE 10 MHz scenario [100] is chosen for the upcoming simulation test. It is important to mention that the extra overhead in LTE for the guardband, CP...etc, is not taken into consideration in the following, as it is the same for all systems. Table. 4.3 shows the system parameters for the upcoming simulation test. SEFDM α values are adjusted here to ensure OFDM and SEFDM systems have the same spectral efficiency. The test is held over an AWGN channel, with external interleaver and 8

Table 4.3: SEFDM versus OFDM test parameters.

System label	α	R_s Msymbol/sec	N	$\alpha \times B$ (MHz)	M -QAM	R_c	η (b/s/Hz)
OFDM-1	1	9.00	600	9.00	8	1/3	1
SEFDM-1	2/3	9.00	600	6.00	4	1/3	1
OFDM-2	1	9.00	600	9.00	32	1/3	1.67
SEFDM-2	4/5	9.00	600	7.20	16	1/3	1.67

decoder iterations. The simulation results are shown in Fig. 4.15.

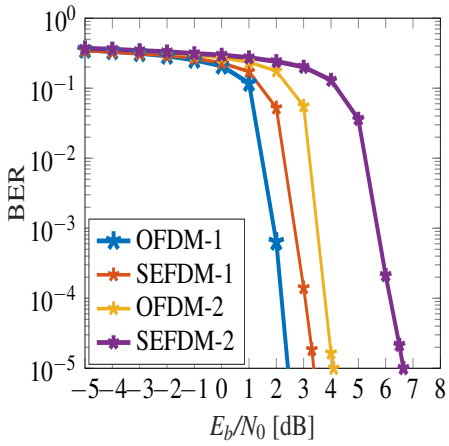

Figure 4.15: A comparison test between OFDM and SEFDM turbo coded systems.

The results indicate that for the same complexity and the same spectral efficiency, OFDM still outperforms SEFDM and the gap between the two systems increases for a higher η. Thus, unlike AWGN noise impairments, even a powerful channel coding such as turbo coding cannot fully mitigate the effect of ICI and a more powerful interference canceller is necessary. Although results show OFDM is superior to SEFDM, in specific scenarios, it might be preferable to achieve a higher η by bandwidth compression, rather than using higher modulation order.

4.7 Conclusions

This chapter presented the basics of coded SEFDM systems, where different channel coding techniques were applied to enhance SEFDM error performance in AWGN and frequency selective channels. The first trial for applying turbo coding to SEFDM was not successful, as the error penalty of using SEFDM with 20% bandwidth savings, instead of OFDM was approximately 4 dB. Thereafter, system model issues were solved, such as the replacement of the hard demapper by a soft demapper and an accurate tail-biting of the turbo encoder was implemented to return the encoder to its zero state at the end. These two alternations, plus utilising an MMSE channel equaliser instead of ZF to take into account the noise variance, showed a huge impact on the error performance and the advantages of using SEFDM became

evident. This study is not limited only to turbo coding, the capability of RS, convolutional and serially concatenated codes in eliminating the interference effect in SEFDM was investigated too. However, the results favoured turbo coding over the other techniques, particularly with high SEFDM compression levels, with gain up to 67% with limited power penalty, when compared to OFDM systems.

This conclusion initiated the investigation of the effect of different parameters of turbo channel coding, when dealing with the interference in SEFDM. It is found that SEFDM is more sensitive to code puncturing, relative to OFDM, with higher power penalty gap for higher compression levels. Also, by increasing the number of the turbo decoder iterations, the error performance improves, up to a limit where it saturates and further increase will have a negligible effect.

An external interleaver was proposed to interleave the coded bits of the SEFDM signals before the mapper to help in maintaining the channel coding randomness, which is affected due to high levels of interference. This adjustment to the system model proved to be of great advantage as it showed up to 1 dB enhancement in coded SEFDM error performance.

Finally, to summarise this work, a fair comparison between OFDM and SEFDM was simulated, given that both have the same spectral efficiency and the same simulation parameters. Results showed that although coding improves the error performance for SEFDM, as it indeed does for OFDM systems, there is still a limitation, which is ICI. Therefore, further improvements in spectral efficiency and the reduction in the power penalty require better removal of the interference from the received signal. This has led to the development of a new type of SEFDM receivers with interference cancellation, which is the topic of the next chapter.

Chapter 5

The Application of Successive Interference Cancellation for SEFDM Satellite Systems

This chapter is, in a way, an extension to the previous chapter where channel coding proved its efficacy as a detector, even with high compression levels. This conclusion has led to the successive interference canceller design, to benefit from the channel decoder and to estimate the interference and cancel it gradually. The new SEFDM receiver design is tested for satellite broadcast and broadband scenarios, where multiple carriers are frequency division multiplexed with a substantial overlap. In such satellite communication systems, variable coding and modulation (VCM) is adjusted to satisfy pre-defined spectral efficiency values for a given quality index (QI) for associated application. SEFDM adds more flexibility to the satellite systems by introducing adjustable compression level variable. In this chapter, a mathematical model and simulation studies are presented, indicating promising gains to be achieved for SEFDM transmission with advanced transceiver architectures.

The outline of this chapter is: Section 5.1 gives an overview of SIC types and applications. Section 5.2 describes the digital broadcast satellite model to which SEFDM signal with SIC is applied to. Section 5.3 details the simulation model, followed by results analysis in section 5.4. Finally, conclusions are provided in section 5.5.

5.1 Successive Interference Cancellation

SIC may be defined as an iterative detection scheme, which aims to cancel the unwanted interference gradually from a given received signal. Thus, SIC usage guarantees a better estimate of the transmitted signal. The idea of an iterative detector first appeared after the substantial performance gains of turbo coding and decoding algorithms [93]. The first SIC was proposed by Douillard *et al.* to eliminate the effect of ISI when the signal propagates through a multipath channel [101]. This SIC consisted of a MAP detector and a convolutional decoder exchanging soft information for a certain number of iterations.

There are different types of SIC, depending on: *i*) the detector type (sometimes called equaliser); *ii*) the decoder type; *iii*) the exchanged data format type (i.e. soft or hard data). Soft linear detectors, such as ZF and MMSE are dominant in many communication systems dealing with interference, where the detector feeds the decoder with soft information as $a-priori$ probabilities [102]. However, these detectors would perform poorly in ill-conditioned systems like SEFDM, because they require matrix inversion. Non-linear detectors cope with the ill-conditioned issue, mentioned above, better than linear detectors. For example, soft non-linear MAP detector generates soft information in the form of $a-priori$ probabilities without any matrix inversion operations [103]. However, the main drawback of MAP detectors is in its high complexity [103]. An alternative less complex SIC design is the hard SIC, where the interference is estimated in each iteration, then subtracted gradually in the following iteration [104].

Exhaustive analysis of soft and hard SIC to cancel ISI, ICI and multi-antenna interference for OFDM systems is provided in the survey paper [105]. SIC has been broadly used in different applications to deal with different kinds of interference impairments, such as:

1. Code-division multiple access (CDMA): SIC is used to cancel the effect of multi-access interference and ISI. In [102], a soft SIC is implemented, where a soft-input/soft-output (SISO) linear MMSE detector exchanges extrinsic information with a convolutional decoder at each iteration, just as turbo decod-

ing does.

2. Ad hoc network: One of the applications of SIC is to minimise the schedule length in an ad hoc network by decoding multiple transmissions at a time [106] and enhance the network capacity [107]. In this application, hard SIC allows a certain node to decode and subtract signals intended for the other nodes within the network first, then decode their own signals [107]. Consequently, it was shown that SIC leads to significant capacity gains [107].

3. Non-orthogonal signals: SIC has been successfully implemented for non-orthogonal signals to estimate the ICI and/or ISI components and suppress them from the received signal. For instance, a soft SIC, consisting of a MAP detector and a turbo decoder, is used in single user FTN [108] and MIMO FTN [109] systems, to estimate and subtract the interfering FTN signal at each iteration. Furthermore, in [11], TFP signals use the same soft SIC, but with LDPC decoder. In [13], hard SIC has been implemented for SEFDM signals for use with convolutional coded signals, where within each loop, a hard decision is made after the convolutional decoder, to estimate the interference amount from other subcarriers and then subtract it from the desired one.

4. NOMA: Hard SIC is widely used in power NOMA, to separate different users by detecting and cancelling the multi-user interference gradually, starting with the closer one from the base station (highest power level), up to the farthest user with the lowest power level, or worst channel conditions [110].

5. Vehicle to vehicle (V2V): A new application to hard SIC is V2V communications. SIC is used to to mitigate the effect of collision between signals sent from different vehicles, by estimating the other interfering signals, then subtract them from the desired one [111].

6. MIMO: SIC is used to remove co-channel interference in a layered space-time MIMO architecture, where the interference resulting from MIMO-

OFDM signals propagating in a multi-path environment [112] and from other transmitted antennas at the receiver [113] will be estimated and subtracted. For example, the authors in [114] use a soft SIC composed of a MAP detector and a turbo decoder, while in [104], a hard SIC is implemented to reduce complexity with minimal performance losses.

7. Non-linearities: SIC based on Volterra-series expansion is designed in [115] to cope with the ISI and non linearities resulting from the high power amplifier (HPA) used in satellite systems.

In this work, the design philosophy of the hard SIC may be viewed as a synthesis of the processes used in [104] and for convolutional coded SEFDM in [13]. The SIC is formed of an LDPC decoder generating soft LLR values for the encoded bits, which are used to generate, through mapping and ICI estimation processes, approximate ”replicas” of the received symbols. Thereafter, these approximated symbols in turn are used to cancel the interference, iteratively. The mathematical model of the suggested SIC is provided in detail later in this chapter, as a part of the implemented system model section. The following section gives an overview of DVB-S2 multi-carrier system and discusses how the introduction of SEFDM to such systems would be beneficial.

5.2 Applications on Satellite Systems

In DVB-S2 [116], VCM is commonly applied to optimise the spectral efficiency and provide different levels of error protection to different service components (e.g. SDTV and HDTV, audio, multimedia). Interference avoidance has been the dominant paradigm in the design of conventional satellite communication systems. Frequency division multiplexing (FDM) is used in the current DVB-S2 [116] and beyond the second generation (DVB-S2X) [117]. In such a system, multiple users (subcarriers) share the same transponder to enhance payload mass efficiency [118]. The number of subcarriers is limited to ($1 \leq N \leq 6$) per transponder and the subcarriers are shaped using a RRC filter with different roll-off factors ($0 \leq \beta \leq 1$) [119].

Fig. 5.1 depicts the normalised frequency spectrum of DVB-S2 transpon-

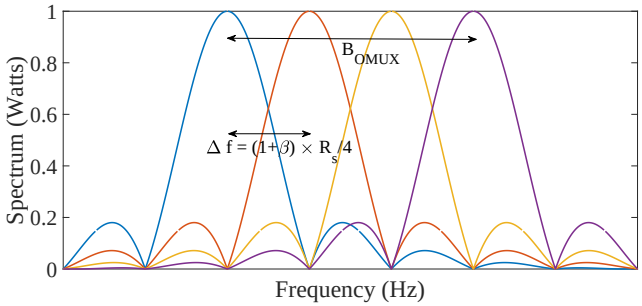

(a) RRC ($\beta = 0.25, \alpha = 1$) case.

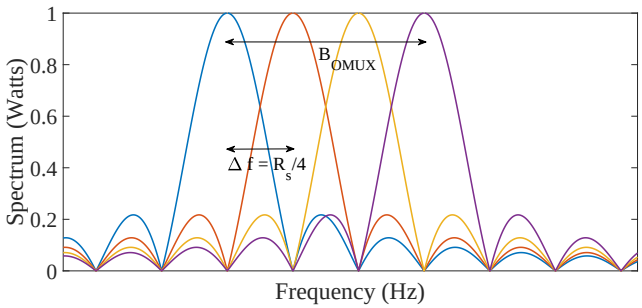

(b) OFDM ($\beta = 0, \alpha = 1$) case.

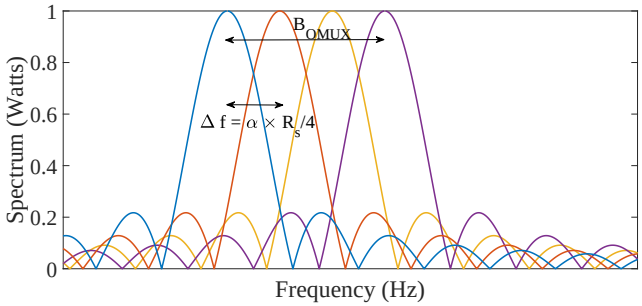

(c) SEFDM ($\beta = 0, \alpha = 0.8$) case.

Figure 5.1: DVB-S2 transponder for four carriers and different signals formats.

der, for the case $N = 4$ and the transponder bandwidth B_{OMUX}. In Fig. 5.1(a), to avoid ICI between the subcarriers and to ensure that a simple receiver structure can effectively recover the transmitted information, the frequency spacing is $\Delta f = (1+\beta) \times R_s/4$, where $\beta = 0.25$ and R_s is the symbol rate. RRC shaped carriers lead to a wider bandwidth when compared to OFDM ($\beta = 0$) for the same symbol rate, as shown in 5.1(b). Furthermore, RRC pulse shaping results in higher PAPR, but the OOBE decays at a faster rate than that of unshaped OFDM signals, resulting in lower interference between adjacent users.

SEFDM may serve the same purpose of enhancing the spectral efficiency for DVB-S2 systems by reducing the transponder required bandwidth, as demonstrated

in Fig. 5.1(c) for $\alpha = 0.8$. Improving the achievable spectral efficiency without increasing the constellation order can be considerably convenient, since it is well-known that low-order constellations are more robust to channel impairments, such as time-varying phase-noise and non-linearities [120]. The concept of packing the adjacent channels within a transponder beyond orthogonality was firstly introduced to satellite systems in 2002, where the spacing between the RRC subcarriers was reduced [121]. A SIC, similar to the one implemented for CDMA systems [102], was implemented to reduce the interference effect. Later, different methods were proposed purposely to deal with the ICI and non-linear interference in DVB-S2 systems. For instance, a Volterra filter, at the receiver, was implemented for two users (two RRC subcarriers) sharing the same transponder in [122]. Consequently, this Volterra filter was used either as a part of a SIC [123] or as a pre-distorter at the transmitter [118], for DVB-S2 systems with three or four subcarriers per transponder for further performance enhancement.

The spectral efficiency issue of DVB-S2 system attracted other non-orthogonal signalling formats. In [124], time packing, which is another term for Faster-than-Nyquist was studied. The resulting interference from time packing is reduced using either the soft-input soft-output Volterra-series expansion or an MMSE turbo equaliser [115]. However, results showed a no guaranteed spectral efficiency advantage of time packing with the aforementioned filters [124]. TFP is applied in [120], to maximize the spectral efficiency for a single-carrier-per-transponder DVB-S2/S2X system. The results show that even with a suboptimal detector, similar to [115], it is possible to achieve up to 40% spectral efficiency advantage.

In this Chapter, when SEFDM spectral efficiency and BER performance are examined, OFDM is the reference because SEFDM does not use any pulse shaping. DVB-S2/ DVB-S2X systems employing SEFDM may deliver broadcasting services over multiple transport streams, providing differentiated error protection (variable coding compression and modulation (VCCM) mode) to different service components (e.g. SDTV and HDTV, audio, multimedia). The lookup Table 5.1 (which may be stored in the memory of the transmitter) can be utilised to adjust the system

parameters according to a given service QI. In this work, the modulation and coding examined are taken from the satellite standards DVB-S2 [116] and DVB-S2X [117], where eight different coding rates (R_c) are used with two constellation (M) levels (QPSK, 8-PSK) and the use of seven SEFDM compression factors is further examined. Adapting the standard definition of spectral efficiency (η) bit/s/Hz [116], to account for the compression factor α, η becomes

$$\eta = \frac{\log_2(M) \times R_c \times R_s}{B_{OMUX}}, \tag{5.1}$$

where R_s is the symbol rate and $B_{OMUX} = (1+\beta) \times \alpha \times R_s$ is the output multiplexer (OMUX) bandwidth. SEFDM reduces the total occupied bandwidth, as shown in Fig. 5.1, or increases the throughput by increasing the number of users (subcarriers) per transponder. For example, if an SEFDM system with $\alpha = 0.8$ were to be used assuming the same coding and modulation order as in an OFDM system serving four users, then an SEFDM system would be capable of serving five users per transponder while maintaining the OFDM bandwidth or alternatively serve four users whilst saving 20% of the OFDM bandwidth. The second case is adopted in this work (i.e. the transponder bandwidth is adjustable).

Although this study focuses on optimising satellite systems spectral efficiency and assumes the system is operating in the linear region of the amplifier, it is important to emphasise the interesting results in [78], which shows that SEFDM exhibits lower PAPR compared to OFDM and that the PAPR of SEFDM decreases by increasing bandwidth compression. Thus, the possibility of SEFDM signal to reach the saturation region of the HPA is lower than that of OFDM signal and this is considered as an extra advantage for the use of SEFDM in satellite systems.

A question that may be raised is: Instead of bandwidth compression, why not increase M or reduce R_c to achieve a better spectral efficiency? To address this and validate the main argument of SEFDM employment and show its usefulness, extensive simulations are carried out for each group in Table 5.1 where the BER performance is compared to indicate the best VCCM. Four different signal groups are studied where, in each group, the SEFDM signal occupies smaller bandwidth

Table 5.1: Lookup table for mapping QI to compression factor, coding rate and modulation

Group (QI)	η (bit/s/Hz)	α	R_c	$\log_2(M)$
I	0.67	1.0	1/3	2
		0.75	1/4	2
II	1.8	1.0	9/10	2
		1.0	3/5	3
		0.67	3/5	2
III	2.25	1.0	3/4	3
		0.8	3/5	3
		0.89	2/3	3
		0.71	4/5	2
IV	2.7	1.0	9/10	3
		0.83	3/4	3
		0.67	3/5	3
		0.67	9/10	2

than that of an OFDM signal, therefore, the SEFDM and OFDM signals studied have the same spectral efficiency.

5.3 SEFDM DVB-S2X Transceiver System Model

5.3.1 Transmitter

Consider the SEFDM system architecture depicted in Fig. 5.2. At the transmitter, in the first stage, a stream of bits $\mathbf{b} \in \{0,1\}$ are encoded by the outer BCH encoder followed by an LDPC inner encoder. The BCH encoder is used to correct sporadic errors made by the LDPC decoder. The QI specified at the transmitter sets the code rate.

LDPC coding is a linear block channel coding technique. Gallager invented LDPC in 1962, during his doctoral studies [125], which was supervised by Elias, who invented convolutional coding [87]. However, the limitation in technology

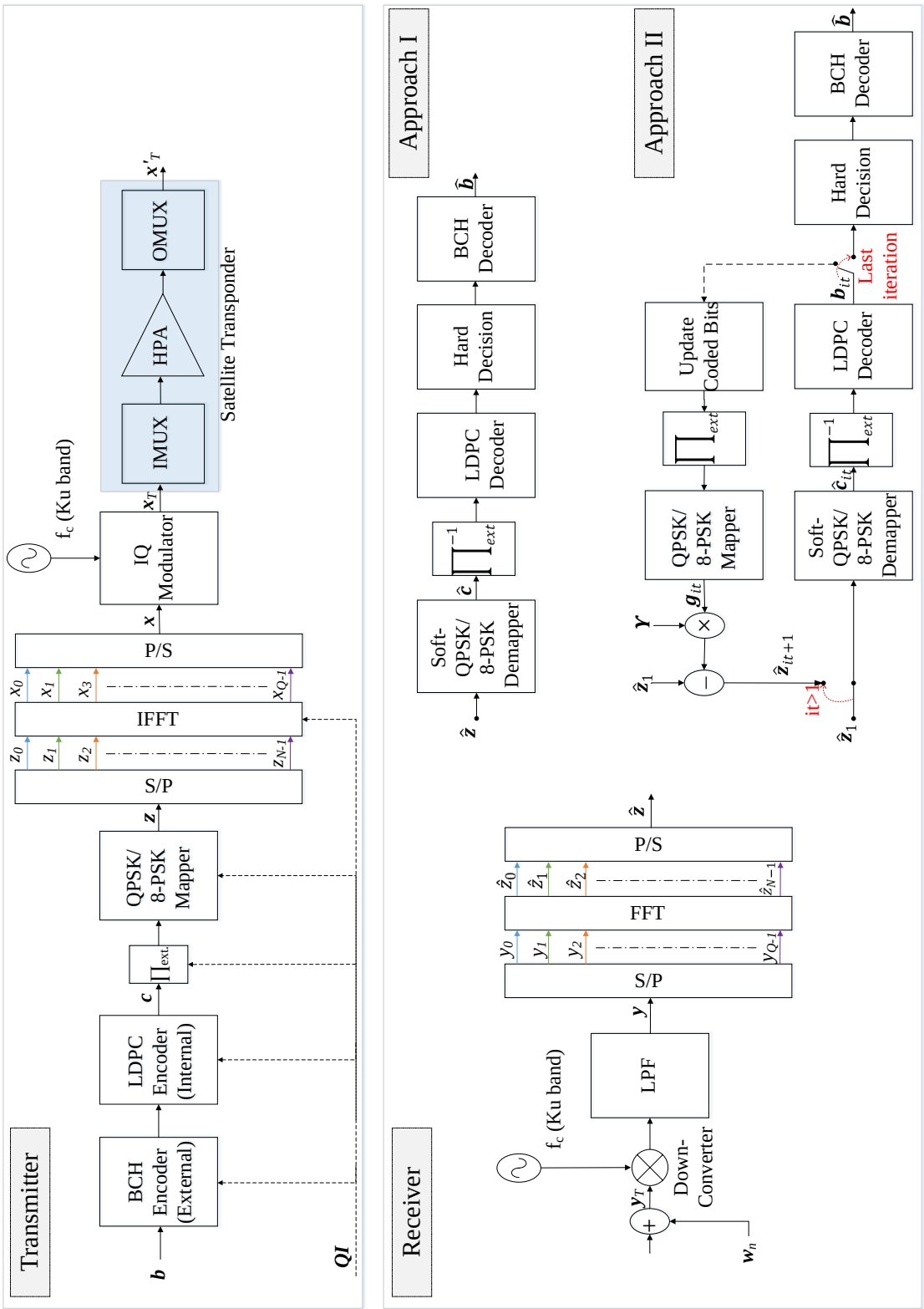

Figure 5.2: Transceiver block diagram.

by that time margined LDPC, and it only became well-known and used after the success of the iterative turbo decoding [87]. An LDPC encoder invokes multiplying by a sparse parity check matrix $\mathbf{H}_{(n_c-k_c)\times k_c}$, where each k_c bits are encoded to a codeword of size n_c bits [125]. There are two types of LDPC coding depending on the sparse matrix form; regular and irregular [87].

In DVB-S2, irregular LDPC coding is used, where for each code rate, a parity check matrix is specified. The output is always of size $n_c = 64,800$, while the length of the information bits (k_c) depends on the desired coding rate R_c [117].

The encoded bits $\mathbf{c} \in \{0,1\}$ are interleaved by an external block interleaver ($\prod_{\text{ext}}$) with equivalent size of 64,800 bits [116]. The interleaver ensures that the independence of $\mathbf{c}$ approximately holds for several turbo equalisation iterations at the receiver.

The encoded bits $\mathbf{c}$ of the baseband frame are then mapped. The QPSK/ 8-PSK mapper converts each $\log_2 M$ bits to a symbol z from the M-PSK symbol alphabet $Z = \{z_1, z_2, ..., z_M\}$, $z \in \mathbb{C}$. The mapping considered here is taken from the DVB standards [117] [116], with the symbol alphabet of zero mean ($M^{-1}\sum_{j=1}^{M} z_j = 0$) and unity energy ($M^{-1}\sum_{j=1}^{M} |z_j|^2 = 1$).

The mapped symbols sequence $\mathbf{z}$ is then divided into N parallel streams. In DVB-S2X, the maximum number of subcarriers per transponder is six [117]. These may be divided into filtered groups [119] or taken as one group of subcarriers [118], where four FDM subcarriers are used per transponder. Here, we adopt similar specifications to [118], with four subcarriers, but we apply OFDM and SEFDM modulation characteristics. Each parallel stream is modulated onto SEFDM subcarriers by means of an IFFT as shown previously in the SEFDM system model, where the QI defines the compression factor (α). The sampled parallel output of the IFFT is multiplexed to $\mathbf{x}$, up-converted to the Ku frequency band (f_c GHz) using the in-phase and quadrature components (IQ) modulator to obtain the bandpass signal given by

$$\mathbf{x}_T = \Re\{\mathbf{x}e^{j2\pi f_c t}\}. \tag{5.2}$$

Subsequently, the real modulated stream of the SEFDM symbols $\mathbf{x}_T$ goes through

the input multiplexer (IMUX) filter to select the desired group of N subcarriers and limit the interference with adjacent subcarriers. The IMUX output is then amplified by an HPA and finally, filtered again by the OMUX filter at the far end of the gateway to limit the interference to neighbouring subcarriers before $\mathbf{x}_T^{'}$ is transmitted over the satellite downlink channel.

In multi-carrier formats satellite-based physical layer modulation studies, the large scale variation and co-channel interference may be ignored since these are independent of the signalling format used [126] and with high power signal being sent along a line of sight channel, small signal variations are negligible as well. For simplicity, the HPA is assumed to operate in its linear region as assumed by other work of [121]. The IMUX, OMUX and HPA transfer characteristics are also assumed to be ideal, since the standards (H.7) in [116] consider linearised HPAs and a highly selective IMUX and OMUX filters. Hence, in this model, ICI and AWGN ($\mathbf{w}$) are the main distortions of the received signal $\mathbf{y}$. The full details of such impairments in SEFDM signals have been already explained in the SEFDM system model in Chapter 3.

5.3.2 Receiver

At the first stage of the receiver, shown in Fig. 5.2, the received bandpass signal $\mathbf{y}_T$ is down-converted to its baseband complex equivalent $\mathbf{y}$, using a down-converter and a low pass filter (LPF) combination. To obtain estimates $\hat{\mathbf{z}}$ of the transmitted symbols, demodulation of $\mathbf{y}$ is then performed using matched filters by means of an FFT. Subsequently, the symbols estimates will be used to detect the message transmitted. In the following, the design model of the two approaches implemented to remove ICI is detailed.

5.3.2.1 Matched filter:

The block diagram of approach I in Fig. 5.2, shows the design for a classical receiver. In the first stage, the estimated symbols $\hat{\mathbf{z}}$ are demodulated by employing an approximate LLR algorithm to obtain soft bit estimates $\hat{\mathbf{c}}$. Then, the soft bits are deinterleaved and the LDPC decoder decodes the deinterleaved soft bit values to

generate hard decisions. LDPC decoding is similar to that of turbo coding, where a belief propagation method runs iteratively until a valid codeword has been found, or a pre-determined maximum number of iterations is reached (50 iterations is the most common). In irregular LDPC coding, the bit nodes with high degrees (i.e. higher number of connections between bit and check nodes) collect more information from their connected check nodes while decoding, and they get corrected first after a small number of iterations. Then, they help the other bit nodes get corrected through iterative decoding [127]. Finally, the BCH decoder works on these hard decisions to create the final estimate of the received bits $\hat{\mathbf{b}}$.

5.3.2.2 SIC:

The receiver implementation is shown at the bottom of Fig. 5.2 (Approach II), where the feedback processes are shown in dashed lines. At the first iteration ($it = 1$), the initial estimate vector $\hat{\mathbf{z}}_1$ is the output of the FFT. The LDPC decoder is fed by soft bits $\mathbf{c}_{it}$ from the de-interleaver, where the index (it) indicates the iteration number. There are two outputs from the LDPC decoder; the soft LLRs of the encoded bits $\mathbf{c}_{it}$ used to update the encoded stream shown in the figure and the extrinsic LLR information (inside the LDPC decoder block and therefore not shown explicitly in the figure) that will be fed to the LDPC decoder as $a-priori$ information in the next iteration. The updated encoded stream is mapped again via QPSK/ 8-PSK mapper to $\mathbf{g}_{it}$. The new estimate $\mathbf{g}_{it}$ of the transmitted symbols is then used to cancel the interference. The non-diagonal elements of the cross correlation matrix Λ (discussed previously in Chapter 3 (3.7)) represent the ICI between subcarriers in SEFDM systems and can be expressed by the $N \times N$ interference canceller matrix Υ. This special matrix is generated by setting the diagonal of Λ to zeros as shown below

$$\Upsilon = \Lambda - \mathbf{I}_N, \tag{5.3}$$

where $\mathbf{I}_N$ is an $(N \times N)$ identity matrix. The resulting Υ is then multiplied by the estimated vector symbols $\mathbf{g}_{it}$ to evaluate the estimated ICI, given by the term $(\Upsilon \times \mathbf{g}_{it})$. The estimated ICI is subtracted from the initial estimates $\hat{\mathbf{z}}_1$, as stated in (5.4),

to give $\hat{\mathbf{z}}_{it+1}$, which forms the input to the next iteration.

$$\begin{aligned}\hat{\mathbf{z}}_{it+1} &= \hat{\mathbf{z}}_1 - \Upsilon\hat{\mathbf{g}}_{it} \\ &= \hat{\mathbf{z}}_1 - (\Lambda - \mathbf{I}_N)\hat{\mathbf{g}}_{it} \\ &= \hat{\mathbf{z}}_1 - \Lambda\hat{\mathbf{g}}_{it} + \hat{\mathbf{g}}_{it}.\end{aligned} \tag{5.4}$$

For clarification, consider the case of the first iteration, where the input to the SIC is the output of the receiver FFT $\hat{\mathbf{z}}_1$. By substituting $\hat{\mathbf{z}}_1$ in (5.4)

$$\hat{\mathbf{z}}_2 = \hat{\mathbf{g}}_1 + \Lambda(\mathbf{z} - \hat{\mathbf{g}}_1) + \Phi^{\mathrm{H}}\mathbf{w}. \tag{5.5}$$

The second term on the right hand side of (5.5) represents the difference between the actual interference and estimated interference, hence, if the SIC is converging properly, this term should become smaller after each iteration. After the last iteration, a hard decision is made on the output of the LDPC decoder and the BCH decoder in the final stage estimates the transmitted information bits $\hat{\mathbf{b}}$.

5.4 Results

In this section, simulated BER and constellation diagrams are generated for the case of DVB-S2/S2X TV broadcasting. The signal and system parameters used are shown in Table 5.2.

Table 5.2: Signal and system modelling parameters

Parameters	Value
Symbol rate	27.5 Msymbols/s
Symbol duration (T_s)	36.36 ns
SEFDM symbol size (N)	4
SEFDM symbol duration (T)	$N \times T_s$
Subcarrier Spacing	$\alpha/(N \times T_s) = \alpha \times 6.875$ MHz
Satellite transponder bandwidth	$\alpha \times 27.5$ MHz
Modulation format	QPSK; 8-PSK
Coding Rate	1/3; 1/4; 9/10; 3/5; 3/4; 2/3; 4/5
α	1; 0.75; 0.67; 0.8; 0.89; 0.71
LDPC decoder number of iterations	50
SIC number of iterations	1

5.4.1 Without SIC

Fig. 5.3 shows the BER results versus E_b/N_0 in dB, using the single-user matched filter receiver described previously with 50 LDPC decoder iterations for the different groups of Table 5.1. The minimum BER achieved in the simulations is 10^{-5}, which leads to almost free packet error rate (PER) [116].

In the simulations to follow, to allow fair comparison for given values of spectral efficiencies, both the bit rate and occupied bandwidth were adjusted for each group and the results are shown in Fig. 5.3. For clarity, the arrangement is held by subdividing the results according to the spectral efficiency (i.e. QI used), where the legend contains three values; α, R_c and $\log_2 M$, respectively. The first group ($\eta = 0.67$ bit/s/Hz) in Fig. 5.3(a) shows the advantage of using SEFDM with a lower coding rate rather than OFDM, as 0.8 dB power advantage is evident for the same BER performance, with a detector similar to what is typically used in multi-carrier satellite systems. This SEFDM scenario occupies 25% smaller bandwidth relative to an OFDM system with the same spectral efficiency.

The results of group II and III for higher values of η show that if the compression factor satisfies Mazo's limit (i.e. $\alpha \geq 0.8$), SEFDM slightly outperforms OFDM and with lower α there is no performance advantage of using SEFDM (e.g. Fig. 5.3(b)) in terms of power savings. Finally, for $\eta = 2.7$ bit/s/Hz for group IV in Fig. 5.3(d), the system becomes more prone to ICI, thus, for α less than Mazo's limit, the error floor is high and the system does not converge.

To conclude, in terms of power saving, SEFDM with a single-user matched filter receiver is beneficial but only for low η. To attain a system advantage, a more sophisticated receiver is required. Consequently, the SIC, discussed above, is implemented and examined in the following section.

5.4.2 With SIC

The constellation diagrams of Fig. 5.4 prove the capability of the SIC in reducing the ICI with only one turbo equaliser iteration for the case of $\alpha = 0.8$. The first column is for the case of QPSK, where the SEFDM constellation of (b) turns into (c) after one iteration and this constellation is similar to the interference-free case

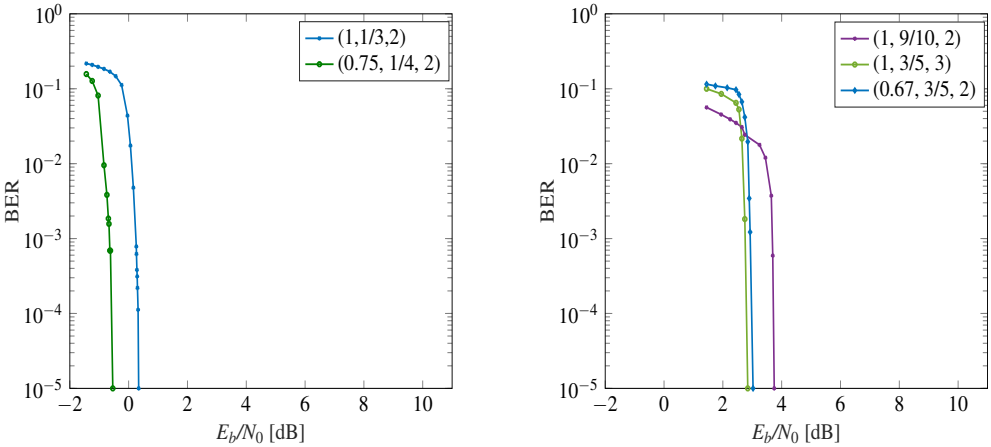

(a) Group I: $\eta = 0.67$ bit/s/Hz **(b)** Group II: $\eta = 1.8$ bit/s/Hz

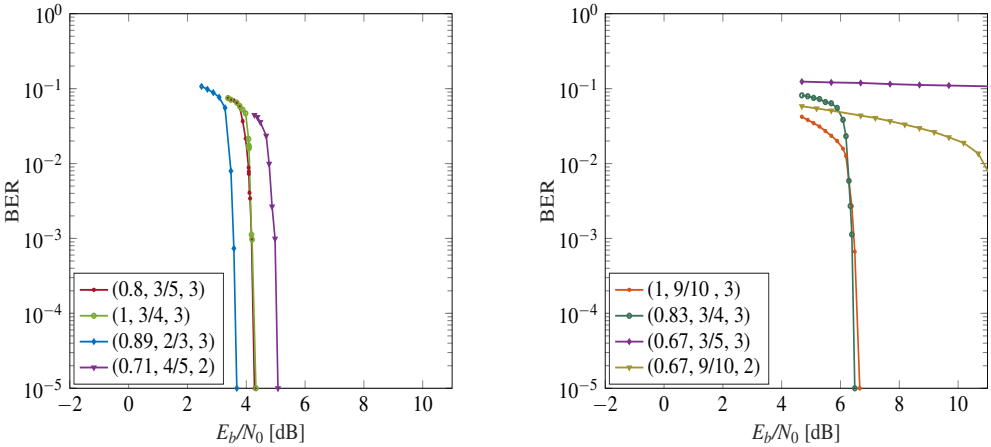

(c) Group III: $\eta = 2.25$ bit/s/Hz **(d)** Group IV: $\eta = 2.7$ bit/s/Hz

Figure 5.3: SEFDM system BER performance for the different QI groups with matched filter receiver design and different VCCM parameters (α, R_c, $\log_2(M)$).

of OFDM (a). The same can be observed with the second column of Fig. 5.4 for the 8PSK case.

The system advantage of using SIC becomes even more apparent when considering the BER performance for SIC approach, which is tested for the same parameters of matched filter approach and results are shown in Fig. 5.5. The advantage of SEFDM over OFDM with one SIC iteration for the same η is clear for the four different groups. SEFDM saves bandwidth compared to OFDM and requires less power while maintaining the same BER performance. For instance, a 33% bandwidth and 2.8 dB power savings are guaranteed for group IV ($\eta = 2.7$ bit/s/Hz). However, no enhancement is gained without a pay-off and, in this case, it is the increase in detector complexity compared to the matched filter approach.

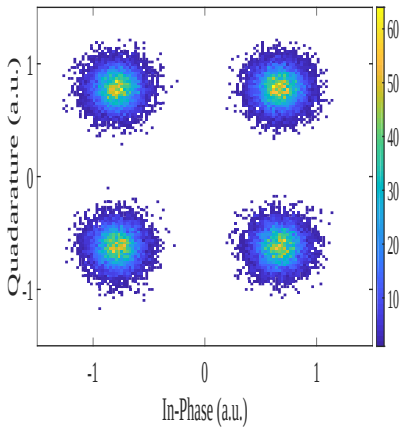

(a) QPSK OFDM

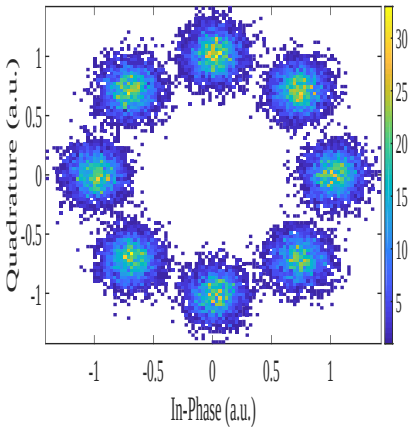

(d) 8PSK OFDM

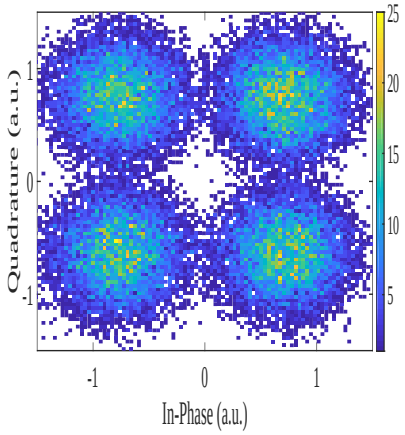

(b) QPSK SEFDM (before SIC)

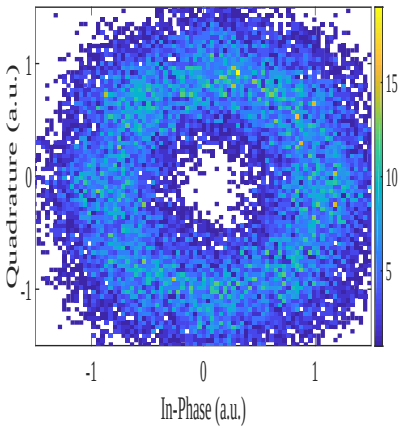

(e) 8PSK SEFDM (before SIC)

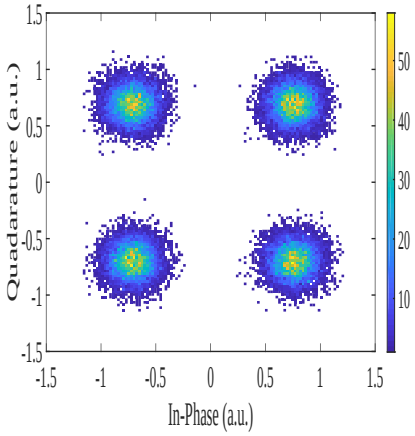

(c) QPSK SEFDM (after SIC)

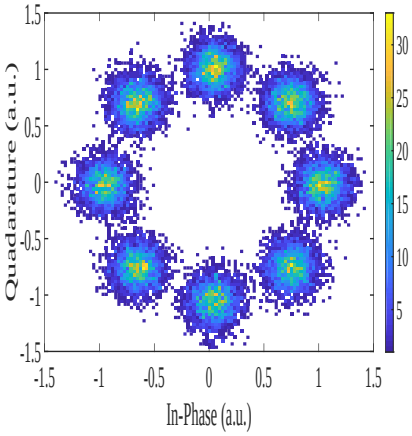

(f) 8PSK SEFDM (after SIC)

Figure 5.4: The constellation diagrams for the received QPSK/ 8PSK symbols (a) & (d) OFDM, (b) & (e) SEFDM ($\alpha = 0.8$) before SIC iteration and (c) & (f) SEFDM ($\alpha = 0.8$) after one SIC iteration.

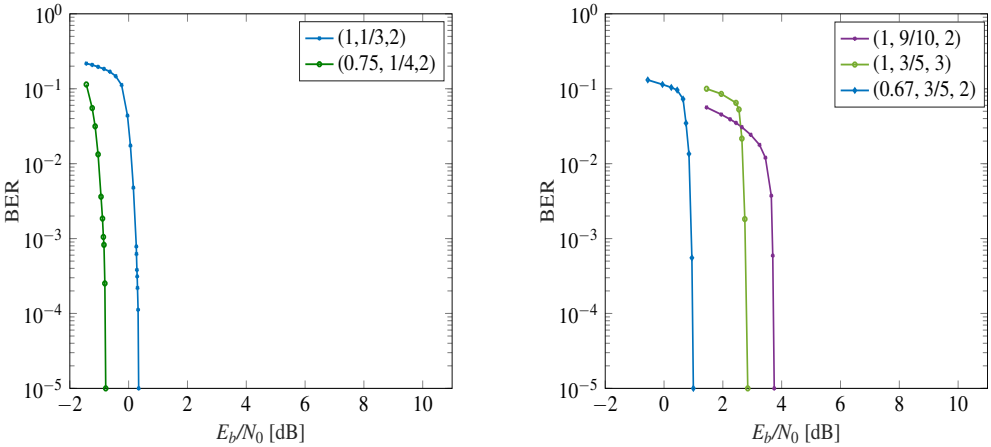

(a) Group I: $\eta = 0.67$ bit/s/Hz **(b)** Group II: $\eta = 1.8$ bit/s/Hz

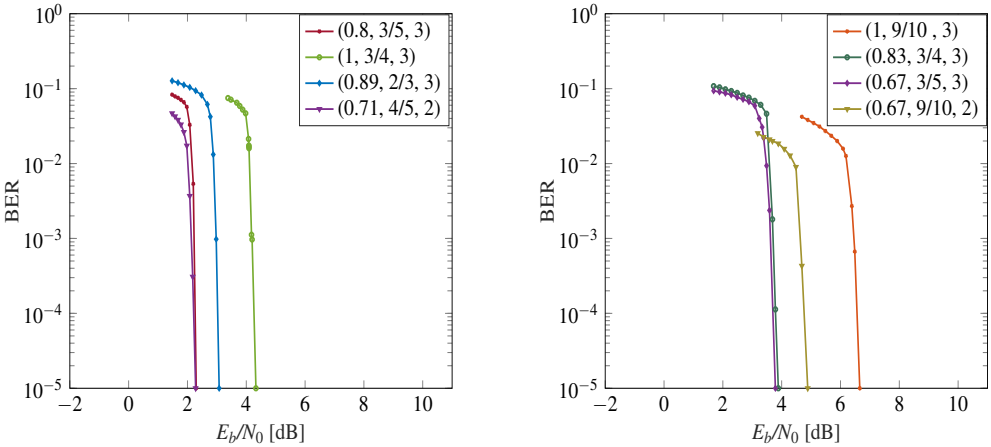

(c) Group III: $\eta = 2.25$ bit/s/Hz **(d)** Group IV: $\eta = 2.7$ bit/s/Hz

Figure 5.5: SEFDM system BER performance for the different QI groups with SIC receiver design and different VCCM parameters (α, R_c, $\log_2(M)$).

The results reported here are based on system parameter adjustments to effect the same spectral efficiency values, in other words the number of subcarriers was the same for all experiments ($N = 4$) but the bandwidth and information bit rates were changed to maintain equal values of η. It is worth noting that the advantages of SEFDM can be also demonstrated when comparing systems of the same bandwidth, where the number of SEFDM subcarriers is increased relative to that of an OFDM system of the same spectral efficiency. For such scenarios, the number of required iterations will be increased but the error rates will be the same as those of Fig. 5.5.

5.5 Conclusions

This chapter discusses new system design to increase the spectral efficiency of high spectral efficiency satellite communication systems through the employment of a finite constellation SEFDM signals, coupled with LDPC channel coding and advanced interference cancellation processing via SIC turbo equalisation system. A special case for DVB-S2 is considered, where SEFDM provides more degrees of freedom to optimise the system, compared to orthogonal signals, by using VCCM.

In addition to the original single-user matched filter receiver with soft demapping (approach I), a turbo equaliser based on SIC (approach II) has been developed. The second approach overcomes the ICI problem and ameliorates ICI effects by subtracting the interference gradually.

BER performance analysis, obtained by system modelling and computer simulations, provide significant insight to these two approaches. A fair comparison is held by amending the bandwidth and information bit rates of SEFDM and OFDM signals to maintain the same spectral efficiency. Results show that SEFDM saves bandwidth compared to OFDM and requires less power while preserving the same BER performance. For high spectral efficiency values, interference cancellation becomes necessary to gain the predicted SEFDM advantages. For this purpose, the SIC method proposed shows its capability of reducing interference even with only one iteration.

SEFDM can be beneficial in another scenario, where the number of SEFDM subcarriers per transponder increases to maintain OFDM bandwidth rather than saving bandwidth for the same OFDM spectral efficiency. For such scenarios, the number of required iterations will be increased when the system is operating at relatively high spectral efficiency values, but for the same BER performance.

The analyses presented in this work allows the choice of an appropriate equalisation method for the given scenario. Our studies show that SIC is the most suitable method, as SIC is based on simple mathematical subtraction operation. Although there are compromises in terms of additional receiver complexity and added latency due to the iterations, the results of this work indicate possible new system design

directions to improve further the spectral efficiency beyond what is used in today's FDM based DVB standards.

The work done in this chapter may be further extended to account for non-linearities introduced by the HPA. This is essential to show the PAPR advantage of SEFDM besides BER performance. Finally, the recent work in [128], introduced a new layer of multi-carrier modulation to satellite systems, where each user within a transponder is an OFDM signal instead of a conventional single-carrier signal. This introduces a new potential for SEFDM to enhance future satellite systems spectral efficiency, where each sub-channel within a transponder is an SEFDM signal.

Chapter 6

Robust Channel Estimation and Application to 5G New Radio

When a signal propagates through a multipath channel, it will be impaired by the channel effects, which varies according to the type of the channel encountered. Usually, an equaliser is used at the receiver, to compensate for the channel effects. To do so, a knowledge of the channel state information (CSI) is required and such knowledge is typically acquired by performing channel estimation.

In general, channel estimation is a topic extensively researched for OFDM systems, while most published research articles on non-orthogonal signals assume a perfect knowledge of the channel. Channel estimation may be a hindrance to SEFDM signals practicability, considering the compressed subcarriers feature. Thus, it is essential to consider channel estimation methods and to realise their effects on system performance.

In a multi-carrier signal transmission, the channel estimation is processed either in the time domain or the frequency domain. For a time-varying frequency selective channel, time domain channel estimation is proved to perform better than frequency domain [129]. However, time domain estimation suffers from cubic complexity growth, because it requires matrix inversions and this is a burden that limits its practical utilisation. The matrix size depends on the OFDM symbol size and the number of channel delay taps (i.e. the number of paths the signal propagates through in a multipath channel) [86]. This limitation was among the main reasons of OFDM

adoption in current communication systems, as it allows a simple yet accurate estimation and equalisation of channel effects in the frequency domain. However, in SEFDM, the dual distortion of non-orthogonality interference and multipath channel effects compounds the difficulty and reduces the accuracy of channel estimation relative to those of OFDM systems.

This chapter explains the structure of the SEFDM signals in the time domain to design a novel frequency domain channel estimation scheme for SEFDM signals. The proposed scheme is distinguished by its simplicity, low computational complexity and high accuracy. Owing to the explicit benefit of the proposed frequency-domain channel estimation scheme, any substantial increase in the system complexity is not imposed regardless of the SEFDM compression factor and number of channel taps. In order to provide further insights, the proposed estimation scheme efficacy is assessed by evaluating its: *i*) estimation accuracy; *ii*) computational complexity; *iii*) pilot generation and *iv*) the application of the new estimation scheme to 5G new radio (NR) framework to enhance its spectral efficiency. The development of this new estimation scheme has also brought forward an issue not studied before about the generation of continuous CP for SEFDM.

The outline of this chapter is: Section 6.1 summarises the developed time domain channel estimation schemes for non-orthogonal signals. In section 6.2, the current frequency domain channel estimation schemes for non-orthogonal signals are outlined and the novelty of the developed work here is highlighted. Section 6.3 demonstrates a mathematical model of SEFDM transmission over multipath frequency selective channels. Section 6.4 describes two frequency domain channel estimation schemes, while section 6.5 introduces the scheme developed as part of this work. To justify the proposed scheme efficiency, section 6.6 compares the complexity and performance of the different frequency estimation schemes. Thereafter, section 6.7 describes a simulation study of the application of the developed scheme to SEFDM 5G new radio (NR) frames, before conclusions are drawn in section 6.8.

6.1 Time Domain Estimation Schemes

In time domain channel estimation schemes, a burst of transmitted symbols are dedicated to convey a pre-determined pilot sequence. The receiver works out the channel response based on the received signal and the knowledge of the pilots used [8].

Two time domain channel estimation schemes for SEFDM systems were developed in [15] to estimate the CSI circulant matrix coefficients. In the first scheme, an SEFDM symbol carrying the pilot signals is transmitted, while in the second scheme, the pilot signals modulate a pre-defined mutually orthogonal subset from the SEFDM symbol to reduce the ICI effect [15]. Both estimation schemes proved to be reasonably accurate, however, their complexity is impractical because they require matrix inversion. For example, the SEFDM transmission over the static 60 GHz radio over fiber experiment in [71], utilised the former estimation scheme, given the fact that the channel was static and the estimation process was done off-line.

Another time domain channel estimation scheme was designed explicitly for SEFDM visible light communication (VLC) systems in [82]. This scheme, termed recursive least square (RLS), recursively finds the filter coefficients that minimize a weighted linear least square cost function related to the input signals [130]. Again, the limitation of this scheme is in its complexity, as the training symbols have to go through multiple iterations (1,000 in this experiments) to achieve a reasonably accurate estimation.

As verified in the previous chapter, the iterations between the detector and the decoder in the SIC result in more accurate estimates of the transmitted signal, when compared to other suboptimal receivers. This conclusion led researchers to apply an iterative channel estimation and decoding process. Recently, a joint iterative time domain channel estimation and decoding scheme is proposed for FTN systems in [131]. The advantage of this scheme is in reducing the number of pilot symbols and enhancing the estimation accuracy. However, the complexity of this scheme is dominated by multiple matrix inversions in each iteration, where the matrix size

depends on the length of FTN-induced ISI considered at the receiver and the number of channel taps (channel length). The complexity is even higher, given the iterations between the channel estimator and the decoder [131]. To conclude, an iterative time domain estimation scheme is impractical when dealing with non-static or fast fading channels. If the channel time variance is faster than the channel estimation process, then the estimation accuracy will get worse.

6.2 Frequency Domain Estimation Schemes

To estimate the channel in the frequency domain, pilot symbols are sent at predefined frequencies to determine the channel response at such frequencies [8].

For single-carrier FTN systems, a joint iterative channel estimation and equalisation scheme in the frequency domain is proposed in [132]. If this scheme is implemented for a coded FTN system, then three decoders exchanging information in each iteration are required. Although the estimation accuracy is enhanced gradually in each iteration, the complexity and delay due to the estimator iterative nature limit the scheme practicality, which is a similar problem to the limitation of the time domain iterative scheme of [131].

To allow using the existing OFDM frequency domain channel estimation scheme for non-orthogonal signals, the concept of dividing the transmitted signals into orthogonal and non-orthogonal multiplexing regions was firstly proposed in [133]. In this work, to enhance the LTE system spectral efficiency, the information signals are FTN OFDM/ O-QAM while the pilot signals are multiplexed in the orthogonal region to decrease the ISI and ICI incurred from the FTN signalling to a very low level. The same concept was followed in the 24 Gbps SEFDM signals coherent optical transmission experiment reported in [16], where the transmitted block is divided into orthogonal and non-orthogonal multiplexing regions. The orthogonal region is used specifically for channel estimation based on LS [16]. However, in this work interpolation is required, which increases the estimation complexity and reduces its accuracy [16]. Section 6.6 evaluates the complexity and performance of this scheme.

A new frequency domain channel estimation scheme is developed to allow a real-time accurate channel estimation for SEFDM systems. In this scheme, the pilot symbols, in the orthogonal region, use the same number of subcarriers and the same frequency spacing of SEFDM signals used to transmit data, while maintaining the orthogonality. As a result, a simple and accurate channel estimation is guaranteed at the expense of slightly increased pilot duration overhead [21].

In the meantime, [134] and [135] were published along the lines of the aforementioned idea. In [134], the authors implemented an estimation scheme termed robust channel processor (RCP), which uses OFDM pilot symbols to estimate the channel frequency response (CFR). The implemented scheme is applied to an experimental FTN non-orthogonal FDM VLC testbed and managed to transmit data at 1.76 Gbps rate over 2 m free-space transmission [134]. The work of [135], uses OFDM training pilot symbols to estimate the channel in an SEFDM LTE like system.

Against this background, the novelty of the work developed as part of this PhD and presented in [21], [24] and this chapter, are as follows:

1. The structure of SEFDM signal in the time domain, which led to developing the proposed scheme, is explained.

2. The estimation accuracy of the proposed scheme is compared to the other frequency domain channel estimation schemes.

3. The computational complexity of the proposed scheme is compared to the other frequency domain channel estimation schemes.

4. The generation of the pilot symbol for the proposed scheme is explained, where the IFFT used to generate the data SEFDM symbols, generates the pilot symbol too.

5. Based on the structure of SEFDM signal in the time domain, an explanation of the proper generation of continuous CP for SEFDM signals is given.

6. The efficiency of the proposed scheme is validated by applying it to a 5G NR framework and compare its error results and throughput to a 5G OFDM based system.

6.3 SEFDM Signals Over Multipath Channels

In this thesis, up to this point, SEFDM signals transmission was modelled for AWGN channels only. In this section, a mathematical model of SEFDM transmission over multipath frequency selective channel is demonstrated. It should be noted that some of the upcoming equations were previously introduced in SEFDM system model in Chapter 3, but repeated here for ease of reference. An SEFDM-modulated symbol is expressed as

$$x_k(t) = \sum_{n=0}^{N-1} z_{k,n} \exp(2\pi jn\alpha\Delta f(t-kT)), \tag{6.1}$$

where $\mathbf{z} \in \mathbb{C}^{N\times 1}$ are a complex QAM baseband symbol of duration T_s, N denotes the number of subcarriers, $z_{k,n}$ is the QAM symbol modulated by the n^{th} subcarrier, $T = N \times T_s$ is the SEFDM signal duration and $\Delta f = 1/T$ is the orthogonal frequency spacing between subcarriers and $\alpha \in (0,1]$ is the compression factor. If the signal in (6.1) were to be transmitted over a frequency-selective multipath channel of L paths, the received signal can be expressed as

$$y_k(t) = \sum_{L} \gamma_l x_k(t-\tau_l) + w_k(t), \tag{6.2}$$

where γ_l, τ_l are the complex amplitude and delay of the l^{th} path, respectively. w_k is the AWGN.

At the receiver, the estimated symbol at the n^{th} subcarrier $\hat{z}_{k,n}$ affected by the channel and contaminated by interference resulting from the non-orthogonal nature

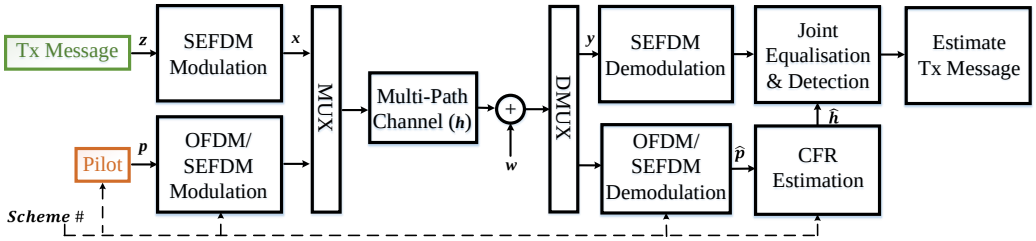

Figure 6.1: Transceiver block diagram.

of the SEFDM signal can be expressed as

$$\begin{aligned}\hat{z}_{k,n} &= y_k(t)\exp(-2\pi jn\alpha\Delta ft)\\ &= \sum_{L}\gamma_l[\sum_{m=0}^{N-1} z_{k,m}\Lambda(m,n)\times\exp(-2\pi jm\alpha\Delta f(kT+\tau_l))]+w_k(t)\exp(-2\pi jn\alpha\Delta ft)\\ &= \sum_{m=0}^{N-1} z_{k,m}h_{k,m}\Lambda(m,n)+w_k(t)\exp(-2\pi jn\alpha\Delta ft),\end{aligned} \tag{6.3}$$

where $h_{k,m}=\sum_L \gamma_l\exp(-2\pi jm\alpha\Delta f(kT+\tau_l))$ is the multi-path CFR acting on the m^{th} subcarrier of the k^{th} SEFDM symbol and $\Lambda(m,n)$ is the cross correlation between the subcarriers m and n represented earlier in (3.7).

A high level transceiver design is shown in Fig. 6.1, to give a general idea about CFR estimation for SEFDM signals over a multipath channel. In this work, a CP of sufficient length is added to validate the assumption of null ISI between adjacent SEFDM symbols.

It is convenient to describe the transceiver process in the digital domain through a linear model. A demodulated SEFDM symbol $\hat{\mathbf{z}}_k$ from (6.3) can be expressed in a matrix form as

$$\hat{\mathbf{z}}_k = \Lambda\mathbf{H}_k\mathbf{z}_k+\Phi^{\mathrm{H}}\mathbf{w}_k, \tag{6.4}$$

where $\hat{\mathbf{z}}_k$, $\mathbf{z}_k$ and $\mathbf{w}_k$ are $\mathbb{C}^{N\times 1}$ vectors of the k^{th} demodulated, transmitted baseband symbols and the white noise, respectively. $\mathbf{H}_k\in\mathbb{C}^{N\times N}$ is a diagonal matrix, where its diagonal element $H_{n,n}$ is the CFR coefficient on the n^{th} subcarrier of the SEFDM signal and $\Lambda\in\mathbb{C}^{N\times N}$ is the subcarriers correlation matrix.

Let $\mathbf{p}\in\mathbb{C}^{N\times 1}$ be the pilot symbol with the same characteristics of $\mathbf{z}$. Then,

from (6.4), the demodulated pilot may be presented as

$$\hat{\mathbf{p}} = \Lambda \mathbf{h} \odot \mathbf{p} + \mathbf{w}, \tag{6.5}$$

where $\odot$ denotes element-wise multiplication and $\mathbf{h}$ is the diagonal of $\mathbf{H}$.

6.4 Modelling and Analysis of Existing Frequency Domain Estimation Schemes

In this section, two existing frequency domain channel estimation schemes are discussed and a newly developed one is introduced and explained afterwards. Scheme I is based on the time domain channel estimation scheme of [15], but is implemented here in the frequency domain instead. Scheme II is similar to the estimation scheme of the optical experimental work of [16].

6.4.1 Scheme I: Interpolated Partial Channel Estimation

Partial channel estimation (PCE) is based on the observation that there are subsets within the SEFDM subcarriers that can be mutually orthogonal. For $\alpha = b/c$ where $b, c \in \mathbb{Z}$, $b < c$, $N > c$, there are $\lceil N/c \rceil$ mutually orthogonal subcarriers ($|\Lambda_{m,n}| = 0$) for $\alpha(m-n) \in \mathbb{Z}$, where $\lceil . \rceil$ is the ceiling function [15]. A visual representation of this scheme is given in Fig. 6.2, for $N = 16$ and $\alpha = 0.8$. From the figure, the pilot symbol consists of a subset of $\lceil 16/5 \rceil = 4$ mutually orthogonal subcarriers, located at the frequencies $(0, 4\Delta f, 8\Delta f, 12\Delta f)$. Another subset may be used, as long as the subcarriers are orthogonal. Thus, the pilot is sent only over the mutually orthogonal subcarriers while the rest of the subcarriers are unmodulated during pilot transmission. This type of arrangement overcomes the SEFDM ill-conditioning problem [15], as the condition number of its correlation matrix Λ increases by reducing α and/or increasing N.

The first step to estimate the channel via PCE is LS estimation. Thereafter, the CFRs over the rest $N - \lceil N/c \rceil$ subcarriers are interpolated. For simplicity, linear interpolation is used. Algorithm 1 summarises the PCE algorithm for CFR estimation, where $f(p)$ is the frequency of the subcarrier modulated by the pilot p.

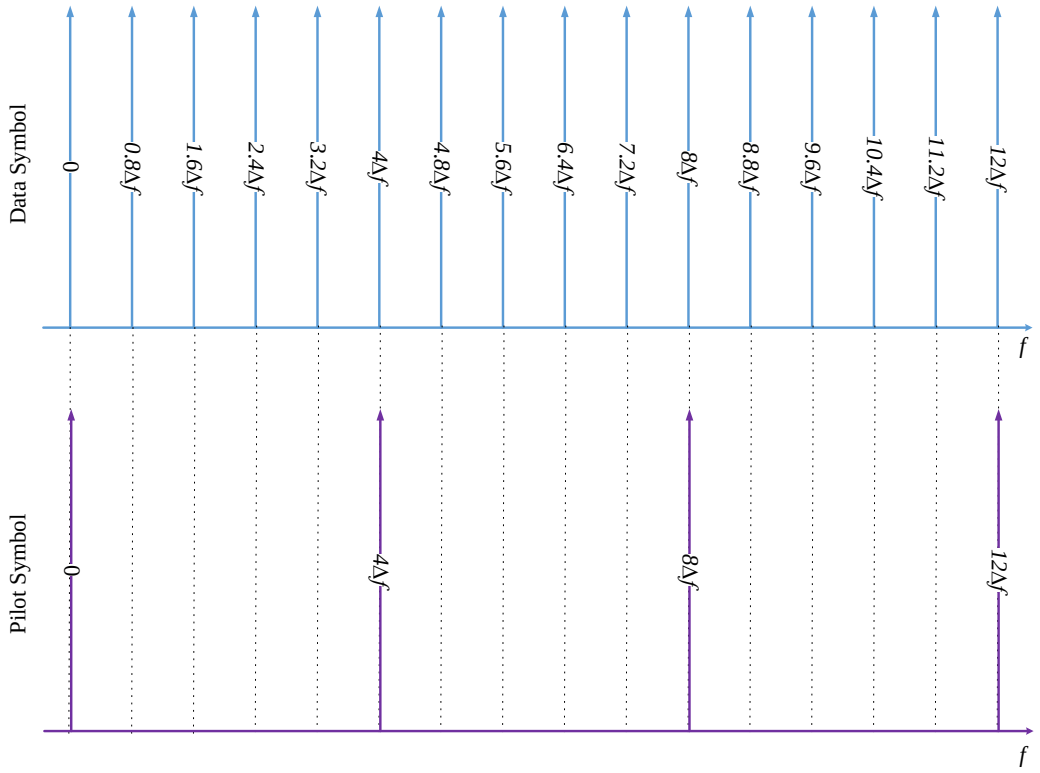

Figure 6.2: A graphical representation of scheme I pilot design for $N = 16$, $\alpha = 0.8$.

Algorithm 1 Scheme I: PCE

Input: $(N, \mathbf{p}, \hat{\mathbf{p}}, c)$
Output: CFR $(\hat{\mathbf{h}})$

for $i = 0 : N-1$ **do** {Receiver}
  if $\alpha \times i \in \mathbb{Z}$ **then** {LS}
    $\hat{h}_i = \hat{p}_i / p_i$
  end if
end for
for $i = 1 : \lfloor N/c \rfloor$ **do**
  $\vartheta(i) = \frac{\hat{h}(p(i\times c)) - \hat{h}(p((i-1)\times c))}{f(p(i\times c)) - f(p((i-1)\times c))}$ {Slope between two pilots}
end for
for $i = 1 : \lfloor N/c \rfloor$ **do** {Linear interpolation}
  $p_o = p((i-1)\times c)$, $\hat{h}_o = \hat{h}(p_o)$
  for $j = (i-1)\times c + 1 : (i\times c) - 1$ **do**
    $\hat{h}_j = \vartheta(i) \times (f(j) - f(p_o)) + \hat{h}_o$
  end for
end for

6.4.2 Scheme II: OFDM Pilots with Interpolation

Another way to solve the SEFDM ill-conditioning problem is using an OFDM pilot, as in [16]. SEFDM packs more subcarriers in the same bandwidth relative to OFDM. Thus, for the OFDM pilot, in order to occupy the same bandwidth as SEFDM, the number of subcarriers of the OFDM pilot (N_p) for a specific α is given by

$$N_p = \lceil \alpha \times N \rceil, \tag{6.6}$$

where the transmitted OFDM pilot can be presented as

$$p(t) = \sum_{n=0}^{N_p-1} p_n \exp(2\pi jn\Delta ft). \tag{6.7}$$

For $\alpha = b/c$ where $b, c \in \mathbb{Z}$, $b < c$, $N > c$, there are $\lceil N/c \rceil$ subcarriers out of N_p

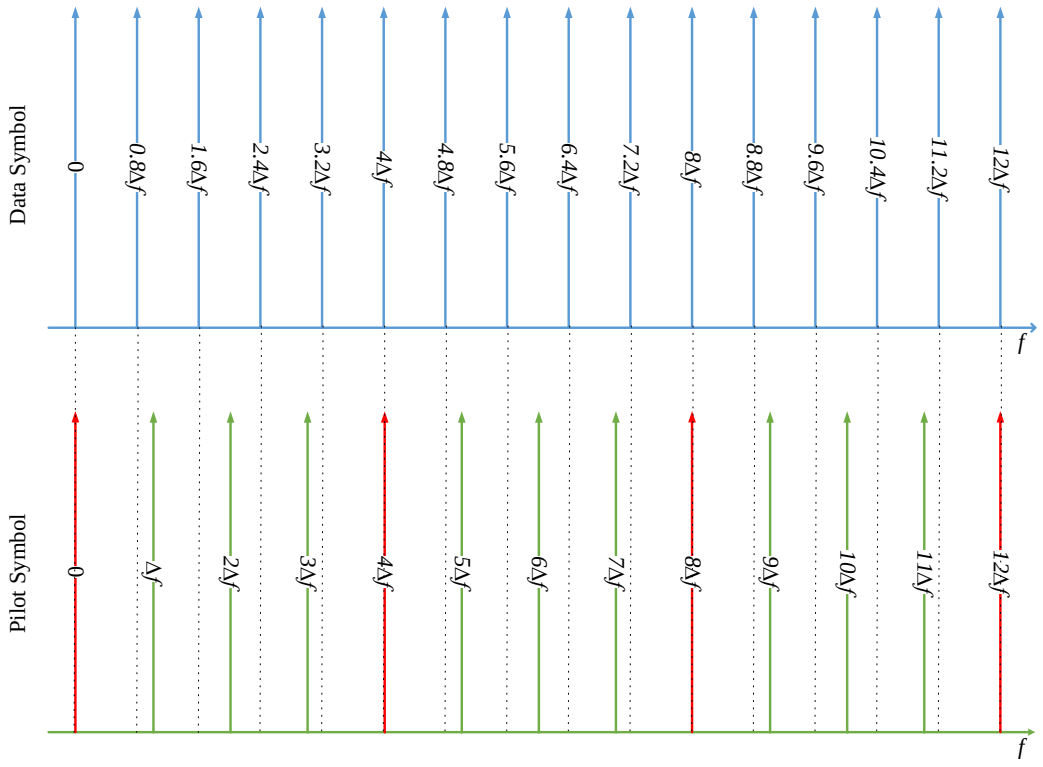

Figure 6.3: A graphical representation of scheme II pilot design for $N = 16$, $\alpha = 0.8$.

subcarriers with an integer multiple of $(\alpha\Delta f)$. Hence, the CFRs on these subcarriers can be found directly by LS estimation. Thereafter, the CFRs on the rest $N - \lceil N/c \rceil$

are obtained through interpolation. A graphical illustration of this scheme is demonstrated in Fig. 6.3 for $N = 16$, $\alpha = 0.8$ and $N_p = 13$ according to (6.6). The figure shows the $\lceil 16/5 \rceil = 4$ pilot subcarriers aligned with the subcarriers of the SEFDM symbol at the frequencies $(0, 4\Delta f, 8\Delta f, 12\Delta f)$. These subcarriers do not require interpolation, while linear interpolation will be required to estimate the CFR on the rest of the subcarriers. Algorithm 2 summarises Scheme II for CFR estimation. Next, the new channel estimation scheme developed here and published in [21] is introduced and discussed.

Algorithm 2 Scheme II: OFDM Pilots with Interpolation

Input: $(N, N_p, \mathbf{p}, \hat{\mathbf{p}}, \alpha)$
Output: CFR $(\hat{\mathbf{h}})$
for $i = 0 : N_p - 1$ **do** {LS}
  $\hat{r}_n = \hat{p}_n / p_n$
end for
for $i = 0 : N - 1$ **do**
  if $i/c \in \mathbb{Z}$ **then**
    $\hat{h}_i = \hat{r}(i \times \alpha)$ {No interpolation}
  else
    $g = \lfloor \alpha \times i \rfloor$ {Linear interpolation}
    $\hat{h}_i = \hat{r}(g) + \frac{\hat{r}(g+1) - \hat{r}(g)}{f(g+1) - f(g)} (f(i) - f(g))$
  end if
end for

6.5 Modelling and Analysis of a New Frequency Domain Estimation Scheme (III)

The previous method of OFDM pilot utilization shows the advantage of solving the SEFDM ill-conditioning problem. However, the required frequency-domain interpolation results in an increase in the estimation scheme complexity and a dependency on α.

To overcome the interpolation drawback, the main challenge is to have an OFDM pilot symbol that occupies the same bandwidth of the SEFDM information symbols in (6.1), with the same number of subcarriers N and frequency separation. These requirements, if satisfied, result in estimating the channel directly via LS

without interpolation as given below

$$\hat{\mathbf{h}} = \hat{\mathbf{p}}./\mathbf{p}, \tag{6.8}$$

where $./$ denotes an element-wise division. Hence, to maintain the orthogonality of the pilot with a subcarreirs separation $\Delta f = \alpha/T$, the OFDM pilot symbol duration (T_p) increases by a factor of $(1/\alpha)$, such as $T_p = T/\alpha$.

To have better understanding, Fig. 6.4 compares an OFDM pilot of duration T_p, with an SEFDM information symbol of duration T for the case of $\alpha = 0.8$. This figure presents the real part of the first three subcarriers $\{f_n = 0, \Delta f, 2\Delta f\}$ in

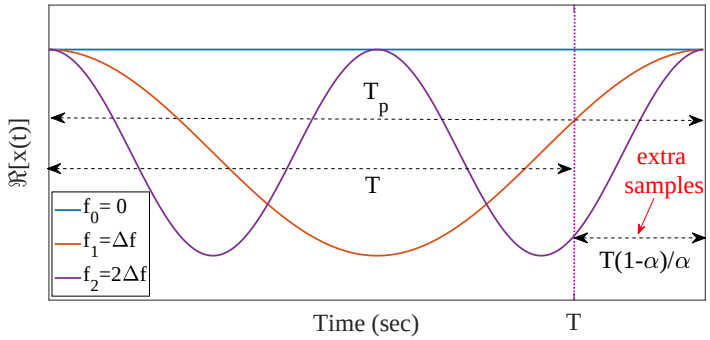

Figure 6.4: The real part of $x_k(t)$ in the time domain for $f_n = 0, \Delta f, 2\Delta f$ with $\alpha = 0.8$.

(6.1). Clearly, unlike SEFDM, the OFDM pilot has to maintain an integer number of cycles to preserve its orthogonality. Therefore, to complete a cycle, extra samples to cover the $T(1-\alpha)/\alpha$ overhead are needed, resulting in an extended pilot symbol period.

The added redundancy of this scheme compared to others depends on how frequently the pilot is sent. For instance, if the pilot is sent every G information symbols, then, the added redundancy is $((1-\alpha)/(G+1)) \times 100\%$. In the following discussion, and for the purpose of illustrating the utility of this new channel estimation scheme, two scenarios for slow varying or static channels, where a pilot symbol is sent ahead of information symbols, are presented. For fast varying channels, the same technique may be applied but with more frequent pilot transmission, in line with other mobile system practices.

6.6 Comparative Study of Schemes Performance & Complexity

Based on (6.5) and the algorithms discussed above, the received pilot symbol $\hat{\mathbf{p}}$ is used to calculate the estimated CFR $\hat{\mathbf{h}}$. Thence, $\hat{\mathbf{h}}$ is used to equalise the channel effects on the SEFDM information symbols via a joint equalisation and detection method similar to that implemented in Chapter 4 and 5. In this following, mean square error (MSE) is used to evaluate the performance of the schemes considered. MSE is given by

$$\text{MSE} = \mathbb{E}\{[\hat{\mathbf{h}} - \mathbf{h}]^{\text{H}}[\hat{\mathbf{h}} - \mathbf{h}]\}, \tag{6.9}$$

where $\mathbb{E}[\cdot]$ is the expectation operator and $(\cdot)^{\text{H}}$ is the Hermitian operator. In the simulation study, the effects of the following system parameters are considered:

1. Channel Condition:

   Two different channel conditions are examined. Channel 1 with impulse response given by (6.10), is the static channel in [96] which has been used before in [15] and Chapter 4, for SEFDM system.

$$\begin{aligned} h(t) =& 0.8765\delta(t) - 0.2279\delta(t - T_q) + 0.1315\delta(t - 5T_q) \\ & - 0.4032e^{\frac{i\pi}{2}}\delta(t - 7T_q), \end{aligned} \tag{6.10}$$

   where $\delta(.)$ is the Dirac delta function and $T_q = T/Q$ is the sample time-duration in seconds and $Q = 2 \times N$ is the number of time samples per SEFDM symbol. Channel 2 is a quasi static Rayleigh channel that does not significantly change within an SEFDM symbol transmission but is time variant over the duration of the transmission of few symbols. Table. 6.1 summarises simulation parameters of Channel 2, while Fig. 6.5 illustrates the CFRs for static Channel 1 and a snapshot of Channel 2 at a given time instant. From the figure, the CFR of Channel 1 is flatter (i.e. less frequency selective) than the CFR of Channel 2. Furthermore, it can be noticed that Channel 2 suffers from deep fading at different frequencies.

Table 6.1: Channel 2 simulation parameters.

Parameter	Value
Number of delay taps	8
Maximum delay (τ)	$0.2T < \tau < 0.5T$

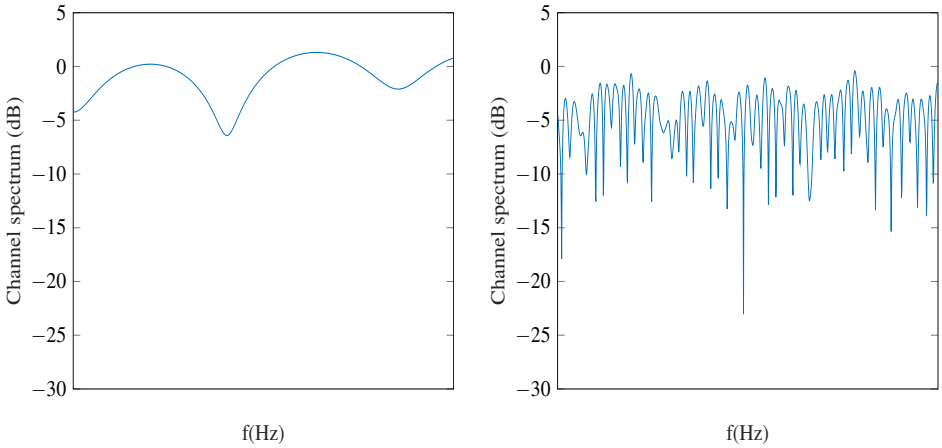

(a) Channel 1 **(b)** Channel 2

Figure 6.5: Channel frequency responses for channels 1 & 2.

2. Pilot size (number of subcarriers):

   The performance of the three different schemes depends on N. Given B is the channel bandwidth in Hz, then, the OFDM subcarrier spacing $\Delta f = B/N$ Hz becomes narrower by increasing N. A narrower subcarrier spacing is expected to enhance the estimation accuracy, because the frequency response per subcarrier becomes flatter and narrower fluctuations may be captured. In this work three different pilot sizes are chosen ($N = 16, 128, 1024$).

3. SEFDM Compression level (α):

   In Schemes I and II the number of subcarriers which requires interpolation depends on the value of α. In this simulation study, two values are used ($\alpha = 4/5, 2/3$).

The simulation results of Fig. 6.6 show the MSE versus E_b/N_0 in dB for the three CFR estimation schemes (I:PCE; II:OFDM with interpolation; III: OFDM without interpolation) using QPSK mapped pilot symbols and the parameters mentioned above. In the figure, each column is dedicated to one of the channels, while each row is for a certain N. Every single sub-figure presents the MSE results for the

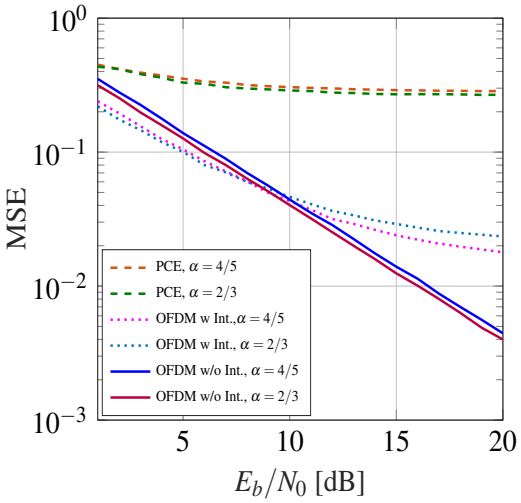

(a) Channel 1, $N = 16$

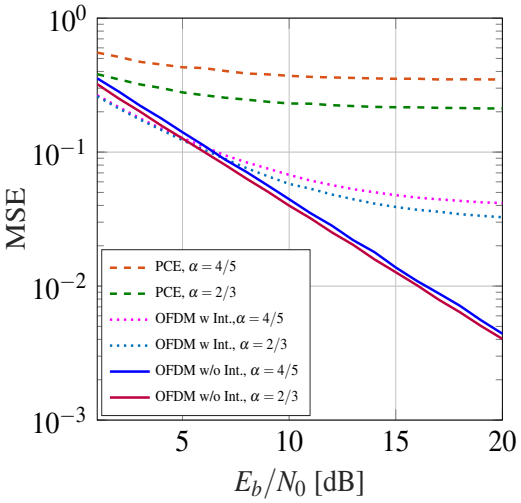

(d) Channel 2, $N = 16$

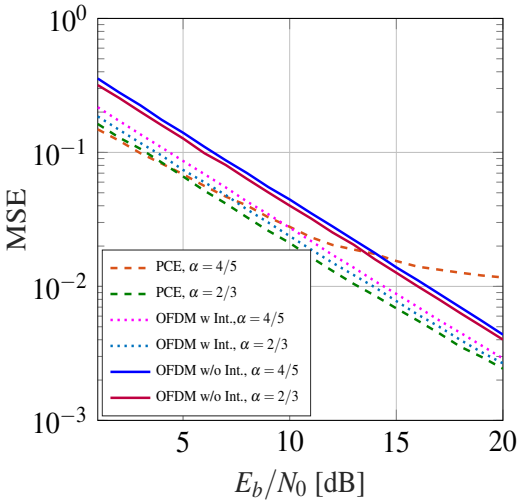

(b) Channel 1, $N = 128$

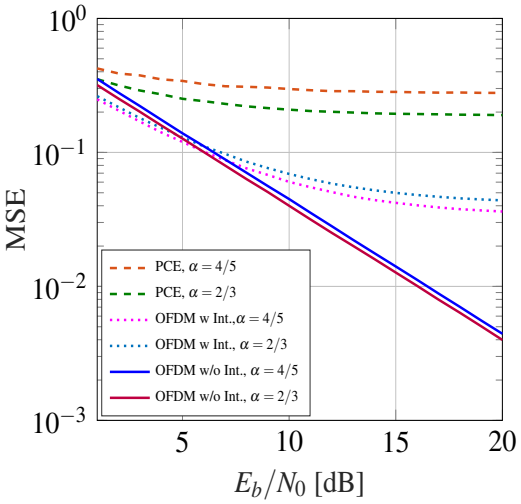

(e) Channel 2, $N = 128$

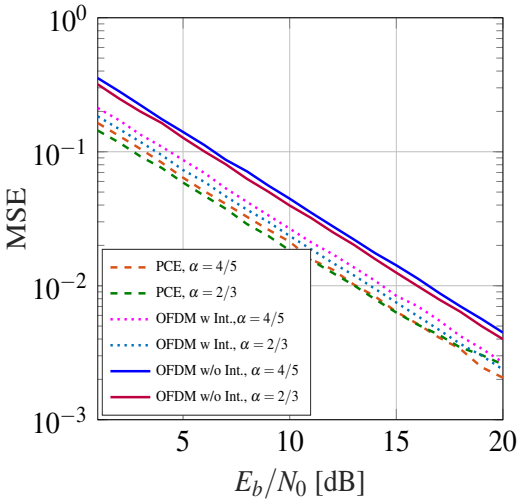

(c) Channel 1, $N = 1024$

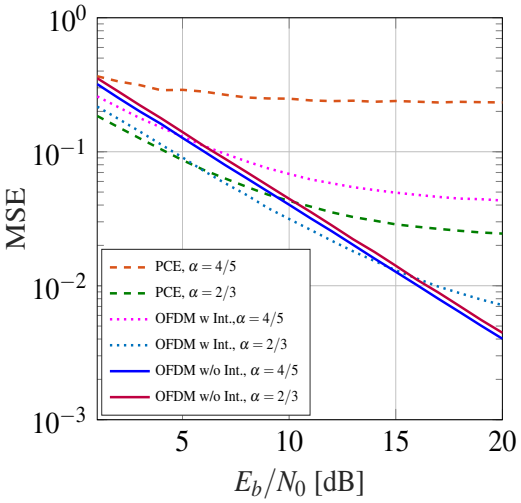

(f) Channel 2, $N = 1024$

Figure 6.6: MSE results for the three estimation schemes over channel 1 & channel 2, for different values of N and α.

three different estimation schemes and the two different α. From the results, the following may be observed:

- Scheme III accuracy is independent of N, α and the channel condition.
- Schemes I and II performance is enhanced by increasing the number of subcarriers under different channel conditions.
- Unlike scheme III, schemes I and II estimation accuracy is affected by the channel condition.
- In scheme I, the estimator for the case of $\alpha = 2/3$ appears to be more accurate than $\alpha = 4/5$ for different N and channel conditions. As shown in Algorithm 1, the reason is because the number of modulated subcarriers of the pilot symbol is inversely proportional to c, which is 5 and 3 for $\alpha = 4/5$ and $\alpha = 2/3$, respectively.
- Scheme II is more accurate than scheme I because the number of modulated subcarriers of the pilot symbol is higher.
- In contrast to scheme I, the number of subcarriers in scheme II is directly proportional to α ($N_p = \lceil N \times \alpha \rceil$). Yet, higher α does not guarantee a better performance, because the number of subcarriers which can be estimated directly without interpolation is inversely proportional to c ($\lceil N/c \rceil$). For instance, in Fig. 6.6 (a) the case of $\alpha = 4/5$ performs better than $\alpha = 2/3$ because the number of the subcarriers is higher, however, in Fig. 6.6 (d) for the same N, but a more frequency selective channel, $\alpha = 2/3$ performs better given that less interpolation is required.
- For the case of Channel 1, it is observed that schemes I and II perform better than the new scheme (III) for high N. The reason is the averaging used in interpolation, which reduces AWGN noise effect. However, this does not apply to Channel 2.

In conclusion, the performance of the first two schemes is a function of α, the flatness of the CFR and N. Second, due to the interpolation implemented in the first two schemes, they outperform the third scheme for the case of Channel 1 with $N = 128, 1024$. Finally, the advantage of the new scheme can be seen from its enhanced performance that is independent of N, α and the channel condition.

Besides performance, complexity is another key factor to consider. The total number of operations for the three schemes discussed above are counted using Algorithm 1, 2 and (6.8). Table 6.2 summarises the computational complexity of all schemes in terms of the number of complex additions and multiplications. Clearly, scheme III has the lowest complexity. It is important to emphasize here that the complexities of scheme I and II depend on α unlike scheme III. Thus, the performance and complexity of the proposed scheme make its implementation practical.

Table 6.2: Computational complexities (in terms of number of complex operations) for the three channel estimation schemes.

	Multiplications	Additions
Scheme I	$N + \lceil N/c \rceil - 1$	$2(N-1)$
Scheme II	$2(N - \lceil N/c \rceil) + \lceil N \times c \rceil - 1$	$4(N - \lceil N/c \rceil) - 1$
Scheme III (new)	N	0

After proving the efficiency of the proposed channel estimation scheme for SEFDM systems, the next section details the application of this scheme to 5G NR SEFDM frame.

6.7 SEFDM 5G NR Frame

A key feature of the 5G NR frame structure is its scalability, where the OFDM subcarriers spacing and subframe duration can change to support diverse use cases (i.e. higher data rates and reduced latency) [39] [40]. Boosting up the data rates is achieved by using a higher modulation order and/or transmitting over higher bandwidth. Another degree of freedom can be achieved in optimizing the 5G frame structure by using SEFDM. The advantage of 5G NR SEFDM-based frame is interpreted as the increase of the system throughput without increasing the modulation order, where more subcarriers will occupy the same bandwidth of a radio frame

when compared to OFDM. To start with, the next section describes the resource grid design for SEFDM 5G NR frame.

6.7.1 Resource Grid Design

In the recent 3GPP standards (release 15) [40] [1], the standard numerology (subcarriers spacing and symbol length) of the 5G NR is one radio frame of length 10 ms consisting of 10 subframes, each of length 1 ms. Each subframe consists of an OFDM subcarrier spacing dependent number of slots, as it goes from one up to eight slots per subframe. Each slot consists of 14 OFDM symbols (12 OFDM symbols in case of extended CP). In the following, the case of 15 KHz subcarrier spacing is investigated, which results in 1 slot per subframe [40].

The resource grid width is equal to the number of OFDM/ SEFDM symbols within a subframe, while the height corresponds to the number of resource blocks. For the case of original 5G NR frame with normal CP, the width is 14 symbols [39] and the number of resource blocks depends on the available bandwidth. Each resource block for OFDM has total width equal to one slot in time and total height equal to 12 subcarriers of 15 kHz subcarriers spacing each, which is equal to 180 kHz. If SEFDM symbols are used instead of OFDM, then instead of 12 subcarriers per resource block, $\lfloor 12/\alpha \rfloor$ subcarriers are used and the subcarriers spacing is $(15 \times \alpha)$ kHz resulting in the same height for OFDM (180 kHz). Fig. 6.7 demonstrates the resource block design for $\alpha = 0.8$, where each resource block contains 15 subcarriers of subcarriers spacing equals to 12 kHz.

One type of the reference signals sent in each subframe is the cell-specific reference (CSR), also known as pilot signals, which is used to estimate the CFR. For the special case of SEFDM signalling format, the pilot is sent over all subcarriers of the first SEFDM symbol as shown in Fig. 6.7. However, to obtain the channel response without ICI effect, as shown before, the pilot symbol duration will be longer than that of SEFDM symbols used to transmit data by a factor of $(1-\alpha)/\alpha$ [21]. Therefore, if each column is of duration $(1/14)$ ms, then the first column of

[1] This standard was released in July, 2018, by the end of this PhD work and during writing up this thesis.

each subframe, is of duration $(1/14\alpha)$ ms.

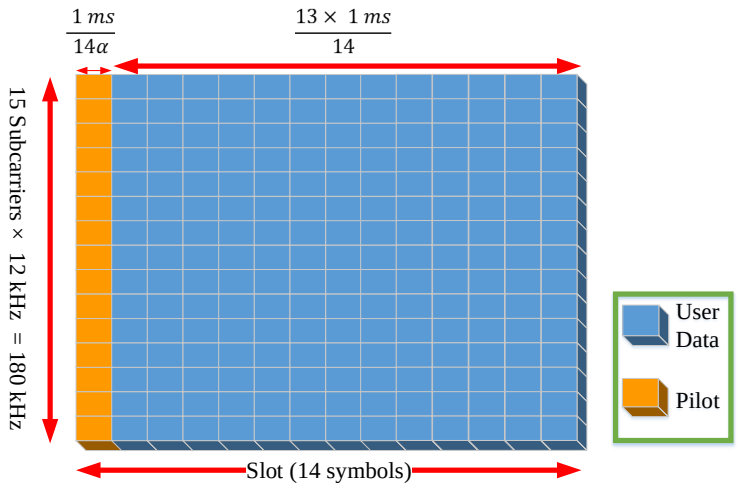

Figure 6.7: 5G NR SEFDM-based resource block content for $\alpha = 0.8$.

After resource grid mapping, the OFDM/ SEFDM signal generation operates in the resource grid, where it takes one column in a time. The ease and accuracy of OFDM signals generation using an IFFT was one of the main reasons to OFDM being adopted in LTE (4G) cellular network standards [136]. SEFDM signal generation by means of a single or multiple IFFT has been already implemented in [57]. However, the capability of generating a 5G SEFDM-based frame via a single IFFT is more challenging for two reasons: i) the proposed channel estimation scheme requires a generation of OFDM pilot; ii) the generation of continuous CP SEFDM signal to maintain the signal continuity. The next section explains SEFDM signals generation using a single IFFT.

6.7.2 IFFT Based SEFDM Transmitter

In this work, the case of 20 MHz bandwidth is investigated. According to [39], the number of resource blocks for this case is 100. Thus, the number of subcarriers will be either 1200 or 1500 for OFDM symbol or SEFDM symbol ($\alpha = 0.8$), respectively. The IFFT size is 2048, where at its input the data is packed and reordered. In NR resource blocks, no explicit DC subcarrier is reserved and the presence or absence of it is known to the receiver. Here, the DC subcarrier is not present, as no special handling of the DC subcarrier at the receiver has been specified yet by the

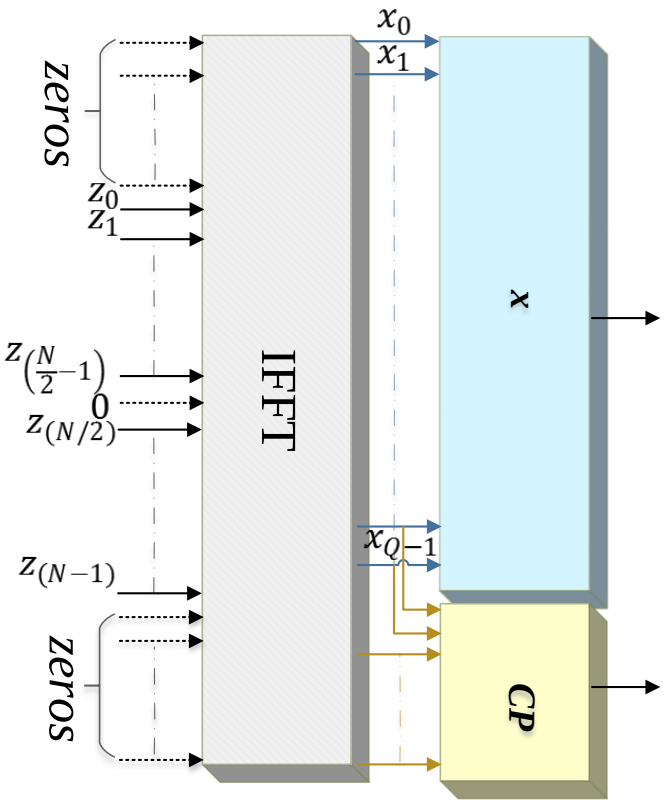

Figure 6.8: SEFDM signal generation with continuous CP via a single IFFT.

standards of [40].

If the IFFT is used for OFDM modulation, then all samples at the output of the IFFT will be taken to a parallel to serial (P/S) converter, then CP will be added before processing the signal by the digital to analog converter (DAC) converter. However, for SEFDM signal generation, the output of the IFFT is adjustable to generate the SEFDM data signals, the pilot symbol and continuous CP as explained below.

6.7.2.1 SEFDM data signals:

To generate the SEFDM signal **x**, as shown in Fig. 6.8, the input to the IFFT is the reordered 1500 complex symbols **z**, with $\alpha = 0.8$. At the output of the IFFT, the first $\lceil 2048 \times \alpha \rceil = 1639$ samples are taken while the rest are discarded. The discarded samples at the IFFT output affect the subcarriers compression in SEFDM [57].

6.7.2.2 Pilot generation:

The pilot symbols **p**, from the first column of the resource grid in Fig. 6.7, are the input to the IFFT in a similar way to the data symbols **z**. At the output of the IFFT, in contrary to SEFDM data symbols generation, all samples are taken resulting in an OFDM pilot **s**, with the same number of subcarriers and frequency spacing of the SEFDM signal **x**. This results in an overhead of $\lceil((1-\alpha)/\alpha)\times Q\rceil$ samples for the pilot symbol compared to SEFDM data symbols [21]. The CP of the pilot symbol is added directly because the pilot is an OFDM symbol.

6.7.2.3 Continuous cyclic prefix:

A guard band or CP of a duration longer than the channel delay spread of a wireless multipath channel is used to protect the transmitted symbols from ISI [137]. CP is chosen instead of guard band in 5G because CP maintains the transmitted symbol continuity. Hence, the circular convolution in time domain is transferred into multiplication in frequency domain, which allows using a one-tap equaliser to equalise the channel effect. Thus, the property of continuity has to be maintained for SEFDM.

In OFDM, the CP of duration d samples, is created by preceding the symbol with a copy of the last d samples of that same symbol. However, if the same method is followed to create the CP of SEFDM symbols, it will result in a non-continuous CP as shown in Fig. 6.9 (a), for the first two SEFDM ($\alpha = 0.8$) symbols ($f_1 = 12$ kHz, $f_2 = 24$ kHz). To overcome this problem, the CP samples (the samples inside the red circle in the figure) have to be taken from the last d discarded samples of the IFFT as shown in Fig. 6.8. The effect of this can be seen in Fig. 6.9 (b), where the CP is taken from the discarded part (presented by dashed lines). Furthermore, generating CP properly for SEFDM signals improves the overall system performance as it reduces the OOBE level compared to the non-continuous case. Fig. 6.10 demonstrates the normalized spectrum of the SEFDM symbol generated above, after adding the CP and the P/S stage of the transmitter for both cases.

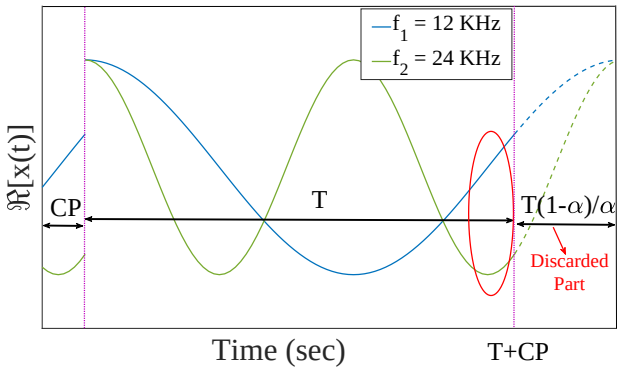

(a) Non-continuous CP (existing methods).

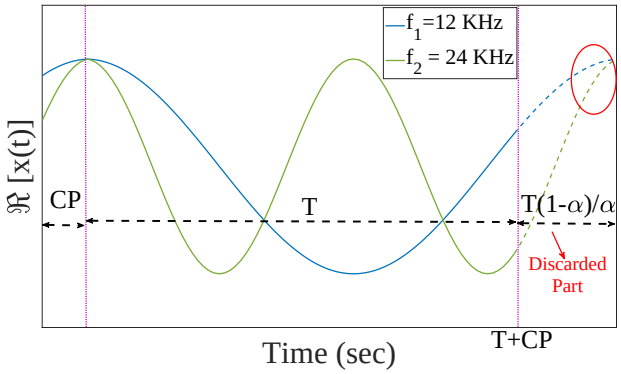

(b) Continuous CP (new method).

Figure 6.9: The real part of x(t) in the time domain for $f_1 = 12$ kHz, $f_2 = 24$ kHz with $\alpha = 0.8$.

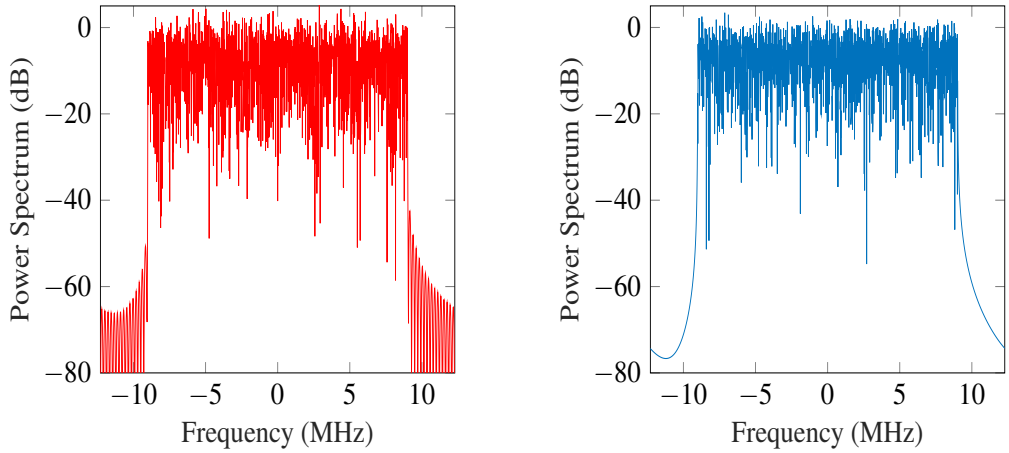

(a) Non-continuous CP.

(b) Continuous CP.

Figure 6.10: The spectrum of x(t) for 20 MHz bandwidth with $\alpha = 0.8$ and different CP addition cases.

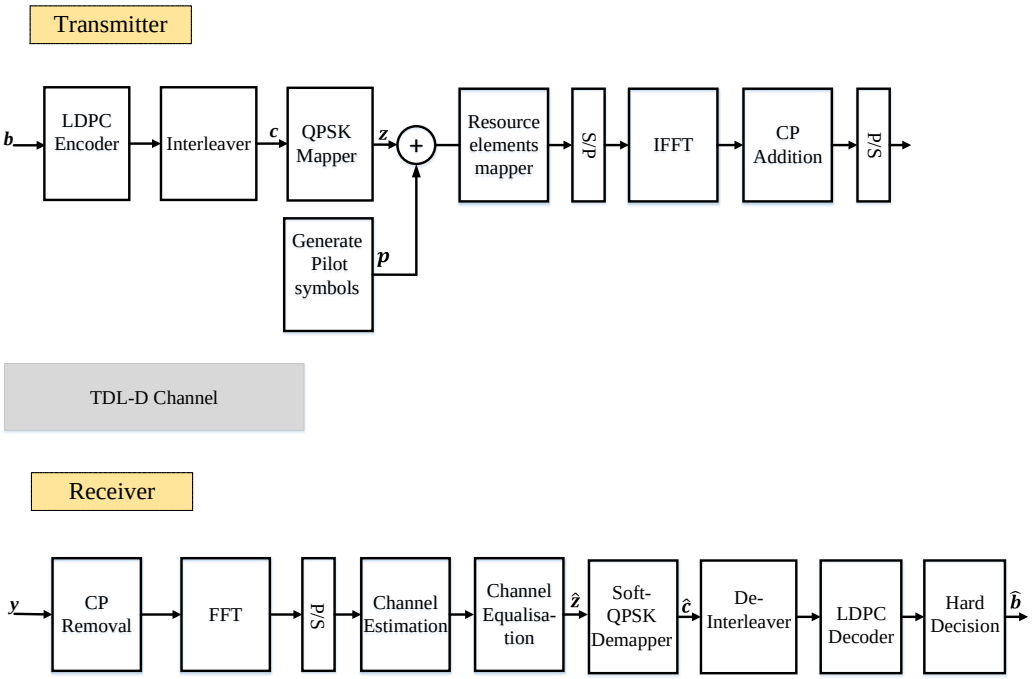

Figure 6.11: High level transceiver descriptive design for 5G NR SEFDM-based system.

6.7.3 BER and Throughput Simulation Results

To prove the validity of the suggested SEFDM transmission design, a 5G NR signal transmission scenario is simulated. The scenario is for a specific modulation order (QPSK) and coding rate (1/3), 20 MHz bandwidth and subcarrier spacing 15 KHz, 12 KHz for $\alpha = 1$ and 0.8, respectively. As the main focus of this work is at the transmitter, the receiver simulated here is similar to that of OFDM. However, with higher compression level (i.e. lower α) and/or higher modulation order, the use of SIC, explained in Chapter 5, becomes necessary.

Fig. 6.11 is a high level illustrator of the transceiver model designed and developed in MATLAB as part of this study. Starting from the far left, first the message bits are encoded by an LDPC encoder of a coding rate $R_c = 1/3$. Then, the coded bits are interleaved with the random external interleaver and mapped to QPSK complex symbols. Simultaneously, QPSK pilot symbols are generated by the gold sequence [138]. Then both pilot and data symbols are mapped into the resource blocks similar to Fig. 6.7, where the number of resource blocks within the resource grid is 100 for the case of 20 MHz bandwidth. The IFFT in Fig. 6.8 is used for OFDM/ SEFDM ($\alpha = 0.8$) modulation and a normal CP of length (7%) is added to each

symbol. The resultant samples are sent over a tapped delay line (TDL) 5G channel model of type (D), which has been defined in the new 5G 3GPP standards [139] and it represents a line of sight (LoS) channel. The first tap of the TDL-D channel follows a Ricean distribution with a K-factor=7 dB and the rest of the taps follow Rayleigh distribution (given in Table 7.7.2-4 of the standards [139]). The channel simulation parameters are given in Table 6.3.

Table 6.3: Channel simulation parameters.

Parameter	Value
Channel delay profile	TDL-D
Delay spread	300 ns
User terminal velocity	30 km/hour
Maximum Doppler shift	111.2 Hz
K-factor	7 dB

At the receiver, firstly, resource elements demapping is performed. The pilot is processed to acquire the CFR, where the CP samples distorted by ISI are discarded and pilot samples are demodulated by means of an FFT, which has the exact arrangement of the IFFT at the transmitter. The output symbols from the FFT are used to estimate the CFR [21]. Consequently, the rest of the symbols in a subframe are processed by removing the CP and demodulation via the FFT, followed by one-tap equaliser using the estimated CFR to equalise the channel effect. Then, the equalised symbols go through a soft QPSK demapper followed by an inverse interleaver and LDPC decoder to obtain the estimated message bits.

Fig. 6.12 illustrates the BER performance versus E_b/N_0 in dB, for 5G OFDM-based systems and 5G SEFDM-based systems with ($\alpha = 0.8$) continuous CP. The perfect knowledge of CFR is the benchmark to assess the estimation accuracy. Results show that a spectral efficiency can be gained for SEFDM at the expense of an error penalty just below 1 dB. The SIC, if used, can further reduce the penalty of SEFDM compared to OFDM at the expense of receiver complexity. Furthermore, a comparable degradation is noticed in the error performance for OFDM and SEFDM, relative to the results of perfect knowledge of the CFR.

The throughput (η) is calculated by evaluating the total number of subcarriers

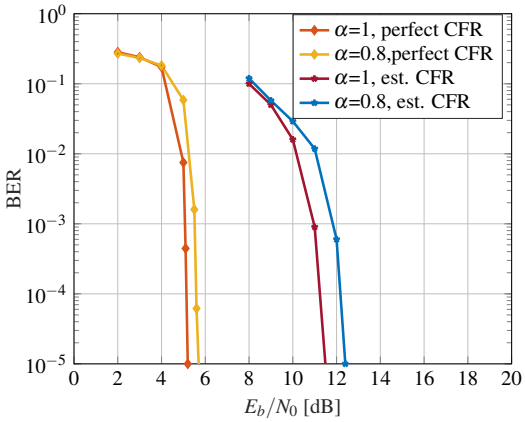

Figure 6.12: BER results for 5G SEFDM and OFDM based with perfect and estimated CFR.

in a subframe multiplied by the number of bits per modulation symbol, over the subframe duration, such as

$$\eta = \frac{\log_2(M) \times N_s \times N}{\frac{(13+1/\alpha)\times 10^{-3}}{14}}, \tag{6.11}$$

where N_s is the number of symbols per subframe, which is 14 for this case, and M is the constellation order (e.g. $M = 4$ for QPSK). For instance, if the channel bandwidth is 20 MHz, then number of subcarriers per resource grid is 1200 for $\alpha = 1$ and 1500 when $\alpha = 0.8$. The throughput using the parameters of the system simulated above for the case of OFDM is 33.60 Mbps and 41.26 Mbps for SEFDM $\alpha = 0.8$.

Using SEFDM in the NR 5G is beneficial in terms of throughput. For example the case above allows an increase in throughput by a factor of 22.8% compared to OFDM. The throughput is calculated by taking into consideration the overhead used for channel estimation. In both SEFDM and OFDM cases, the overhead percentage from synchronisation and the redundant bits added by channel coding...etc is the same, under the assumption that OFDM will use the pilot structure discussed here. However, if compared to the pilot structure of the current 3GPP standards [40], then the throughput advantage is slightly lower than the above. The reason is that the number of pilot signals in [40] is less than the number of pilot signals used

here, as pilot signals are sent on certain subcarriers, while interpolation is used to estimate the channel response on the rest of the subcarriers.

6.8 Conclusions

This work investigates various channel estimation schemes for SEFDM signals and devises a new robust frequency domain channel estimation scheme. In the proposed scheme, the transmitted block is divided into orthogonal and non-orthogonal multiplexing regions. Specifically, the pilot is sent over orthogonally spaced subcarriers as an OFDM symbol, while information symbols are sent over SEFDM; both using the same number of subcarriers and the same subcarrier spacing.

To provide significant insight to the proposed scheme, system modelling of the multipath channel effect on SEFDM signals is shown. Then, simulation studies are used to compare the suggested scheme to another two existing frequency domain estimation schemes; partial channel estimation and full channel estimation with interpolation. The MSE results show that in a good channel condition and high number of subcarriers, the other schemes tend to be slightly more accurate than the proposed one, because averaging in interpolation reduces the noise effect. For applications with low number of subcarriers and/or worse channel conditions, these schemes feature a high error floor. Unlike these two schemes, the scheme proposed in this chapter maintains accurate estimation of the channel regardless of the channel condition, number of subcarriers or the compression level. Besides the aforementioned advantage, the numerical analysis shows substantial reduction in the computational complexity for the proposed scheme when compared to the other two schemes. However, there are compromises in terms of increased pilot duration overhead, which depends on how often the pilot is sent. For instance, such overhead is lower in semi-static or slow fading channels, compared to fast varying channels with more frequent pilot transmission.

To verify the proposed scheme suitability for practical systems, it is applied to SEFDM 5G NR system model. First, a proposal is given for a single reconfigurable IFFT design capable of generating SEFDM symbols, as well as continuous cyclic

prefix and the OFDM pilot of the proposed estimation scheme. To maintain the CP continuity property, it is found that the CP of SEFDM has to be created in a different way to that of OFDM. The single IFFT efficiency is shown by system modelling and simulations for 5G frames transmission over TDL-D channel. Results show that for the case of $\alpha = 0.8$, with a less than 1 dB error penalty, SEFDM can enhance the throughput by a factor of 22.8% compared to OFDM. The error penalty can be further reduced and higher subcarriers compression can be used, to increase the throughput, by using the successive interference canceller in Chapter 5.

The work done in this chapter may be further extended to account for the effective throughput, where the error rate is taken into consideration to achieve better insight of the spectral efficiency advantage of SEFDM. The accuracy performance of all schemes may be tested under the condition of fast fading channel where the channel varies within the transmission of an OFDM/ SEFDM symbol.

Chapter 7

Experimental Demonstration of SEFDM Transmissions at E-Band

The continuous growth of data-hungry services pushes the current microwave spectrum towards saturation. Recently, research interest has shifted to higher frequencies to benefit from the larger available bandwidth. The E-band is defined as the frequency spectrum from 71 to 76 GHz and 81 to 86 GHz.

Up to this point, the E-band transmission is limited to single carrier or orthogonal signals transmission, which constricts the system spectral efficiency. This work, and for the first time, presents an experimental demonstration of SEFDM signal wireless transmission over the E-band (81-86) GHz frequency range. The experimental demonstration here uses the powerful LDPC codes and the newly implemented CFR estimation scheme of Chapter 6 and a newly developed technique for timing synchronization, where the orthogonal pilot symbols are also used for timing synchronization to reduce system overhead. The experimental results show highest transmission rate of 12 Gbps over a bandwidth varying between 2.67 to 4 GHz depending on the compression level of the SEFDM signals, which results in a spectral efficiency improvement by up to 50% compared to OFDM.

This demonstration represents an important milestone for SEFDM transmission. The employment of LDPC codes and the new CFR estimation scheme with no complex transmitter and receiver signal processing, highlights the potential of a real-time implementation.

This chapter is organized as follows: Section 7.1 gives an overview about the E-band spectrum and the existing multi-carrier experiments held. Section 7.2 describes the SEFDM transmission experimental demonstrator and gives a detailed explanation of the system setup and the transmitter and receiver digital processing part to ameliorate the effect of ICI and system impairments. In Section 7.3, an analysis of the experiment results and measurements are given to evaluate the system performance. Finally, conclusions are drawn in Section 7.4.

7.1 E-band Overview

The recent Federal Communications Commission (FCC) spectrum frontiers ruling has assigned many bands above 30 GHz, for mobile and backhaul communications [140]. E-band in particular has gained a lot of interest for multiple reasons [141]:

1. The 5-10 GHz of available bandwidth allows multi-gigabits per second transmission;

2. The low atmospheric absorption compared to the 60 GHz and beyond-100 GHz bands, as shown in Fig. 7.1 [140], allows data transmission over relatively long distances;

3. The light-licensing requirements of the E-band spectrum simplify and reduce the operating cost.

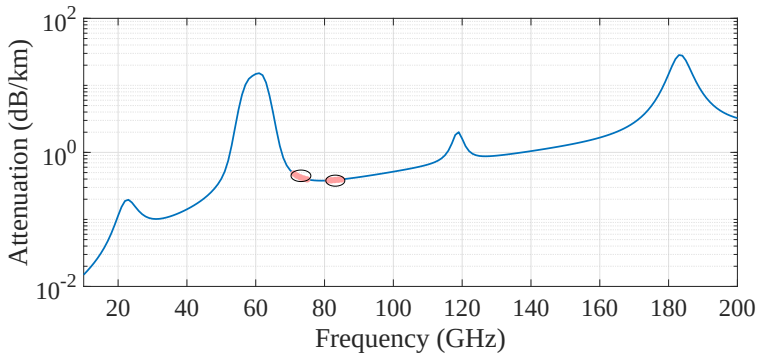

Figure 7.1: Atmospheric absorption of electromagnetic waves at sea level versus frequency, with the E-band highlighted [140].

In a multipath environment, the mm-wave channel exhibits frequency selective characteristics. To combat frequency selectivity and to simplify channel equalisation, OFDM converts the frequency selective channel into a parallel collection of orthogonal frequency flat sub-channels [142]. This is the reason for the popularity of OFDM for many of today's wireless applications and experiments. A comprehensive and complete study of OFDM versus single carrier mm-wave transmission by Rappaport *et al.* in [143] concludes that the superior frequency selectivity mitigation capabilities of OFDM offset the power amplifier non-linearity benefits of single carrier, at least when robust channel coding is used. For instance, OFDM is chosen for the WiFi 802.11ad and wireless personal area network (WPAN) IEEE 802.15.3c new standards over the mm-wave spectrum [144] and the future 5G standards [141].

Much transmission experiments have been reported on different mm-bands for OFDM ranging from 39 GHz [145], 40 GHz [146], 60 GHz [147] and up to 94 GHz [148] for different applications and scenarios. More experiments can be found in the references therein of the above mentioned papers. Only a few trials have been carried out in the E-band transmission to gain a better understanding of the channel propagation characteristics and to prove its viability. Rappaport *et al.* investigated the deployment of highly directional steerable antennas with beamforming for data transmission over the 71-76 GHz spectrum, in an indoor scenario [149] and an outdoor scenario [150] in NY City for future 5G communication systems. A demonstration of adaptive OFDM-based transmission over the 70 GHz band has been reported in [144], where different modulation orders to different subcarriers groups are implemented to cope with channel impairments and enhance system total capacity.

Other FDM based systems have been implemented too, such as the 6 Gbps demonstrator reported in [151], where the 81-86 GHz bandwidth is divided into sub-channels. Each sub-channel is filtered with an RRC filter to reduce the interference between subcarriers.

Up to this point, all E-band transmission multi-carrier systems have been lim-

ited to orthogonal signals transmission, which constricts the system spectral efficiency. This work presents an experimental demonstration of SEFDM signal wireless transmission over the E-band 81-86 GHz frequency range. Improving the spectral efficiency is not the only motivation for using SEFDM signals. There are also noise advantages when bandwidth is reduced, such as the overall reduction of noise power and as was shown in [152], the impact of white phase noise depends on the bandwidth of the signal. Therefore, the impact of white phase noise in SEFDM will be less than that of OFDM for the same transmission rate, while the severity of near carrier phase noise will not be affected [153] [154]. Additionally, improving the achievable spectral efficiency without increasing the constellation cardinality can be considerably convenient, since it is well known that low-order constellations are more robust to channel impairments such as time-varying phase-noise and nonlinearities. The next section describes the experimental demonstration of SEFDM signals transmission over the E-band.

7.2 E-Band SEFDM Transmission Demonstrator

The experiment was held at the Microwave Electronics Laboratory, Department of Microtechnology and Nanoscience, Chalmers University of Technology in Gothenburg, Sweden from the 11th of November to the 17th of November, 2017. The setup is shown in Fig. 7.2(a); the E-band SEFDM Tx and Rx chips in the experiment are TSC0023B and RSC0015D, shown in Fig. 7.2(b) and (c), respectively [155]. Both Tx and Rx are designed by Gotmic AB for this collaborative work. The design topology of the transmitter and receiver chips and measurements are given in Appendix 2. In the following, a description of the experiment setup is given.

7.2.1 Experiment Setup

The arbitrary waveform generator (AWG) (Keysight M8195A) was used as a DAC, with a vertical resolution of 8 bits, to convert digital baseband signal to analogue input to the E-band Tx. The AWG provides two differential outputs (+I, -I, +Q, -Q), each operates at 16 GHz and are connected to the four inputs of the Tx chip (TSC0023B) which up converts the input signal to the RF range around the center

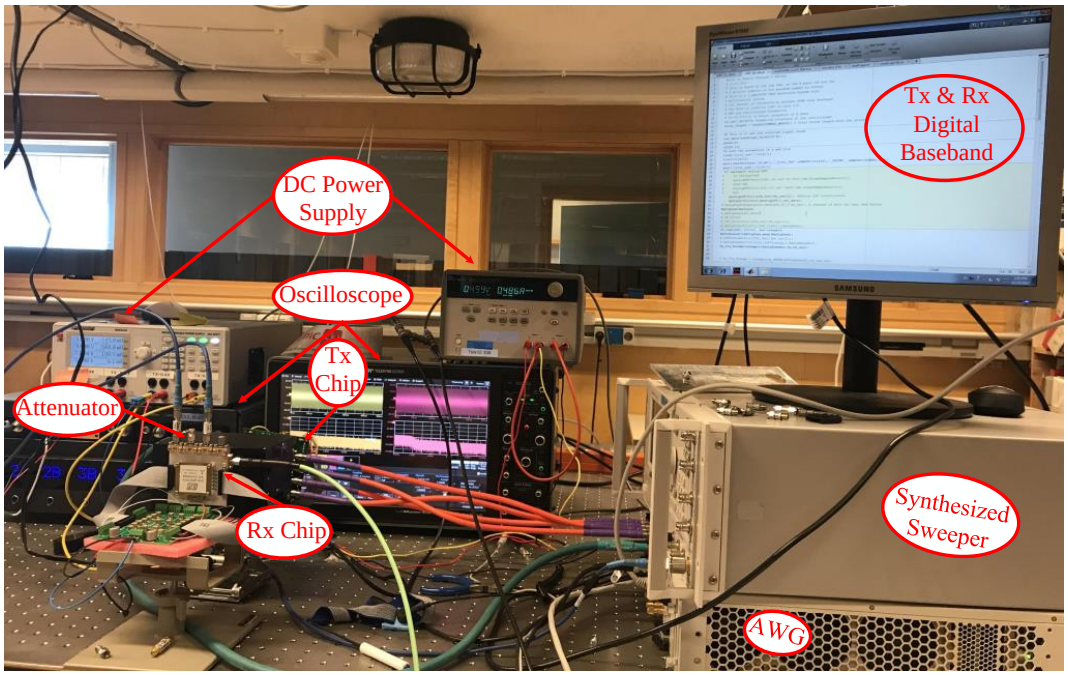

(a) SEFDM E-band transmission test bed

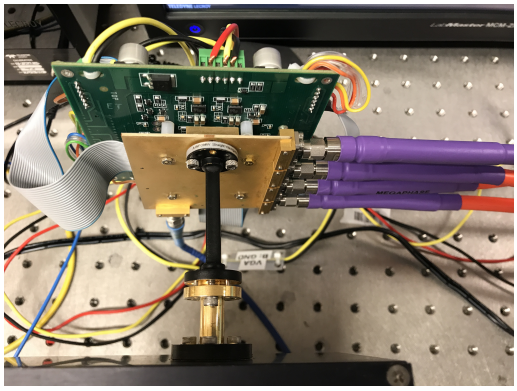

(b) Transmitter chip

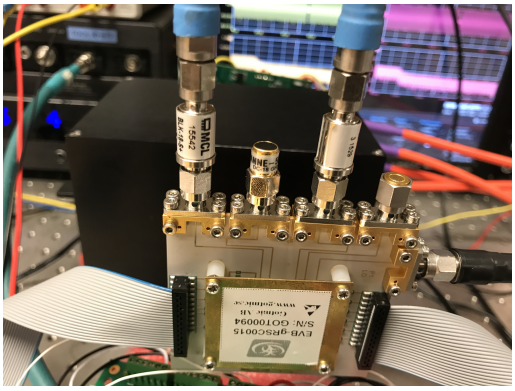

(c) Receiver chip

Figure 7.2: Photos of the SEFDM E-band experiment test bed.

frequency 83.5 GHz. It is important to mention that the AWG buffer size (10 million samples) limits the number of transmitted samples in this experiment. The RF signal propagates through the E-band waveguide (WR12) and the digital variable attenuator (Mi-Wave's 511 Series Precision Programmable Rotary Vane) is inserted to introduce a controlled frequency selective environment and to avoid the receiver from reaching its saturation region. The measured channel frequency amplitude and phase responses and group delay and are shown in Fig. 7.3. From the measurements, the combination of waveguides and attenuator may be characterised as a frequency selective channel and almost linear phase, resulting in minimal fluctuations

in the channel group delay. Such channel, appears in a multi-path environment, where signals propagate through different paths.

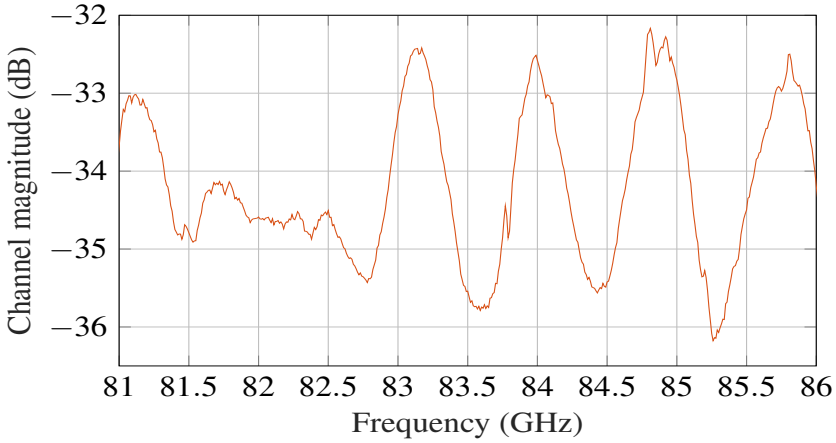

(a) Channel magnitude response.

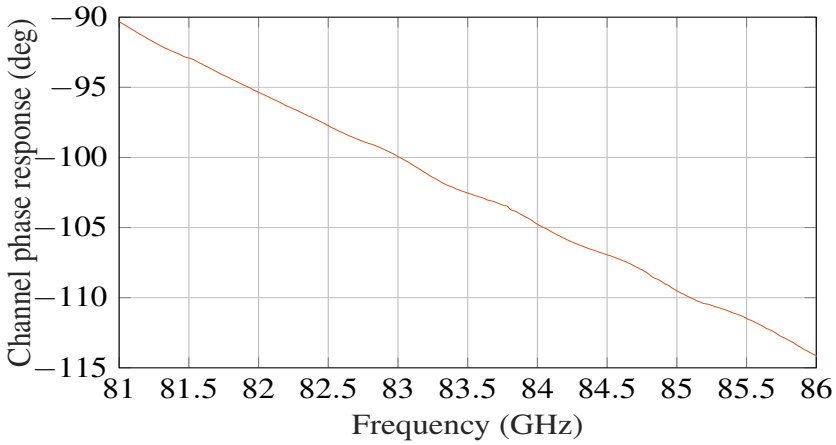

(b) Channel phase response.

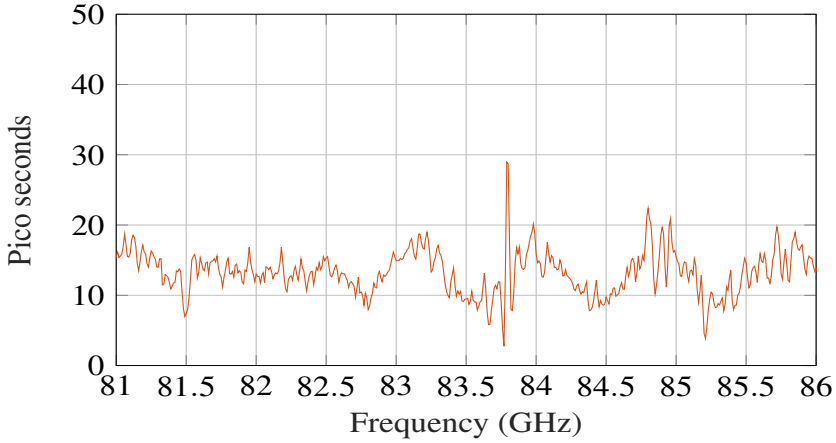

(c) Channel group delay.

Figure 7.3: The attenuator measured channel magnitude and phase responses, and group delay.

Table 7.1:
System Parameters.

Parameter	Value
Sampling Rate (f_s)	16 Gsample/sec
Number of subcarriers (N)	16
Number of pilot OFDM symbols	5
OFDM/ SEFDM symbol duration (T)	4 ns
Compression factor (α)	$2/3, 4/5, 1$
Pilot symbol duration (T_p)	$4/\alpha$ ns
Subcarrier Bandwidth (Δf)	$\alpha \times 250$ MHz
Bandwidth (BW)	$\alpha \times 4$ GHz
RF Center carrier frequency (f_c)	83.5 GHz
Transmission frequency band	$(-\frac{\alpha \times BW}{2}) - (\frac{\alpha \times BW}{2}) + f_c$
Transmission symbol rate (R_s)	4 Gsymbol/sec
Modulation cardinality (M)	4, 8
LDPC coding rate (R_c)	$1/3$
LDPC decoder number of iteration	50
Interleaver size	64800 bits

At the receiver, the Rx chip (RSC0015D) down converts the RF signal back to the baseband region and the received IQ outputs are connected to the (Teledyne Lab Master 10-100 Zi) oscilloscope, operating as an analog to digital converter (ADC), with a vertical resolution of 8 bits, at 80 GHz sampling rate (interleaved) and 36 GHz analog bandwidth. The sampled signals are fed to the digital baseband receiver which is implemented offline in MATLAB to recover the transmitted symbols and evaluate system performance, as will be discussed in the next section. The experiment system parameters are summarized in Table 7.1.

7.2.2 Digital Baseband Tx & Rx

A descriptive block diagram is depicted in Fig. 7.4, starting from the Tx digital baseband part through up-conversion to radio RF band, and the signal E-band trans-

mission and then, to down-conversion from RF to baseband again to recover the transmitted bits.

At the transmitter, in the first stage, a stream of bits $\mathbf{b} \in \{0,1\}$ are encoded by the LDPC encoder. In this work, the coding rate is ($R_c = 1/3$), meaning that two parity bits are sent for each information bit. The encoded bits $\mathbf{c} \in \{0,1\}$ are interleaved by a random block interleaver ($\prod$) of size 64,800 bits to scatter burst errors. Hence, the possibility of loosing the information bit together with its parity check bits reduces, as was shown earlier in Chapter 4. The QPSK/ 8-PSK modulator maps each $\log_2(M)$ bits to a symbol z, from the M-ary symbol alphabet. Thereafter, the mapped symbols sequence $\mathbf{z}$ is divided into $N = 16$ parallel streams. Each symbol z_n is modulated by the n^{th} subcarrier of the SEFDM symbol, where the frequency separation between adjacent subcarriers is ($\alpha \times BW/N = \alpha \times 250$ MHz). The spectrum of the resultant signal after RF up-conversion is shown in Fig. 7.5. The density of the demonstrated spectrum results from using a high sampling frequency to plot the spectrum without any filtering, to guarantee a high resolution.

In concurrent with the process of preparing the message bits for SEFDM modulation, a pilot is generated. The pilot consists of five consecutive OFDM symbols, the first of these is used to estimate the CFR coefficients and the other four are used to estimate the system phase offset. The pilot symbols have the same constellation order of the data symbols. The special feature of these pilot symbols is that they have the same frequency spacing ($\alpha \times 250$ MHz) and number of subcarriers of SEFDM symbols, but they are designed to be orthogonal, as explained in Chapter 6 and reported in [21]. The added redundancy of this scheme depends on how frequent the pilot is sent. For instance, in this experiment, as the environment is static, the pilot is sent only once at the beginning before sending data of length $L_d = 3 \times 10^6$ symbols. Hence, the added redundancy, given by $((1-\alpha)/(L_d+1)) \times 100\%$, is insignificant. Finally, the last stage is a parallel to serial converter, so the data stream generated, is ready for the AWG IQ output.

Fig. 7.6 shows the spectrum of the received samples captured from the oscilloscope. It is important to note that the OOBE level of SEFDM is slightly lower than

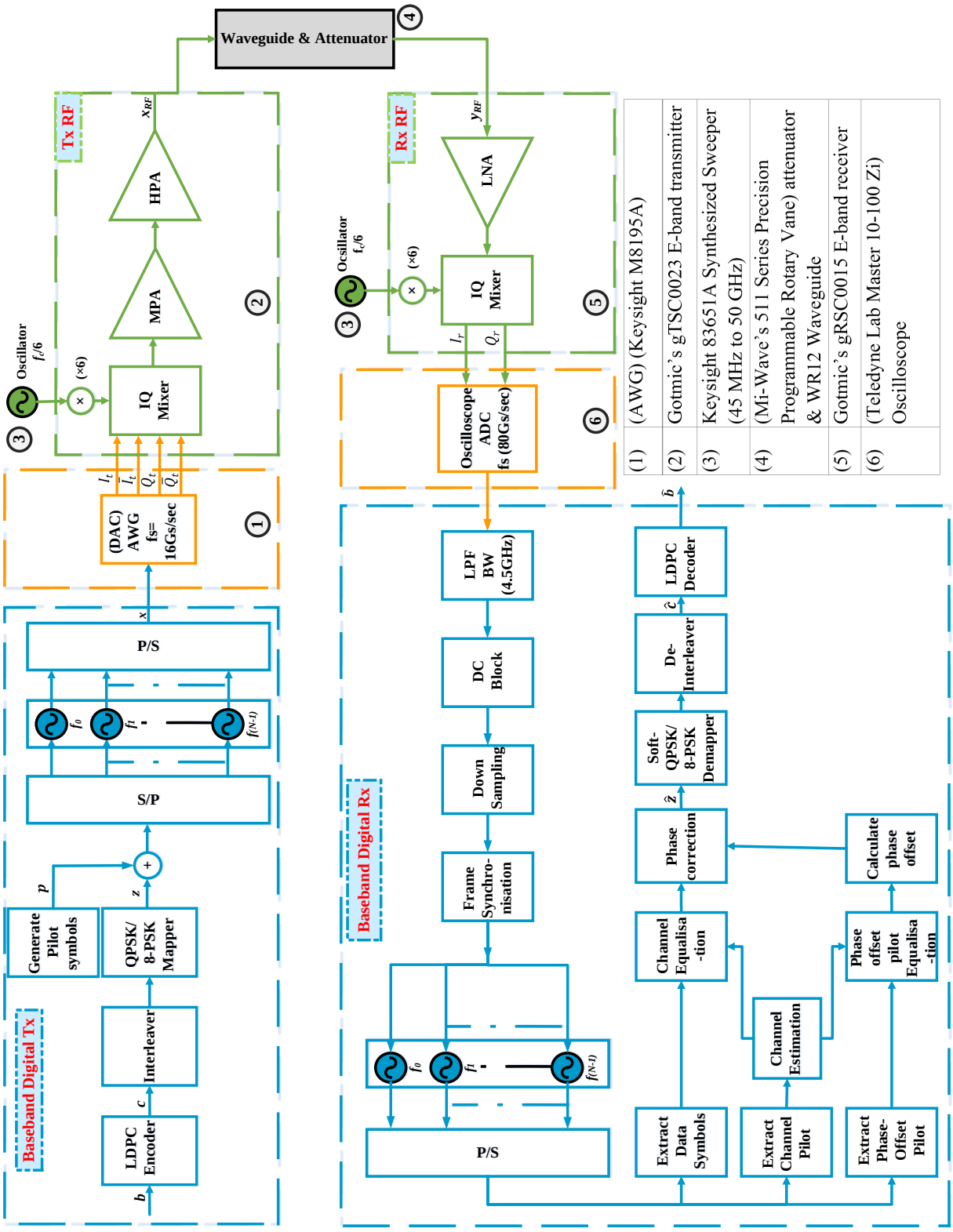

Figure 7.4: A descriptive block diagram of the system with a list of the equipment used.

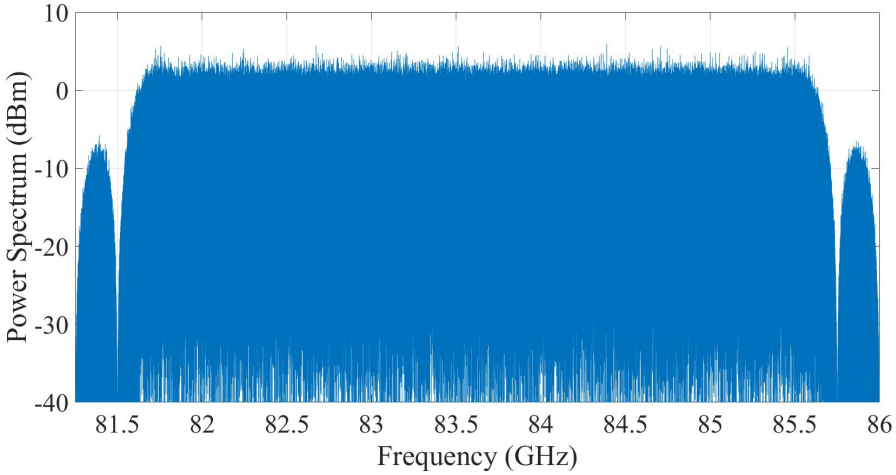

(a) OFDM ($\alpha = 1$), BW = 4 GHz

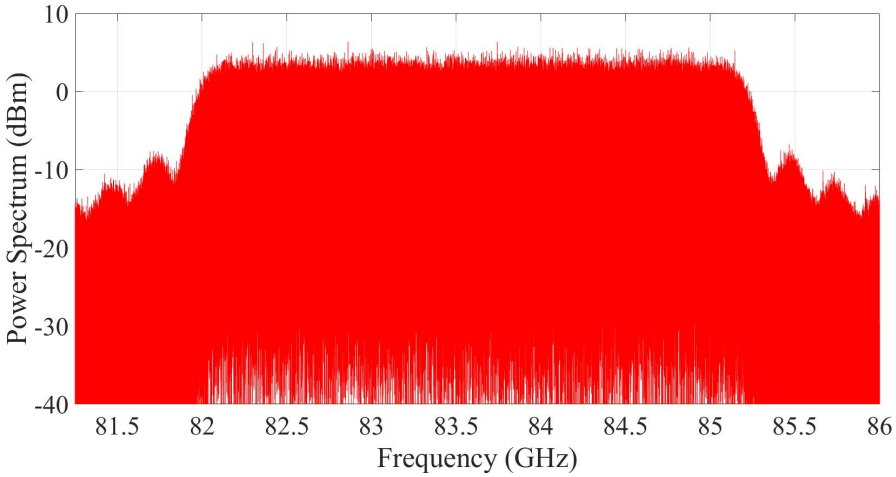

(b) SEFDM ($\alpha = 4/5$), BW = 3.2 GHz

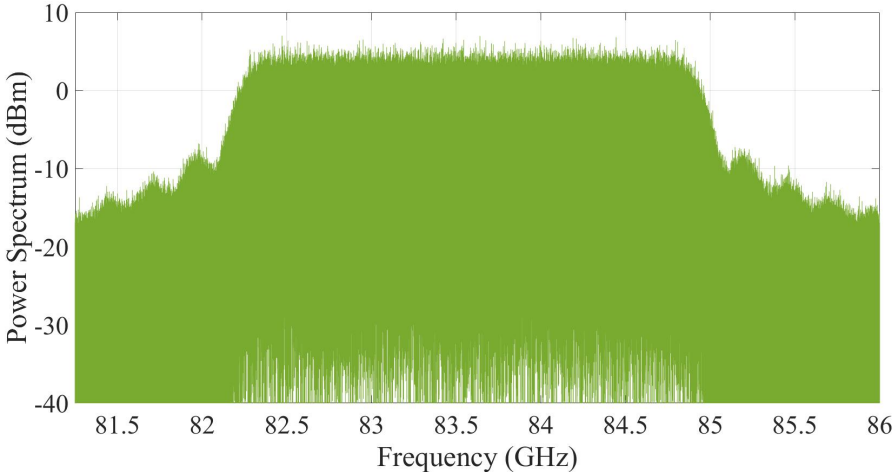

(c) SEFDM ($\alpha = 2/3$), BW = 2.67 GHz

Figure 7.5: A comparison of OFDM ($\alpha = 1$) and SEFDM ($\alpha = 4/5, 2/3$) spectra at the transmitter for the same transmission rate 8 Gbps.

that of OFDM. Consequently, extra subcarriers, or signals of other users may use the saved bandwidth.

At the first stage of the digital receiver, a LPF of bandwidth (4.5 GHz) is implemented followed by a DC block. Thereafter, a down sampler is used to re-sample the samples captured from the oscilloscope from 80 Gsample/sec to 16 Gsample/sec, which is the sampling rate of the transmitted signal.

As the pilot symbols in this experiment are sent ahead of the data symbols, a new technique is developed in this work for timing synchronization where the pilot symbols (normally used for channel estimation only) are also used here for timing synchronization. This is made possible because of the orthogonal nature of the pilot symbols, discussed above, allowing the known transmitted pilot samples to be correlated with the received samples at the receiver to give a correlation peak indicating the beginning of the received data samples, thus, establishing timing synchronization.

The received samples are demultiplexed into channel pilot symbol, phase offset pilot symbols and data symbols. The channel pilot symbol enters the bank of demodulators, then the output is used to estimate the CFR. Following, the phase offset pilot symbols are demodulated, then equalised using the estimated CFR and a one-tap equaliser. Afterwards, the four equalised pilot symbols are used to calculate the phase offset. Here, four pilots are used for the phase offset estimation to gain a more accurate estimation. Thereafter, the received data symbols are equalised using a one tap-equaliser. Then, the equalised received symbols are rotated by the estimated phase offset. After this stage, the symbols are de-mapped, de-interleaved and decoded by an LDPC decoder with 50 iterations. The output of the decoder are the estimated transmitted bits.

7.3 Measurement, Analysis and Results

In this section, to evaluate the system performance and prove its viability, the analysis of the system setup and results are divided into three categories: spectral efficiency gain; the advantage of OFDM pilot over SEFDM pilot; and SEFDM error

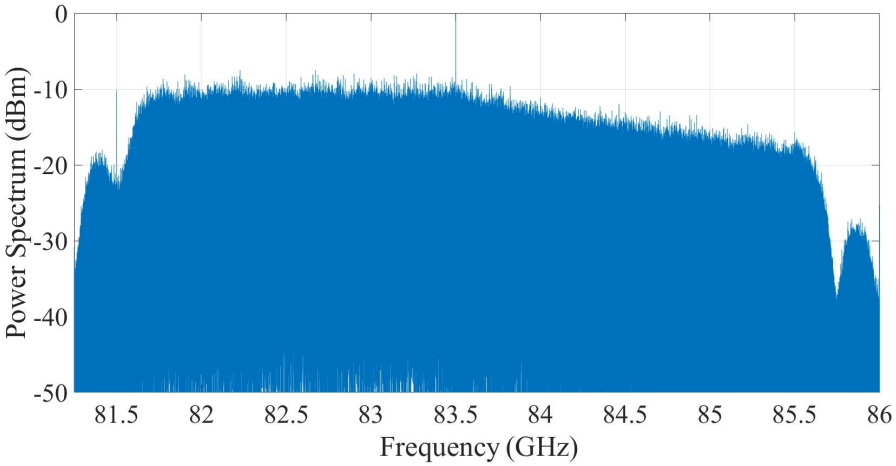

(a) OFDM ($\alpha = 1$), BW=4 GHz

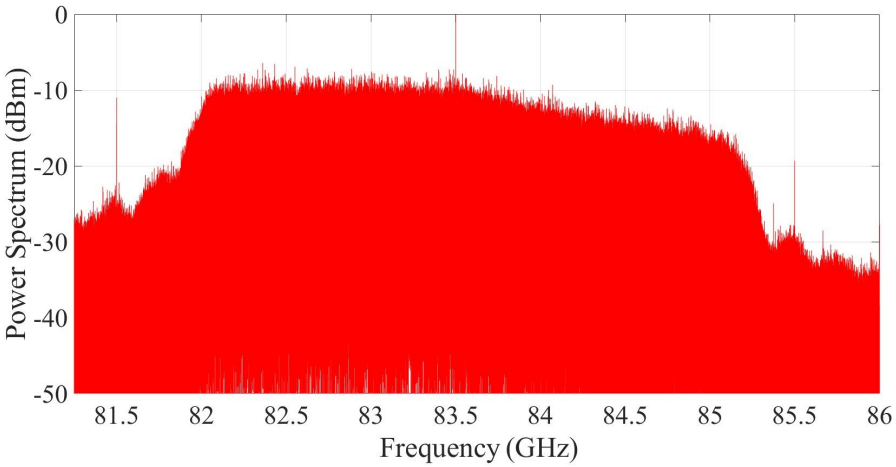

(b) SEFDM ($\alpha = 4/5$), BW=3.2 GHz

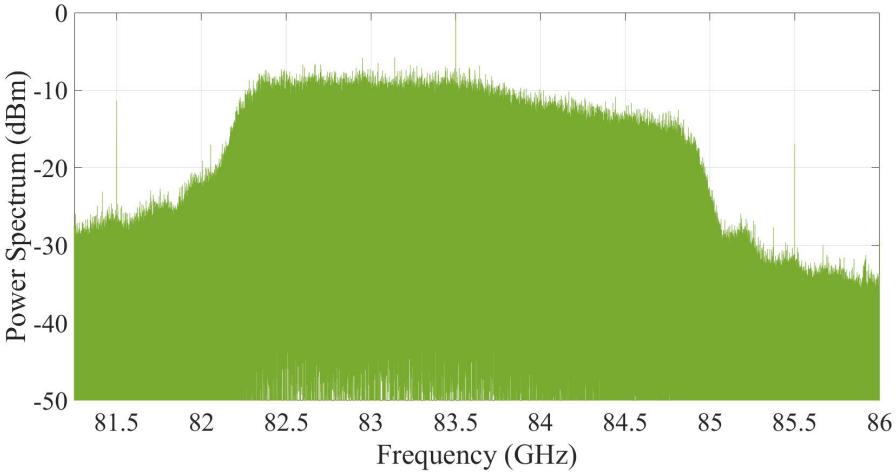

(c) SEFDM ($\alpha = 2/3$), BW=2.67 GHz

Figure 7.6: The spectra of the received samples obtained from the experiment for OFDM ($\alpha = 1$) and SEFDM ($\alpha = 4/5, 2/3$) for the same transmission rate 8 Gbps.

performance.

7.3.1 SEFDM Spectral Efficiency Gain

The constellation diagrams of the received symbols, for QPSK and 8PSK, before and after equalisation and phase correction (before the decoder stage), are shown in Table 7.2 along with the spectral efficiency (η bit/s/Hz) for each case. This constellation is for the 9^{th} subcarrier that is located at the center frequency ($f =$ 83.5 GHz). It is chosen given that this is the only subcarrier that has the same frequency for all compression factors, because the compression is applied on both sides as shown in Fig. 7.5. Furthermore, the constellation given here is for the same receiver input power level, given the signal to noise ratio ($SNR = 25$ dB), where the transmission is error free (i.e. BER $< 5 \times 10^{-6}$), even for the case of 8-PSK and $\alpha = 2/3$, due to the powerful LDPC decoder.

From Table 7.2, we can notice that higher spectral efficiency improvement is gained for lower α and the percentile improvements (ζ) calculated by (4.4) are 25% and 50% for $\alpha = 4/5$ and $\alpha = 2/3$, respectively.

This gain is achieved in this experiment as the transmitted SEFDM signal occupies less bandwidth for the same OFDM signal transmission rate. Another scenario, that has not been tested yet but will also be beneficial, is that of increasing the number of subcarriers for the SEFDM case to maintain the same OFDM bandwidth rather than saving bandwidth. For such case, the transmission data rate will be increased relative to OFDM by the same ζ percentage.

7.3.2 SEFDM vs OFDM Pilots

To evaluate the effect of the special OFDM pilot used to estimate the CFR and phase offset, a comparison is held when this pilot is used versus the use of an SEFDM pilot, similar to SEFDM transmitted data symbols. The evaluation is done by checking the level of impairment on each transmitted symbol, using the root mean square (RMS) of the normalised error vector magnitude (EVM) E_k of the data symbols after the equalisation and phase offset correction stage at the same Rx input

Table 7.2: The spectral efficiency and constellation of experimentally obtained received and equalised symbols before channel decoding.
For the 9^{th} subcarrier ($f = 83.5$ GHz) and different compression factors and constellation sizes.

M & R_b	Measurements	$\alpha = 1$	$\alpha = 4/5$	$\alpha = 2/3$
QPSK 8 Gbps	Constellation Before Equalisation	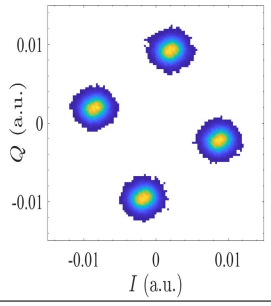	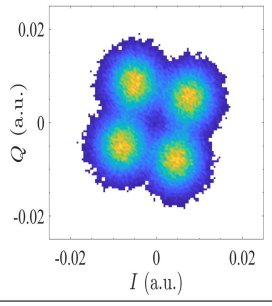	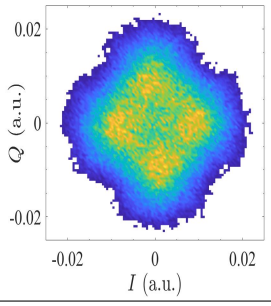
	Constellation After both Equalisation and Phase Correction	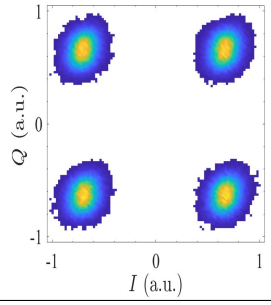	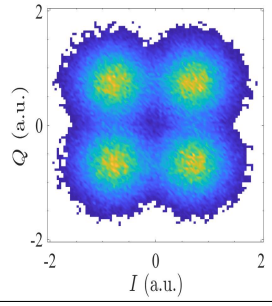	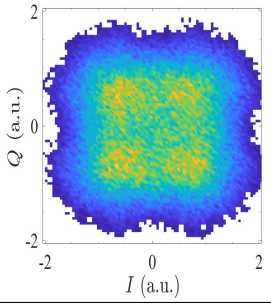
	Spectral Efficiency (η)	0.67 b/s/Hz	0.83 b/s/Hz	1 b/s/Hz
8PSK 12 Gbps	Constellation Before Equalisation	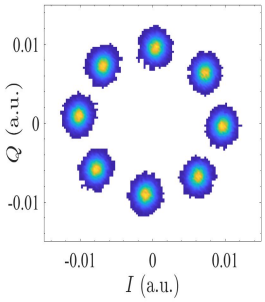	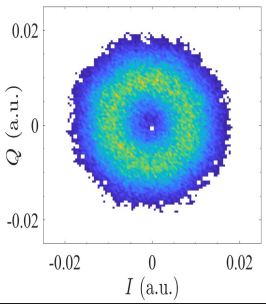	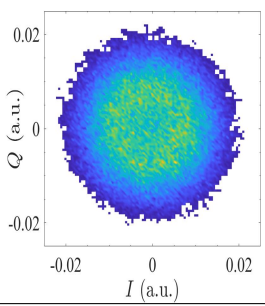
	Constellation After both Equalisation and Phase Correction	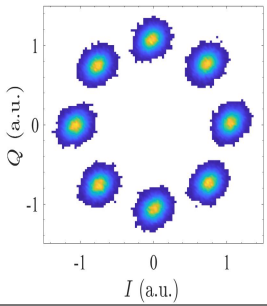	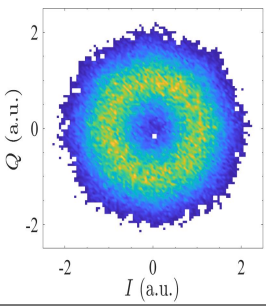	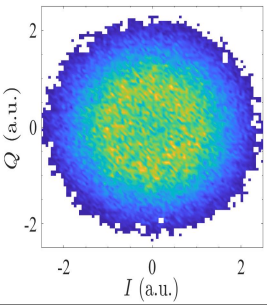
	Spectral Efficiency (η)	1 b/s/Hz	1.25 b/s/Hz	1.5 b/s/Hz

power value ($SNR = 25$ dB). The normalised EVM values are calculated as

$$E_k = \sqrt{\frac{(I_k - \tilde{I}_k)^2 + (Q_k - \tilde{Q}_k)^2}{(I_k + Q_k)^2}}, \quad 1 \leq k \leq L_d, \tag{7.1}$$

where L_d is the vector size of the transmitted symbols, I_k, Q_k are the in-phase and quadrature-phase elements of the k^{th} transmitted symbol, while $\tilde{I}_k$, $\tilde{Q}_k$ are the in-phase and quadrature-phase elements of the k^{th} received symbol after equalisation and phase correction. Consequently, the RMS of EVM (EVM_r) is evaluated by taking the square root of the mean square of the EVM across all values. EVM_r in dB scale is given by

$$EVM_r = 20\log\sqrt{\frac{1}{L_d}\sum_{k=1}^{L_d} {E_k}^2}. \tag{7.2}$$

Fig. 7.7 illustrates the advantage of using the special OFDM pilot over SEFDM pilot, where the EVM drops by approximately 2 and 2.5 dB for $\alpha = 4/5$ and $\alpha = 2/3$, respectively. The spectrum of the equalised received signal, obtained by the experiment, for the case of $\alpha = 0.8$, is shown for comparison. Clearly, the equalised spectrum using OFDM pilot is closer to the transmitted spectrum, compared to that of the SEFDM pilot case.

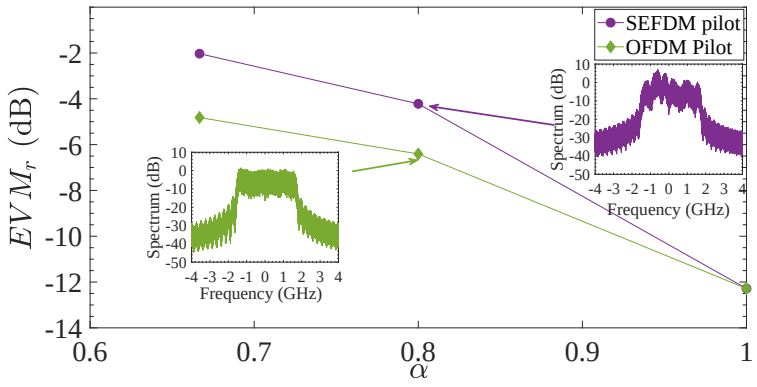

Figure 7.7: EVM_r calculation to compare the utilization of OFDM pilots over SEFDM pilots.

The advantage of such pilot design can also be considered from another perspective; by calculating the absolute phase difference between the transmitted and equalised symbols, using SEFDM and OFDM pilots. Fig. 7.8 demonstrates the

absolute phase difference values for the OFDM and SEFDM pilots cases. From the figure, it can be noticed that by using an OFDM pilot, the phase difference is lower compared to the case with SEFDM pilot. Furthermore, the phase difference increases by decreasing α (i.e. increase the compression level).

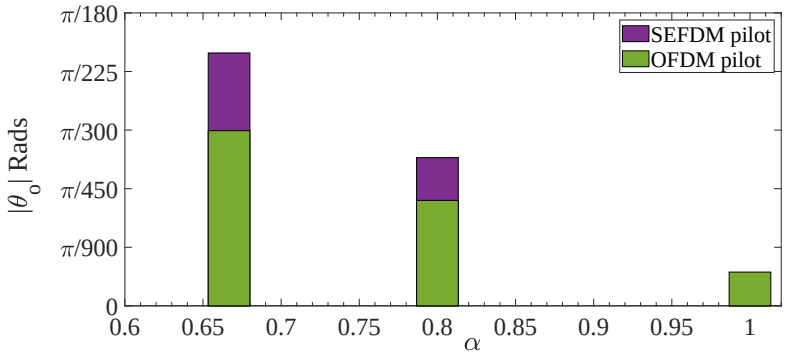

Figure 7.8: The absolute phase difference calculation to compare the utilisation of OFDM pilots over SEFDM pilots.

7.3.3 BER Results

Finally, due to steep nature of the waterfall BER curves of LDPC coded schemes [87] and measurement equipment limitations; specifically the AWG buffer size limits the number of transmitted samples, the BER results collected lacked resolution and detail and the error performance displayed either high numbers of errors or simply error free behaviour (i.e. BER $< 5 \times 10^{-6}$). As such, BER curves are not plotted here, instead Table 7.3 gives the *SNR* values at the receiver input for which the transmission becomes error free, for the different combinations of α and M used in the experiment, when (64800×90) bits are transmitted.

Clearly from the table, the spectral efficiency improvement results in a power penalty of few dBs compared to OFDM. For instance, for the QPSK case, 1.4 and 2.9 dB increase in the power level is required, to increase the spectral efficiency by 25% and 50%, respectively. On the other hand, for the higher constellation order (8PSK), the signal appears to be slightly more sensitive to bandwidth compression, resulting in a slightly higher power penalty. It is worth noting that the noise level and non-linear impairments of the time-interleaved high-speed oscilloscope scale with the power of the received signal, therefore, in a more ideal setup, the *SNR*

Table 7.3:
Measured *SNR* values at receiver input for error free transmission.

	M	α	*SNR* (dB)
QPSK	4	1	5.1
	4	4/5	6.5
	4	2/3	8.0
8-PSK	8	1	7.0
	8	4/5	9.2
	8	2/3	11.8

required to achieve error free operation will be lower (better) than what is measured and reported here in Table 7.3. Chapter 5 has shown that this power penalty gap can be further reduced, by using a SIC. However, as the aim of this demonstration is to validate the concept of utilising SEFDM for E-band data transmission, a simple detector similar to OFDM is used, which can be implemented in real time.

Finally, referring to Table 7.3 and the reported attenuation levels from the digital attenuator (item 4 in Fig. 7.4) for each *SNR* value, coupled with a 46 dBi-gain E-band antenna at both the Tx and Rx, it can be anticipated that the best-case hop link is between 2.4 and 4.1 kilometres. Such calculation takes into account the free space path loss only, without other impairments like oxygen absorption, rain, humidity and others. Thus, the reported distance values may be considered as the upper-bound values for future experiments, where the E-band link will be affected by environmental and weather conditions.

7.4 Conclusions

This work reports an experimental demonstration of SEFDM signals transmission over an E-band (81-86) GHz frequency range. The experimental setup design is divided into two sections; hardware setup and digital signal processing. The testbed design and the equipment used are detailed in the hardware setup section. The measurements of the channel magnitude and phase responses and time delay guaranteed dealing with a controlled frequency selective environment. GaAs microwave inte-

grated circuits transceiver chips, especially designed for the transmission of multi-carrier signals in the E-band are utilised for filtering, amplifying and conversing from baseband to RF spectrum and vice versa.

In the digital signal processing part, each step starting from message bits generation, all the way to detect the message bits at the receiver, are demonstrated. The channel estimation scheme developed in Chapter 6, contributed to the capability of accurate estimation of the channel response, which is essential to mitigate the channel impairments. Furthermore, the orthogonal nature of the pilot symbols in this estimation scheme allowed developing a new timing synchronization method. In this method, the pilot symbols are also used here for timing synchronization, as the pilot symbols in this experiment are sent ahead of the data symbols. Consequently, the overall system overhead size will be reduced. In addition to this, the powerful LDPC channel coding and coded bits interleaving are implemented to enhance error performance.

The results reported a successful transmission of SEFDM signals in the E-band at a highest rate of 12 Gbps. Such transmission, with judicious selection of modulation format and SEFDM signal compression, allows up to 50% improvement in spectral efficiency (relative to OFDM) with some loss of performance that may be ameliorated by using more sophisticated detection techniques. Furthermore, the EVM results proved the efficiency of the aforementioned channel estimation scheme when compared to conventional channel estimation schemes. In the future, this experiment will be proceeded to transmit over a higher distance in non-line of sight multipath indoor and outdoor environments.

Chapter 8

Design and Performance of SEFDM Signals with Power Allocation

Power allocation is a technique used to distribute a certain amount of power among the available resources at the transmitter. The policy followed to allocate power, differs according to the application it serves. The concept of power allocation was suggested for multiuser OFDM systems, to increase capacity and improve robustness to interference caused by multipath channels [156]. More recently, the concept of power allocation has become popular, after the successful application of power NOMA techniques to 5G and beyond cellular systems [110].

In multiuser OFDM, multiple users are allowed to share the same OFDM symbol. A dynamic allocation of power among users in a multiuser OFDM introduces a new dimension to the system optimisation problem. In [156], the advantage of power allocation in maximising the transmission rate among users for a given transmitted power level is proven. Power allocation is also applied to OFDM to maintain fairness among users experiencing different channel conditions. Thus, the worse the channel condition, the higher the power level allocated to a user, depending on the total available power [157]. Furthermore, power allocation is combined with adaptive OFDM in [158], to achieve a better throughput performance for a fixed BER target.

Power allocation was implemented in LTE systems to improve the channel estimation accuracy, which is crucial for maintaining good system performance [159].

This is achieved by allocating more power to the subcarriers carrying channel reference symbol (CRS) signals, compared to the data subcarriers [159].

More recently, the NOMA technique has attracted substantial attention for 5G and beyond cellular systems. The application of NOMA results in: *i*) increase in the overall system throughput; *ii*) support of diverse quality of service (QoS) requirements; *iii*) and low latency and massive connectivity [160]. NOMA assigns to multiple users the same time and frequency resources, while it realises multiple access via power domain or code domain multiplexing [160]. In power NOMA, the users suffering from worse channel conditions are allocated more power. At the receiver SIC is applied to detect and cancel the interference from other users, where the user with the higher power level is detected first, then cancelled from other users received signal. Additionally, Soft defined multiple access (SoDeMA) is a newly proposed concept, where orthogonal multiple access (OMA) and different NOMA techniques can coexist to enhance the total system spectral efficiency [110].

Inspired by the power domain multiplexing of OFDM and NOMA, this work of this chapter, and for the first time, introduces a similar power allocation method to SEFDM, where different subcarriers within the same SEFDM symbol are allocated different power levels. Despite the fact that the power allocation scheme is not novel on its own, its application to serve a different purpose, which is reducing the effect of ICI is new. The advantages of power allocation to SEFDM systems proved in this chapter are summarised below:

1. Enhancement of the system stability by reducing the condition number of the correlation matrix and making it independent of the number of subcarriers. The essential limitation of SEFDM is in its correlation matrix resulting from the interference between subcarriers. The condition number of this matrix is substantially high, especially with high compression level and/or relatively high number of subcarriers, thus, the system becomes ill-conditioned [50].

2. Substantial reduction in detector complexity. The detection of the SEFDM signal with power allocation is processed through two stages. First, the information transmitted on the subcarriers of high-power level is estimated and

the interference coming from these subcarriers to the rest of the subcarriers is calculated and then cancelled in the second stage. This detection design will reduce the complexity compared to conventional methods as will be shown in this work.

3. Power allocation results in PAPR reduction compared to conventional SEFDM and OFDM signals.

4. Channel estimation becomes more accurate. Similar to current LTE systems, the same power allocation scheme is applied, where the CRS (pilot) signals are allocated with higher power when compared to data signals. However, in SEFDM, with the interference taken into account, the pilot signals require higher power to overcome the random fluctuations in system performance due to ICI.

The outline of this chapter is as follows; section 8.1 applies power allocation to SEFDM signals to enhance its detection, where the system model is implemented and the advantages of such method are explored. Section 8.2 explores the application of power allocation to SEFDM to enhance its channel estimation accuracy. The simulation study in this section is for a specific scenario of LTE physical downlink channel dedicated to transmit user data. Finally, section 8.3 wraps up the findings and draws conclusions.

8.1 Power Allocation for SEFDM Signal Detection

The proposed power allocation method is characterised by transmitting subcarriers at different power levels. The SEFDM feature of overlapped mutually orthogonal subsets, described in Chapter 6 for partial channel estimation scheme, is applied here too. For $\alpha = b/c$ where b and c are integers, $b < c$ and $c < N$, there are $\lceil N/c \rceil$ mutually orthogonal subcarriers ($|\Lambda_{m,n}| = 0$) for $\alpha(m-n) \in \mathbb{Z}$. Thus, the subset of $\lceil N/c \rceil$ mutually orthogonal subcarriers will be transmitted at higher power level (P_H), as the subcarriers in this subset will not interfere with each others. The rest $N - \lceil N/c \rceil$ subcarriers are allocated with the lower power level (P_L).

A visual representation of power allocation is given in Fig. 8.7, where the spectrum of an SEFDM symbol with $N = 16$, $\alpha = 4/5$ is shown. In this case, $b = 4$ and $c = 5$, which results in $\lceil 16/5 \rceil = 4$ subcarriers with power level P_H and the rest of the 12 subcarriers with power level P_L. From the spectrum, the mutual orthogonality feature of the 4 subcarriers is observed, as at the peak of any of them, the rest of the subcarriers within the orthogonal subset are zero. In spite of the fact that the interference on the rest 12 subcarriers becomes higher, this interference may be detected better at the receiver and then deducted. This will enhance the overall system performance as will be shown in the next section.

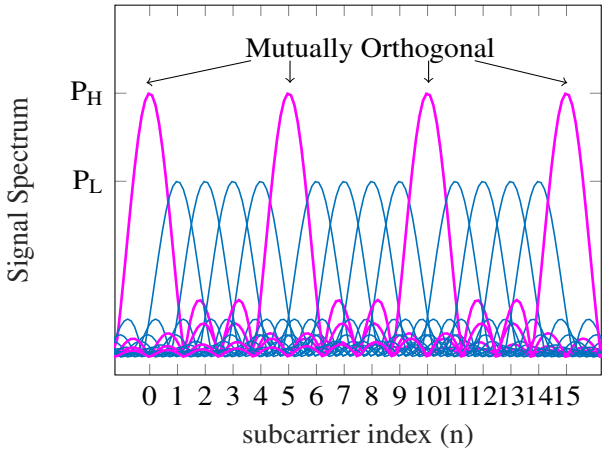

Figure 8.1: SEFDM signal spectrum for $N = 16$, $\alpha = 4/5$, $b = 4$ and $c = 5$.

In order to have a fair comparison with SEFDM signals without power allocation, it is important to maintain the same total transmitted power (P_T). Hence, the increase in the power level of some subcarriers, will result in a reduction of the power level of the rest, such that the total power P_T remains unchanged. The relation between P_T, P_H and P_L is given by

$$P_T = P_H \lceil N/c \rceil + P_L (N - \lceil N/c \rceil). \tag{8.1}$$

The parameter ρ is defined as the ratio between the upper and lower power levels (i.e. P_H/P_L) and ρ optimum value is a function of the system parameters N and α,

as will be shown in the next section. Given this, (8.1) becomes

$$P_T = P_L\lceil N/c\rceil(\rho-1)+P_L N. \tag{8.2}$$

In the following, the transceiver design of SEFDM signals with power allocation transmission is described.

8.1.1 System Design

A high level descriptive transceiver design of SEFDM signals with power allocation transmission is shown in Fig. 8.2. The transmitter here is similar to the previously discussed SEFDM system model in Chapter 3, but an extra stage is inserted before SEFDM modulation to perform power allocation. This is achieved by multiplying the $\mathbf{z} \triangleq \{z_0, z_1, .., , z_{N-1}\}$ complex baseband symbols by the diagonal matrix $\rho \in \mathbb{C}^{N\times N}$. The matrix element ρ_{ii} takes one of the two weighting factors value to reflect the variation in power level (i.e. P_L and P_H), depending on the subcarrier position within the SEFDM symbol. The equation below represents the discrete SEFDM-modulated symbol vector, $\mathbf{x} \in \mathbb{C}^{Q\times 1}$, at the transmitter side with power allocation

$$\mathbf{x} = \Phi(\rho\mathbf{z}), \tag{8.3}$$

Assuming the SEFDM signal in (8.3) were to be transmitted over AWGN channel. The SEFDM received signal $\mathbf{y} \in \mathbb{C}^{Q\times 1}$, will be detected in two stages. In the first

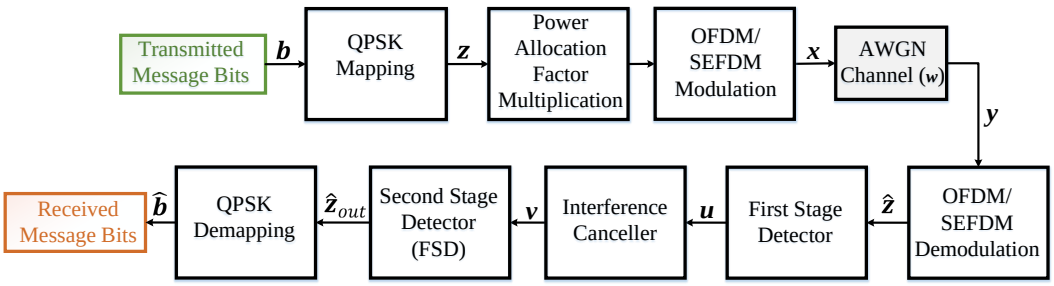

Figure 8.2: A high level descriptive transceiver design of SEFDM signals with power allocation.

stage, the mutually orthogonal subcarriers are detected, by taking a hard decision

on these high-power level subcarriers, while the rest are set to zero as shown below

$$u_n = \begin{cases} \lfloor \hat{z}_n \rceil, & n \bmod c = 0 \\ 0, & \text{otherwise,} \end{cases} \tag{8.4}$$

where $\lfloor . \rceil$ is the slice function and mod is the modulo operation. Thereafter, $\mathbf{u} \in \mathbb{C}^{N\times 1}$ is used to calculate and cancel the interference from the subcarriers with high-power on the rest of the low-power subcarriers, as shown in (8.5). This interference cancellation method is similar to the one of Chapter 5, which was applied with SIC in an SEFDM satellite scenario. The resultant vector $\mathbf{v} \in \mathbb{C}^{N\times 1}$ is given by

$$\mathbf{v} = \hat{\mathbf{z}} - \Lambda \mathbf{u}. \tag{8.5}$$

As a consequence of the first stage interference cancellation, the correlation matrix Λ is updated to $\acute{\Lambda}$ in the second detection stage, where the elements describing the interference already cancelled in the first stage are set to zero and this is given by

$$\acute{\Lambda}_{m,n} = \begin{cases} 0, & n \bmod c = 0 \\ \Lambda_{m,n}, & \text{otherwise} \end{cases} \tag{8.6}$$

This adjustment to the correlation matrix results in several orders of magnitude reduction in its condition number, as will be explained in the next section. The resultant $\mathbf{v}$ and $\acute{\Lambda}$ are the input to the second stage detector FSD.

The FSD algorithm fixes the complexity of SD by restricting the search within a limited subspace of the SD problem. FSD was first applied to MIMO systems in [161] and then to SEFDM in [12]. At every level (k), a fixed number of nodes, or in other words tree width ($T_w = 2^k$), are examined. The FSD estimate ($\hat{\mathbf{z}}_{out}$) is obtained from the minimisation problem stated in [162]

$$\hat{\mathbf{z}}_{out} = \arg \min_{\tilde{\mathbf{z}} \subset \mathscr{H}, \tilde{z} \in M} \|\mathbf{L}(\mathbf{p} - \tilde{\mathbf{z}})\|^2 \leq \breve{g}, \tag{8.7}$$

where $\|.\|$ is the Euclidean norm, $\tilde{\mathbf{z}}$ is a candidate SEFDM symbol within the search

subspace $\mathscr{H}$, M is the constellation cardinality, $\mathbf{L}$ is an upper triangular matrix defined by the Cholesky decomposition as $\acute{\Lambda}^{\mathrm{H}}\acute{\Lambda} = \mathbf{L}^{\mathrm{H}}\mathbf{L}$, $(.)^{\mathrm{H}}$ is the Hermitian operator and $\mathbf{p}$, given in [162], by

$$\mathbf{p} = (\acute{\Lambda}^{\mathrm{H}}\acute{\Lambda})^{-1}\acute{\Lambda}\mathbf{v}, \tag{8.8}$$

and $\breve{g}$ is the radius of the search sphere, which corresponds to the distance from the ZF estimate $\hat{\mathbf{z}}_{\mathrm{ZF}} = \lfloor \acute{\Lambda}^{-1}\mathbf{v} \rceil$ and is given by [162]

$$\breve{g} = \|\mathbf{v} - \acute{\Lambda}\hat{\mathbf{z}}_{\mathrm{ZF}}\|^2, \tag{8.9}$$

From the above, it is noticed that the first stage detector affects both the ZF estimate $\hat{\mathbf{z}}_{\mathrm{ZF}}$ and the correlation matrix $\acute{\Lambda}$ for FSD detection. The output of the FSD is demapped to recover the received bits $\hat{\mathbf{b}}$, then determine the system error rate. For a detailed mathematical treatment about the application of FSD to SEFDM, readers are referred to [63] and [162]. In the following, the benefits of power allocation in this given scenario are explored.

8.1.2 Power Allocation Benefits

Here, the benefits of power allocation are divided into three main categories. Simulation results are provided for each, to prove the efficiency of power allocation in SEFDM systems.

8.1.2.1 Condition number reduction

The condition number of a matrix is defined as the ratio of its maximum eigenvalue to its minimum eigenvalue. Previously, in [50], it was shown that eigenvalues of the correlation matrix (Λ) tend to zero with higher N and/or lower α. Hence, the correlation matrix becomes ill-conditioned, because the condition number turn out to be very high. The computation of the inverse of an ill-conditioned matrix for a linear detector will be prone to large numerical errors in such case. In SEFDM, the condition number of Λ increases rapidly with increasing the compression level and/or the number of subcarriers [50].

Fig. 8.3 demonstrates the logarithmic value of the condition number

(log(cond)) versus N for the correlation matrix Λ and the resultant matrix after interference cancellation $\acute{\Lambda}$ with different values of α. The figure shows that the resultant correlation matrix $\acute{\Lambda}$ has a drastic reduction in its condition number compared to conventional SEFDM and it is independent of N, similar to the OFDM case.

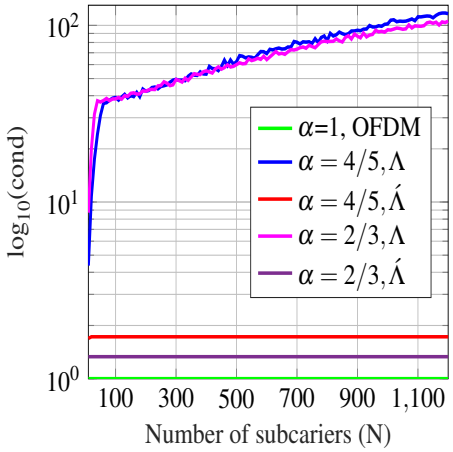

Figure 8.3: Condition number of Λ and $\acute{\Lambda}$ versus N for different values of α.

The reward of this correlation matrix adjustment is highly significant for sub-optimal and low complex detectors that requires matrix inversion. For instance the FSD requires an inversion of the correlation matrix for an initial ZF estimate as shown in (8.7). If the initial estimate is compromised by contributions of the ill-conditioned system then the deviations from the received statistics point will propagate to the final solution. It is worth noting that there is no purpose of using power allocation in optimal detectors, such as ML, or detectors that do not require matrix inversion, like the SIC discussed in Chapter 5.

8.1.2.2 Complexity reduction

In preparation for the study of the error performance and complexity of SEFDM with power allocation, the optimum power ratio ρ is to be determined first. The optimum ρ is defined here as the value that minimises the required E_b/N_0 value for a given error performance and found through numerical simulations. Fig. 8.4 demonstrates the E_b/N_0 value required to achieve a BER of 10^{-3}, using the two stages detector in Fig. 8.2, with $T_w = 2$ for the FSD. It can be noticed that the

optimum value of ρ depends on N and α and it moves towards higher values for higher N and/or lower α, as the interference level becomes higher. Furthermore, the starting ρ value varies as well, because it has been found that the BER curve reaches an error floor at values higher than 10^{-3}, as the error caused by ICI is dominant one in this region.

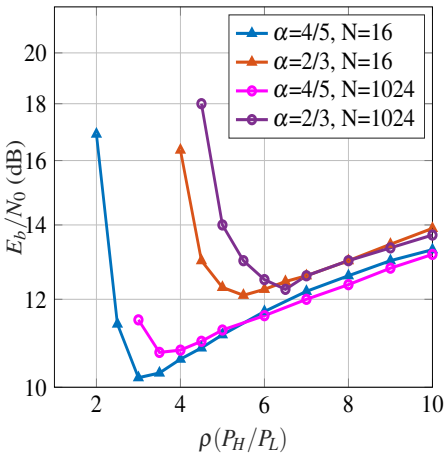

Figure 8.4: E_b/N_0 required to achieve a BER$= 10^{-3}$ versus ρ, for different values of N and α.

Consequently, the optimum ρ values are then used to evaluate and compare the BER performance of the new method to conventional SEFDM. Fig. 8.5 demonstrates the BER results versus E_b/N_0 for $M = 4$, $\alpha = 4/5$ and $\alpha = 2/3$ and for small and large number of subcarriers. The FSD is of unity level when power allocation scheme is used, however, the FSD detector becomes more complex and of higher level order for conventional SEFDM. Earlier work has shown that for number of subcarriers exceeding 32, the FSD performance degrades substantially rendering its impractical use [63]. From the results, it can be noticed that the tree width of conventional FSD (diamond marker in Fig. 8.5(a)) needs to be increased substantially to achieve BER performance comparable to the new method with power allocation and unity level FSD. For instance, when $N = 16$, the tree width increases from 2 to 16 for $\alpha = 4/5$ and $\alpha = 2/3$ to 32, factors of 800% and 1600%, respectively. For $N = 1024$ only the results with power allocation are shown, as for conventional FSD with high number of subcarriers the correlation matrix is almost singular (refer to Fig. 8.3), thus, FSD is not capable of signal detection.

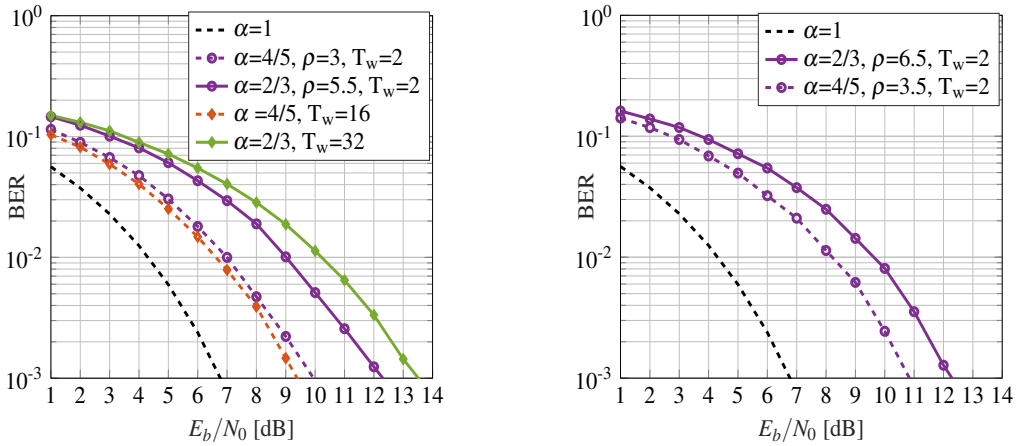

(a) $N = 16$ **(b)** $N = 1024$

Figure 8.5: A comparison of SEFDM signals BER performance with and without power allocation for $M = 4$, $\alpha = 4/5, 2/3$ and (a) $N = 16$, (b) $N = 1024$.

Table 8.1: Computational complexity (in terms of number of real operations).

Process description	Number of operations
1^{st} stage multiplications	$4N^2$
1^{st} stage additions	$4N^2$
2^{nd} stage (FSD) multiplications	$\sum_{n=1}^{w} 2^n[2n+1] + \sum_{m=w+1}^{2N} T_w[2m+1]$
2^{nd} stage (FSD) additions	$\sum_{n=1}^{w} 2^n[2n-1] + \sum_{m=w+1}^{2N} T_w[2m-1]$ $+4{T_w}^2(2N-w)$

The computational complexity for the detector of two stages of Fig. 8.2, in terms of real-valued multiplications and real-valued additions, is summarised in Table 8.1. A detailed computation of FSD complexity can be found in [162]. Table 8.2 calculates the complexity for the simulated BER results of Fig. 8.5(a) using Table 8.1. Clearly, the new method is an order of magnitude less complex than the stand-alone FSD detector without power allocation.

8.1.2.3 PAPR reduction

As defined before in Section 3.5, PAPR is a parameter that holds information about the range of power variation in the signal, which is vital in design optimisation to choose the system components. In [78], it was shown that for SEFDM the PAPR is dependent of the compression level in SEFDM and PAPR reduces by reducing α,

Table 8.2: Comparison of total number of operation between conventional FSD and FSD with power allocation.

Case	Multiplications	Additions
Conventional FSD, $T_w = 16$	17250	44966
Conventional FSD, $T_w = 32$	34274	143014
FSD with power allocation, $T_w = 2$	3200	3566

compared to OFDM. Thus, SEFDM signals are less prone to the non-linear effect when amplifiers are used, which is considered as an added advantage of SEFDM besides improving the spectral efficiency. Recently, [79] and [80] investigated the PAPR of MFTN, which is similar to an SEFDM case with RRC shaped subcarriers [73]. The results agree with the previous conclusion of [78] that SEFDM and MFTN have a better PAPR behaviour than OFDM. Thence, it is important to ensure that the PAPR behaviour of SEFDM with power allocation will not degrade performance.

The PAPR performance is usually evaluated by the complementary cumulative distribution function (CCDF), which is defined as the probability that the PAPR surpasses a certain value ($\text{PAPR}_0 > 0$). Fig. 8.6 shows the PAPR distribution for two different compression values ($\alpha = 4/5, 2/3$), given $N = 16$ and $M = 4$. The PAPR of OFDM is the benchmark to be compared to.

From the results, it can be noticed that the PAPR performance is improved by lowering α. For example, given $\rho = 1$, the probability of PAPR$=$ 8 dB is 3%; 2% and 1% for $\alpha = 1$; $4/5$ and $2/3$, respectively. Power allocation seems to enhance the PAPR performance further, when compared to the case of $\rho = 1$. Logically, this is because the total power is fixed, so the power is lowered on the majority of the subcarriers to compensate for the power boost of the chosen orthogonal subcarriers set. Therefore, the peak resulting from the alignment of subcarriers with lowered power level, which is the majority, is less than that peak when no power allocation is used, as their power will be higher. However, the average power will not be affected and this results in lower PAPR. Furthermore, by increasing ρ, the power allocated for subcarriers with low power level gets even lower and this explains the better PAPR for higher ρ.

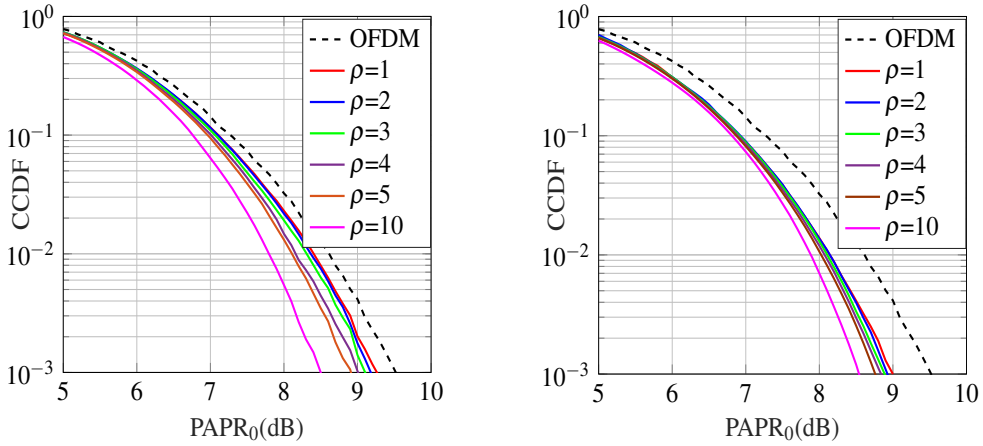

(a) $\alpha = 4/5$ **(b)** $\alpha = 2/3$

Figure 8.6: PAPR distribution of SEFDM signals with different power ratios (ρ) and $N = 16$, $M = 4$, (a) $\alpha = 4/5$, (b) $\alpha = 2/3$.

Methods introduced to reduce PAPR for OFDM, SEFDM and MFTN, such as SLW [78] and partial transmit sequence [79] reduction algorithms can be applied here as well, for further PAPR reduction.

Taking all the above into account, power allocation has proved to be beneficial for SEFDM systems with sub-optimal detectors. Given the importance of channel estimation, the following section explores the application of power allocation for channel estimation.

8.2 Power Allocation for Channel Estimation

A similar concept to SoDeMA in [110] may be applied to multiplexing, leading to soft defined FDM (SoDeFDM). SoDeFDM allows the coexistence of different FDM schemes in a given system and provides more flexibility in modulation and multiplexing to support different services and applications, while taking into consideration the channel conditions. For example, if an eNodeB is serving a UE located in the middle of the cell with relatively good channel condition, SEFDM with high compression level can be applied, while for the case of bad channel condition or ultra reliable services, OFDM scheme is preferable. [1] This adds another degree of freedom for systems similar to the work in Chapter 6.

[1]The work in this section was done at BT research labs in Adastral Park, Ipswich, United kingdom as a part of an internship, funded by BT and the EPSRC Impact Acceleration Award.

In SoDeFDM, the generation and detection of the different FDM schemes have to use the same hardware architecture and the switching between these schemes must be fast and flexible. The above condition is met for SEFDM/ OFDM signals, given that the generation and detection of SEFDM signals is implemented in a similar way to OFDM using an IFFT/ FFT pair, as elaborated in Chapter 6 and the work done before in [57]. Although the newly developed channel estimation scheme proved to be robust and accurate, it requires different resource block design for SEFDM, compared to OFDM and this limits its application to SoDeFDM systems. This being the case, in this work, power allocation is proposed to solve the problem of channel estimation accuracy in SEFDM, whilst preserving the same resource block design of OFDM. The case study, described in the following section, is for the application of SoDeFDM to the LTE downlink shared channel reserved for user data transmission.

8.2.1 SoDeFDM LTE PDSCH System Design

In this work, the case of SoDeFDM 10 MHz-LTE physical downlink shared channel (PDSCH) is simulated. PDSCH is the channel that carriers the downlink user data from eNodeB to UE. Fig. 8.7 demonstrates the normalised power spectra of LTE SoDeFDM downlink signals, for different values of α.

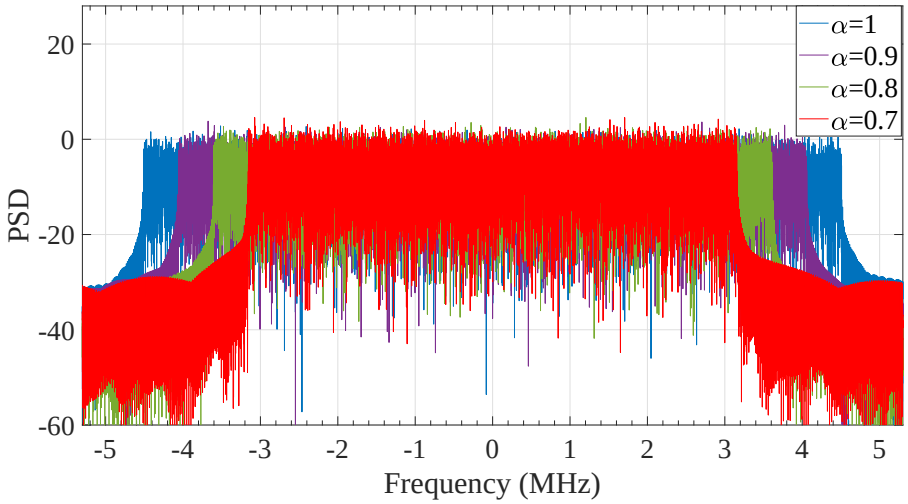

Figure 8.7: LTE power spectra for SoDeFDM signals with different compression levels.

Consider the system architecture depicted in Fig. 8.8. A turbo encoder of rate

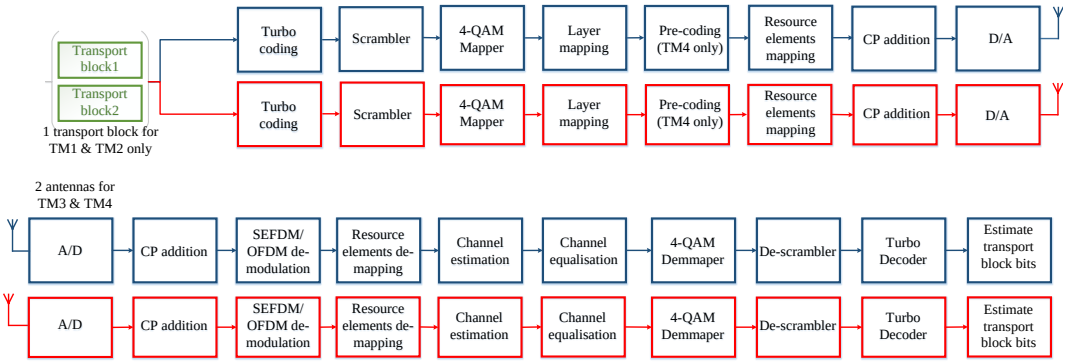

Figure 8.8: A high level descriptive block diagram of the PDSCH LTE SoDeFDM transceiver design.

($R_c = 1/2$) generates redundancy bits to protect the information bits. The output is referred to as a codeword. In LTE, it is either 1 or 2 codewords depending on the transmission mode [163]. 3GPP introduced 10 transmission modes, which are defined according to the number of antennas and their functionality [163]. These codewords are mapped into layers, then precoded into antenna ports. In this work, four transmission modes are examined:

- TM1: A single-input single-output mode, where the base station and the user equipment operate with a single antenna each.

- TM2: Transmitter diversity scenario with 2 antennas at the transmitter and 1 at the receiver (2×1). Space frequency block coding based on Alamouti coding [164] is used to enhance the error performance.

- TM3: An open-loop based precoding 2×2 spatial multiplexing system, where the input stream is divided into two independent streams to increase the system throughput. Open-loop means there is no feedback from the UE to eNodeB and its found to be suitable for good condition channels or when the user speed is relatively high.

- TM4: A closed-loop based precoding 2×2 spatial multiplexing system. It is similar to TM3 but with a feedback from the UE, to take into account the current channel state in the precoding process.

For further information about the above transmission modes and others implemented in LTE systems, readers are referred to the 3GPP standards [163].

After mapping the input coded bit stream to the antenna ports, the bits are scrambled using an external interleaver and mapped into a 4-QAM data symbols. Afterwards, the mapped data symbols and CRS, or in other words pilot signals, are mapped into resource blocks. In the case of 10 MHz, the number of resource blocks is 50 and each consists of 12 subcarriers of frequency spacing $\Delta f = \alpha \times 15$ KHz. Thereafter, the resource blocks are mapped into subframes, where each subframe is of length 1 ms and consists of 14 SoDeFDM symbols for the case of normal CP. 8 CRS signals are allocated in different resource elements scattered through each resource block [163].

The resource elements within a subframe are the input to SoDeFDM modulation using an IFFT of size $Q = 1024$ and the number of subcarriers is $N = 600$. At the output of the IFFT, the first $\lfloor \alpha \times Q \rfloor$ are transmitted while the rest are truncated. This truncation results in subcarriers frequency spacing compression as explained previously in Chapter 6. Given this SoDeFDM LTE generation method, the sampling rate (f_s) in Hz is a function of α and is calculated by

$$f_s = \frac{(\lfloor \alpha \times 1024 \rfloor \times 14) + L_{CP}}{10^{-3}}, \tag{8.10}$$

where L_{CP} is the total number of samples used for CP per subframe, which is 1024 samples for normal CP (i.e. 7%) [163]. For simplicity, the number of CP samples is the same for any value of α. If the sampling rate is 15.36 MHz for OFDM, referring to (8.10), it will become 12.49 MHz for SEFDM ($\alpha = 0.8$).

As a side note, it is possible to fix the system sampling rate regardless of α, if the IFFT is replaced by an IDFT of size ($\lceil 1024/\alpha \rceil$) and the first 1024 samples are only taken from the output of the IFFT. The drawbacks are the IDFT complexity is higher than the IFFT and a separate IDFT/ DFT pair for each value of α will be required.

After modulation, a digital to analog converter (D/A) followed by an up-converter are used to get the signal ready for transmission. The impairments consid-

ered in this study are the multipath channel effect and AWGN. The channel model used is a normalized LTE extended pedestrian A model (EPA) [165] and the Doppler frequency is 5 Hz, while the antennas correlation is low.

At the receiver, after down conversion and A/D conversion, the symbol is demodulated by an FFT, whose input is adjusted by replacing the discarded samples at the transmitter with zeros. Afterwards, CRS signals are extracted and used to estimate the CFR. The channel is estimated every frame (i.e. 10 ms) by an MMSE estimator, followed by time and frequency averaging and interpolation. The estimated channel effect is reversed using a one tap-equaliser, then, the equalised symbols are soft de-mapped and the turbo decoder of 5 iterations estimates the transmitted message bits from the received codeword.

Power allocation is already implemented in current LTE systems, such as the resource elements carrying CRS are allocated with a higher power level when compared to resource elements carrying transmitted information. The power allocation factor is determined according to the the channel condition and leads to a potential enhancement in estimation accuracy of channel impairments, which is crucial for an accurate detection at the receiver. With this in mind and taking into account the interference in SEFDM, the same power allocation technique may be applied to SoDeFDM to ameliorate the effect of ICI in CRS signals. In the next section, the simulation results of SEFDM with power allocation for this case study are demonstrated.

8.2.2 Simulation Results

A new metric termed effective spectral efficiency (ESE) is introduced to evaluate the efficiency of SEFDM and power allocation. The difference between ESE and the spectral efficiency calculations in the previous chapters is that in ESE, the error rate is taken into account. ESE is calculated by

$$ESE = \sum_{k} \frac{(1 - BLER) \times b_s}{t \times \alpha \times BW}, \tag{8.11}$$

where k is the number of transmitted blocks, $BLER$ is the block error rate and it takes a value of 1 if there is an error in the block or 0 in the case of error free reception. Each block in this simulation study is of size equal to one LTE subframe and the total number of transmitted blocks is 1000. b_s is the number of information bits (uncoded) transmitted per block, t is the subframe duration (1 ms) and BW is the subframe bandwidth, which is $\alpha \times 10$ MHz in this case. First, for the purpose of benchmarking, a perfect knowledge of the CFR is assumed. Fig. 8.9 presents the ESE results versus SNR for the four transmission modes and different compression values. SNR is used instead of E_b/N_0, because these simulations uses the current LTE framework and in practice SNR is more informative. The following may be identified by looking at the results:

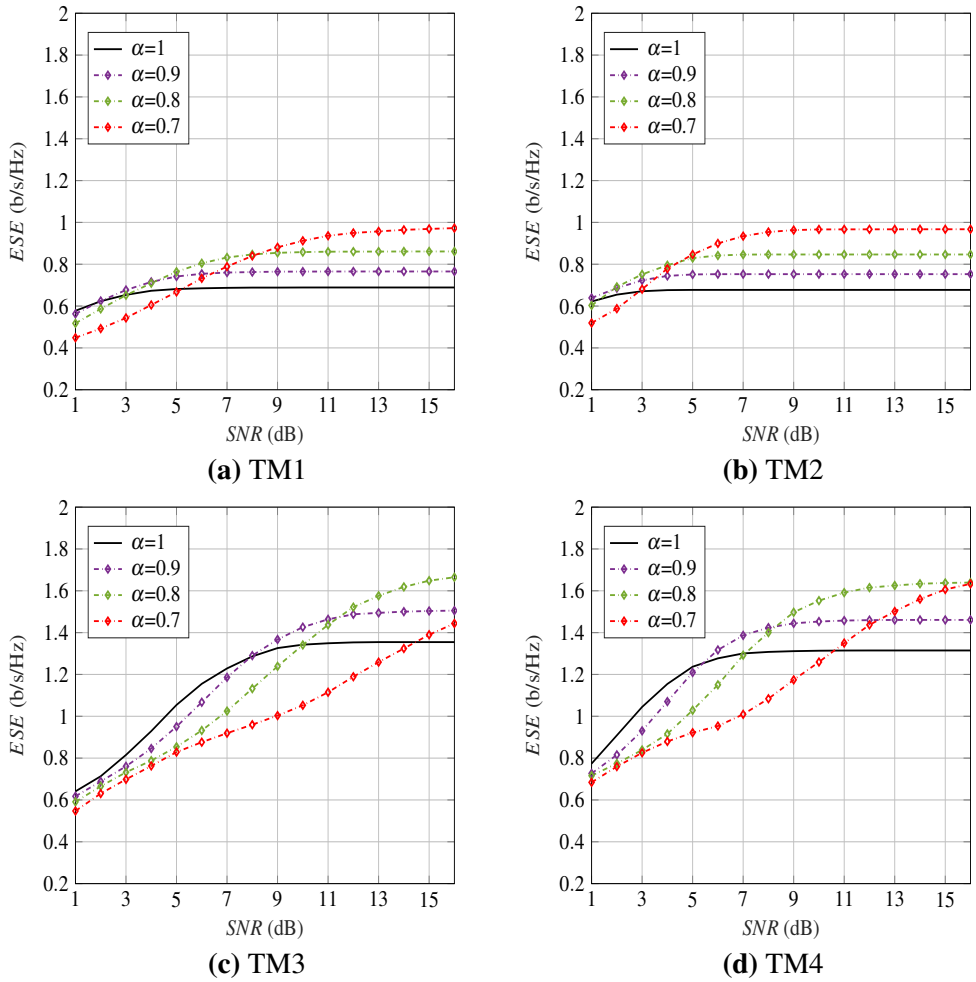

Figure 8.9: *ESE* vs. *SNR* for OFDM/SEFDM LTE PDSCH TM(1-4) with perfect channel estimation and different values of α.

- A general observation from the different transmission modes is that by increasing the transmission power level, the ESE increases up to a point where it saturates. The reason is an error free transmission is achieved at this power level and this maximises the ESE, as shown in (8.11).

- Given that the percentage of resource elements used for signalling per resource grid is 20-25% and the CP length is 7% of the transmitted signal, if the modulation cardinality is 4-QAM and the channel coding rate is $1/2$, then the maximum ESE would be around 0.7 bit/s/Hz for TM1 and TM2 and $\alpha = 1$. By looking at Fig. 8.9(a) and (b), as expected, the maximum ESE is 0.7 b/s/Hz for $\alpha = 1$ and the lower α is, the higher ESE, where the gain may reach up to 40%. However, higher *SNR* is required to achieve error free transmission due to ICI. Therefore, the advantage of SEFDM is more obvious in high *SNR* regions.

- In Fig. 8.9(b), it can be noticed that the required *SNR* to achieve maximum ESE for a given α is lower than that of TM1 in Fig. 8.9(a), due to transmission diversity. TM2 sends the same information in both antennas and this results in power advantage but not throughput. Thus, the maximum ESE is comparable to that of TM1. Furthermore, the advantage of bandwidth compression is obvious and the gain is more than 40% for $\alpha = 0.7$ and $SNR \geq 9$ dB.

- The spatial multiplexing in TM3 and TM4 almost duplicates the ESE, compared to TM1 and TM2. However, higher power level is required. The power penalty of TM4 is less than TM3 due to the feedback connection. Also, the advantage of SEFDM is still valid here, however, the maximum gain is less than 25% for $\alpha = 0.7$.

- The advantage of applying SoDeFDM is in optimising the ESE regarding the channel condition and available *SNR* without changing the modulation cardinality or coding rate. For example, if an eNodeB is operating at $SNR = 8$ dB, then from the results, the optimum α is 0.8 for TM1, while it is 0.7, 1, 0.9

for TM2, TM3 and TM4, respectively. This flexibility in altering α optimises the resources utilisation.

If the current channel estimation scheme of LTE without power allocation is applied to SoDeFDM, the estimated CFR will be significantly affected by the interference on the pilot symbol, mainly coming from neighbouring symbols. The estimation scheme will not be able to distinguish between the channel effect and interference. Fig. 8.10 demonstrates simulated ESE results when channel estimation is used, but

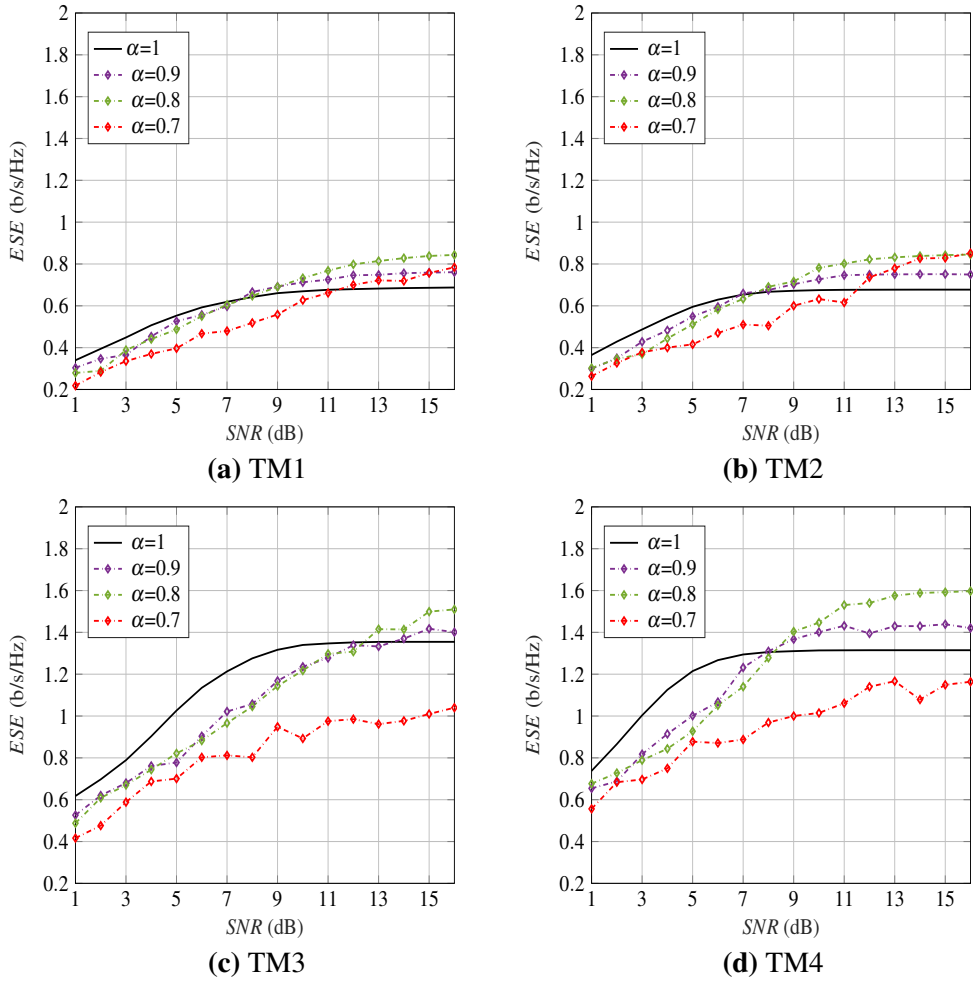

Figure 8.10: *ESE* vs. *SNR* for OFDM/SEFDM LTE PDSCH TM(1-4) with conventional channel estimation method and different values of α.

without power allocation. From the results, it can be noticed that the estimation inaccuracy due to the interference coming from other subcarriers within the same SEFDM symbol causes the fluctuations in the ESE curves. This interference is

random as it depends on the data being transmitted on other subcarriers and the fluctuations level tends to be higher for lower α, because the interference level becomes higher. The power gap due to channel estimation is the highest for TM2, because the transmitter diversity creates reliable transmission in the low *SNR* and the pilot estimation does not benefit from this diversity.

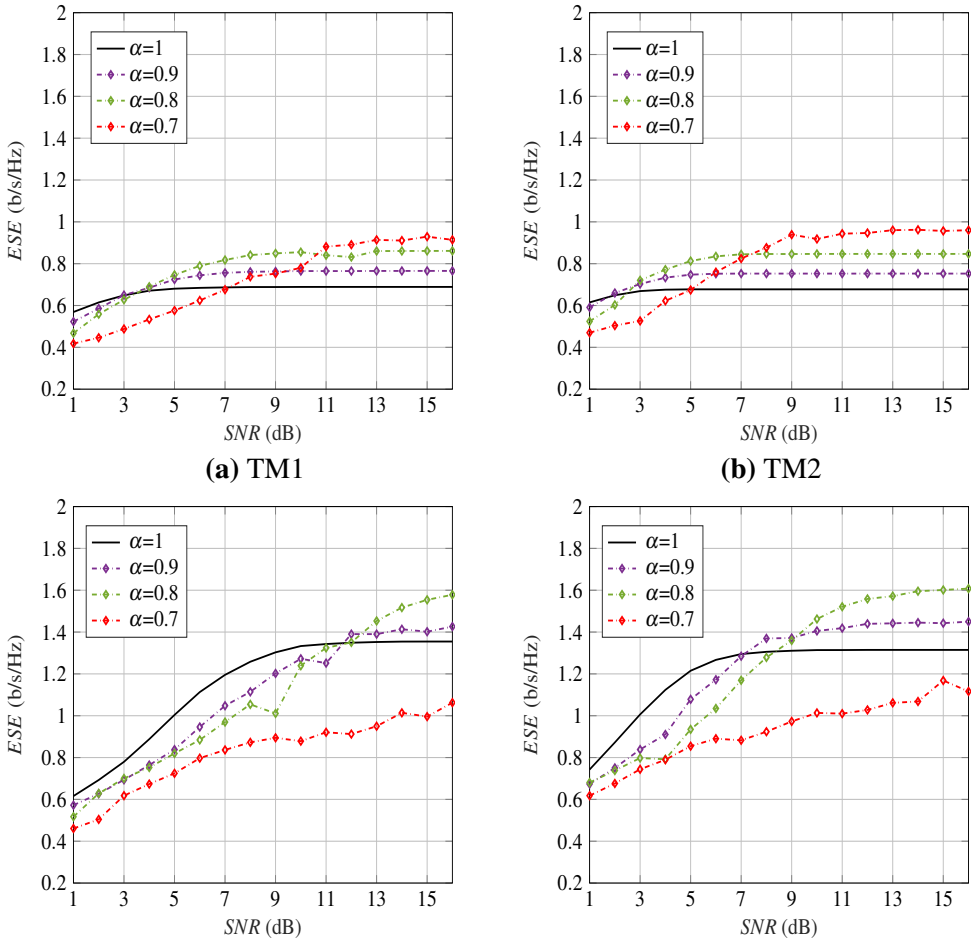

(a) TM1 **(b)** TM2

(c) TM3 **(d)** TM4

Figure 8.11: *ESE* vs. *SNR* for OFDM/SEFDM LTE PDSCH TM(1-4) with conventional channel estimation method and power allocation ($\rho = 2$) for different values of α.

To conclude, bandwidth compression shows a potential of significant enhancement in ESE as demonstrated in the case of perfect knowledge of CSI, however, in practice this is not the case. If the pilot design and estimation scheme of LTE without power allocation were to be used, the performance degrades and fluctuates. To solve this issue, a preliminary study is undertaken to address the utility of power

allocation in a similar manner to the power allocation currently used in LTE. In the following, only one value of power allocation factor is investigated, which is $\rho = 2$ (or 3 dB higher). This value is not the optimal one, because in a system such as LTE, many parameters are to be considered in the optimisation problem and this research is still in its early stage.

Fig. 8.11 demonstrates the ESE results with power allocation. From the results, it can be noticed that the fluctuation level is lower (i.e. the ESE curves are smoother) when compared to those of Fig. 8.10, especially for $\alpha \geq 0.8$. This is justified by the fact that the interference level compared to the CRS signals level turns to be lower. In addition, the ESE performance tends to be closer to the perfect channel estimation scenario in Fig. 8.9, when compared to Fig. 8.10. Finally, the advantage of power allocation in current LTE systems may be also noticed, when comparing the ESE results of $\alpha = 1$ to the ones in Fig. 8.10, as the channel estimation tends to be more accurate.

8.3 Conclusions

This chapter explores current power allocation methods used in different systems, such as OFDM and NOMA and proposes a new power allocation method to SEFDM. Power allocation is employed in SEFDM to overcome the impairments resulting from ICI by allocating different power levels to the different subcarriers within the same symbol. This implication of power allocation to SEFDM systems is tested from two perspectives: signal detection and channel estimation.

Regarding signal detection, a new system architecture based on double stage detection techniques has been designed, and the presented results prove that such power allocation is beneficial to SEFDM as: *i*) It solves the main limitation of SEFDM signals, which relates to its ill-conditioning nature resulting from ICI; such as its correlation matrix condition number becomes independent of the number of subcarriers, unlike conventional SEFDM where the condition number increases substantially for $N > 32$; *ii*) it reduces the detector complexity drastically compared to conventional SEFDM without power allocation, for the same error performance,

with a particular case presented here for the sub-optimal FSD detector; *iii*) FSD detector is capable of detecting the signal even with high number of subcarriers, because of power allocation adjustment to the correlation matrix; *iv*) finally, the use of power allocation enhances the PAPR behaviour of SEFDM, which is essential for non-linear systems.

Concerning the channel estimation problem, an SEFDM LTE PDSCH downlink channel is implemented. Results show that SEFDM has a significant throughput advantages as it can enhance the throughput by up to 40% compared to OFDM. However, this throughput advantage is affected by the accuracy of channel estimation. If the channel estimation method currently used in LTE, were to be used for SEFDM, power allocation can reduce the penalty error in channel estimation due to ICI. This conclusion is of great importance for SEFDM, especially when it comes to SEFDM deployment as part of SoDeFDM LTE systems. The work done here is still at an early stage and there is ongoing research to further investigate the optimal power ratio and the optimal location of the CRS resource elements within a resource block.

Chapter 9

Conclusions

Improving the spectral efficiency of future communication systems is essential to cope with the emergence of new applications and technological trends connecting billions of people and machines. Accordingly, the theme of this thesis is the employment of spectrally efficient signals (namely SEFDM) to enhance spectrum utilisation. In this thesis, new techniques have been proposed and explored to establish end-to-end comprehensive and practical SEFDM systems.

9.1 Summary and Discussion

The feasibility of SEFDM is hindered by many design and implementation obstacles due to orthogonality violation. Previous work focused on SEFDM signal generation and detection. However, other issues have not been fully tackled by previous work, such as the application of channel coding, practical channel estimation and equalisation and importantly, the design of a full end-to-end system. Towards the ultimate goal of considering SEFDM in future wireless standardisation, work in this thesis was conducted in three main parts; firstly, the fundamentals of SEFDM signals and communication system were mathematically modelled, using deterministic and statistical processes, to facilitate system design under different channel conditions. Second, new methods were developed and communication system techniques were adapted and applied to SEFDM to improve its performance. Third, the mathematical studies and new techniques developed were applied to practical systems that were tested both by simulation and experimentation.

This thesis commenced by a general overview of existing multi-carrier orthogonal signals. The focus was on OFDM signals, where a mathematical model was presented and the signal characteristics were compared to existing non-orthogonal signals, which violate the orthogonality of their subcarriers by either compressing the signal frequency spacing, by pulse shaping or by using both methods simultaneously. This overview set the main background for this thesis and then moved on to an extensive survey of the active research work on SEFDM. This survey helped in identifying a number of shortcomings, which paved the way to the research carried out through this thesis. The SEFDM signal was studied and mathematically modelled, where a statistical model of ICI in SEFDM was derived to complement the well-known SEFDM deterministic model. Detailed mathematical and simulation studies concluded that ICI in SEFDM approximates a Gaussian distribution, of a variance which depends largely on the compression level and to a much lesser extent on the number of subcarriers. This is because the interference power (of the ICI) on a given subcarrier largely results from the neighbouring subcarriers on both sides. The developed ICI model was used to derive a closed form of SEFDM probability of error bounds, when a simple matched filter receiver and AWGN channel are assumed. The results indicated that, unlike OFDM, increasing the signal power will not improve the error performance and an error floor appears by increasing the compression level of SEFDM signals. This set of results led to the conclusion that some powerful interference cancellation method is required and such was developed in this thesis. In the final part of signal mathematical studies, SEFDM upper-bound spectral efficiency was derived using the statistical signal model and showed the advantage of SEFDM over OFDM, for different signal powers and system operating conditions.

To ameliorate the effect of ICI in SEFDM and improve its error performance, different channel coding techniques were applied; specifically RS block code and convolutional and turbo probabilistic codes. Furthermore, a serial concatenation of RS and turbo codes was studied through system modelling and simulations. Results expectedly favoured the use of turbo coding over the other techniques, particularly

when high compression levels are used, with spectral efficiency gains of 67% resulting in a maximum of 3 dB power penalty relative to OFDM. Consequently, further investigations were undertaken, to evaluate the impact of different operational parameters on ICI mitigation capabilities of turbo coding. Results showed that lower coding rates (i.e. more redundant bits generated per information bit) mitigates ICI effects better. Moreover, SEFDM error performance degrades more than OFDM error performance with code puncturing (i.e. increase coding rate by puncturing the output of the encoder) especially for higher compression levels. The second parameter studied was the number of turbo decoder iterations, where it was proven that SEFDM error performance improves by increasing the iterations but only up to a certain extent. A new method was developed to further improve coded SEFDM error performance, where a random interleaver was implemented to interleave coded bits. Although channel impairments were limited to AWGN, yet the interleaver proved to be beneficial in terms of error rate reduction because of ICI. Thus, the employment of such interleaver is essential, especially with high compression level. The channel coding studies were concluded by performing a fair comparison between OFDM and SEFDM, where both systems have the same spectral efficiency and the same system simulation parameters. Results showed that although coding significantly improves system performance, yet it is not sufficient by its own and better methods to remove the interference may be required.

The above conclusion led to the design and implementation of successive interference cancellation with LDPC channel coding, where the detector estimates and then subtracts ICI iteratively. Such interference canceller is distinguished by; *i*) its simplicity, as it is based on mathematical subtraction operation and does not require matrix inversion; *ii*) its interference estimation efficiency, because the channel decoder plays a part in this process. Mathematical modelling and simulations were provided to investigate the SIC performance in a broadband and broadcasting scenario (DVB-S2). Taking into account that in DVB-S2 systems, each transponder serves multiple users, SEFDM provided more degrees of freedom in optimising the system compared to OFDM by adding a compression parameter to the existing

variable coding and modulation operational parameter. Results evidenced SIC capability of solving the interference limitations of SEFDM, by reducing interference even with only one iteration. Furthermore, SEFDM proved to accomplish bandwidth savings compared to OFDM while preserving the same BER performance, at the cost of higher detector complexity.

The second addressed issue of SEFDM signals was channel estimation. A new robust and practical frequency domain channel estimation scheme was devised, which allowed real-time SEFDM signals transmission and detection. In this scheme, a pilot symbol is sent over orthogonally spaced subcarriers as an OFDM symbol, while information symbols are sent as SEFDM symbols; both symbols use the same number of subcarriers and the same subcarrier spacing. A mathematical model was designed to compare the new scheme to two other existing SEFDM frequency domain estimation schemes; partial channel estimation and channel estimation with interpolation. Results proved that the new scheme is more robust and more accurate, regardless of the channel condition, number of subcarriers and the compression level. Furthermore, the computational complexity of the proposed scheme is substantially less than the computational complexity of the other two schemes. Finally, the new scheme slightly increases the pilot duration overhead, thus, it is deemed more suitable for semi-static or slow fading channels, where the pilot is sent less often.

For further justification of the proposed channel estimation scheme suitability, the proposed scheme was applied to new 5G NR system model transmitting SEFDM frames over TDL-D channel. A new reconfigurable IFFT design was proposed, which is capable of generating SEFDM symbols, pilot OFDM symbols and continuous cyclic prefix. It was proven that if the cyclic prefix of SEFDM signals is generated in a similar way to OFDM signals, it would violate signal continuity. Thereafter, a new method to maintain cyclic prefix continuity was proposed and it was shown that this method results in lower out-of-band emission, compared to the existing method.

Inspired by the successful implementation of power NOMA in 5G, preliminary

work in this thesis explored the advantages of applying power allocation to SEFDM to overcome the impairments resulting from ICI. In this method, different subcarriers within the same symbol are allocated different power levels. A new system architecture was suggested, where signal detection was divided into two stages. In the first stage, subcarriers allocated with higher power are detected and their interference on the rest of the subcarriers is estimated and cancelled. Thereafter, the rest of the subcarriers are detected by a second stage sub-optimal fixed sphere decoder. This new architecture solved SEFDM ill-conditioning problem, as it was proven that the correlation matrix condition number reduces substantially and becomes independent of the number of subcarriers. Further advantages of applying power allocation with the new system architecture were presented, such as substantial reduction of detector computational complexity and better PAPR behaviour, when compared to conventional SEFDM systems.

Another study on power allocation for channel estimation in SEFDM systems was discussed in this thesis. The ultimate goal of this study was to explore the possibility of coexistence of SEFDM and OFDM systems. Thus, a new system design with minimum modifications to existing PDSCH LTE system was implemented. Power allocation was suggested to enhance SEFDM channel estimation accuracy, where the power level of the pilot signals is higher than that of data signals. Consequently, the power of interference coming from other subcarriers to the pilot, will become relatively lower. Results proved the potential of power allocation in enhancing channel estimation accuracy and reducing error rate. However, this study is still at an early stage and further work is going for further enhancement.

Finally, the world first experimental demonstration of SEFDM signals transmission over E-band (81-86) GHz frequency range was reported, with a highest transmission rate of 12 Gbps and up to 50% improvement in spectral efficiency, relative to OFDM. The testbed setup consisted of GaAs microwave integrated circuit transceiver chips, especially designed for the transmission of multi-carrier signals in the E-band. To guarantee a controlled frequency selective environment, an E-band waveguide was used, with well characterised magnitude and phase responses

and time delay parameters. In the digital signal processing part, each step starting from message bits generation, all the way to detect the message bits at the receiver, were designed and implemented. The channel estimation scheme developed in this thesis proved again its capability, in practice, of accurate estimation of the channel response. Furthermore, the orthogonal nature of the pilot symbols in this estimation scheme allowed developing a new timing synchronization method. In this method, the pilot symbols were also used here for timing synchronization to reduce the overall system overhead. In addition, the powerful LDPC channel coding and coded bits interleaving were employed to enhance error performance. This demonstration not only verifies the design techniques developed in this thesis, but also represents an important milestone for SEFDM transmission, given the importance of using mm-waves in expanding transmission rates for future wireless communication systems.

To summarise, the appealing SEFDM concept is challenged by the loss of orthogonality that complicates the required transmitter and receiver tasks and degrades performance. The work presented in this thesis tackled both complexity and performance issues, by introducing new design and verifying their efficacy experimentally.

9.2 Future Work

The work and conclusions developed through out this thesis motivate further investigations, some of which are listed below as potential future research lines:

- **E-band over air transmission for in-door and out-door environments.** The experiment of SEFDM transmission over the E-band (81-86) GHz, reported in [27] and in Chapter 7 of this thesis, may be extended to replace the waveguide connecting the transmitter to receiver with an over air channel. To achieve this and given the high path loss at the E-band, transmitter and receiver antennas become essential. Furthermore, the robustness of SEFDM signals to impairments in different transmission environment has to be investigated and compared not only to OFDM, but also to single carrier experiments as in [150] and [149].

- **Satellite non-linearities mathematical modelling:** The work reported in [20] and in Chapter 5 of this thesis concerning the application of SEFDM to DVB-S2 system, may be extended further. First, the channel linear model should be extended to take into account non-linearities introduced by the low and high power amplifiers at the transmitter. It is expected that such model will show the advantage of SEFDM, when compared to OFDM, given the former better PAPR behaviour. This channel model, termed Saleh model, has been implemented in different publications by Baidas, such as in [118] and [122]. Second, the recent work in [128], introduced a new layer of multi-carrier to satellite systems, where each user within a transponder is an OFDM symbol instead of a conventional single-carrier signal. This introduces a new potential for SEFDM to enhance future satellite systems, where each sub-channel within a transponder is an SEFDM symbol.

- **Investigate the new channel estimation scheme behaviour in a fast fading environment.** Expand the use cases of the new channel estimation scheme developed during this PhD, which is reported in [21] and in Chapter 6 of this thesis. In the new channel estimation scheme, the pilot is sent ahead of data symbols. This might degrade estimation accuracy of the new scheme in fast fading channels, unless, the pilot is sent more often. Consequently, operational parameters, such as how often the pilot is sent and effective throughput may be calculated to get a better grasp on the big picture. Furthermore, the new channel models introduced in the recent 3GPP standards [139] may be modelled, to evaluate the new channel estimation scheme in other scenarios not considered in this thesis.

- **Optimise power allocation technique for channel estimation.** Power allocation in LTE [163] is used to boost the power level of pilot reference signals. This will result in a better estimate of channel impairments and better equalisation. If SEFDM is applied to LTE framework, such as the work reported in Chapter 8 of this thesis, then, the following points are to be taken into consideration. First, unlike OFDM LTE, the pilot signals must be modulated

on an orthogonal subset of subcarriers, i.e. pilot signals should not interfere with each others. Second, after estimating the channel response using the pilot reference signals, the interference from these pilot signals into the rest of subcarriers within a resource block, should be calculated and subtracted, before signal detection.

- **Formal system optimisation:** Several methods and tools may be used to optimise SEFDM system design and parameters, in a formal manner. EXIT chart tool was firstly proposed as a powerful semi-analytical tool devised for analysing the convergence behaviour of iteratively decoded systems, where mutual information between data bits at the transmitter and the soft values at the receiver are used to describe the exchange of extrinsic information between constituent decoders [166]. Recently, EXIT charts were employed to predict the convergence behaviour of iterative turbo equalizers, where soft information is circulated between the detector and decoder, such as the SIC in this thesis. Therefore, EXIT chart may be used to optimise the SIC system design and parameters. The second tool is machine learning, which showed great potentials to revolutionise current communications systems. Although the mathematical model of ICI in SEFDM exists, yet, the application of machine learning to SEFDM may highlight new potentials and solutions. For instance, machine learning can be used to optimise the interference cancellation and detection blocks in SEFDM systems, such as [68]. Furthermore, there is evidence that "learned" algorithms could be executed faster than existing programs and algorithms [167].

Overall, this thesis and its underlying research work have explored mathematical, engineering design and practical aspects of the SEFDM system. It is hoped that this work will serve as a further step towards the implementation and and use of SEFDM symbols in future communication systems.

Appendix A

Preliminaries on MAP Decoding

The trellis presentation of convolutional coding has to be explained to understand MAP decoding. Fig. A.2 shows the trellis for the RSCC (5,7,3) of Fig. A.1.

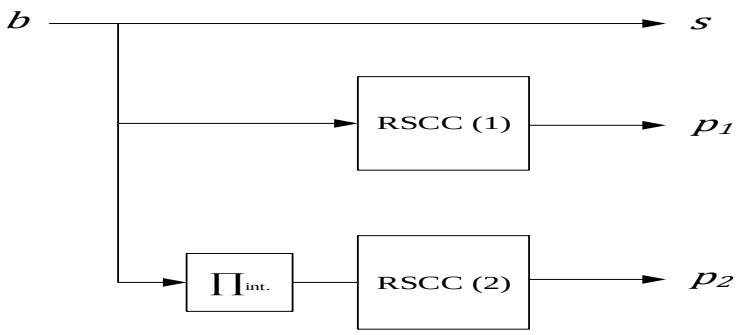

Figure A.1: RSCC for (5,7,3) and $R_c = 1/2$.

The content of the memory registers of the encoder at any time is referred to as the trellis states (S). Thus, the number of possible states, at a certain point, is equal to 2^{m_c}, which is 4 in this case. Therefore, the number of trellis rows depends on m_c while the trellis depth depends on the input sequence **b** length k_c.

The initial stage always starts with all zeros state, then, with the first input (b_1), the content of the memory registers is shifted one step forward to the right and the output of the generator sequences is calculated. The trellis presentation, calculates the output for all possible input values, which in this case is $b_i \in \{0,1\}$ and updates the trellis state according to it. The arrows here have two values (b_i/c_i).

The transition from a state to the next one depends on the encoder input value. Thus, if the previous state ($S_{i-1} = s^{'}$) and present state ($S_i = s$) are known, then the

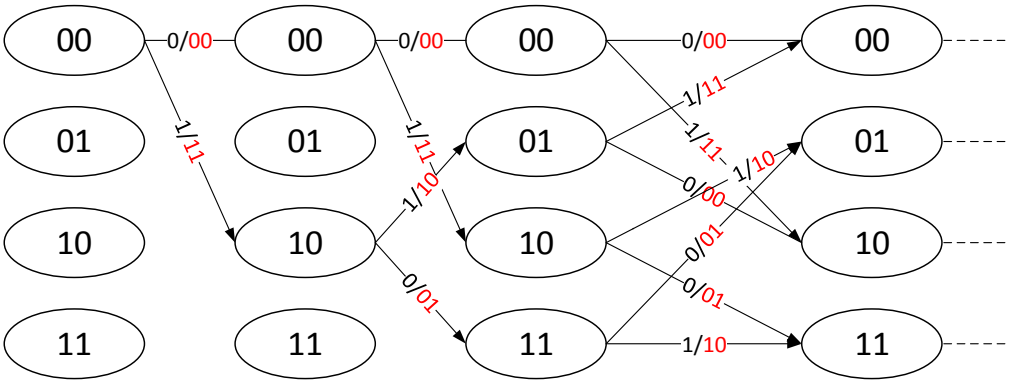

Figure A.2: Trellis diagram presentation for RSCC (5,7,3).

input that triggered this transition can be figured out [90].

MAP algorithm gives the probability that the i^{th} transmitted bit value is $\mathrm{P}(b_i = 0)$ or $\mathrm{P}(b_i = 1)$, using the received coded bits sequence $\hat{\mathbf{c}}$, such as [90]

$$L(b_i|\hat{\mathbf{c}}) = \ln\left(\frac{\mathrm{P}(b_i = 1|\hat{\mathbf{c}})}{\mathrm{P}(b_i = 0|\hat{\mathbf{c}})}\right), \tag{A.1}$$

where $L(b_i|\hat{\mathbf{c}})$ is the *a posteriori* LLR.

The LLR in (A.1) can be rewritten using Bayes' rule [1] and the exclusive mutuality of the trellis states [2] as [90]

$$L(b_i|\hat{\mathbf{c}}) = \ln\left(\frac{\sum_{(s'\to b_i=1)}\mathrm{P}(S_{i-1} = s' \wedge S_i = s \wedge \hat{\mathbf{c}})}{\sum_{(s'\to b_i=0)}\mathrm{P}(s_{i-1} = s' \wedge s_i = s \wedge \hat{\mathbf{c}})}\right). \tag{A.2}$$

To evaluate this probability, two rules are used; Bayes' rule and Marcov Chains, which is exploited for memoryless channels. In a memoryless channel, the future received sequence will depend only on the present state and not on the previous states [90], [91]. Consequently, the numerator and denominator of (A.2) becomes [90]

$$\mathrm{P}(s_{i-1} = s' \wedge s_i = s \wedge \hat{\mathbf{c}}) = \alpha_{i-1}(s') \times \gamma_L(s', s) \times \beta_i(s) \tag{A.3}$$

where $\alpha_{i-1}(s')$ is referred to as the forward recursion, $\beta_i(s)$ is the backward re-

[1] $\mathrm{P}(b_i|\hat{\mathbf{c}}) = \mathrm{P}(b_i \wedge \hat{\mathbf{c}})\mathrm{P}(\hat{\mathbf{c}})$

[2] only one of the states could occur at the encoder at a certain stage

cursion and $\gamma_L(s^{'},s)$ is the transition branch metric. These three parameters are calculated as [90]

$$\alpha_i(s^{'}) = \mathrm{P}(s_{i-1} = s^{'} \wedge \hat{\mathbf{c}}_0^{i-1}), \tag{A.4}$$

$$\beta_i(s) = \mathrm{P}(\hat{\mathbf{c}}_{i+1}^{k_c-1} | s_i = s), \tag{A.5}$$

$$\gamma_i(s^{'},s) = \mathrm{P}(s_{i+1} = s, \hat{c}_i | s_i = s^{'}) = \mathrm{P}(\hat{c}_i|b_i)\mathrm{P}(b_i), \tag{A.6}$$

where $\hat{\mathbf{c}}_0^{i-1}$ is a vector of previous outcomes from stage 0 till the $i-1$ stage and $\hat{\mathbf{c}}_{i+1}^{k_c-1}$ is a vector of future outcomes from stage $i+1$ till k_c-1. $\mathrm{P}(c_i)$ is the $a-priori$ probability and $\mathrm{P}(\hat{c}_i|c_i)$ is the conditional density that the channel sequence $\hat{c}_i$ is received given that c_i is transmitted. In MAP decoder, usually $\mathrm{P}(\hat{c}_i|c_i)$ is assumed to have AWGN PDF for simplification.

To calculate the above, first, $\gamma_i(s^{'},s)$ is calculated assuming that the $a-priori$ probability is equally likely to happen for $b_i = \{0,1\}$ (i.e. $\mathrm{P}(b_i = 0) = \mathrm{P}(b_i = 1) = 0.5$). Then, using $\gamma_i(s^{'},s)$, (A.4) and (A.5) can be calculated by [90]

$$\alpha_i(s^{'}) = \sum_{\text{all } s^{'}} \alpha_{i-1}(s^{'}) \times \gamma_L(s^{'},s), \tag{A.7}$$

$$\beta_{i-1}(s) = \sum_{\text{all } s} \beta_i(s) \times \gamma_L(s^{'},s). \tag{A.8}$$

In (**??**) and (**??**), it is assumed that at the encoder starts and terminates at all zeros memory state. For example, the RSCC (5,7,3) of Fig. A.1 $\alpha_0(s_0 = [00]) = \beta_{k_c-1}(s_{k_c-1} = [00]) = 1$.

Finally, the conditional LLR of b_i in (A.2) is found by [90]

$$L(b_i|\hat{\mathbf{c}}) = \left(\frac{\sum_{(s^{'} \to b_i=1)} \alpha_{i-1}(s^{'}) \times \gamma_L(s^{'},s) \times \beta_i(s)}{\sum_{(s^{'} \to b_i=0)} \alpha_{i-1}(s^{'}) \times \gamma_L(s^{'},s) \times \beta_i(s)} \right). \tag{A.9}$$

Then, the hard decision is made according to the sign of $L(b_i|\hat{\mathbf{c}})$. However, (A.9) turned to be very complex and different methods have been studied to reduce the MAP decoder complexity. For instance, a method called max-log-MAP [168] is used, where it takes the natural logarithm for α, β, γ to turn multiplication into

simple addition, then, it uses Jacobian approximation [7] to simplify the calculation of $\ln(e^x + e^y)$.

[7] $(\ln(e^x + e^y) = max(x,y) + \ln(1 + e^{-|x-y|}))$

Appendix B

E-band Transmitter & Receiver Integrated Circuits Design

The E-band SEFDM MMIC Tx and Rx in the experiment reported in Chapter 7 of this thesis were TSC0023B and RSC0015D, respectively. Both Tx and Rx are designed by Gotmic AB for this collaborative work. Based on WIN Semiconductors' 100 nm GaAs pHEMT process (PP10-10), the Tx and the Rx circuits are one-chip solutions that contain integrated frequency sextupler (X6) and balanced IQ modulator. The two MMICs were each mounted on Taconic Taclamplus printed circuit board (PCB) of size 3×3 mm^2, having 100 um thick substrate on 1 mm copper hardback with edge-launch SMA connectors for the local oscillator (LO) and IQ ports and a WR12 waveguide interface for the RF. Additional PCBs were used, taking only $\pm$5 V, for making the E-band SEFDM transmitter and receiver plug'n'play solutions for quick deployment and ease-of-use.

B.1 Design Topology of the Transmitter and the Receiver

The Tx integrated circuit contains a variable-gain amplifier (VGA), a medium power amplifier, and a power detector for monitoring RF output power and LO leakage. These components are integrated after the quadrature mixer, as shown in the block diagram and the corresponding chip photo in Fig. B.1(a) citeWebsite. The quadrature mixer comprises a differential branchline coupler and a Marchand balun on

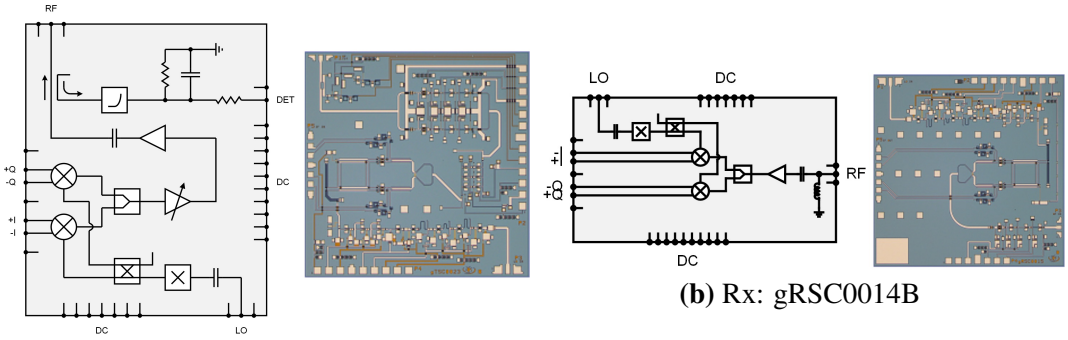

(a) Tx: gTSC0023B

(b) Rx: gRSC0014B

Figure B.1: The E-band block diagram and chip photo: (a) transmitter; (b) receiver.

the LO side and is based on the topology in [169]. Such design provides LO-RF isolation and quadrature interface, suitable for direct modulation. The frequency sextupler makes use of a differential stage amplifier, which in saturation is rich of odd harmonics, and a common-source transistor biased at threshold, which is rich of even harmonics. These two sources extract the X3 and the X2 frequency products respectively, and together with the amplifiers, they boost the signal level, such that the output power level reaches 16 dBm. The detailed schematic of the frequency sextupler is described in [170]. The VGA utilizes a travelling wave type amplifier for gain control, which over 25 dB gain control range has consistent flat gain response and return loss better than 10 dB. The medium power amplifier consists of 4-stages and in two parallel branches to increase linearity. A gradual increase in the gate width of the transistors from 150 um to 400 um has been adopted in the design, to balance the transmitter's power consumption and third-order intermodulation product. At the output, the RF signal is 10-dB coupled to a power detector, thus, the detector is sensitive enough to detect all power levels across the gain control range.

In terms of the receiver, the Rx circuit of Fig. B.1(b), consists of a low-noise amplifier (LNA) placed in front of the quadrature mixer. The LNA is used to buffer the noise figure, such that the conversion gain and noise figure of the whole receiver chip are 15 dB and 5 dB, respectively. The LNA consists of a three-stage amplifier design, where the first transistor is biased at a low drain voltage and low current for optimum noise figure. Similar to the medium power amplifier in the transmitter, the

second and third stages have a gradual increase in their transistors size to improve linearity. The quadrature mixer and the frequency sextupler are identical to the ones described of the transmitter above.

B.2 Measurements of the Transmitter and the Receiver

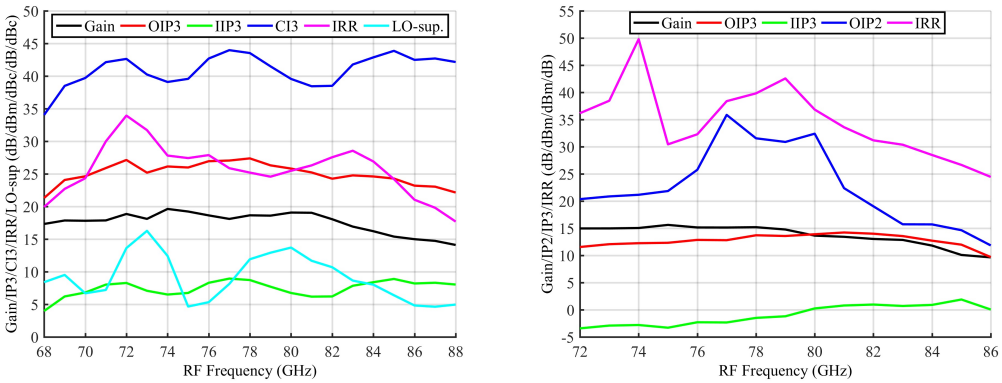

(a) Transmitter **(b)** Receiver

Figure B.2: Measured performance of the SEFDM E-band transmitter and receiver at different RF frequencies.

The suitability of the Tx circuit is evaluated in Fig. B.2(a). The results show that the measured maximum conversion gain, third-order output intercept point (OIP3) and image rejection ratio (IRR) are 18 dB, 26 dBm, and 25 dB, respectively. This implies that the transmission of multi-carrier modulation formats including OFDM and SEFDM, even at a relatively high peak-to-average power ratio (PAPR) is viable. Nevertheless, because of the limited frequency response of the branchline coupler, it is noticed that the IRR is high at the center frequency and starts to deviate at the corner frequencies. LO suppression can be further improved (around 40 dBc), by applying DC offset to the +I, -I and +Q, -Q channels.

For the receiver, the measured input linearity may be described by measuring the third-order input intercept point (IIP3) and the IRR , which are 1 dBm and 25 dB, respectively, as shown in Fig. B.2(b). We can notice that the performance is similar to that of the transmitter, indicating the suitability to multiple-subcarrier modulation format.

For direct modulation and demodulation, intermodulation product, such as IM2, is a critical parameter because it falls within the modulated signal bandwidth. Thus, OIP2 has been measured and the results indicate that OIP2 is higher than 30 dBm at the center frequency, but decreases to 12 dBm at 86 GHz. This effectively limits the maximum received signal power of the SEFDM receiver chain.

Appendix C

The Relation between SNR and E_b/N_0

In this thesis, the system performance is usually evaluated by presenting results (e.g. MSE, BER, ESE) versus either E_b/N_0 or SNR. In experiments and practical systems SNR is used more often, however, E_b/N_0 is more common in theoretical studies for normalisation purposes. The flowchart demonstrated below summarises the steps taken to transfer from SNR to E_b/N_0 and vice versa.

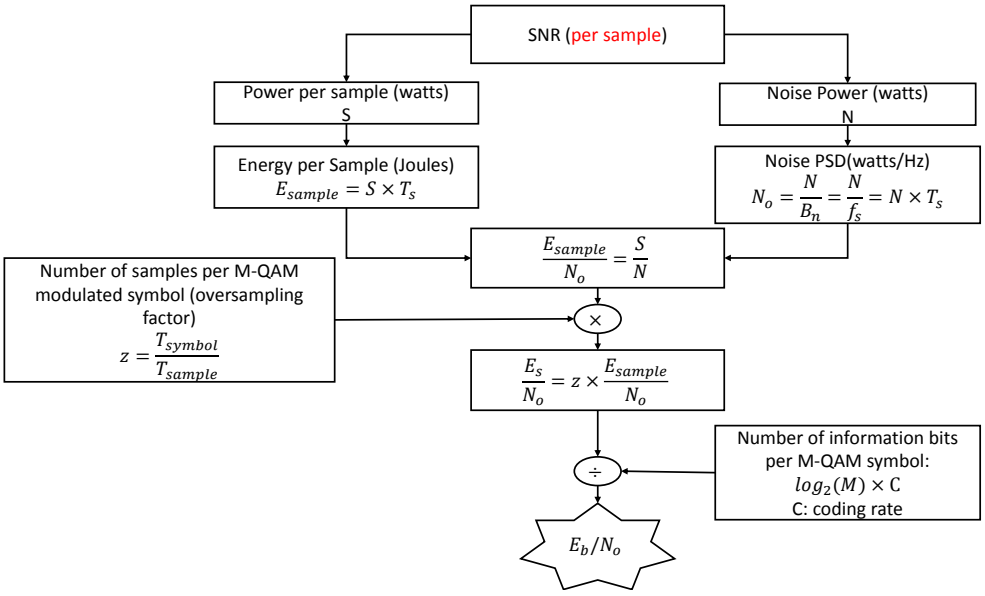

Figure C.1: A flow chart of the relation between SNR and E_b/N_0.

List of References

[1] Jack L. Burbank, Julia Andrusenko, Jared S. Everett, and William T. M. Kasch. *Fourth-Generation (4G) Cellular Communications*, pages 712–. Wiley-IEEE Press, 2013.

[2] J. G. Andrews, S. Buzzi, W. Choi, S. V. Hanly, A. Lozano, A. C. K. Soong, and J. C. Zhang. What Will 5G Be? *IEEE Journal on Selected Areas in Communications*, 32(6):1065–1082, June 2014.

[3] Walid Saad, Mehdi Bennis, and Mingzhe Chen. A Vision of 6G Wireless Systems: Applications, Trends, Technologies, and Open Research Problems. *arXiv e-prints*, page arXiv:1902.10265, Feb 2019.

[4] P. Banelli, S. Buzzi, G. Colavolpe, A. Modenini, F. Rusek, and A. Ugolini. Modulation Formats and Waveforms for 5G Networks: Who Will Be the Heir of OFDM?: An Overview of Alternative Modulation Schemes for Improved Spectral Efficiency. *IEEE Signal Processing Magazine*, 31(6):80–93, Nov 2014.

[5] T. Hwang, C. Yang, G. Wu, S. Li, and G. Y. Li. OFDM and Its Wireless Applications: A Survey. *IEEE Transactions on Vehicular Technology*, 58(4):1673–1694, May 2009.

[6] M.R.D. Rodrigues and Izzat Darwazeh. A Spectrally Efficient Frequency Division Multiplexing Based Communications System. In *Proc. 8th Int. OFDM Workshop*, pages 48–49, 2003.

[7] I. Kanaras. *Spectrally Efficient Multicarrier Communication Systems: Signal Detection, Mathematical Modelling and Optimisation*. PhD thesis, University College London, 2010.

[8] Safa I. Ahmed. *Spectrally Efficient FDM Communication Signals and Transceivers: Design, Mathematical Modelling and System Optimization*. PhD thesis, University College London, 2011.

[9] T. Xu. *Bandwidth Compressed Waveform and System Design for Wireless and Optical Communications: Theory and Practice*. PhD thesis, University College London, 2017.

[10] F. Rusek and J. B. Anderson. Multistream Faster than Nyquist Signaling. *IEEE Transactions on Communications*, 57(5):1329–1340, May 2009.

[11] A. Barbieri, D. Fertonani, and G. Colavolpe. Time-Frequency Packing for Linear Modulations: Spectral Efficiency and Practical Detection Schemes. *IEEE Transactions on Communications*, 57(10):2951–2959, October 2009.

[12] I. Kanaras, A. Chorti, M. R. D. Rodrigues, and I. Darwazeh. A Fast Constrained Sphere Decoder for Ill Conditioned Communication Systems. *IEEE Communications Letters*, 14(11):999–1001, November 2010.

[13] T. Xu and I. Darwazeh. A Soft Detector for Spectrally Efficient Systems with Non-Orthogonal Overlapped Sub-Carriers. *IEEE Communications Letters*, 18(10):1847–1850, Oct 2014.

[14] I. Darwazeh, H. Ghannam, and T. Xu. The First 15 Years of SEFDM: A Brief Survey. In *IEEE Porc. 11th International Symposium on Communication Systems, Networks Digital Signal Processing (CSNDSP), Budapest*, pages 1–7, July 2018.

[15] S. Isam and I. Darwazeh. Robust Channel Estimation for Spectrally Efficient FDM System. In *2012 19th International Conference on Telecommunications (ICT)*, pages 1–6, April 2012.

[16] D. Nopchinda, T. Xu, R. Maher, B. C. Thomsen, and I. Darwazeh. Dual Polarization Coherent Optical Spectrally Efficient Frequency Division Multiplexing. *IEEE Photon. Technol. Lett*, 28(1):83–86, Jan 2016.

[17] H. Ghannam and I. Darwazeh. SEFDM: Spectral Efficiency Upper Bound and Interference Distribution. In *IEEE Proc. 11th International Symposium on Communication Systems, Networks Digital Signal Processing (CSNDSP), Budapest*, pages 1–6, July 2018.

[18] H. Ghannam and I. Darwazeh. Comparison of Turbo Decoder and Turbo Equalizer for Spectrally Efficient FDM System. In *IEEE Proc. 10th Int. Symp. Commun. Syst. Networks and Digital Signal Process. (CSNDSP), Prague*, pages 1–6, July 2016.

[19] H. Ghannam and I. Darwazeh. Signal Coding and Interference Cancellation of Spectrally Efficient FDM Systems for 5G Cellular Networks. In *2017 IEEE Proc. 24th Int. Symp. International Conference on Telecommunications (ICT), Cyprus*, pages 1–6, May 2017.

[20] H. Ghannam and I. Darwazeh. SEFDM over Satellite Systems with Advanced Interference Cancellation. *IET Communications*, 12(1):59–66, January 2018.

[21] H. Ghannam and I. Darwazeh. Robust Channel Estimation Methods for Spectrally Efficient FDM Systems. In *IEEE 87th Vehicular Technology Conference VTC (Spring) workshop; Technology Trials and Proof-of-Concept Activities for 5G and Beyond 2018 (TPoC5G 2018), Porto*, June 2018.

[22] W. Ozan, H. Ghannam, P. A. Haigh, and I. Darwazeh. Experimental Implementation of Real-time Non-orthogonal Multi-carrier Systems in a Realistic Fading Channel. In *IEEE proc. Radio and Wireless Symposium (RWS), California*, pages 121–124, January 2018.

[23] H. Ghannam and I. Darwazeh. Low Complexity Channel Estimation Scheme for Spectrally Efficient FDM Systems in 5G Cellular Networks. In *Wireless World Research Forum (WWRF) Meeting 39 Workshop, Castelldefels, Barcelona*, October 2017.

[24] H. Ghannam and I. Darwazeh. A Proposal for Scalable 5G New Radio Frames with Enhanced Throughput. In *IEEE 89th Vehicular Technology Conference (Spring), Kuala Lumpur*, April 2019.

[25] H. Ghannam and I. Darwazeh. Power Allocation for Detection Performance Enhancement of SEFDM Signals. In *2018 IEEE 29th Annual International Symposium on Personal, Indoor and Mobile Radio Communications (PIMRC), Bologna*, pages 584–585, September 2018.

[26] H. Ghannam and I. Darwazeh. Design and Performance of SEFDM Signals with Power Allocation. In *IEEE Proc. Wireless Communications and Networking Conference (WCNC), Marrakech*, April 2019.

[27] H. Ghannam, D. Nopchinda, M. Gavell, H. Zirath, and I. Darwazeh. Experimental Demonstration of Spectrally Efficient Frequency Division Multiplexing Transmissions at E-Band. *IEEE Transactions on Microwave Theory and Techniques*, 67(5):1911–1923, March 2019.

[28] H. Ghannam T. Xu and I. Darwazeh. Practical Evaluations of SEFDM: Timing Offset and Multipath Impairments. *Infocommunications Journal*, January 2019.

[29] H. Ghannam and I. Darwazeh. Turbo Coding and Iterative Interference Cancellation of Spectrally Efficient FDM Systems. In *IEEE Wireless Communications and Networking Conference ((WCNC) - Student Outreach Program-Poster, San Francisco*, March 2017.

[30] W. Ozan, H. Ghannam, T. Xu, P. A. Haigh, and I. Darwazeh. Experimental Evaluation of Channel Estimation and Equalisation in Non-Orthogonal FDM Systems. In *IEEE 11th Proc. International Symposium on Communication Systems, Networks Digital Signal Processing (CSNDSP), Budapest*, July 2018.

[31] L. Cimini. Analysis and Simulation of a Digital Mobile Channel Using Orthogonal Frequency Division Multiplexing. *IEEE Transactions on Communications*, 33(7):665–675, Jul 1985.

[32] M. L. Doelz, E. T. Heald, and D. L. Martin. Binary Data Transmission Techniques for Linear Systems. *Proceedings of the IRE*, 45(5):656–661, May 1957.

[33] R. R. Mosier and R. G. Clabaugh. Kineplex, A Bandwidth-Efficient Binary Transmission System. *Transactions of the American Institute of Electrical Engineers, Part I: Communication and Electronics*, 76(6):723–728, Jan 1958.

[34] John G. Proakis. *Digital Communications*. McGraw-Hill series in electrical and computer engineering. McGraw-Hill, New York, 1995.

[35] P. Guan, D. Wu, T. Tian, J. Zhou, X. Zhang, L. Gu, A. Benjebbour, M. Iwabuchi, and Y. Kishiyama. 5G Field Trials: OFDM-Based Waveforms and Mixed Numerologies. *IEEE Journal on Selected Areas in Communications*, 35(6):1234–1243, June 2017.

[36] Qualcomm Research. Making 5G NR a Reality. Technical report, Qualcomm Technologies, Inc., 12 2016.

[37] J. Benedetto, C. Heil, and D. F. Walnut. *Gabor Systems and the Balian Low Theorem*, pages 85–122. 1998.

[38] C. Kim, Y. H. Yun, K. Kim, and J. Y. Seol. Introduction to QAM-FBMC: From Waveform Optimization to System Design. *IEEE Commun. Mag.*, 54(11):66–73, Nov. 2016.

[39] 3rd Generation Partnership Project; Technical Specification Group Radio Access Network; Study on New Radio (NR) access technology (Release 14). Technical report, 3GPP, 06 2017.

[40] 3rd Generation Partnership Project; Technical Specification Group Services and System Aspects; Release 15 Description; Summary of Rel-15 Work Items (Release 15). Technical report, 3GPP, 07 2018.

[41] X. Zhang, L. Chen, J. Qiu, and J. Abdoli. On the Waveform for 5G. *IEEE Communications Magazine*, 54(11):74–80, November 2016.

[42] L. Zhang, A. Ijaz, P. Xiao, M. M. Molu, and R. Tafazolli. Filtered OFDM Systems, Algorithms, and Performance Analysis for 5G and Beyond. *IEEE Transactions on Communications*, 66(3):1205–1218, March 2018.

[43] N. Michailow, M. Matth, I. S. Gaspar, A. N. Caldevilla, L. L. Mendes, A. Festag, and G. Fettweis. Generalized Frequency Division Multiplexing for 5th Generation Cellular Networks. *IEEE Transactions on Communications*, 62(9):3045–3061, Sept 2014.

[44] Y. Tao, L. Liu, S. Liu, and Z. Zhang. A Survey: Several Technologies of Non-orthogonal Transmission for 5G. *China Communications*, 12(10):1–15, Oct 2015.

[45] J.E. Mazo. Faster-than-Nyquist Signaling, year=1975, volume=54, number=8, pages=1451-1462, doi=10.1002/j.1538-7305.1975.tb02043.x, issn=0005-8580, month=Oct.,. *The Bell System Technical Journal*.

[46] J. B. Anderson, F. Rusek, and V. wall. Faster-Than-Nyquist Signaling. *Proceedings of the IEEE*, 101(8):1817–1830, Aug 2013.

[47] MRD Rodrigues and Izzat Darwazeh. Fast OFDM: A Proposal for Doubling the Data Rate of OFDM Schemes. In *Proceedings of the International Conference on Telecommunications*, pages 484–487, 2002.

[48] Ji Zhou, Yaojun Qiao, Zhanyu Yang, Mengqi Guo, and Xizi Tang. Capacity Limit for Faster-than-Nyquist Non-Orthogonal Frequency-Division Multiplexing Signaling. In *Scientific Reports*, 2017.

[49] P. N. Whatmough, M. R. Perrett, S. Isam, and I. Darwazeh. VLSI Architecture for a Reconfigurable Spectrally Efficient FDM Baseband Transmitter. *IEEE Transactions on Circuits and Systems I: Regular Papers*, 59(5):1107–1118, May 2012.

[50] I. Kanaras, A. Chorti, M. R. D. Rodrigues, and I. Darwazeh. Spectrally Efficient FDM Signals: Bandwidth Gain at the Expense of Receiver Complexity. In *Proc. IEEE Int. Conf. Commun. (ICC)*, pages 1–6, June 2009.

[51] A. D. Liveris and C. N. Georghiades. Exploiting Faster-than-Nyquist Signaling. *IEEE Transactions on Communications*, 51(9):1502–1511, Sept 2003.

[52] F. Rusek and J. B. Anderson. The Two Dimensional Mazo Limit. In *Proceedings. International Symposium on Information Theory, 2005. ISIT 2005.*, pages 970–974, Sept 2005.

[53] S. Isam and I. Darwazeh. Characterizing the Intercarrier Interference of Non-Orthogonal Spectrally Efficient FDM System. In *2012 8th International Symposium on Communication Systems, Networks Digital Signal Processing (CSNDSP)*, pages 1–5, July 2012.

[54] Lajos L. Hanzo, C. H. Wong, and M. S. Yee. *Adaptive Multicarrier Modulation*. Wiley-IEEE Press, 2002.

[55] D. Rainnie, Y. Feng, and J. Bajcsy. On Capacity Merits of Spectrally Efficient FDM. In *MILCOM 2015*, pages 581–586, Oct 2015.

[56] C. E. Shannon. Communication in the Presence of Noise. *Proceedings of the IRE*, 37(1):10–21, Jan 1949.

[57] S. Isam and I. Darwazeh. Simple DSP-IDFT Techniques for Generating Spectrally Efficient FDM Signals. In *2010 7th International Symposium on Communication Systems, Networks Digital Signal Processing (CSNDSP 2010)*, pages 20–24, July 2010.

[58] R. C. Grammenos, S. Isam, and I. Darwazeh. FPGA Design of a Truncated SVD Based Receiver for the Detection of SEFDM Signals. In *2011 IEEE 22nd International Symposium on Personal, Indoor and Mobile Radio Communications*, pages 2085–2090, Sept 2011.

[59] M. R. Perrett and I. Darwazeh. Flexible Hardware Architecture of SEFDM Transmitters with Real-Time Non-Orthogonal Adjustment. In *2011 18th International Conference on Telecommunications*, pages 369–374, May 2011.

[60] S. Isam, I. Kanaras, and I. Darwazeh. A Truncated SVD Approach for Fixed Complexity Spectrally Efficient FDM Receivers. In *2011 IEEE Wireless Communications and Networking Conference*, pages 1584–1589, March 2011.

[61] I. Kanaras, A. Chorti, M. Rodrigues, and I. Darwazeh. Investigation of a Semidefinite Programming Detection for a Spectrally Efficient FDM System. In *2009 IEEE 20th International Symposium on Personal, Indoor and Mobile Radio Communications*, pages 2827–2832, Sept 2009.

[62] I. Kanaras, A. Chorti, M. R. D. Rodrigues, and I. Darwazeh. A Combined MMSE-ML Detection for a Spectrally Efficient non Orthogonal FDM Signal. In *2008 5th International Conference on Broadband Communications, Networks and Systems*, pages 421–425, Sept 2008.

[63] S. Isam and I. Darwazeh. Design and Performance Assessment of Fixed Complexity Spectrally Efficient FDM Receivers. In *2011 IEEE 73rd Vehicular Technology Conference (VTC Spring)*, pages 1–5, May 2011.

[64] I. Darwazeh, T. Xu, T. Gui, Y. Bao, and Z. Li. Optical Spectrally Efficient FDM System for Electrical and Optical Bandwidth Saving. In *2014 IEEE International Conference on Communications (ICC)*, pages 3432–3437, June 2014.

[65] I. Kanaras, A. Chorti, M. Rodrigues, and I. Darwazeh. A New Quasi-Optimal Detection Algorithm for a Non Orthogonal Spectrally Efficient FDM. In *2009 9th International Symposium on Communications and Information Technology*, pages 460–465, Sept 2009.

[66] S. Isam and I. Darwazeh. Precoded Spectrally Efficient FDM System. In *21st Annual IEEE International Symposium on Personal, Indoor and Mobile Radio Communications*, pages 99–104, Sept 2010.

[67] R. G. Clegg, S. Isam, I. Kanaras, and I. Darwazeh. A Practical System for Improved Efficiency in Frequency Division Multiplexed Wireless Networks. *IET Communications*, 6(4):449–457, March 2012.

[68] T. Xu and I. Darwazeh. Deep Learning for Interference Cancellation in Non-Orthogonal Signal Based Optical Communication Systems. In *PIERS (invited)*, August 2018.

[69] T. Xu and I. Darwazeh. Transmission Experiment of Bandwidth Compressed Carrier Aggregation in a Realistic Fading Channel. *IEEE Transactions on Vehicular Technology*, PP(99):1–1, 2016.

[70] S. Mikroulis, T. Xu, J. E. Mitchell, and I. Darwazeh. First Demonstration of a Spectrally Efficient FDM Radio over Fiber System Topology for Beyond 4G Cellular Networking. In *2015 20th European Conference on Networks and Optical Communications - (NOC)*, pages 1–5, June 2015.

[71] T. Xu, S. Mikroulis, J. E. Mitchell, and I. Darwazeh. Bandwidth Compressed Waveform for 60-GHz Millimeter-Wave Radio Over Fiber Experiment. *Journal of Lightwave Technology*, 34(14):3458–3465, July 2016.

[72] X. Zhang, L. Chen, J. Qiu, and J. Abdoli. On the Waveform for 5G. *IEEE Commun. Mag.*, 54(11):74–80, Nov. 2016.

[73] T. Xu and I. Darwazeh. Nyquist-SEFDM: Pulse Shaped Multicarrier Communication with Sub-carrier Spacing below the Symbol Rate. In *2016 10th International Symposium on Communication Systems, Networks and Digital Signal Processing (CSNDSP)*, pages 1–6, July 2016.

[74] Sergey V. Zavjalov, Sergey B. Makarov, Sergey V. Volvenko, and Wei Xue. Waveform Optimization of SEFDM Signals with Constraints on Bandwidth and an Out-of-Band Emission Level. In Sergey Balandin, Sergey Andreev, and Yevgeni Koucheryavy, editors, *Internet of Things, Smart Spaces, and Next Generation Networks and Systems*, pages 636–646, Cham, 2015. Springer International Publishing.

[75] S. V. Zavjalov, S. V. Volvenko, and S. B. Makarov. A Method for Increasing the Spectral and Energy Efficiency SEFDM Signals. *IEEE Commun. Lett.*, 20(12):2382–2385, Dec 2016.

[76] R. C. Grammenos, S. Isam, and I. Darwazeh. FPGA Design of a Truncated SVD Based Receiver for the Detection of SEFDM Signals. In *2011 IEEE 22nd International Symposium on Personal, Indoor and Mobile Radio Communications*, pages 2085–2090, Sept 2011.

[77] T. Xu, R. C. Grammenos, and I. Darwazeh. FPGA Implementations of Real-time Detectors for a Spectrally Efficient FDM System. In *ICT 2013*, pages 1–5, May 2013.

[78] S. Isam and I. Darwazeh. Peak to Average Power Ratio Reduction in Spectrally Efficient FDM Systems. In *2011 18th International Conference on Telecommunications*, pages 363–368, May 2011.

[79] S. Peng, A. Liu, K. Wang, and X. Liang. PAPR Reduction of Multicarrier Faster-Than-Nyquist Signals with Partial Transmit Sequence. *IEEE Access*, 5:24931–24937, 2017.

[80] S. Peng, A. Liu, L. Song, I. Memon, and H. Wang. Spectral Efficiency Maximization for Deliberate Clipping-Based Multicarrier Faster-Than-Nyquist Signaling. *IEEE Access*, 6:13617–13623, 2018.

[81] E. O. Antonov, A. V. Rashich, D. K. Fadeev, and N. Tan. Reduced Complexity Tone Reservation Peak-to-Average Power Ratio Reduction Algorithm for SEFDM Signals. In *2016 39th International Conference TSP*, pages 445–448, June 2016.

[82] Y. Wang, Y. Zhou, T. Gui, K. Zhong, X. Zhou, L. Wang, A. P. T. Lau, C. Lu, and N. Chi. SEFDM Based Spectrum Compressed VLC System Using RLS Time-domain Channel Estimation and ID-FSD Hybrid decoder. In *ECOC 2016; 42nd European Conference on Optical Communication*, pages 1–3, Sept 2016.

[83] C. E. Shannon. A Mathematical Theory of Communication. *The Bell System Technical Journal*, 27(3):379–423, July 1948.

[84] K. Sathananathan and C. Tellambura. Forward Error Correction Codes to Reduce Intercarrier Interference in OFDM. In *ISCAS 2001. The 2001 IEEE International Symposium on Circuits and Systems (Cat. No.01CH37196)*, volume 4, pages 566–569 vol. 4, May 2001.

[85] A. G. Burr and G. P. White. Performance of turbo-coded OFDM. In *IEE Colloquium on Turbo Codes in Digital Broadcasting - Could It Double Capacity? (Ref. No. 1999/165)*, pages 8/1–8/8, Nov 1999.

[86] S. Sugiura. Frequency-Domain Equalization of Faster-than-Nyquist Signaling. *IEEE Wireless Communications Letters*, 2(5):555–558, October 2013.

[87] D. J. Costello and G. D. Forney. Channel Coding: The Road to Channel Capacity. *Proceedings of the IEEE*, 95(6):1150–1177, June 2007.

[88] P. Elias. Error-Free Coding. *Transactions of the IRE Professional Group on Information Theory*, 4(4):29–37, September 1954.

[89] A. Burr. *Modulation and Coding for Wireless Communications*. Pearson Education Limited, 2001.

[90] L. Hanzo, J. P. Woodard, and P. Robertson. Turbo Decoding and Detection for Wireless Applications. *Proceedings of the IEEE*, 95(6):1178–1200, June 2007.

[91] E. Boutillon, C. Douillard, and G. Montorsi. Iterative Decoding of Concatenated Convolutional Codes: Implementation Issues. *Proceedings of the IEEE*, 95(6):1201–1227, June 2007.

[92] L. Bahl, J. Cocke, F. Jelinek, and J. Raviv. Optimal Decoding of Linear Codes for Minimizing Symbol Error Rate. *IEEE Transactions on Information Theory*, 20(2):284–287, Mar 1974.

[93] C. Berrou, A. Glavieux, and P. Thitimajshima. Near Shannon Limit Error-Correcting Coding and Decoding: Turbo-codes. 1. In *IEEE Int. Conf. on Comm., 1993. ICC '93 Geneva.*, volume 2, pages 1064–1070 vol.2, May May 1993.

[94] A. Burr. Turbo-codes: the ultimate error control codes? *Electronics Communication Engineering Journal*, 13(4):155–165, Aug 2001.

[95] Ioannis Chatzigeorgiou, M.R.D. Rodrigues, I.J. Wassell, and R. Carrasco. Can Punctured Rate-1/2 Turbo Codes Achieve a Lower Error Floor than their Rate-1/3 Parent Codes? In *Information Theory Workshop, 2006. ITW '06 Chengdu. IEEE*, pages 91–95, Oct 2006.

[96] Xianbin Wang, P. Ho, and Y. Wu. Robust Channel Estimation and ISI Cancellation for OFDM Systems with Suppressed Features. *IEEE Journal on Selected Areas in Communications*, 23(5):963–972, May 2005.

[97] Pei Xiao, E. Strom, and R. Carrasco. Comparison of Different Soft Demodulation and Decoding Algorithms in Coded M-ary Orthogonal DS-CDMA Systems. In *Second IFIP International Conference on Wireless and Optical Communications Networks, 2005. WOCN 2005.*, pages 578–583, March 2005.

[98] Evolved Universal Terrestrial Radio Access (E-UTRA); Multiplexing and Channel Coding, 3GPP Rel-13, ts 36.212, version 13.1.0. Technical report, 3GPP, 2016.

[99] M. Tuchler, A. C. Singer, and R. Koetter. Minimum Mean Squared Error Equalization Using A Priori Information. *IEEE Trans. Signal Process.*, 50(3):673–683, Mar. 2002.

[100] Evolved Universal Terrestrial Radio Access (E-UTRA); Physical Channels and Modulation, 3GPP Rel-10, ts 36.211, version 10.0.0. Technical report, 3GPP, 2011.

[101] Catherine Douillard, Michel Jézéquel, Claude Berrou, Département Electronique, Annie Picart, Pierre Didier, and Alain Glavieux. Iterative Correction of Intersymbol Interference: Turbo-Equalization. *European transactions on telecommunications*, 6(5):507–511, 1995.

[102] Xiaodong Wang and H. V. Poor. Iterative (turbo) Soft Interference Cancellation and Decoding for Coded CDMA. *IEEE Transactions on Communications*, 47(7):1046–1061, July 1999.

[103] M. Tuchler, R. Koetter, and A. C. Singer. Turbo Equalization: Principles and New Results. *IEEE Trans. Commun.*, 50(5):754–767, May 2002.

[104] A. F. Molisch, M. Toeltsch, and S. Vermani. Iterative Methods for Cancellation of Intercarrier Interference in OFDM Systems. *IEEE Trans. Veh. Technol.*, 56(4):2158–2167, July 2007.

[105] N. I. Miridakis and D. D. Vergados. A Survey on the Successive Interference Cancellation Performance for Single-Antenna and Multiple-Antenna

OFDM Systems. *IEEE Communications Surveys Tutorials*, 15(1):312–335, First 2013.

[106] M. Kontik and S. Coleri Ergen. Scheduling in Successive Interference Cancellation Based Wireless Ad Hoc Networks. *IEEE Communications Letters*, 19(9):1524–1527, Sep. 2015.

[107] S. Toumpis and A. J. Goldsmith. Capacity Regions for Wireless Ad Hoc Networks. *IEEE Transactions on Wireless Communications*, 2(4):736–748, July 2003.

[108] D. Dasalukunte, F. Rusek, and V. Owall. An Iterative Decoder for Multicarrier Faster-Than-Nyquist Signaling Systems. In *2010 IEEE International Conference on Communications*, pages 1–5, May 2010.

[109] K. Yagishita, Y. Kakishima, and M. Sawahashi. Effects of Antenna Receiver Diversity with Faster-than-Nyquist Signaling Using OFDM/OQAM in Multipath Fading Channel. In *2014 International Symposium on Wireless Personal Multimedia Communications (WPMC)*, pages 351–355, Sep. 2014.

[110] L. Dai, B. Wang, Y. Yuan, S. Han, C. l. I, and Z. Wang. Non-Orthogonal Multiple Access for 5G: Solutions, Challenges, Opportunities, and Future Research Trends. *IEEE Commun. Mag.*, 53(9):74–81, September 2015.

[111] T. Ute, Y. Watanabe, K. Sato, T. Fujii, T. Shimizu, and O. Altintas. Multiantenna Successive Interference Cancellation to Improve Reliability of V2V Communication. In *2017 IEEE Vehicular Networking Conference (VNC)*, pages 29–30, Nov 2017.

[112] Y. G. Li, J. H. Winters, and N. R. Sollenberger. MIMO-OFDM for Wireless Communications: Signal Detection with Enhanced Channel Estimation. *IEEE Transactions on Communications*, 50(9):1471–1477, Sep. 2002.

[113] G. J. Foschini. Layered Space-Time Architecture for Wireless Communication in a Fading Environment when Using Multi-element Antennas. *Bell Labs Technical Journal*, 1(2):41–59, Autumn 1996.

[114] J. Ylioinas and M. Juntti. Iterative Joint Detection, Decoding, and Channel Estimation in Turbo-Coded MIMO-OFDM. *IEEE Transactions on Vehicular Technology*, 58(4):1784–1796, May 2009.

[115] G. Colavolpe and A. Piemontese. Novel SISO Detection Algorithms for Nonlinear Satellite Channels. *IEEE Wireless Communications Letters*, 1(1):22–25, February 2012.

[116] Digital Video Broadcasting (DVB); Second Generation Framing Structure, Channel Coding and Modulation Systems for Broadcasting, Interactive Services, News Gathering and Other Broadband Satellite Applications (DVB-S2). Technical report, European Standard (Telecommunications series), 08 2009.

[117] Digital Video Broadcasting (DVB); Second Generation Framing Structure, Channel Coding and Modulation Systems for Broadcasting, Interactive Services, News Gathering and other Broadband Satellite Applications; Part 2: DVB-S2 Extensinos (DVB-S2X). Technical report, European Standard (Telecommunications series), 10 2014.

[118] B. F. Beidas, R. I. Seshadri, and N. Becker. Multicarrier Successive Predistortion for Nonlinear Satellite Systems. *IEEE Trans. Commun.*, 63(4):1373–1382, April 2015.

[119] A. Ugolini, Y. Zanettini, A. Piemontese, A. Vanelli-Coralli, and G. Colavolpe. Efficient Satellite Systems Based on Interference Management and Exploitation. In *2016 50th Asilomar Conference on Signals, Systems and Computers, Pacific Grove.*, pages 492–496, Nov Nov 2016.

[120] A. Piemontese, A. Modenini, G. Colavolpe, and N. S. Alagha. Improving the Spectral Efficiency of Nonlinear Satellite Systems through Time-Frequency Packing and Advanced Receiver Processing. *IEEE Transactions on Communications*, 61(8):3404–3412, August 2013.

[121] B. F. Beidas, H. El Gamal, and S. Kay. Iterative Interference Cancellation for High Spectral Efficiency Satellite Communications. *IEEE Trans. Commun.*, 50(1):31–36, Jan 2002.

[122] B. F. Beidas and R. I. Seshadri. Analysis and Compensation for Nonlinear Interference of Two High-order Modulation Carriers over Satellite Link. *IEEE Transactions on Communications*, 58(6):1824–1833, June 2010.

[123] B. F. Beidas. Intermodulation Distortion in Multicarrier Satellite Systems: Analysis and Turbo Volterra Equalization. *IEEE Transactions on Communications*, 59(6):1580–1590, June 2011.

[124] A. Ugolini, A. Modenini, G. Colavolpe, G. Picchi, V. Mignone, and A. Morello. Advanced Techniques for Spectrally Efficient DVB-S2X Systems. In *2014 7th Advanced Satellite Multimedia Systems Conference and the 13th Signal Processing for Space Communications Workshop (ASMS/SPSC)*, pages 158–164, Sep. 2014.

[125] R. Gallager. Low-Density Parity-Check Codes. *IRE Trans. Inf. Theory*, 8(1):21–28, Jan. 1962.

[126] A. Morello and V. Mignone. DVB-S2: The Second Generation Standard for Satellite Broad-Band Services. *Proceedings of the IEEE*, 94(1):210–227, Jan 2006.

[127] Mustafa Eroz, Feng-Wen Sun, and Lin-Nan Lee. DVB-S2 Low Density Parity Check Codes with Near Shannon Limit Performance. *International Journal of Satellite Communications and Networking*, 22(3):269–279.

[128] B. F. Beidas and R. Iyer Seshadri. OFDM-like Signaling for Broadband Satellite Applications: Analysis and Advanced Compensation. *IEEE Transactions on Communications*, 65(10):4433–4445, Oct 2017.

[129] and P. J. Voltz and F. A. Cassara. On Channel Estimation and Detection for Multicarrier Signals in Fast and Selective Rayleigh Fading Channels. *IEEE Transactions on Communications*, 49(8):1375–1387, Aug 2001.

[130] Yiguang Wang, Xingxing Huang, Li Tao, Jianyang Shi, and Nan Chi. 4.5-Gb/s RGB-LED Based WDM Visible Light Communication System Employing CAP Modulation and RLS Based Adaptive Equalization. *Opt. Express*, 23(10):13626–13633, May 2015.

[131] N. Wu, W. Yuan, Q. Guo, and J. Kuang. A Hybrid BP-EP-VMP Approach to Joint Channel Estimation and Decoding for FTN Signaling over Frequency Selective Fading Channels. *IEEE Access*, 5:6849–6858, 2017.

[132] T. Ishihara and S. Sugiura. Iterative Frequency-Domain Joint Channel Estimation and Data Detection of Faster-than-Nyquist Signaling. *IEEE Transactions on Wireless Communications*, 16(9):6221–6231, Sept 2017.

[133] T. Hirano, Y. Kakishima, and M. Sawahashi. TDM based Reference Signal Multiplexing for Faster-than-Nyquist Signaling using OFDM/OQAM.

In *2014 IEEE International Conference on Communication Systems*, pages 437–441, Nov 2014.

[134] Z. Hu, S. Gao, Y. Shao, L. Chen, and C. Chan. A Robust Channel Processor for Faster-than-Nyquist Non-orthogonal FDM Visible Light Communication Systems. In *2018 European Conference on Optical Communication (ECOC)*, pages 1–3, Sep. 2018.

[135] S. Gorbunov and A. Rashich. BER Performance of SEFDM Signals in LTE Fading Channels. In *2018 41st International Conference on Telecommunications and Signal Processing (TSP)*, pages 1–4, July 2018.

[136] S. Weinstein and P. Ebert. Data Transmission by Frequency-Division Multiplexing Using the Discrete Fourier Transform. *IEEE Transactions on Communication Technology*, 19(5):628–634, October 1971.

[137] B. Muquet, Zhengdao Wang, G. B. Giannakis, M. de Courville, and P. Duhamel. Cyclic Prefixing or Zero Padding for Wireless Multicarrier Transmissions? *IEEE Trans on Commun*, 50(12):2136–2148, Dec 2002.

[138] J.K. Ahn, K.J. Kim, D. Lee, and J.H. Lee. Reference Signal Generation Using Gold Sequences, September 23 2009. EP Patent App. EP20,090,155,364.

[139] 5G; Study on Channel Model for Frequencies from 0.5 to 100 GHz (3GPP TR 38.901 version 14.0.0 Release 14). Technical report, 3GPP, 05 2017.

[140] T. S. Rappaport, J. N. Murdock, and F. Gutierrez. State of the Art in 60-GHz Integrated Circuits and Systems for Wireless Communications. *Proceedings of the IEEE*, 99(8):1390–1436, Aug 2011.

[141] P. Wang, Y. Li, L. Song, and B. Vucetic. Multi-Gigabit Millimeter Wave Wireless Communications for 5G: from Fixed Access to Cellular Networks. *IEEE Commun. Mag.*, 53(1):168–178, Jan. 2015.

[142] Y. Shoji, C. S. Choi, and H. Ogawa. 70-GHz-Band OFDM Transceivers Based on Self-Heterodyne Scheme for Millimeter-Wave Wireless Personal Area Network. *IEEE Trans. Microw. Theory Tech.*, 54(10):3664–3674, Oct. 2006.

[143] Theodore S Rappaport, (Robert William) Heath, (Robert Clark) Daniels, and (James Nelson) Murdock. *Millimeter Wave Wireless Communications*. Prentice Hall, 2015.

[144] C. S. Choi, Y. Shoji, and H. Ogawa. Implementation of an OFDM Baseband with Adaptive Modulations to Grouped Subcarriers for Millimeter-Wave Wireless Indoor Networks. *IEEE Trans. Consum. Electron.*, 57(4):1541–1549, Nov. 2011.

[145] C. Lin, Y. Chi, C. Tsai, H. Wang, and G. Lin. 39-GHz Millimeter-Wave Carrier Generation in Dual-Mode Colorless Laser Diode for OFDM-MMWoF Transmission. *IEEE J. Sel. Topics Quantum Electron.*, 21(6):609–618, Nov. 2015.

[146] Z. Cao, F. Li, Y. Liu, J. Yu, Q. Wang, C. W. Oh, Y. Jiao, N. C. Tran, H. P. A. van den Boom, E. Tangdiongga, and A. M. J. Koonen. 61.3-Gbps Hybrid Fiber-Wireless In-Home Network Enabled by Optical Heterodyne and Polarization Multiplexing. *J. Lightw. Technol.*, 32(19):3227–3233, Oct. 2014.

[147] M. Martinez-Ingles, C. Sanchis-Borras, J. Molina-Garcia-Pardo, J. Rodríaguez, and L. Juan-Llacer. Experimental Evaluation of an Indoor MIMO-OFDM System at 60 GHz Based on the IEEE802.15.3c Standard. *IEEE Antennas Wireless Propag. Lett.*, 12:1562–1565, Nov. 2013.

[148] C. Sanchis-Borrás, M. Martínez-Inglés, J. Molina-García-Pardo, J. P. García, and J. Rodríguez. Experimental Study of MIMO-OFDM Transmissions at 94 GHz in Indoor Environments. *IEEE Access*, 5:7488–7494, Apr. 2017.

[149] S. Nie, G. R. MacCartney, S. Sun, and T. S. Rappaport. 72 GHz Millimeter Wave Indoor Measurements for Wireless and Backhaul Communications. In *2013 IEEE 24th Annual International Symposium on PIMRC*, pages 2429–2433, Sept. 2013.

[150] G. R. MacCartney and T. S. Rappaport. 73 GHz Millimeter Wave Propagation Measurements for Outdoor Urban Mobile and Backhaul Communications in New York City. In *2014 IEEE ICC*, pages 4862–4867, June 2014.

[151] V. Dyadyuk, J. D. Bunton, J. Pathikulangara, R. Kendall, O. Sevimli, L. Stokes, and D. A. Abbott. A Multigigabit Millimeter-Wave Communication System with Improved Spectral Efficiency. *IEEE Trans. Microw. Theory Tech.*, 55(12):2813–2821, Dec. 2007.

[152] M. R. Khanzadi, D. Kuylenstierna, A. Panahi, T. Eriksson, and H. Zirath. Calculation of the Performance of Communication Systems from Mea-

sured Oscillator Phase Noise. *IEEE Trans. Circuits Syst. I, Reg. Papers*, 61(5):1553–1565, May 2014.

[153] J. Chen, Z. S. He, D. Kuylenstierna, T. Eriksson, M. Hörberg, T. Emanuelsson, T. Swahn, and H. Zirath. Does LO Noise Floor Limit Performance in Multi-Gigabit Millimeter-Wave Communication? *IEEE Microw. Wirel. Co.*, 27(8):769–771, Aug. 2017.

[154] J. Chen, D. Kuylenstierna, S. E. Gunnarsson, Z. S. He, T. Eriksson, T. Swahn, and H. Zirath. Influence of White LO Noise on Wideband Communication. *IEEE Trans. Microw. Theory Tech.*, 66(7):3349–3359, July 2018.

[155] Gotmic. Gotmic. `http://www.gotmic.se`.

[156] Cheong Yui Wong, R. S. Cheng, K. B. Lataief, and R. D. Murch. Multiuser OFDM with Adaptive Subcarrier, Bit, and Power Allocation. *IEEE J. Sel. Areas Commun.*, 17(10):1747–1758, Oct 1999.

[157] and J. G. Andrews and B. L. Evans. Optimal Power Allocation in Multiuser OFDM Systems. In *GLOBECOM '03. IEEE Global Telecommunications Conference (IEEE Cat. No.03CH37489)*, volume 1, pages 337–341 Vol.1, Dec 2003.

[158] Lei Ye and Alister Burr. Power Allocation for Adaptive Turbo Coded OFDM System. *Chinese Journal of Electronics*, 20(3), July 2011.

[159] 3rd Generation Partnership Project; LTE; Evolved Universal Terrestrial Radio Access (E-UTRA); User Equipment (UE) Radio Transmission and Reception (Release 14). Technical report, 3GPP, 11 2017.

[160] Z. Ding, X. Lei, G. K. Karagiannidis, R. Schober, J. Yuan, and V. K. Bhargava. A Survey on Non-Orthogonal Multiple Access for 5G Networks: Research Challenges and Future Trends. *IEEE Journal on Selected Areas in Communications*, 35(10):2181–2195, Oct 2017.

[161] L. G. Barbero and J. S. Thompson. A Fixed-Complexity MIMO Detector Based on the Complex Sphere Decoder. In *2006 IEEE 7th Workshop on Signal Processing Advances in Wireless Communications*, pages 1–5, July 2006.

[162] Tongyang Xu, Ryan C Grammenos, Farokh Marvasti, and Izzat Darwazeh. An Improved Fixed Sphere Decoder Employing Soft Decision for the Detection of Non-Orthogonal Signals. *IEEE Commun. Lett.*, 17(10):1964–1967, October 2013.

[163] Evolved Universal Terrestrial Radio Access (E-UTRA); Physical Layer Procedures. Technical report, 3GPP, May 2016.

[164] S. M. Alamouti. A Simple Transmit Diversity Technique for Wireless Communications. *IEEE Journal on Selected Areas in Communications*, 16(8):1451–1458, Oct 1998.

[165] Evolved Universal Terrestrial Radio Access (E-UTRA); Base Station (BS) Radio Transmission and Reception. Technical report, 3GPP, May 2008.

[166] M. El-Hajjar and L. Hanzo. EXIT Charts for System Design and Analysis. *IEEE Communications Surveys Tutorials*, 16(1):127–153, First 2014.

[167] Zhijin Qin, Hao Ye, Geoffrey Ye Li, and Biing-Hwang Fred Juang. Deep Learning in Physical Layer Communications. *arXiv e-prints*, page arXiv:1807.11713, Jul 2018.

[168] P. Robertson, E. Villebrun, and P. Hoeher. A Comparison of Optimal and Sub-Optimal MAP Decoding Algorithms Operating in the Log Domain. In *Communications, 1995. ICC '95 Seattle, 'Gateway to Globalization', 1995 IEEE International Conference on*, volume 2, pages 1009–1013 vol.2, Jun 1995.

[169] M. Gavell, H. Zirath, M. Ferndahl, and S. E. Gunnarsson. A Linear 70-95 GHz Differential IQ Modulator for E-band Wireless Communication. In *2010 IEEE MTT-S International Microwave Symposium*, pages 788–791, May 2010.

[170] D. Nopchinda, Z. He, G. Granström, M. Gavell, and H. Zirath. 8-PSK Upconverting Transmitter Using E -Band Frequency Sextupler. *IEEE Microw. Wirel. Co.*, 28(2):177–179, Feb. 2018.